Dissertation

submitted to the

Combined Faculties for the Natural Sciences and for Mathematics

of the Ruperto-Carola University of Heidelberg, Germany

for the degree of

Doctor of Natural Sciences

presented by

Dipl.-Biochem. Manon Eckhardt

born in Frankfurt am Main, Germany

Oral examination: May 12, 2010

Quantitative analysis of the early steps of virus host cell interaction of human immunodeficiency virus type 1 and hepatitis C virus

Referees:

Prof. Dr. Hans-Georg Kräusslich

Prof. Dr. Ralf Bartenschlager

Summary

Viruses are obligatory intracellular pathogens; hence an essential step of their replication cycle is the entry into a host cell. Enveloped viruses like the human immunodeficiency virus type 1 (HIV-1) and the hepatitis C virus (HCV) enter cells by fusion with cellular membranes. The current knowledge of this process relies mostly on bulk measurements, which often comprise the outcome of several distinct replication steps in a non-synchronized manner. The recent development of novel quantitative approaches has opened the door for deeper understanding of the process by analyses on a single cell and single particle level.

Fluorescently labelled viruses allow studying single steps in the interaction of individual virions with the host cell. A strategy for labelling HIV-1 with organic dyes using the recently described SNAP-tag was established and evaluated in this thesis. Introduction of the SNAP-tag did not significantly interfere with virus entry and infectivity and allowed specific labelling of the Gag structural polyprotein in the context of virions and virus producing cells. Combining fluorescently labelled HIV-1 with the HCV pseudoparticle system (HCVpp) allowed the analysis of virion attachment and entry dependent on the envelope protein of HCV on a single particle level. In addition, the β-Lactamase virion fusion assay was adapted to and optimized for HCVpp, allowing the detection of virus-cell fusion. The dependency of virus particle binding, endocytic uptake and fusion on various stimulating and inhibiting agents was investigated. The virus binding assay developed for HCVpp was subsequently adapted to HIV-1 and revealed cell-type specific kinetics of virion attachment. Interestingly, the expression level of the cellular virion tethering factor CD317 was shown to have no effect on exogenous virus binding.

The main part of this thesis aimed at the acquisition and analysis of quantitative multi-parameter data of HIV-1 entry. Besides the receptor CD4, HIV-1 entry depends on the presence of either one of the two major co-receptors, CXCR4 or CCR5. The ability of a virus variant to use a co-receptor defines the tropism of the virus and is at least in part determined by the sequence of the third variable loop (V3-loop) of the viral envelope protein (Env). In summary, HIV entry efficiency is determined by a complex interplay between Env sequence, receptor and co-receptor densities. A deeper insight into the interdependencies of these critical parameters provides a basis for the understanding of the mechanism of action of HIV entry inhibitors as well as of pathways of resistance development against these compounds. Mathematical models describing the interdependencies will also aid in the refinement of algorithms for the genotypic prediction of co-receptor tropism, which is essential for the use of co-receptor antagonists in antiretroviral therapy. Here, experimental systems were developed which allow acquisition of detailed quantitative data on the interdependencies between these parameters as a basis for a mathematical model of the HIV-1 entry process. This comprised the selection and characterization of suitable model cell

lines and experimental conditions, the generation and characterization of defined isogenic virus variants and the establishment and calibration of virological assay systems. Multivariant data sets were acquired under standard conditions and algorithms for multivariant data analysis which have been developed in collaboration with bioinformaticians were evaluated. A comprehensive data set was obtained by studying a subset of viruses carrying patient-derived Env variants which revealed quantitative differences in receptor and co-receptor dependency as well as sensitivity to prototype entry inhibitors beyond the overall results of common phenotyping/genotyping methods.

Zusammenfassung

Viren sind obligatorische Zellparasiten; der Eintritt in die Wirtszelle stellt daher einen essentiellen Schritt im Replikationszyklus jedes Virus dar. Umhüllte Viren wie das humane Immundefizienzvirus Typ 1 (HIV-1) und das Hepatitis C Virus (HCV) treten durch Fusion der Virushülle mit einer zellulären Membran in die Wirtszelle ein. Bisherige Analysen des Viruseintritts beruhen überwiegend auf Ensemblemessungen, in denen oft mehrere aufeinanderfolgende Replikationsschritte in nicht synchronisierten Messungen zusammengefasst werden. Neuere Methoden erlauben jedoch die eingehende quantitative Analyse einzelner Replikationsschritte auf der Ebene einzelner Zellen und Partikel.

Fluoreszenzmarkierte Viren ermöglichen es, die Interaktion einzelner Virionen mit der Wirtszelle zu visualisieren. In dieser Arbeit wurde eine Strategie zur Markierung von HIV mit synthetischen Fluoreszenzfarbstoffen durch Einführung des ‚SNAP-tags' entwickelt und evaluiert. Der SNAP-tag beeinträchtigte die virale Eintrittseffizienz und Infektiösität nur geringfügig und ermöglichte die spezifische Markierung von Viren und dem viralen Strukturprotein in virusproduzierenden Zellen. Durch Kombination fluoreszenzmarkierter HIV Partikel mit dem HCV Pseudopartikel-System (HCVpp) sowie durch Anpassung des β-Lactamase Fusionsassays an HCVpp konnten einzelne Schritte des durch die HCV Hüllproteine vermittelten Eintrittsprozesses und deren Abhängigkeit von stimulierenden und inhibierenden Faktoren untersucht werden. Die Anwendung der zuvor mit HCVpp entwickelten Methode zur Untersuchung der Virusbindung auf HIV-1 zeigte zelltyp-spezifische Unterschiede in der Kinetik der Virusbindung. Weiterhin wurde gezeigt, dass die Menge des zellulären Virusbindungsfaktors CD317 an der Zelloberfläche keine Rolle bei der Bindung exogener Viren spielt.

Der Hauptteil dieser Arbeit befasst sich mit der Aufnahme und Analyse multivarianter Daten zum Zelleintritt von HIV. Neben dem Rezeptor CD4 benötigt HIV einen der beiden Korezeptoren CCR5 oder CXCR4. Der Tropismus für einen oder beide dieser Korezeptoren wird weitgehend von der Aminosäuresequenz in der 3. variablen Schleife (V3-loop) des HIV Hüllproteins (Env) bestimmt. Die Eintrittseffizienz des Virus wird von einem komplexen Zusammenspiel zwischen Env-Sequenz, Rezeptor- und Korezeptordichte bestimmt. Eine genauere quantitative Analyse dieser Abhängigkeiten ist die Grundlage für ein besseres Verständnis der Wirkungsweise von Inhibitoren des HIV Eintritts sowie der Entwicklung von Resistenzen gegen diese Präparate. Ein mathematisches Modell des Eintrittsprozesses wird auch zur Verbesserung von Algorithmen zur Vorhersage des Korezeptor Tropismus beitragen, die für den therapeutischen Einsatz von Korezeptor-Antagonisten essentiell ist. In dieser Arbeit wurden experimentelle Systeme entwickelt, die die Erhebung detaillierter quantitativer Daten zur Abhängigkeit der Eintrittseffizienz und Inhibitorsensitivität von Rezeptor- und Korezeptordichte

erlauben. Dies umfasste die Auswahl und Charakterisierung geeigneter Modell-Zellinien, die Herstellung und Charakterisierung einer Auswahl isogener Virusvarianten, sowie die Etablierung und Kalibrierung virologischer Testsysteme. Diese Daten bilden die Grundlage zur Erstellung mathematischer Modelle des Eintrittsprozesses. Systematische multivariante Datensätze wurden aufgenommen und Algorithmen zur Datenanalyse wurden in Zusammenarbeit mit Bioinformatikern evaluiert. Die Analyse eines umfassenden Datensatzes zur Eintrittseffizienz von isogenen Viren mit aus Patientenisolaten gewonnenen viralen V3-loop Sequenzen ergab individuelle Eintrittsprofile der Virusvarianten, die durch bisher gebräuchliche Geno- und Phänotypisierungsmethoden nicht erfasst werden.

Table of contents

1 Introduction

Viruses are minute pathogens that lack the machinery for replication and therefore are highly dependent on their host cells. The most basic viruses consist only of a genome (RNA or DNA) packed into a protein shell for protection from the outer environment. In order to replicate viruses need to deliver their genomes into the cytoplasm or even nucleus of a susceptible cell. In case of enveloped viruses this step is accomplished by fusion of the viral envelope with a cellular membrane. After replication of the virus genome and expression of viral proteins with the help of cellular enzymes, new virus particles assemble within the cell. The egress of the progeny virus can be accomplished by lysis of the host cell or by budding off cellular membranes and release into the surrounding medium. The new virus particles then infect further target cells so that the virus eventually spreads within the organism and beyond.

The replication cycle of different viruses has been studied in great detail. Most of these studies however, relied on bulk measurements due to restrictions of the respective methods. These traditional virological methods often merged multiple steps of the replication cycle due to indirect readouts and limited temporal resolution. The recent development of various quantitative methods allows the investigation of individual steps in much greater detail. Introduction of single-virus techniques such as fluorescent labelling of viruses significantly enhances the temporal, spatial as well as quantitative resolution of results. Advances in microscopic techniques such as stimulated emission depletion (STED) or stochastic optical reconstruction microscopy (STORM) furthermore circumvent the diffraction limited resolution of fluorescence microscopy allowing even deeper analyses of single-virus data. With these new quantitative single-cell methods, the distinct steps of the viral replication cycle can be visualized (for review see [26]). To date, virus cell interactions have been studied on the single-particle level for several viruses, including non-enveloped viruses like simian virus 40 and poliovirus, as well as enveloped viruses like influenza, murine leukaemia virus, human immunodeficiency virus (HIV) and very recently also hepatitis C virus (HCV) [25, 41, 129, 147, 179, 203]. In addition to trafficking of viral proteins within host cells and the interactions of viral and cellular proteins, those methods have also been applied to study viral egress, for example for HIV [101, 109]. Theses methods provide quantitative data of cellular systems which represent a basis for mathematical modelling. The comprehension and simulation of complex cellular processes by mathematical models is a major goal of systems biology approaches. In this regard, the relative low complexity of a virus represents a benefit for the development of mathematical models of biological processes and the preciseness of their outcome.

This work focuses on two enveloped RNA viruses, the human immunodeficiency virus type 1 (HIV-1) and the hepatitis C virus (HCV), specifically on their entry into and egress out of host cells. The following chapter will therefore introduce these two viruses.

1.1 Human Immunodeficiency Virus type 1 – HIV-1

HIV is the major member of the virus genus of lentiviruses among the family of retroviruses. It is the causative agent for the acquired immunodeficiency syndrome (AIDS) [10, 70] with app. 33.4 million people infected worldwide and 2 million deaths due to AIDS in 2008 alone [229]. There are two types of HIV, HIV-1 and HIV-2, with HIV-1 accounting for the majority of infections. Therefore, this chapter will focus only on HIV-1.

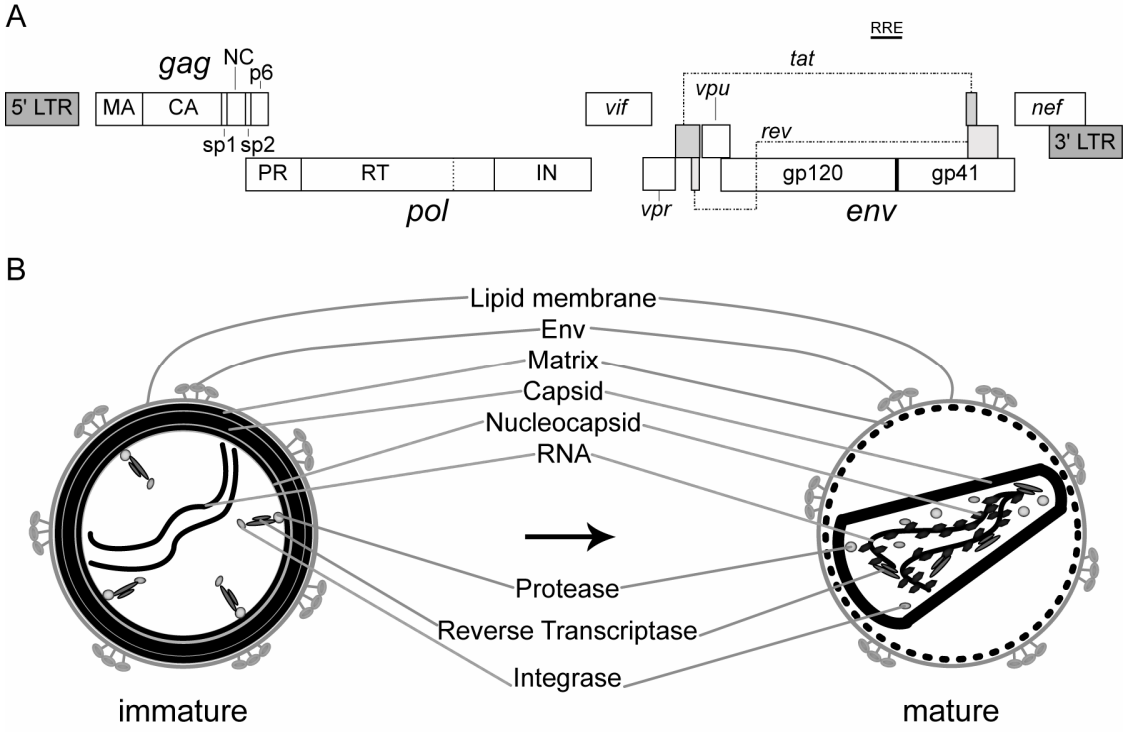

Fig. 1.1: HIV-1 genome and particle structure. (A) Schematic drawing of the HIV-1 genome. Vertical positions denote each of the three different reading frames that encode viral proteins. An RNA structural element, the Rev-responsive element (RRE) is depicted with a bold horizontal line. Two long terminal repeats (LTR, dark grey) are flanking the open reading frames (ORF) of the three major genes, *gag* (group specific antigen), *pol* (polymerase) and *env* (envelope) and six accessory genes coding for Vif (virion infectivity factor), Vpr (viral protein R), Tat (transactivator), Rev (regulator of virion), Vpu (viral protein U) and Nef (negative factor). Abbreviations of fully processed gene products are depicted in regular type within the gene region coding for them; compare text for details. The two exons of *tat* and *rev* genes (shades of grey) are connected with dotted lines, respectively. Viral protease cleavage sites are indicated with vertical lines within the three major ORFs, the cleavage site of the cellular protease in *env* is indicated with a bold vertical line. Dotted vertical line in *pol* indicates RNAse H domain of reverse transcriptase (RT) gene product. This figure is modified from [130]. (B) Schematic drawing of HIV-1 particles in immature (left) and mature (right) conformation. Accessory proteins packaged into the virion are ommited. This figure is modified from[103].

HIV-1 is an enveloped virus forming particles with an average diameter of app. 145 nm [28]. It carries two copies of a single-stranded 9.7 kb RNA genome in plus orientation. In addition to the three major genes *group specific antigen* (*gag*), *polymerase* (*pol*) and *envelope* (*env*), which are shared by all retroviruses, lentiviruses code for accessory proteins that have regulatory functions in gene expression, replication capacity and pathogenicity. The HIV-1 genes are partially overlapping, arranged in all three reading frames and harbour splice signals so that multiple splice variants of the HIV-1 RNA can be processed. The open reading frames (ORF) of retroviruses are flanked by two long terminal repeats (LTR), which harbour enhancer elements and the promoter and are necessary for reverse transcription of the genome. The structure of the viral genome is depicted in Fig. 1.1 A. As depicted in Fig. 1.1 B, HIV-1 virions are surrounded by a lipid membrane. Inside this membrane the structural proteins, encoded by the *gag* gene, form the viral core, which encloses the viral RNA. The *pol* gene codes for the viral enzymes, which are packaged into the virion as well. The last major ORF carries the *env* gene, which encodes for the envelope proteins which are incorporated into the viral lipid membrane.

The Gag precursor protein, which in immature particles radially lines the inside of the viral membrane, is subsequently processed into matrix (MA), capsid (CA), spacer peptide 1 (sp1), nucleocapsid (NC), spacer peptide 2 (sp2) and protein of 6 kDa (p6). CA and NC build up the inner structure of the mature virion and protect the viral genome. The Gag-Pol precursor protein is also processed further, yielding the enzymes needed for replication, reverse transcriptase (RT) and integrase (IN) as well as the viral protease (PR). PR fulfils all the sequential enzymatic cleavages of the precursor proteins starting with an autocatalytic activation event [221]. The Env precursor is processed by cellular subtilisin proteases into gp41, the membrane anchor, and gp120, the surface domain of Env [81, 83]. The accessory proteins Vpr (viral protein R), Vif (virion infectivity factor), Vpu (viral protein unique) and Nef (negative factor) account for pathogenicity, whereas Tat (transactivator) and Rev (regulator of virion) regulate viral gene expression.

The HIV-1 virion occurs in two distinct forms (Fig. 1.1 B,): the immature virus incorporating the uncleaved Gag and Gag-Pol precursor proteins is non-infectious and is only rendered infectious upon full processing by the viral PR into its mature form. In the mature virion, MA forms a thin protein layer underneath the viral membrane, whereas CA is organized into the characteristically cone-shaped structure surrounding the viral RNA. NC lines the two RNA copies and protects it from nuclease digestion, while the viral enzymes RT and IN are also closely associated with the nucleoprotein complex. HIV-1 virions also incorporate the accessory proteins Vpr, Nef and Vif.

1.1.1 HIV-1 replication cycle

The HIV-1 replication cycle is schematically depicted in Fig. 1.2 and begins with the entry of the virus into the host cell. This process will be discussed in detail below, due to its importance to this study. In brief, the viral protein gp120 binds to its cellular receptor CD4 and one of two major co-receptors, the chemokine receptors CXCR4 or CCR5, respectively. Binding triggers the fusion of viral and cellular membranes and the release of the viral core into the cytoplasm of the target cell. After disassembly of the core, the so-called reverse transcription complex (RTC) is formed, in which reverse transcription of the viral RNA by RT takes place. Subsequently, the double-stranded viral cDNA is transported towards the nucleus, incorporated into the so-called preintegration complex (PIC), which contains at least IN and Vpr, but potentially several other viral and cellular proteins [30].

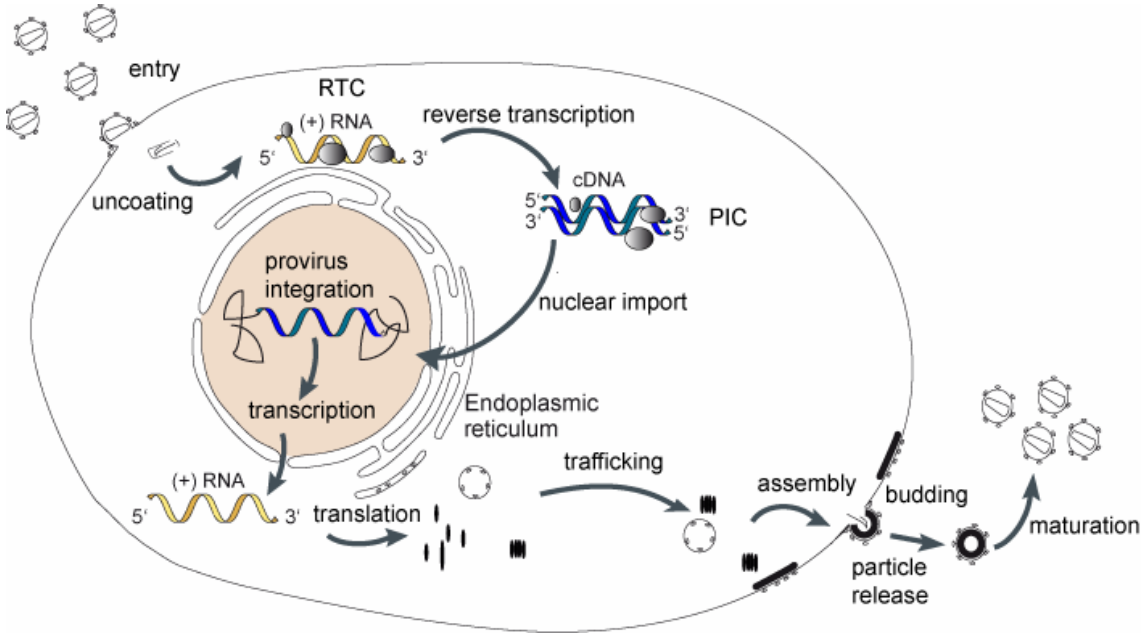

Fig. 1.2: Replication cycle of HIV-1. Schematic drawing of the major steps during HIV-1 replication. See text for details. RTC = reverse transcription complex; PIC = preintegration complex.

After nuclear import, the viral DNA is integrated into the cellular genome with the help of the viral IN. This integrated provirus can persist quiescently in cells for prolonged time periods – up to many years – and will, upon activation of the cell, be transcribed by the cellular RNA polymerase II. Early gene products comprise Tat, Rev and Nef, which are translated from fully spliced mRNA species. Efficient gene expression can take place only upon binding of Tat to the LTR. Tat-independent transcription is driven by cellular transcription factors, which also recognize the LTR, but to a lesser extent. Partially spliced or unspliced viral mRNAs have to be actively exported from the nucleus with the help of Rev, which binds to the RRE (rev-responsive element), an RNA stem loop structure located in the *env* gene (Fig. 1.1 A). Those intron-containing mRNAs serve as templates for the late gene products, Vpr, Vif, Vpu and Env, whereas

Gag and the Gag-Pol precursor are translated from fully unspliced mRNA that also serves as viral genome for progeny virus. All viral proteins are translated on free ribosomes in the cytoplasm, except the transmembrane protein Env, which is translated at the rough endoplasmic reticulum (ER). From there, it will be transported via the secretory pathway to the plasma membrane, where assembly of new progeny virus takes place. All other viral proteins which will be incorporated into the virion also travel to the plasma membrane, as described in greater detail below. Gag alone is necessary and sufficient to form virus like particles [72], although it engages cellular factors of the endosomal sorting complex required for transport (ESCRT) machinery, which helps to pinch off the curved budding structure in an ATP-dependent membrane fission event [233]. Concomitant with or shortly after release, PR starts to process the viral precursor proteins into their final functional units. After this so-called maturation step, which includes also the rearrangement of the inner viral structure, the mature virus is ready for the next round of infection.

1.1.1.1 HIV-1 Gag trafficking

The HIV-1 Gag precursor protein is translated in the cytosol of infected cells on polysomes. It is then thought to oligomerize, maybe with the help of cellular proteins [256]. However, significant multimerization only takes place when Gag is bound to membranes [74]. Gag membrane binding is mediated by several factors. The N-terminal myristate and the basic cluster within the first 31 amino acids (aa) of MA, forming an amphipathic β-sheet, confer membrane binding [192]. MA alone nevertheless shows reduced membrane binding affinities compared to full length Gag, which can be explained by the myristyl-swich model [193, 218]: the myristic acid covalently attached to the N-terminus of MA is hidden in a hydrophobic groove in the monomeric protein. Upon Gag oligomerization the myristate is exposed which increases membrane affinity dramatically without changing the overall conformation of MA. Gag multimerization is mainly driven by intermolecular interactions between the CA, NC, sp1 and MA basic cluster region of neighbouring Gag molecules [32] as well as the interaction with RNA. In addition, it also seems to be stimulated by membrane binding, thus leading to a cumulative mechanism of multimerization and membrane binding of Gag [192].

As mentioned above, budding of HIV-1 particles takes place at the plasma membrane of infected cells. Also, the majority of Gag is found at the plasma membrane in steady-state [92], hence requiring a plasma membrane targeted trafficking of Gag. The specificity of targeting to the plasma membrane is achieved by interaction with phosphatidyl-4,5-bisphosphate ($PI(4,5)P_2$) which predominantly resides within the plasma membrane [174]. Interactions with the adaptor protein AP-3 have also been suggested to play a role [52]. The exact pathway in which Gag travels towards the plasma membrane is however still under debate. It was suggested that after diffuse cytoplasmic distribution Gag forms perinuclear accumulations from which it will travel on

through the multivesicular body (MVB) [182]. The involvement of the endocytic pathway was favoured for a long time as budding seemed to take place at MVB membranes in certain cell types, e.g. primary macrophages [178]. The "Trojan exosome hypothesis" [78] also favours the model of MVB as an intermediate trafficking location. In this theory, however, Gag is not transported to the plasma membrane via endosomes, but complete viral particles bud into the MVB and are released from the cell via exocytosis [166]. However, Welsch and colleagues [241] could show that the plasma membrane is the primary site for HIV-1 budding also in macrophages. This does not exclude that trafficking through the endosomal pathway could still be an intermediate step on the way towards the budding site.

1.1.2 HIV-1 entry mechanism

The first step in the replication cycle of every virus is the entry into its host cell. Viruses achieve the crossing of the plasma membrane by several distinct mechanisms (reviewed in [145]). Clathrin-dependent and -independent endocytic processes are used by non-enveloped viruses as well as several enveloped viruses. Some viruses rely on acidification of early endosomes to activate their fusion protein. Other viruses have been described to directly fuse with the cellular plasma membrane.

The mechanism of HIV-1 entry is overall well understood, but is still a topic of ongoing research. As HIV-1 entry into target cells is pH-independent, it has long been thought to occur at the plasma membrane. However, evidence for involvement of clathrin-dependent endocytosis in productive entry was reported some years ago [45, 80], and has recently been suggested to be the exclusive route of entry [152]. Independent of the location of the fusion event, the mechanism proposed remains the same and will be described in the following paragraph.

1.1.2.1 The HIV-1 Env protein

The HIV-1 Env protein is a type I fusion protein displaying predominantly α-helical secondary structure. It is translated from the singly spliced mRNA at the rough endoplasmic reticulum (ER) as the precursor protein, gp160, which is cotranslationally edited by N-glycosylation. During gp160 transport to the plasmamembrane, it is cleaved into its functional parts, gp41 and gp120, by cellular proteases within the Golgi complex. Here, further addition of highly complex glycosylation also takes place. The two separated protein parts stay noncovalently attached to each other, though this interaction is fairly weak, resulting in frequent Env-shedding – the loss of gp120 from its membrane anchor, gp41. The functional unit of Env is a trimer [251, 252], which will eventually be incorporated into the budding virion at the plasma membrane. Within this trimer, gp120 conveys virus binding to the cellular receptor and co-receptor, whereas gp41 serves as a membrane anchor for Env and provides the machinery for membrane fusion.

The surface unit of Env, gp120, is a highly variable protein among different HIV-1 isolates, which hampers the development of an active immunization strategy against the virus. As depicted in Fig. 1.3 A, it consists of five variable (V1 to V5) and five conserved (C1 to C5) interspersed regions and harbours 18 highly conserved cystein residues [219]. Four of the variable regions are linked to large loops by disulfide bonds each [133], with V1 and V2 forming one continuous loop. Gp120 is arranged into an inner, gp41-interacting, and an outer domain, which is exposed at the viral surface, bridged by a β-sheet [126, 250]. Elements of all three domains contribute to CD4-binding, which occurs over an area of ~800 Å2 [251]. Co-receptor binding on the other hand, is believed to mostly depend on interactions with the third variable loop (V3-loop) [40], although other variable (V1/V2-loop, [176]) as well as conserved regions have been discussed to play a role in co-receptor binding [195]. Fig. 1.3 B depicts a structure-based model of the trimeric Env protein, including both gp41 (brown) and gp120 (blue). Interaction sites with the cellular receptor (grey) and a CD4-induced (CD4i) epitope (orange) as well as the V3-loop (cyan) which is protruding outwards from gp120, pointing away from the viral membrane, are shown.

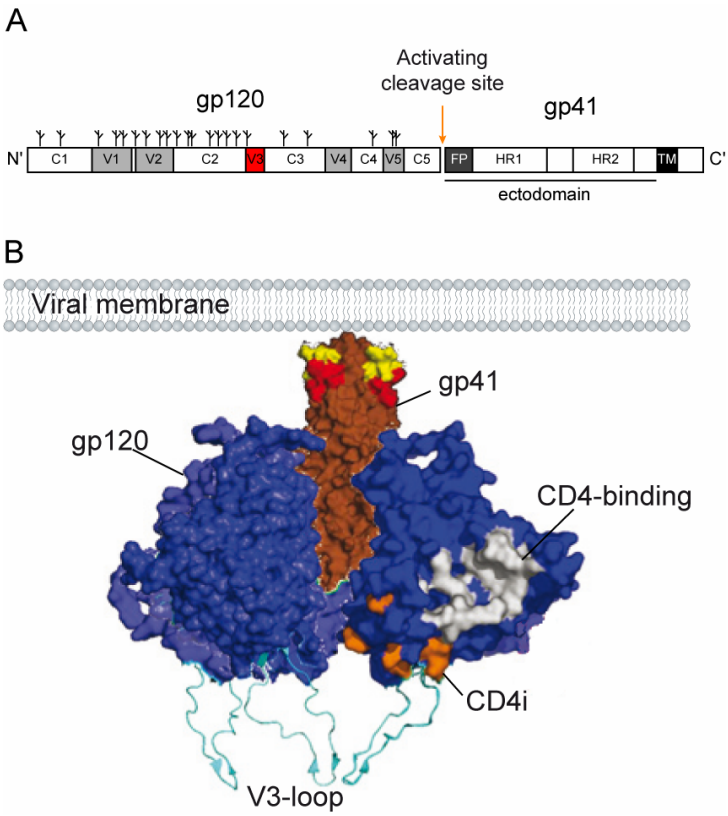

Fig. 1.3: The HIV-1 Env protein. (A) Domain structure of gp120 and gp41. The five conserved (C1-C5) and variable (V1-V5) domains in gp120 are separated by horizontal lines. Positions of conserved glycosylation sites are marked by branched structures. The V3-loop is highlighted in red. Arrow indicates cleavage site of a protease. In gp41, the fusion peptide (FP), two heptad repeat regions (HR1 and HR2) and the transmembrane domain (TM) are depicted. (B) Structure-based model of the extraviral part of HIV-1 Env protein in its trimeric state. The extraviral gp41 is shown in brown, whereas the surface unit of Env (gp120) is depicted in blue. The outwards protruding third variable loop (V3 loop) is shown in cyan. The interaction site of Env with CD4 (CD4-binding) is highlighted in grey and the CD4-induced epitope (CD4i) is shown in orange. Pictures were modified from [223] and [112].

In contrast to the multiple interaction sites in gp120, the gp41 transmembrane unit of Env does not directly contribute to receptor or co-receptor binding, but rather provides an ectodomain that is mostly responsible for trimerisation [213], a membrane-spanning anchor domain (TM) and a long cytoplasmic tail (CT). The exact function of this among retroviruses unconventionally long CT is not known, yet. It may take part in Env internalization through an endocytosis signal [199] and Env incorporation into the newly formed virion through interactions with MA [163]. The N-

terminus of gp41 harbours a glycine rich stretch, the so-called "fusion peptide" (FP) [36]. It is buried underneath gp120 in the fusion incompetent stage of Env and is only exposed upon gross conformational changes, thereby preventing early fusion. Gp41 also exhibits two amphipathic heptad repeat regions (HR), HR1 and HR2, which are able to form a coiled-coil structure with an interconnecting loop. They are arranged in an antiparallel packing, with HR1 in the centre and HR2 fitting in the hydrophobic grooves [33].

1.1.2.2 The cellular receptor and co-receptors of HIV-1

Cluster of differentiation 4 (CD4), a member of the immunoglobulin (Ig) superfamily has been identified as the primary receptor of HIV-1 shortly after the discovery of the virus itself [144]. CD4 is a 55 kDa transmembrane protein and physiologically functions as a co-receptor of the T-cell receptor by stabilizing the interaction with major histocompatibility complex type II (MHC-II) molecules on antigen-presenting cells [23]. However, the presence of CD4 alone is not sufficient to render cells susceptible to HIV-1, but a co-receptor is needed for successful infection. The two major co-receptors of HIV-1 are both members of the G protein-coupled receptor superfamily of seven-transmembrane proteins: the CXC-chemokine receptor 4 (CXCR4) [64] and the CC-chemokine receptor 5 (CCR5) [5, 48]. The natural ligands for CCR5 are the CC-chemokines macrophage inflammatory protein 1 (MIP-1α and MIP-1β) and RANTES (regulated upon activation, normal T-cell expressed and secreted) [205], while CXCR4 is stimulated by the CXC-chemokines of the stromal cell-derived factor type 1 (SDF-1) family [171]. Other chemokine and orphan receptors can also be utilized by some HIV-1 strains, but do not play an essential role *in vivo* [16]. Therefore, this study focuses on the two major co-receptors, CCR5 and CXCR4.

Although CCR5 and CXCR4share little sequence homology [51], they can be used as interchangeable co-receptors by some, but not all HIV strains (see 1.1.3). Whereas both co-receptors are expressed on primary T-cells and macrophages, only CXCR4 is ubiquitously expressed on T-cell lines as well as a variety of other human cell lines. *In vivo*, CCR5 is exclusively expressed on memory T-cells and to a significantly higher degree on the subset of those cells residing in nonlymphoid tissue (e.g. the gastrointestinal tract) [54]. Only a small percentage of circulating CD4-positive ($CD4^+$) T-cells are $CCR5^+$, whereas CXCR4 is present on 80-90 % of circulating naïve $CD4^+$ T-cells [168].

A 32 base pair (bp) deletion within CCR5, the so-called CCR5/Δ32 mutation, confers resistance to HIV-1 infection of homozygous carriers of this allele [140] due to inefficient cell surface expression of the truncated co-receptor that cannot pursue its function anymore. 1 % of the total European Caucasian population is homozygous and 15 % are heterozygous for this specific mutation, which has no observable effect on the life expectancy or health of affected

persons [140].

1.1.2.3 Membrane fusion

HIV-1 fusion with the host cell membrane is a pH-independent step that has long been thought to solely occur at the plasmamembrane of cells. Over time, it has been shown that clathrin-mediated endocytosis can also play a role [45] and it has recently been proposed to be the major productive entry route [152].

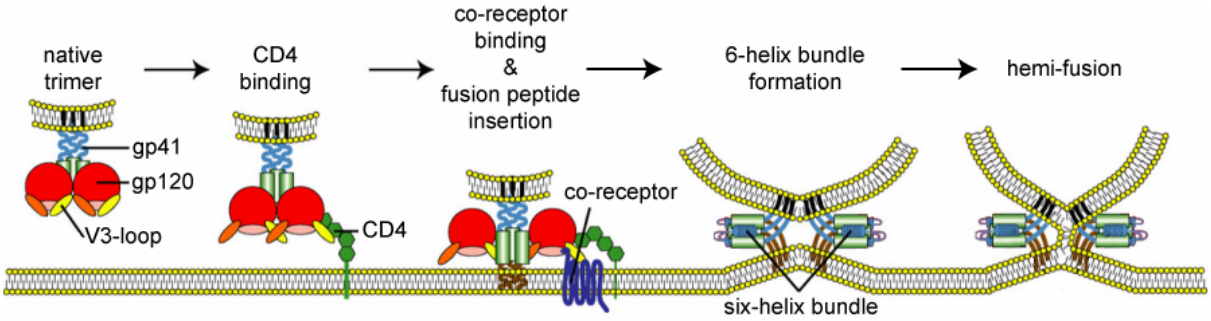

Fig. 1.4: Membrane fusion mechanism of HIV-1. Schematic representation of the consecutive steps of membrane fusion. Details see text. The picture was modified from [223].

Independent of the location of fusion, the mechanism is similar to other retroviruses (e.g. MLV) and to Influenza virus fusion [239]. The first step in HIV-1 entry is unspecific attachment to the cell via heparan sulphate proteoglycans (HSPG) [154] or cellular proteins incorporated into the virus envelope [224]. To illustrate the fusion process in greater detail, the consecutive steps are depicted in Fig. 1.4: First, the specific interaction of gp120 with CD4 is established. The Env protein is thought to be in a metastable, fusion-incompetent conformation prior to CD4 binding. Binding to CD4 represents the trigger for conformational changes within gp120 that allow the exposition of co-receptor binding motifs [249]. Only the subsequent binding of the co-receptor activates gp41 to insert its N-terminal fusion peptide into the opposing host cell membrane [68]. The actual fusion mechanism is believed to appear in analogy to the so-called "spring-loaded model" of influenza virus membrane fusion [31]. This model describes the convergence of the two opposing membranes through the formation of a six-helix bundle of the two heptad repeat regions. Fusion then proceeds through a hemifusion state, in which only the outer membrane sheets of virus and cell have fused, to full fusion of the membranes with both N- and C-termini of gp41 residing in the same membrane, again.

1.1.2.4 Inhibition of HIV-1 entry

HIV-1 is the causative agent for the fatal disease AIDS. The lack of a protective vaccine stresses the need for specific antiviral treatment to suppress HIV-1 replication. Currently, several classes of inhibitors targeting different steps of the viral life cycle are used in highly active antiretroviral therapy (HAART): two classes of reverse transcriptase inhibitors, protease

inhibitors, integrase inhibitors and entry inhibitors.[246] For the latter, several possibilities of interference are illustrated in Fig. 1.5. Today, there are two different classes of entry inhibitors used in clinical practice: a fusion inhibitor and a co-receptor antagonist.

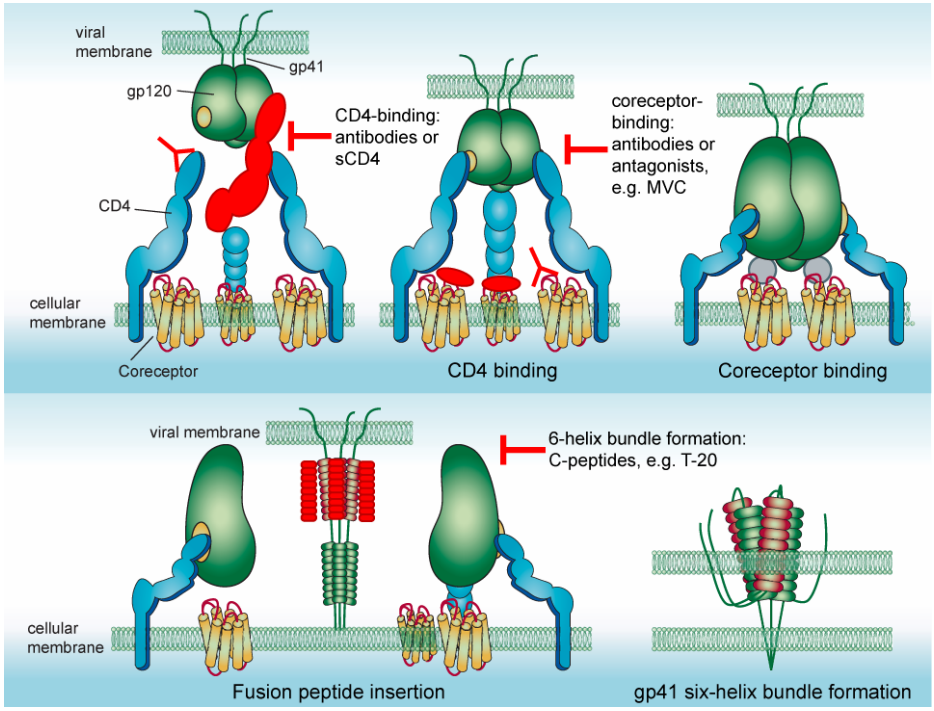

Fig. 1.5: Possible interference points of different drugs with the entry process of HIV-1. Schematic representation of the consecutive steps of membrane fusion with possible interference points highlighted in red. Inhibition of CD4-binding, thus preventing the progression from the first to the second picture, has been attempted with soluble CD4 molecules (sCD4) and antibodies (depicted as a Y) directed against CD4. The next step, namely co-receptor binding, can successfully be inhibited by the usage of co-receptor antagonists (ovals), such as maraviroc (MVC). In addition, antibodies directed against the co-receptor (depicted as Y) are another strategy. The next interference point is the inhibition of six-helix bundle formation, which can be achieved by gp41-derived C-peptides (cylinders). Modified from [60].

Early studies focussed on the usage of soluble CD4 molecules to compete with effective cell binding and in addition to promote premature gp120 shedding which renders the virion non-infectious [155]. After the discovery of the two major co-receptors, their ligands were shown to efficiently block entry of the respective HIV-1 strains by downmodulation of the co-receptor from the cell surface (reviewed in [139]). Based on this, small molecule inhibitors have been developed, as discussed below. Another class of entry inhibitors that has been investigated are humanized monoclonal antibodies directed against CD4 or CCR5. Although it binds to CD4, Ibalizumab [50] (also known as TNX-355, TaiMed Biologics, Taipei, Taiwan) does not show immunosuppressive action, but still inhibits viral entry independent of co-receptor usage [102]. The phase II clinical trial is expected to be completed at the end of this year [169]. An antibody targeting CCR5, PRO 140 (Progenics Pharmaceuticals, Tarrytown, NY, USA), has completed phase II clinical trials and was approved for the "Fast Track" process by the FDA to accelerate medical availability [20].

The first entry inhibitor approved for clinical use, belonged to the class of fusion inhibitors. The small peptidomimetic drug T-20/Enfuvirtide (trade name Fuzeon, Roche Pharmaceuticals, Basel, Switzerland), is a 36 aa HR2-derived peptide, which inhibits fusion at the stage of 6-helix-bundle formation. Peptides derived from HR2 are called C-peptides, as HR2 is closer to the C-terminus of gp41 than HR1. Mimicking their origin, these C-peptides bind to HR1 in the intermediate state of fusion. At this stage, gp41 is easily accessible to the peptides, as it is in its extended conformation with the C-terminus still anchored to the virus membrane while the N-terminal fusion peptide is inserted into the host cell membrane. Due to the mechanism of action, resistance mutations are mostly found in HR1 of gp41 [194]. Other synthetic C-peptides were also shown to inhibit fusion at nanomolar concentrations [247], but have not been developed into antiretroviral drugs due to the disadvantages of peptidic drugs.

The other class of approved entry inhibitors are, as mentioned above, co-receptor antagonists. Antagonists for CXCR4 have been developed and tested early after identification of this co-receptor, but did not get approval for clinical use in HIV-1 patients due to severe adverse effects. AMD-3100, a bicyclam which binds to CXCR4 and blocks HIV-1 entry *in vitro* at nanomolar concentrations, was the first co-receptor antagonist described [47]. The latest tested derivative, AMD11070 (Genzyme, Cambridge, MA, USA), showed promising results but a clinical trial phase II had to be discontinued due to liver toxicity of the compound [160].

CCR5, on the other hand, has always been considered to be the easier target, since individuals homozygous for the CCR5/Δ32 mutation show no signs of decreased life expectancy and remain healthy [140]. Several compounds shown to block CCR5 engagement of HIV-1 Env have entered clinical trials, although most of them are not approved for clinical use yet. A phase II trial with Aplaviroc [236] (GlaxoSmithKline, London, UK) was discontinued in 2006 due to high liver toxicity [44]. Vicriviroc (Schering-Plough, now Merck, Whitehouse Station, NJ, USA) showed promising results and low adverse effects, but trials were discontinued very recently [183]. Nevertheless, in late 2007 the first co-receptor antagonist was finally approved for clinical use. Maraviroc (MVC), sold under the trade name of Celsentri (Selzentry in the USA; ViiV Healthcare, Brentford, UK), is a small molecule that inhibits chemokine binding to CCR5 and ligand-induced signalling, but fails to induce signalling or downmodulation of the co-receptor itself. Therefore, it is termed an inverse agonist or functional antagonist of CCR5 [53]. This compound was shown to be active in the low nanomolar range against a broad spectrum of R5-tropic HIV-1 strains *in vitro* and *in vivo* with no observable increase in adverse effects in comparison to the control group of patients with optimized treatment background only [62]. Resistance to MVC has been reported to occur in such a way that the adapted virus is able to use the drug-bound co-receptor [226, 243]. This resistance was obtained by several mutations within the V3-loop and elsewhere in gp120 and resulted in a reduced maximum inhibition rather than

increased 50 % inhibitory concentration (IC_{50}) values. In contrast to what most people would expect, no tropism-switch from R5- to X4-tropic viruses could be observed in this *in vitro* study. This resistance mechanism of usage of drug-bound co-receptor has also been reported *in vivo* [158]. However, most patients failing MVC treatment showed a switch of co-receptor usage towards X4-tropic viruses, which cannot be inhibited by the drug. It was shown, though, that these patients possessed a reservoir of X4-tropic viruses already before the start of the treatment, which had only occurred at an undetectable level before the start of treatment [157, 242].

1.1.3 Co-receptor tropism and its testing

The range of host cells for HIV-1 is restricted due to the necessity of CD4 expression, although also CD4-independent viruses have been described [95]. Within the human organism, only T-helper cells, macrophages and some populations of dendritic cells are $CD4^+$ and therefore susceptible to HIV-1 entry. Yet, due to the requirement of a suitable co-receptor, not all HIV-1 strains behave similarly in regard to which target cells can be infected. Therefore, the viruses have been classified in different ways over the last two decades.

In the early days of HIV-1 research, mitogen-activated human primary blood mononuclear cells (PBMCs) were used to propagate primary virus isolates. These cells possess both co-receptor molecules and therefore allow the replication of most HIV-1 strains. As soon as human T-cell lines were used to study virus replication, it was noticed that some strains did not replicate in those cells. Those viruses were, on the other hand, able to replicate in human monocyte-derived macrophages and were hence named M-tropic [42]. The remaining primary isolates, mostly from patients with progressed infections, were termed T-tropic in reference to their ability to infect T-cell lines. Another observation was made very early: the rapid replication of isolates from patients with progressed disease (termed RH for rapid/high) compared to the majority of primary isolates from newly infected patients (termed SL for slow/low) [65]. In addition to this, the formation of huge syncytia could be observed when the T-cell line MT-2 was cocultured with PBMCs producing T-tropic isolates. Syncitia are multinucleated cells resulting from membrane fusion of cells infected with HIV-1 and therefore expressing Env and neighbouring non-infected cells expressing CD4 and co-receptor. Those T-tropic isolates were therefore classified as SI – syncytium-inducing – in contrast to the M-tropic isolates that were mostly NSI – nonsyncytium-inducing [120, 198].

All phenotypes described showed interdependencies, though exceptions from the rule could always be observed. Also, those schemes can be misleading in some instances [51], e.g. the term M-tropic implies that those strains cannot enter and replicate in primary T-cells, which is not the case. The designation SI/NSI on the other hand is also misleading, as it refers to the ability to form syncytia in one particular cell line which happens to be negative for CCR5 and

therefore renders CCR5-using viruses to be NSI. If cultured within $CCR5^+$ cells, those viruses are nevertheless also able to form syncytia.

tropism	coreceptor usage	PBMC replication	macrophage replication	T-cell line replication	replicative phenotype	syncytium-inducing phenotype
X4	CXCR4	+	-	+	RH	SI
R5	CCR5	+	+	-	SL	NSI
dual	CXCR4 / CCR5	+	+	+	RH	SI

Tab. 1.1: Different classifications of HIV-1. HIV-1 can be classified into X4-, R5- or dual-tropic strains [15]. The table correlates the tropism with co-receptor usage, the ability to replicate in PBMCs, macrophages or in T-cell lines. The speed of replication RH = rapid/high and SL = slow/low and the ability to form syncytia if infected PBMCs are cocultured with MT-2 cells is also depicted for the different tropic strains. SI = syncytium-inducing, NSI = nonsyncytium-inducing.

To avoid confusion, Berger and colleagues [15] proposed a new classification scheme in 1998. This classification will also be used throughout this thesis. It organizes all HIV isolates into three classes depending on the co-receptor they use for entry. Those viruses that use solely CXCR4 are called X4-tropic, whereas viruses utilizing exclusively CCR5 as a co-receptor are termed R5-tropic. Viruses that are able to use either of the two major co-receptors are classified as dual- or R5X4-tropic. Another term that is commonly used in concordance with this classification system is mixed-tropic, describing a virus population that consists of a mixture of R5-, X4- and possibly also dual-tropic viruses. If working with virus pools derived from patient's samples, dual- or mixed-tropic viruses cannot be distinguished, hence the two latter phenotypes are often combined and referred to as dual/mixed (D/M). Tab. 1.1 summarizes the relation of this current classification to the different earlier used classification schemes.

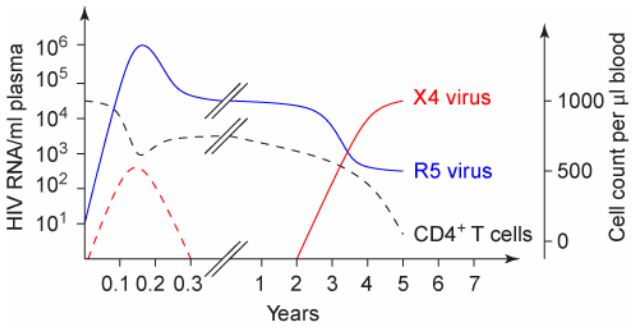

Fig. 1.6: Correlation of co-receptor-usage and $CD4^+$ cell count over the typical course of HIV-1 infection. Viral load in RNA copies per ml (left y-axis) in correlation to $CD4^+$ cell count per µl blood (right y-axis) is schematically depicted with respect to time of infection in years. The acute phase of infection (0 – 0.3 years) is characterized by high viral loads, mostly of R5-tropic viruses (blue line). It coincides with a temporary drop in CD4+ cells (black dotted line). After several years, X4-tropic viruses (red line) begin to emerge, concomitant with a loss in CD4+ cells. At the same time, R5 viruses decrease in abundance, leading to the so-called co-receptor switch. The presence of low levels of X4-tropic virus in the acute phase of HIV-1 infection is depicted with a dotted red line. The figure was modified from [191].

Co-receptor usage is closely associated with disease progression [119] and the efficacy of antiretroviral treatment. While R5-tropic viruses mostly account for acute and early HIV-1 infections [16], X4-tropic variants occur later in infection in about 50 % of cases [220] and hint

towards a more rapid disease progression [143]. As depicted in Fig. 1.6, the occurrence of R5-tropic virus declines with decreasing $CD4^+$ cell count and increasing viral load, while X4- and D/M-tropic viruses can be found independent of those parameters. High natural killer (NK) cell counts on the other hand coincide with increased incidence of R5-tropic variants [161]. While 80 % of patients in the early stage of infection directly after transmission only harbour R5-tropic viruses [29], pure X4-usage is very uncommon in antiretroviral-naïve (0.1 %) as well as experienced patients (3-4 %) [248]. On average, the majority of viruses within a patient stay R5-tropic over the whole course of the infection (56 % in treatment-experienced patients).

With the introduction of co-receptor antagonists into clinical treatment schemes determination of the tropism of the virus population within a patient has become of major interest. Co-receptor tropism testing is required before initializing therapy to ensure sensitivity of the patient's virus population towards the drug. In addition, a drug induced selection of X4-tropic viruses is avoided to prevent increased disease progression. Nevertheless, whether the switch to X4-tropism precedes the more rapid progression towards AIDS or vice versa has not yet been understood [191].

1.1.3.1 Phenotyping

All "old" classification schemes of HIV-1 have been based on phenotypic analyses. Early phenotypic tropism testing has been conducted by cocultivation of patient's PBMCs with other cell lines and deducing the viral tropism by judgement in regard to its obvious replicative characteristics like the ability to replicate in certain cell types, the speed of spread or its cytophathic effect (CPE) [135]. The discovery of the two major co-receptors led to a classification based on this molecular background. The phenotypic analysis of viral tropism is nevertheless still a major tool to classify viral strains of patient's samples.

Current phenotypic analysis is performed on cell lines expressing only CCR5 or CXCR4 respectively and deducing the tropism based on the ability to enter one or the other cell type in the presence or absence of antagonists of either of the two major co-receptors. The first recombinant assay has been described by Trouplin and colleagues [227]. Viral *env* gene sequences comprising the gp120 regions between V1 and V3 were amplified by nested PCR. Those multiple sequences were then introduced into a replication competent reporter virus by homologous recombination. The resulting virus population was then tested for entry efficiency on indicator cells expressing only one of the two major co-receptors. Current assays no longer depend on the usage of replication competent HIV-1 derivatives, which is a marked increase in safety. The PhenoSense entry assay [161, 243] as well as the Trofile assay [244] both make use of pseudoparticles. To this end, the complete gp160 sequence is amplified from patient's plasma samples and cloned into an Env expression vector. Non-replication competent pseudoparticles are produced by cotransfection of this Env expression vector with a non-replication competent

self-inactivating (SIN) vector encoding a luciferase reporter enzyme. Entry in dependence of different drug levels (PhenoSense) and cells with different expression patterns of co-receptors (Trofile) can hence be scored by measurement of luciferase activity through a fluorimetric read-out.

The administration of the CCR5-antagonist MVC is currently governmentally constrained to a preceding phenotypic tropism test, namely Trofile (Monogram Biosciences, Inc., South San Francisco, CA, USA).

1.1.3.2 Genotyping

The term genotypic analysis describes the assignment of the viral phenotype *in silico* based on the nucleotide sequence of the relevant viral gene. With regard to co-receptor analysis, this gene of interest is the viral *env* gene, mostly confined to the V3-loop as the major determinant for co-receptor tropism (compare 1.1.2.1).

Early genotypic co-receptor analyses relied on the observation that different charges within the V3-loop hint at a different tropism. The so-called 11/25 rule predicts that the presence of a positively charged aa at position 11 and/or 25 within V3 is indicative for the SI phenotype [67]. Today, more advanced prediction methods based on complex statistical methods can be used. Among those are decision trees, support vector machines (SVM) and position-specific scoring matrices (PSSM). In decision trees, consecutive yes/no decisions in a tree like fashion lead to a final conclusion. SVM on the other hand is a machine learning technique to classify different samples into two distinct binary groups. PSSM weights the information used, in this case depending on the importance of different positions within the V3-loop, to classify the sample into different classes. Genotyping algorithms using combinations of the aforementioned methods have been described and are available as web-based tools. WetCat ([185], http://genomiac2.ucsd.edu:8080/wetcat/v3.html) makes use of the 11/25 rule, several decision trees and SVM. It is up to now only trained on a small set of data, making prediction less confident [214]. Furthermore, it demands translated aa sequences of the V3-loop exclusively and manual alignment to a reference strain, a time-consuming an error-prone step. WebPSSM ([104], http://indra.mullins.microbiol.washington.edu/webpssm/) uses, as the name implies, PSSM to predict co-receptor usage. It accepts aa sequences in FASTA format and performs automated sequence alignment. The program allows choosing the scoring matrix based on the virus subtype (only subtype B and C) and classification of the training data set (X4/R5 or SI/NSI). Our collaborators in the group of Thomas Lengauer (Department of Computational Biology and Applied Algorithmics, Max-Planck-Institute for Computer Sciences, Saarbrücken, Germany) also developed a web-based prediction program, geno2pheno$_{[co\text{-}receptor]}$ ([216], www.geno2pheno.org), which is based on SVM. Nucleotide as well as aa sequences are accepted as an input, either as FASTA file or pasted directly into a text field on the website. The newest version allows the

inclusion of clinical data such as viral load, CCR5-genotype of the patient, CD4 percentages, $CD4^+$ cell counts and $CD8^+$ cell counts.

An advantage of genotyping over the more conventional technique of phenotyping clearly is the time needed for analysis. Whereas phenotyping takes several weeks, including the shipping of freshly frozen plasma samples, genotyping can be done within a few days. The only requirement is a viral load which allows for PCR amplification of the V3-loop region of *env*. In contrast to this, the Trofile assay can only be performed with viral loads over 1000 viral RNA copies/ml. In addition, the much lower cost of genotypic tropism tests renders this method more attractive in comparison to the very costly phenotypic tests.

1.1.3.3 Viral quasispecies and the need for sensitivity in tropism testing

In regard to viral tropism, it is nevertheless also crucial to keep in mind the existence of viral quasispecies. The term quasispecie is derived from the observance of a rather heterogenous viral population within a patient instead of one single viral clone [18, 59]. This results from the very high error rate of viral replication enzymes. In case of HIV-1, the viral RT has no proofreading function and thus has been shown to have an error rate of 1/1700 per nucleotide incorporated [196]. In addition, selective pressure in terms of the virus' need to escape immunological control and the presence of different drugs play a role in the establishment of viral quasispecies.

Hence, the detection of a pre-existing X4-tropic variant within a patient which could outgrow the prevalent R5-tropic virus population is strongly dependent on the sensitivity of the tropism test. The first established Trofile assay claimed a sensitivity of X4-minority detection of 5-10 % [244]. A newer version of this assay is supposed to detect minorities of 0.3 % [225]. Genotypic assays display a low sensitivity of about 20 % based on bulk sequencing data [132]. The fact that a minority of 0.1 % pre-existing X4-tropic variants has been described to cause a viral rebound [134] implies that an enhanced sensitivity of assay methods is required.

For genotypic analysis, this can be achieved by the so-called ultra-deep sequencing technique. This method is based on a pyrosequencing approach with massive parallel sequencing [197]. It allows the detection of minor differences within a population of sequences, for example within a viral quasispecies.

1.2 Hepatitis C Virus – HCV

HCV is the sole member of the genus hepacivirus, belonging to the family of flaviviruses. There are 7 genotypes, the most common genotype being genotype 1b, and a wide variety of subtypes of HCV, with sequence variations of about 30 % between genotypes and 20 % between subtypes [77, 215]. The virus is the causative agent of Hepatitis C, a liver disease with an estimated 130 million chronically infected individuals worldwide, representing 2.2 % of the total population [6]. The currently available treatment is composed of unspecific antiviral agents like pegylated interferon-α in combination with ribavirin. More specific antiviral drugs are nevertheless in the pipe-line. Though the acute infection is often asymptomatic, the infection becomes chronic in about 80 % of all cases [6]. The symptoms of chronic Hepatitis C range from none to chronic inflammation of the liver, leading to fibrosis, liver cirrhosis and hepatocellular carcinoma.

The virus that causes this disease is a small (app. 55-65 nm in diameter) enveloped virus carrying a single positive stranded RNA genome of app. 9.6 kb. It is a hepatotropic virus replicating in the cytoplasm of only human hepatocytes, although additional target cells have also been discussed [238, 255]. Replication of the viral genome takes place in a virus-induced, ER-derived compartment close to the nucleus the so-called membranous web, which is rich in lipid droplets [76]. The assembly of viral particles in close proximity to lipid droplets and the coupling of viral secretion to the lipoprotein metabolizing pathway most likely explain the fact that HCV particles in patients have been found to be closely associated with several lipoproteins [222].

1.2.1 HCV entry mechanism

The two envelope glycoproteins, E1 and E2, mediate cell attachment and receptor binding and are indispensable for HCV entry. Both of them are type I integral membrane proteins with a C-terminal transmembrane domain and a large N-terminal extracellular domain. They are synthesized at the rough ER as part of the polyprotein precursor and are cotranslationally cleaved off by the cellular signal peptidase. E1 and E2 stay non-covalently linked to each other via interactions of their transmembrane domains and form a functional heterodimer [175] which is retained at the ER [57]. Within the ER, they become heavily glycosylated, a feature proposed to be needed for proper protein folding, the entry process itself and epitope shielding from the immune system [75].

Fig. 1.7 schematically illustrates the early steps of HCV replication: virus attachment, receptor binding, internalization via endocytosis and fusion. The first step of this entry mechanism is unspecific attachment to the host cell. Several attachment factors have been described, including the low density lipoprotein receptor (LDLr) and glycosaminoglycans (GAG) like heparan sulphate (HS) [2, 13]. This cell attachment could serve as a way to retain the viral

particles at the cell surface long enough for receptor recruitment.

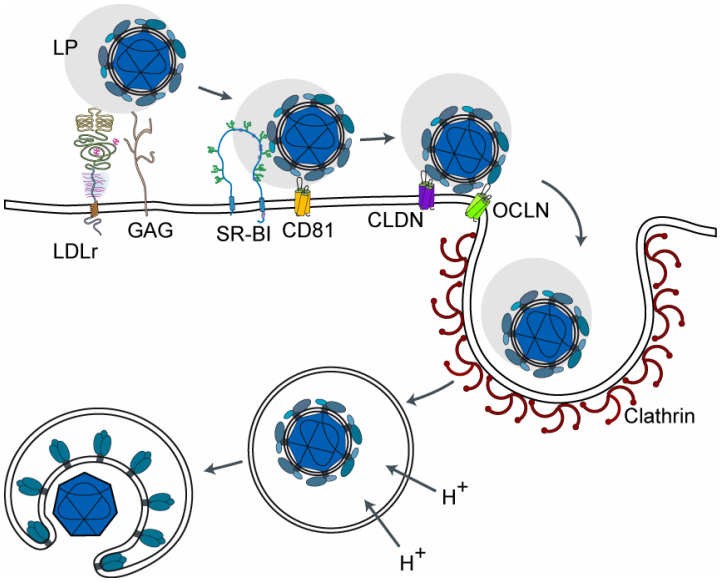

Fig. 1.7: Entry process of HCV. Schematic drawing of the proposed entry mechanism of HCV. Attachment factors, i.e. low density lipoprotein receptor (LDLr) and glycosaminoglycanes (GAG), and four confirmed cellular receptor molecules, i.e. scavenger receptor class B type I (SR-BI), cluster of differentiation 81 (CD81), claudin-1 (CLDN) and occludin (OCLN) are depicted. Uptake of the viral particle, associated to lipoproteins (LP) is thought to occur via clathrin-mediated endocytosis. Fusion with the membrane then occurs in a pH-dependent step after acidification of early endosomes. The picture was modified from [156].

At least four specific receptors have been shown to play major roles in the entry process of HCV. Those comprise the scavenger receptor class B type I (SR-BI), the tetraspanin cluster of differentiation 81 (CD81) and the two tight junction molecules claudin-1 (CLDN1) and occludin (OCLN) [61, 184, 187, 207]. SR-BI is an 82 kDa glycoprotein which is highly expressed in liver hepatocytes. It harbours two transmembrane domains and is involved in the uptake of cholesterol esters through the interaction with high density lipoprotein (HDL) particles. CD81 was the first candidate receptor and is a typical tetraspanin protein with four transmembrane domains, a small and a large extracellular loop (SEL and LEL, respectively) and an intracellular loop. It is widely expressed on a variety of tissues and thus is not considered to be a determinant for the livertropism of HCV. The two tight junction proteins CLDN1 and OCLN both harbour four transmembrane domains with both termini facing to the cytosol, two extracellular loops and an intracellular loop. In addition to CLDN1, two other members of the claudin family, namely Claudin-6 and Claudin-9, have been shown to act as HCV entry receptors [253].

The sequence of receptor engagement is not yet exactly known, however it is speculated that the process starts with interactions of E1/E2 with SR-BI. The virus will then subsequently encounter CD81, which has been proposed to be relocalized to tight junctions upon virus binding [27]. Here, the virus can then bind to the remaining two receptors and finally get internalized by clathrin-mediated endocytosis [21, 148]. The fusion of viral and cellular membrane finally has been shown to be a pH-dependent step, triggered by the low pH of early endosomes [228]. After this step, the viral capsid is released into the cytosol, where protein translation, replication and assembly of new virus progeny take place.

1.2.1.1 Possible ways to interfere with HCV entry

Although no specific HCV entry inhibitors have been developed, yet, there are several ways to interfere with it *in vitro*. One strategy is to block the pH-dependent fusion step. To this end, acidification of endosomes can be inhibited by the addition of alkalizing reagents or specific inhibitors of the proton pumping ATPase (NH_4Cl or Bafilomycin A, respecitively). One step before fusion, the endocytic uptake of viral particles can also be blocked by inhibition of clathrin-mediated endocytosis. To target the four known receptors of HCV entry, RNA interference (RNAi) techniques or neutralizing antibodies can be utilized. Most likely due to the association of HCV particles with lipoproteins and the interaction of those with molecules implicated in entry of the virus (LDLr and SR-BI), it has been described that different lipoprotein complexes can also manipulate HCV entry efficiency. In this regard, HDL has been shown to enhance HCV entry efficiency [56], whereas oxidized low density lipoprotein (oxLDL) has been shown to decrease it [232]. As attachment of HCV to the target cell has been shown to rely on interactions with GAGs, the addition of Heparin can mimic those structures and thus prevent successful virus-cell interactions [122].

1.3 Fluorescently labelled viruses as a tool

To visualize various steps of the viral replication cycle, several methods have been used, including different techniques of electron and fluorescence microscopy. One of the most commonly used techniques is immunofluorescence, in which the protein of interest is detected by specific antibodies in fixed cells. A drawback of this technique is the need for fixation which is preventing live cell observation. In addition, epitopes may be masked due to fixation artefacts or steric inaccessibility. Those points do not apply for fluorescent proteins (FP), which can be fused to the protein of interest and have thus extensively been used to study protein localisation and trafficking within living cells with a high spatial and temporal resolution [138]. The first FP characterized was the green fluorescent protein (GFP), cloned from the jellyfish *Aqueorea victoria* [188]. Like other FPs developed from GFP, it harbours a chromophor build up by aminoacid side chains of a tripeptide inside its beta barrel structure. Optimisation of FPs in regard to quantum yield, spectral properties, stability and folding kinetics has been pursued by site-directed and random mutagenesis. Also, FPs from other species, e.g. corals, have been isolated and found to exhibit desirable properties (reviewed in [46]). Today, enhanced versions of the original FPs, e.g. eGFP, are mostly being used and a broad range of spectral variants is available. More recently, FP variants permitting dynamic analyses have been developed.

The major drawbacks of FPs, include slow maturation kinetics, high light sensitivity leading to fast bleaching, low quantum yield and restricted spectral properties. In contrast to this,

organic dyes have the advantage of higher stability, greater quantum yield and a nearly unlimited choice of excitation and emission wavelength. Those dyes therefore allow for applications with the need of strong fluorescence signals or a special excitation and emission wavelength. To make use of these benefits, the chemical dye has to be specifically attached to the protein of interest. The introduction of a tetracystein-tag into the protein of interest for example allows staining with the FlAsH/ReAsH technique (Invitrogen, San Diego, CA, USA). With this, several groups have been studying HIV-1 Gag trafficking [79, 182, 201] as well as tracking of cytoplasmic and nuclear HIV-1 complexes by labelling the IN [8]. This technique has nevertheless been reported to be accompanied by very high background signals [201].

1.3.1 SNAP-tag as a substitute for fluorescent proteins

Another way to deal with the challenge of specifically labelling a protein of interest with organic dyes within the living cell is the use of the so-called SNAP-tag (New England Biolabs, Ipswich, MA, USA). It is derived from the mammalian DNA repair protein O^6-alkylguanin-DNA-alkyltransferase (AGT) which removes alkyl chains from guanines by covalently adding them to a cystein residue within its active site [177]. Mutational evolution led to a version of this protein with enhanced activity, smaller size (app. 20 kDa), higher substrate specificity and higher activity [113]. SNAP-tag binds to its substrate, O^6-Benzylguanine (BG), with high affinity, allowing the use of low non-toxic concentrations of substrate. It then transfers the benzyl-moiety irreversibly from the substrate to its active site. Thus, SNAP-tag performs a self-labelling reaction if fluorescently labelled derivatives of O^6-Benzylguanine are offered as substrate [114].

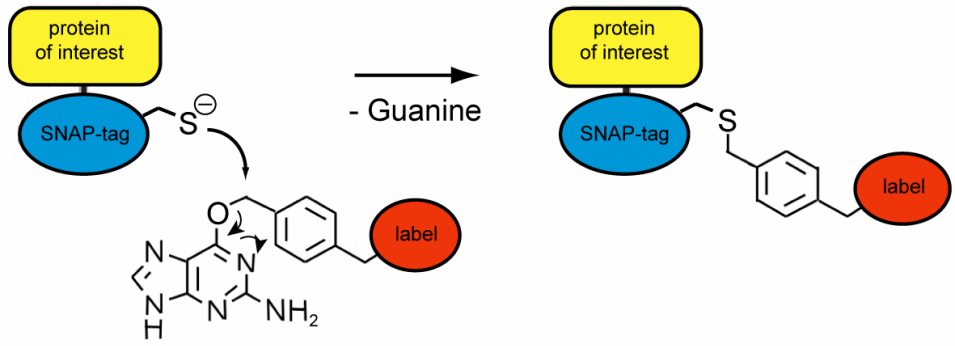

Fig. 1.8: Labelling mechanism of SNAP-tag. Covalent labelling of the SNAP-tag fusion protein with a substrate coupled to a fluorochrome (label). The picture was taken from [114].

To use it as a labelling technique, SNAP-tag can easily be fused N- and C-terminally to the protein of interest. It then allows covalent labelling of the fusion protein by the addition of the substrate of choice [115].

1.3.2 Fluorescently labelled HIV-1 proteins

To study different aspects of the HIV-1 replication cycle, many viral proteins have also been fused to several FPs. Those viral proteins include Vpr [147], Vpu [82, 164], Nef [84] as well as the Gag precursor protein [180], MA [162], IN [4, 49] and the viral membrane by incorporation of membrane anchored FPs [34]. In our department, labelling of HIV-1 derived particles to study attachment and entry has been achieved with the incorporation of Vpr.FP [127] and IN.FP [118] and the fluorescent label directly fused to MA [117, 118, 127, 162]. Viruses incorporating the fusion protein of MA.FP within the complete viral context have been shown to be reduced in infectivity and entry competence. An equimolar cotransfection of wt and the tagged version, however, leads to rescue of full single round infectivity [162]. The C-terminal fusion of a FP to MA allows the observation of its localisation and trafficking within the cell in the context of all other viral proteins that may play a role. In addition, the incorporation of the fluorescent tag within released viral particles allows using those fluorescently labelled viruses as a tool to study attachment and virus entry. Furthermore, the MA.FP fusion protein represents a clear advantage of over the immunofluorescence technique, as the HIV-1 CA protein has been shown to be recognised by antibodies to a much lesser degree within the protein precursor, Gag, than if already processed.

1.4 Aim of the work

Recent advances in the development of quantitative analysis methods on a single cell level open up the possibility to study biological processes in much greater detail as had been possible with bulk assays. Data obtained with those methods can be used to computationally derive mathematical models describing and predicting the studied events. Viruses are ideal study objects because of their relative simplicity compared to the complexity of larger organisms. Viruses are obligatory intracellular pathogens and entry into host cells is the first step in their replication cycle. The aim of this thesis was to quantitatively study entry of two of the most important human pathogens, HIV and HCV, into host cells.

Studying the details of the viral life cycle is facilitated by the visualisation of individual viral particles. Several systems to label viral particles have been implemented, most of which employ fusion of viral components with autofluorescent proteins. New high resolution imaging techniques requiring stronger illumination make the use of more stable organic dyes desirable. To this end, a new labelling technique which allows the covalent coupling of organic dyes to viral structures was applied to HIV-1 and its usefulness was evaluated. The lack of a suitable virus labelling method for HCV at the time implied the adaptation of an already existing approach to this virus, using HIV derivatives carrying the HCV envelope proteins (HCVpp). In addition, a virion fusion assay to study entry independent of later steps of the replication cycle was optimized for HCVpp. These different approaches were used to dissect the early steps of HCVpp entry. The imaging methods established were expanded to HIV-1, and virus binding to cells in dependence of different factors was investigated.

The main focus of this thesis, however, was the quantitative assessment of HIV-1 entry in dependence of multiple cellular and viral parameters. Although the course of events during HIV-1 entry is well-characterized, the major part of this knowledge is based on bulk data. In the light of the employment of co-receptor antagonists in the antiviral treatment of HIV-1 patients, the prediction of sensitivity of a given virus population towards these drugs is of major importance. The detailed investigation of the dependence of HIV entry on the presence of different levels of receptor and co-receptor on the target cell will lead to a greater understanding of this process and allow the development of improved prediction algorithms. Establishing methods that allow the acquisition of reliable quantitative data in relatively high throughput systems was a major goal of this thesis. A comprehensive dataset describing the detailed dependencies of virus entry on receptor and co-receptor levels on the target cell, V3-loop sequence of the viral Env protein and presence of different concentrations of entry inhibitors was generated using an initial subset of patient-derived virus samples.

2 Materials and Methods

2.1 Materials and instruments

Acrylamide	Rotiphorese Gel, Roth, Karlsruhe, Germany
Ampicillin	Roth, Karlsruhe, Germany.
Blasticidin S HCl	Invitrogen, Karlsruhe, Germany
Blotting paper	3 MM Chr, Whatman, Dassel, Germany
BTP SNAP-block	Covalys, Witterswill, Switzerland
CCF2-AM Loading Kit	Invitrogen, Karlsruhe, Germany
CO2-independent medium	Gibco/Invitrogen, Karlsruhe, Germany
Collagen	Collagen A, 1 mg/ml, Biochrom AG, Berlin, Germany
Concanamycin A	Sigma-Aldrich, Steinheim, Germany
Confocal laser scanning microscope Nikon C1Si	Nikon Imaging Center at University Heidelberg, Heidelberg, Germany; Nikon, Düsseldorf, Germany
Confocal laser scanning microscope Leica SP2	Leica Microsystems GmbH, Wetzlar, Germany
DMEM high glucose	Gibco/Invitrogen, Karlsruhe, Germany
DNA gel extraction kit	Nucleospin® Extraction II, Macherey-Nagel, Düren, Germany
ECL substrate	ECL Western blotting substrate, Pierce, Rockford, IL, USA
ELISA plates	Maxisorb, Nunc, Wiesbaden, Germany
Epifluorescence microscope Zeiss Axiovert 200M	Carl Zeiss Imaging Solutions GmbH, München, Germany
Epifluorescence screening microscope Olympus ScanR	Olympus Soft Imaging Solutions GmbH, Münster, Germany
FACSAriaTM	ZMBH, Heidelberg, Germany BD Biosciences, Heidelberg, Germany
FACSCalibur	BD Biosciences, Heidelberg, Germany
FACSCantoTM II	ZMBH, Heidelberg, Germany BD Biosciences, Heidelberg, Germany
FCS	Lot.Nr.: 0251L Biochrom AG / seromed, Berlin, Germany
FCS, tetracycline-free	Biochrom AG / seromed, Berlin, Germany
Fibronectin	Sigma-Aldrich, Steinheim, Germany
Ficoll-Plaque Plus	GE Healthcare Life Science, München, Germany
FugeneHD	Roche, Basel, Switzerland

G418	Calbiochem, Darmstadt, Germany
HDL	Lipoproteins, Low Density, Human Plasma, Calbiochem, Darmstadt, Germany
Hygromycin B	Calbiochem, Darmstadt, Germany
IL-2	Biomol, Hamburg, Germany
Infrared scanner	Odyssey, LI-COR Inc., Lincoln, NE, USA
Kanamycin	Roth, Karlsruhe, Germany
LDL	Lipoproteins, Low Density, Human Plasma, Calbiochem, Darmstadt, Germany
Mircoplate reader	MR5000, Dynatech, Enbrach, Switzerland
Nitrocellulose membrane	Protran, Schleicher & Schüll/Whatman, Dassel, Germany
PHA	Sigma-Aldrich, Steinheim, Germany
Plasmid purification kit	NucleoBond MaxiPrep Kit, Macherey-Nagel, Düren, Germany
Ponasterone A	Invitrogen, Karlsruhe, Germany
Puromycin dihydrochloride	Invitrogen, Karlsruhe, Germany
QuantiBRITE™ PE	BD Biosciences, Heidelberg, Germany
RPMI1640	Gibco/Invitrogen, Karlsruhe, Germany
SDS-PAGE electrophoresis chamber	Mighty small, Hoefer, Almstetten, Germany
Semi-Dry Blotter	Fastblot B32, Whatman Biometra, Göttingen cti GmbH, Idstein, Germany
SNAP-cell TMR-Star	Covalys, Witterswill, Switzerland
Spectrophotometer	DU 640, Beckman Coulter, Fullerton, CA, USA
Tabletop ultracentrifuge	TL-100, Beckman Coulter, Fullerton, CA, USA
Tetracycline	Invitrogen, Karlsruhe, Germany
Trypsin	10x Trypsin/EDTA (0,5% / 0,2%), Biochrom AG, Berlin, Germany
Ultracentrifuge	Optima XL-70, Beckman Coulter, Fullerton, CA, USA
X-ray films for ECL-WB	CL-XPosure, Pierce, Rockford, IL, USA
Zeocin	Invitrogen, Karlsruhe, Germany

2.1.1 Buffers and reagents

Buffer name	**Concentrations**	**Recipe**
10x DNA loading buffer	50 % sucrose	5 g sucrose
(10 ml)	10 mM EDTA	200 µl 0.5 M EDTA
	2 % bromphenol blue	0.2 g bromphenol blue
	2 % orange G	0.2 g orange G
10x PBS	1.37 M NaCl	80 g NaCl
(1000 ml)	27 mM KCl	2 g KCl
	80 mM Na2HPO4	14.4 g Na2HPO4 2H2O
	18 mM KH2PO4	2.4 g KH2PO4

Buffer name	Concentrations	Recipe
10x PonceauS stain (100 ml)	30 % trichloric acetic acid	30 ml trichloric acetic acid
	30 % sulfosalycylic acid	30 ml sulfosalycylic acid
	2 % (w/v) PonceauS	2 g Ponceau S
		40 ml H2O
10x TBST (1000 ml)	200 mM 1M Tris	200 ml 1 M Tris pH 7.5
	150 mM NaCl	87.66 g NaCl
	0.5 % Triton-X100	5 ml Triton-X100
1x SDS-PAGE electrophoresis buffer (1000 ml)	25 mM Tris	3.03 g TRIS
	19.2 M glycine	14.4 g Glycine
	0.1 % SDS	1 g SDS
200x NaN3 stock solution	10 % NaN3 in PBS	5 g NaN3 in 50 ml PBS
2x CaCl2 transfection buffer (1000 ml)	250 mM CaCl2	36.8 g CaCl2 2H2O; filter sterilize through 0.45 µm pore size filters; store at 4°C
2x HeBS transfection buffer (1000 ml)	280 mM NaCl	16.4 g NaCl
	50 mM HEPES	11.9 g HEPES
	1.5 mM Na2HPO4	0.267 g Na2HPO4 H2O
	pH 7.05-7.12	filter sterilize through 0.45 µm pore ters; store at 4°C
30% acrylamide (200:1)	0.15 % bisacrylamide	1.5 g N,N'-Methylen-bis-acrylamid
	30 % acrylamide	1000 ml 30% Rotiphorese Gel A
3x protein sample buffer	125 mM Tris/HCl pH 6.8	prepare for 100 ml, but add H2O only ad 95 ml
	10 % glycerol	before usage, add 0.5 ml β-MeEtOH
	0.02 % bromphenol blue	to 9.5 ml of buffer,
	2 % SDS	store at 4°C up to 4 weeks
	0.5 % β-MeEtOH	
4x separating gel buffer (500 ml)	1.5 M Tris-HCl pH 8.8	90.8 g Tris
	0.4 % SDS	0.2 g SDS
4x stacking gel buffer (500 ml)	0.5 M Tris-HCl pH 6.8	30.3 g Tris
	0.4 % SDS	0.2 g SDS
50x TAE buffer (1000 ml)	2 M Tris-acetate	242 g Tris
	50 mM EDTA	57 ml acetic acid
		100 ml 0.5 M EDTA pH 8.0
acrylamide for stacking gels (30:0.8%)	0.8 % bisacrylamide	8 g N,N'-Methylen-bis-acrylamid
	30 % acrylamide	1000 ml 30% Rotiphorese Gel A
Fixative for cryo-EM (6 ml)	4 % PFA	1.2 ml 20 % PFA
	0.1 % glutaraldehyde	24 µl 25 % glutaraldehyde
	0.1 M PHEM	1.5 ml 0.4 M PHEM
		3.3 ml H_2O

Buffer name	Concentrations	Recipe
Fixative for epon-EM (6 ml)	2.5 % glutaraldehyde	600 µl glutaraldehyde
	0.2 M NaCacodylate	3 ml NaCacodylate
		2.4 ml H2O
LB agar	13 % agar in LB	1 l LB medium
	medium	13 g agar
LB medium	1 % peptone	10 g tryptone
(1000 ml)	0.5 % yeast extract	5 g yeast extract
	171 mM NaCl	5 g NaCl
		0.5 ml 10 N NaOH pH 7.0
Mowiol embedding medium	8 mM Mowiol 4-88	stir 10 g Mowiol in 40 ml PBS for
	in PBS	24 h at RT; add 20 ml 100 %
		glycerol; stir for 24 h; control
		pH (6-7); 12.000 rpm 15 min; make
		1 ml aliquots; store at -20°C
separating gel	17.5 % acrylamide	5.8 ml acrylamide 200:1
(2 minigels; 10 ml)	375 mM Tris-HCl	2.5 ml 4x separating gel buffer
	pH 8.8	1.7 ml H2O
	0.1 % SDS	
	0.1 % APS	for polymerisation add
	0.0017 % TEMED	83 µl 10 % APS; 17 µl TEMED
stacking gel	2 % acrylamide	1.5 ml 30 % acrylamide
(10 ml)	125 mM Tris-HCl	2.5 ml 4x stacking gel buffer
	pH 6.8	6.0 ml H2O
	0.1 % SDS	this mixture can be stored at 4°C
	0.0025 % APS	for polymerisation add per 2 ml
	0.0025 % TEMED	50 µl 10 % APS; 5 µl TEMED
Western blot blocking buffer	5 % milkpowder	in TBST
Western blot buffer I	0.3 M Tris	36.34 g Tris
(1000 ml)	20 % MeOH	200 ml MeOH
Western blot buffer II	25 mM Tris	3.03 g Tris
(1000 ml)	20 % MeOH	200 ml MeOH
Western blot buffer III	25 mM Tris	3.03 g Tris
(1000 ml)	20 % MeOH	200 ml MeOH
	40 mM DL-Norleucine	5.25 g DL-Norleucine

2.1.2 Primers

Number	Sequence (5' -> 3')	See chapter
5251	GGCGCATCGATCCGCCCAGCCCAGGCTTGCC	2.2.4.1
5252	CAGGGATCGATAGGCGGCATGGACAAAGACTGCGAA	2.2.4.1
3159	TGTACAAACGCGTATGGACAAAGACTGC	2.2.4.1
3160	TTTTGGCTTCTAGAGCCCAGCCCAGGC	2.2.4.1
251	CAGGGATCGATAGGCGGCATGGTGAGCAAGGGC	2.2.4.1

Number	Sequence (5' -> 3')	See chapter
252	GGCGCATCGATCCGCCCTTGTACAGCTCGTC	2.2.4.1
2539	TTGTAACATTTCTAGAGC	2.2.4.3
2540	GCTCTAGAAATGTTACAATGTGC	2.2.4.3
2541	TAGTACAGCTGAACACATCTGTAG	2.2.4.3
2542	ACTTCTCCAATTGTCCCTCATATCG	2.2.4.3
2747	TAGTACAATTGAACACATCTGTAGAAATTAATTGTAC	2.2.4.3
2748	TAGTACAATTGAACACATCTGTAGAAATTAATTG	2.2.4.3
2749	TAGTACAATTGAACACATCTGTAGAAATTAATTG	2.2.4.3
2750	TAGTACAATTGAACACATCTGTAGAAATTAATTGTTTCAG	2.2.4.3
2751	TTGCTCTAGAAATGTTACAGTATGC	2.2.4.3

2.1.3 Plasmids

Plasmid name	Description	Reference
pNL4-3	subviral plasmid	[1]
pNLC4-3	subviral plasmid	[127]
pKHIV	non-infectious subviral plasmid	[162]
pCHIV	non-infectious subviral plasmid	[127]
pCHIV.Env(-)	non-infectious subviral plasmid harbouring a frameshift in the *env* gene	B. Müller
pCHIV.eGFP	non-infectious subviral plasmid harbouring the *egfp* gene within the *gag* ORF	[127]
pCHIV.mCherry	non-infectious subviral plasmid harbouring the *mCherry* gene within the *gag* ORF	this work
pBSMAJ.ClaI	intermediate construct	[162]
pVpr.eGFP	expression plasmid for Vpr.eGFP fusion protein	[147]
pMM310	expression plasmid for Vpr.BlaM fusion protein	[35]
pCHIV.SNAP	non-infectious subviral plasmid harbouring the *snap-tag* gene within the *gag* ORF	this work
pNLC.SNAP	subviral plasmid harbouring the *snap-tag* gene within the *gag* ORF	this work
pNLCiSNAP	subviral plasmid harbouring the *snap-tag* gene flanked by two PR cleavage sites within the *gag* ORF	this work
pHIViGFP	subviral plasmid harbouring the *snap-tag* gene flanked by two PR cleavage sites within the *gag* ORF	[98]
pCAGGS-NL4-3	expression plasmid for HIV-1 NL4-3 Env protein	R. Kaiser
pCAGGS-NL4-3-R5	expression plasmid for HIV-1 NL4-3 Env protein, CCR5-tropic	R. Kaiser
pCAGGS-NL4-3*Xba*I	expression plasmid for HIV-1 NL4-3 Env protein additional XbaI restriction site	this work
pCAGGS-220	expression plasmid for HIV-1 NL4-3 Env protein withV3-loop of patient number 220	this work

Plasmid name	Description	Reference
pCAGGS-286	expression plasmid for HIV-1 NL4-3 Env protein with V3-loop of patient number 286	this work
pCAGGS-409	expression plasmid for HIV-1 NL4-3 Env protein with V3-loop of patient number 409	this work
pCAGGS-651	expression plasmid for HIV-1 NL4-3 Env protein with V3-loop of patient number 220	this work
pCAGGS-685	expression plasmid for HIV-1 NL4-3 Env protein with V3-loop of patient number 685	this work
pCAGGS-838	expression plasmid for HIV-1 NL4-3 Env protein with V3-loop of patient number 838	this work
pCAGGS-924	expression plasmid for HIV-1 NL4-3 Env protein with V3-loop of patient number 924	this work
pCAGGSΔEnv	empty expression plasmid	N. Herold
pcDNA3ΔCE1E2	expression plasmid for HCV Con1 Env protein	[208]
pVpu.GFP	expression plasmid for fusion protein of HIV-1 Vpu and GFP	[82]
pSS26m	cloning vector coding for SNAP-tag	Covalys
pC1-Cherry	expression vector for mCherry	Invitrogen
pCMVΔR8.9	CMV-driven HIV-1 packaging construct	[257]
pSEW	SIN-vector carrying a CMV-driven *gfp* reporter gene	[257]

2.1.4 Cell lines

Name	Origin / features	Reference
293T	human embryonic kidney fibroblast, transduced with SV40 large T antigen	[211]
HeLa	human cervix carcinoma	[209]
HeLaP4	HeLa stably expressing CD4	[37]
JC53	HeLa stably expressing high levels of CD4	[186]
Lunet/CD81	human hepatoma, Huh7-derived, cured from replicon, stably expressing CD81	[121]
Lunet/V	human hepatoma, Huh7-derived, cured from replicon, sorted for low CD81 expression	[121]
Affinofile	human embryonic kidney fibroblast, 293-derived, inducible for CD4 and CCR5 expression	[105]
SupT1/CCR5	human Non-Hodgkin's T-cell lymphoma, stably expressing CCR5	R. Doms
C8166/CCR5	human umbrical blood lymphocytes, infected with defect HTLV-I, stably expressing CCR5	M. Malim
C8166	human umbrical blood lymphocytes, infected with defect HTLV-I	[204]
MT-4	human T-cells isolated from a patient with adult T-cell leukemia, HTLV-I transformed	[153]
TZM-bl	HeLa-derived, harbouring a Tat-inducible β-galactosidase and luciferase reporter	[237]

2.1.5 Antibodies

Antibody name	Source	Application	Dilution
mouse anti HIV gp41 Chessie-8	NIH AIDS Research and Reference Reagent Program	WB	1:1000
mouse anti-heparan sulphate clone F58-10E4	Seikagaku Inc.	FACS	1:20
mouse anti-HIVp24 mAb 183-H12-5C	NIH AIDS Research and Reference Reagent Program	WB	1:50
mouse anti-human CCR5 clone 2D7	BD Pharmingen™	IF	1:100
mouse anti-human CCR5 clone 2D7	BD Pharmingen™	FACS	1:10
mouse anti-human CD317	Chugai Pharmaceuticals	FACS	
mouse anti-human CD4 clone RPA-T4	AbDserotec	IF	1:100
mouse anti-human CD4 clone RPA-T4	BD Pharmingen™	FACS	1:20
mouse anti-human CD81 clone JS-81	BD Pharmingen™	neutralization	
mouse anti-human CXCR4 clone 12G5	BD Pharmingen™	FACS	1:20
mouse anti-human IgG	Invitrogen	IF	1:2000
goat anti-rabbit IgG	Invitrogen	IF	1:2000
rabbit anti HIV CA	Kräusslich lab	WB	1:5000
rabbit anti HIV MA	Kräusslich lab	WB	1:5000
rabbit anti-HCV E2 clone H52	Th. Pietschmann	WB	1:500
rabbit anti-HIV RT	Kräusslich lab	WB	1:1000
rabbit anti-HIV Vpr	Kräusslich lab	WB	1:2000
rabbit anti-human Bst-2	Klaus Strebel	IF	
sheep anti-HIV CA	Kräusslich lab	WB	1:5000

2.2 Molecular Biological Methods

2.2.1 Transformation of bacteria and DNA amplification

Chemically competent bacteria were transformed with plasmid DNA (app. 100-500 ng) according to the heat-shock method. Briefly, bacteria were thawed on ice, DNA was added and incubated on ice for at least 10 min and then a heat-shock was performed at 42°C for 45 sec. Then, 450 µl of LB was added and bacteria incubated at 37°C for app. 1 h before plating on LB-Agar plates with the respective selection antibiotic. After over night incubation at 37°C, single

bacterial colonies were picked, inoculated in 1.5 ml (Mini) or 200 ml (Maxi) LB with the respective antibiotic for selection and agitated over night at 37°C. Plasmid DNA was isolated with the alkaline lysis method using the NucleoBond® maxiprep kit (Macherey-Nagel, Düren, Germany). Purified plasmid DNA was dissolved in TE buffer and concentration and purity were determined by measuring the absorption at 260 nm and 280 nm respectively in a UV spectrophotometer (Beckmann Coulter). For Mini preparations, the same buffer set (Macherey-Nagel, Düren, Germany) was used to perform the alkaline lysis and DNA was precipitated using isopropanol. After a washing step with 70 % ethanol, DNA was dissolved in H_2O and subjected to restriction analysis.

2.2.2 DNA digestion and ligation

1 µg of purified plasmid DNA (5 µg for vector preparations) or 30 µl of purified PCR product was incubated with 10 U of the desired restriction enzyme in the appropriate buffer at the temperature recommended by the manufacturer for 0.5-2 h.

Restriction products were checked using gel electrophoresis. To this end, 0.5-2 % agarose (standard 1 %) in TAE buffer was heated until melted, ethidium bromide was added and the cast gel was cooled until solidification. Gel electrophoresis was performed at 90 V for app. 30 min and DNA bands visualized under UV irradiation and compared to a molecular mass standard loaded as a control (1 kb ladder, Invitrogen Ltd., Paisley, UK). DNA fragments for cloning were cut out of the gel and purified using the NucleoSpin kit (Macherey-Nagel, Düren, Germany) according to manufacturer's protocol using 30 µl Millipore H_2O for elution.

In case of a single cut within the plasmid, the vector was dephosphorylated by treatment with 10 U calf intestine alkaline phosphatase for 30 min at 37°C directly after enzyme digestion. Purified digestion products were ligated using 1 µl vector and 3 µl insert DNA (in case this standard did not yield a result, 3 molar excess of insert was used) by the addition of T4-DNA ligase in 15 µl 1X ligase buffer for 2 h at room temperature (or over night at 16°C). The complete ligase reaction was then transformed into 50 µl of chemically competent bacteria (see above).

All enzymes were from Fermentas (Fermentas GmbH, St. Leon-Rot, Germany) or NEB (New England Biolabs GmbH, Frankfurt, Germany).

2.2.3 DNA amplification by polymerase chain reaction (PCR)

Typically 40 ng of purified plasmid DNA was used as a template for amplification using 40 pmol of both forward and reverse primers. The reaction was performed in 20-50 µl total volume in the presence of 250 µM desoxy nucleotide triphospates (dNTPs). In most cases, a proofreading polymerase, e.g. Pfu was used in the recommended buffer. Initial denaturation was performed at 94°C for 5 min, followed by 20-30 circles of a short denaturation at 94°C, followed

by an annealing step for 45 sec at typically 48°C and a synthesizing step at 72°C for 1 min per 1 kb of template length. A final step at 72°C was performed in addition to allow the completion of unfinished products. PCR products were controlled by agarose gel electrophoresis in comparison to mass standards and purified by gel extraction with the NucleoSpin® Kit (Macherey-Nagel, Düren, Germany).

If no or unspecific PCR products were observed, the conditions were optimized regarding annealing temperature of the primers, template input, $MgCl_2$ concentration in the buffer or addition of more efficient polymerase enzyme Taq. Cloning of different V3-loop sequences into pCAGGS-derived vectors (2.2.4.3) was performed using the Phusion high-fidelity DNA polymerase (Finnzymes, Espoo, Finland) with an accelerated protocol according to manufacturer's instructions.

2.2.4 Cloning procedures

All plasmid obtained by cloning including a PCR step were verified by sequencing of the respective inserted fragments. Sequencing was performed by the company GATC Biotech (Konstanz, Germany).

2.2.4.1 Construction of proviral plasmids including the fluorescent protein mCherry

In order to insert the *mcherry* gene into the subviral clone pCHIV at the 3' end of the MA coding sequence, the *mcherry* sequence was amplified by PCR from pC1-Cherry (Invitrogen) with primers 252 and 252, which introduced *Cla*I restriction sites at both ends of the *mcherry* gene. The resulting fragment was inserted into pBSMAJ.*Cla*I harbouring a unique *Cla*I restriction site at position 1171 of the NL4-3 sequence [162] to obtain pBSMAJ.mCherry as an intermediate clone. Then, the *Bss*HII-*Sph*I fragment comprising the modified MA sequence was subcloned into pKHIV to obtain pKHIV.SNAP. The *Age*I-*Xba*I fragment from pKHIV.mCherry was further subloned into pCHIV to obtain pCHIV.mCherry, which expresses higher levels of all HIV-1 proteins to obtain a better particle yield.

2.2.4.2 Construction of proviral plasmids including the SNAP-tag

In order to insert the *snap-tag* gene into the subviral clone pCHIV at the 3' end of the MA coding sequence, the *snap-tag* sequence was amplified by PCR from pSS26m (Covalys) with primers 5252 and 5251, which introduced *Cla*I restriction sites at both ends of the *snap-tag* gene. The resulting fragment was inserted into pBSMAJ.*Cla*I harbouring a unique *Cla*I restriction site at position 1171 of the NL4-3 sequence [162] to obtain pBSMAJ.SNAP as an intermediate clone. Then, the *Bss*HII-*Sph*I fragment comprising the modified MA sequence was subcloned into pKHIV and pNLC4-3 to obtain pKHIV.SNAP and pNLC.SNAP, respectively. The *Age*I-*Xba*I fragment from pKHIV.SNAP was further subloned into pCHIV to obtain pCHIV.SNAP, which

expresses higher levels of all HIV-1 proteins to obtain a better particle yield.

For construction of the subviral clone carrying the SNAP-tag with two flanking PR cleavage sites (pNLCiSNAP), the *snap-tag* sequence was amplified by PCR using primers 3159 and 3160. The forward primer introduced a *Mlu*I and the reverse primer an *Xba*I restriction site. The resulting fragment was inserted into pNLCiGFP to obtain pNLCiSNAP.

2.2.4.3 Construction of Env expression plasmids harbouring different V3-loop sequences

Different patient derived V3-loop sequences were inserted into pCAGGS-NL4-3, a mammalian expression vector for the complete HIV-1 Env protein. To this end, an additional restriction site had to be inserted into the *env* sequence first. *Xba*I was chosen as it was absent from the vector backbone as well as the complete *env* sequence and could be introduced by the introduction of two silent mutations 7 and 8 bp downstream of the 3' end of the V3-loop coding sequence. Two PCRs with overlapping primers introducing the A-T and G-C mutations were performed followed by a fusion PCR of both fragments with the outer primers. The first forward primer, 2541, was overlapping with a unique *Pvu*II restriction site and was used in combination with primer 2540, spanning the complete V3-loop sequence. The second fragment was flanked by the mutated primer 2539 and the reverse primer 2542, overlapping a unique *Mfe*I site. After successful amplification of both fragments, they were purified and used in different dilutions for the fusion PCR step with the outer flanking primers 2541 and 2542. This fragment was then subjected to *Pvu*II/*Mfe*I restriction and inserted in the pCAGGS-NL4-3 vector.

Sequencing of this construct revealed a mutation in the NL4-3 sequence which was found in several clones resulting from this cloning procedure and finally also located in the parental clone. Since this G378V mutation was not found in any HIV-1 Env sequences as confirmed by a BLAST search, and was also absent from the pCAGGS-NL4-3 derivative pCAGGS-NL4-3-R5, the mutation was reversed by a fusion PCR approach. To this end, a primer pair was designed changing the single nucleotide from T to G: 2583 and 2584. Primary PCRs were performed with the pairs 2541 and 2584, as well as 2583 and 2542, products purified and used in the fusion PCR with the flanking primer pair 2541 and 2542, cut by *Pvu*II/*Mfe*I and inserted into the above constructed clone harbouring the additional *Xba*I site. The final construct pCAGGS-NL4-3*Xba*I was confirmed by sequencing and used for further cloning.

V3-loop sequences from patient's samples were amplified by PCR directly on the RT-PCR product amplified from the original sample (for patients 651, 685, 822, 838 and 924) or on mini preparations of inserted patient's sequences into pCAGGS (for patients 220, 286 and 409; performed by E. Heger, group of R. Kaiser, Department of Virology, University of Cologne, Köln, Germany). PCR on patient's samples 286, 409, 685, 838 yielded amplification products that led to positive clones by the partially mismatching original primer pair 2540 and 2541,

whereas new forward primers with perfectly matching sequences had to be used for samples 220 (primer 2747), 651 (primer 2748), 822 (primer 2749) and both forward and reverse primers for 924 (2750 and 2751). PCR products were cleaved with *Pvu*II/*Xba*I yielding small fragments of ~140 bp which were purified via agarose gel electrophoresis and gel extraction and ligated into the vector pCAGGS-NL4-3*Xba*I.

2.3 Biochemical Methods

2.3.1 SDS-Polyacrylamide Gel Electrophoresis (SDS-PAGE) and Western Blot

Protein samples were suspended in 1x SDS-sample buffer containing β-mercaptoethanol and boiled at 95°C for 5-10 min. Low crosslinking-gels of 17.5 % acrylamide containing 0.0875 % bis-acrylamide were used for protein separation at 25 mA per gel for app. 1 h. The gels were then blotted onto a nitrocellulose membrane using a semi-dry blotting machine (Fastblot B32, Whatman Biometra, Göttingen, Germany or one from cti GmbH, Idstein, Germany). To this end, 4 Whatman filter papers were soaked in buffer I, 2 in buffer II, the nitrocellulose and gel were briefly rinsed with buffer II and the gel was finally covered by 5 sheets of Whatman paper soaked in buffer III. Blotting was performed at 0.8 mA/cm^2 for 1 h.

If no prestained protein marker was used, the membrane was briefly stained with ponceauS for 5 min to visualize the marker bands and mark them with a pencil. Otherwise, blocking of the membrane was directly performed in 10 % milkpowder or 2 % BSA in TBST for app. 30 min at RT. Primary antibodies were incubated with the membrane o/n at 4°C in TBST containing 5 % milkpowder or 1-2 % BSA. After washing of the membrane with TBST, secondary antibodies raised against IgGs of the appropriate species directly coupled to horseradish peroxidase were incubated in TBST containing 5 % milkpowder for 1 h at room temperature.

Detection of immunoreactive bands was performed using enhanced chemiluminescence (ECL) with a luminol-based substrate from Pierce (Thermo Fisher Scientific, Bonn, Germany) and the signal recorded by exposure of X-ray films for different time points which were then developed in an automatic film processor.

2.3.2 Quantitative Western Blot

SDS-PAGE separation of protein samples, western blotting, blocking and primary antibody incubation were performed as described in 2.3.1. A prestained protein marker was used that could be visualized on the infrared-imager and ponceauS staining was omitted to prevent background signals. Species specific secondary antibodies were coupled to fluorescent probes

with 700 nm or 800 nm excitation maximum, respectively. Incubation was performed in LiCor blocking buffer diluted 1:3 in PBS for 1 h at room temperature in the dark. The membrane was then washed and immunoreactive bands detected on the infrared imaging system Odyssey® (LI-COR Biosciences GmbH, Bad Homburg, Germany).

Quantitation of p24 amounts in virus samples was performed in comparison to a standard of purified CA-protein (sometimes mixed with purified MA-protein) applied on the gel in parallel.

2.3.3 Dot Blot

The Dot Blot device (Minifold® I, Whatman GmbH, Dassel, Germany) was assembled according to manufacturer's instructions including one Watman filter below the nitrocellulose membrane briefly rinsed in PBS. Protein samples heated in SDS-sample buffer or crude supernatant inactivated with 0.5 % triton-X-100 for 90 min were loaded and applied to the membrane by vacuum. Membrane was dried, blocked for 15 min in 2 % BSA in TBST and incubated with primary and secondary antibodies as described for quantitative western blot membranes (see above).

2.3.4 Enzyme-Linked Immunosorbent Assay (p24-ELISA)

The in-house p24-ELISA for detection of HIV-1 CA-protein in samples was used to determine virus concentrations in p24 equivalents.

Maxisorb 96-well plates (Nunc, Wiesbaden, Germany) were coated with a monoclonal mouse-antibody raised against p24(CA) (183-H12-5C) o/n at room temperature in a moist chamber and then blocked with 10 % FCS/PBST for 2 h at 37°C. Virus dilutions in PBST were added to the single wells and a titration of purified CA-protein was applied as a standard. Samples were incubated o/n at RT in a moist chamber. After washing with PBST, the plate was incubated with a rabbit-antiserum raised against CA protein, followed by another washing step and the incubation with horsereddish peroxidase-coupled secondary antibody raised in goat against rabbit IgG for 1 h at 37°C, each. After washing with PBST and H_2O, the amount of bound antibody was visualized by addition of the chromogenic substrate tetramethyl benzidine (TMB) for 5 min. The labelling reaction was stopped by the addition of 0.5 M sulphuric acid and the absorbance of the coloured reaction product quantitated in a spectrofluorimetric plate-reader at 405 nm wavelength.

2.3.5 Production of oxidized low density lipoproteins (oxLDL)

LDL was diluted to 100 µg/ml in PBS and 1 ml of this solution was oxidized in presence of 10 µM $CuSO_4$ for 18 h at 37°C. The oxidizing reaction was stopped by the addition of 2 µl

0.5 M EDTA, resulting in a final EDTA concentration of 1 mM. All buffers were kept sterile so that the final oxLDL could be stored at 4°C and later on used in the BlaM assay.

2.4 Cell Biological Methods

2.4.1 Cell culture

Adherent cell lines were kept in DMEM high glucose, supplemented with 10 % FCS, 100 U/ml penicillin, 100 µg/ml streptomycin and 20 mM Hepes buffer and incubated at 37°C at 5 % CO_2 in 95 % humidity. The double-inducible 293-derived cell line Affinofile [105] was kept in DMEM, supplemented with 10 % FCS without tetracycline, with penicillin/streptomycin and 20 mM Hepes buffer and the selection antibiotics Hygromycin, Blasticidin, Neomycin and Geneticin were added after each passage of the cells. Suspension cells were kept in RPMI 1640, supplemented with 10 % FCS, Pen/Strep and 20 mM Hepes buffer. SupT1-R5 and C8166-R5 cells, subclones of the SupT1 and C8166 cell lines which stably express CCR5, were kept under permanent selection pressure with 0.3 µg/ml and 0.2 µg/ml Puromycin, respectively. Freshly isolated primary blood mononuclear cells (PBMC) were kept in RPMI 1640.

Cells were passaged every 3-4 days. For that purpose, adherent cells were briefly washed with PBS, detached with 0.05 % Trypsin/EDTA in PBS for 5 min and resuspended in media. Suspension cells were separated and then passaged in the appropriate concentration.

For maintenance, aliquots of cells were cyro-conservated in FCS (w/o Tetracycline for Affinofile cells) supplemented with 10 % DMSO. Then, they were slowly cooled to -80°C and then transferred to liquid nitrogen for long-term storage.

2.4.2 Transfection of cells

Cells were seeded app. 24 h before transfection with one of the different methods.

2.4.2.1 PEI-method

Polyethyleneimmine is a cationic polymer that forms positively charged complexes with DNA that can then enter cells. For this method, DNA was diluted in DMEM without any supplements and 3 times the µg amount of DNA was added in volume of polyethylenimine (1mg/ml in H_2O), mixed well and incubated for at least 30 min at room temperature. The mixture was the added dropwise to the cells.

2.4.2.2 Calcium phosphate precipitation method

DNA was diluted in H_2O and mixed with 1/10 2.5 M $CaCl_2$. This mixture was then

slowly pipetted to the same volume of 2x HeBS buffer while vortexing, incubated for 30 min at RT and then slowly added to the cells. Medium change was performed app. 6 h post transfection.

2.4.2.3 FuGene-method

Two times the µg amount of DNA to be transfected of FuGene6 reagent was added in volume to OptiMEM and incubated for 5 min at room temperature. Then, DNA was added and incubated for further 15 min before adding the mixture to the cells.

2.4.3 SNAP-labelling of cells

Hela cells seeded on coverslips 24 h prior to the experiment were transfected with FuGene method and incubated at 37°C for 24 h. SNAP-labelling was conducted as recommended by the manufacturer. Briefly, cells were incubated with 1 µM TMR-*Star* in DMEM for 15 min at 37°C, washed three times and then incubated in fresh DMEM for 45 min at 37°C to allow diffusion of access substrate. For pulse-chase experiments, cells were first incubated with 10 µM BTP for 5 min at 37°C, washed three times, incubated with fresh DMEM for the indicated chase period and then stained with TMR-*Star* as described above. Cells were then fixed with 3 % PFA for 30 min and counterstained with Hoechst 33258 for 30 min at room temperature, washed with PBS, rinsed with H_2O and embedded in Mowiol.

HIV^{SNAP} infected C8166 cells were subjected to a modified protocol in solution using the same conditions as above. To wash cells, they were centrifuged at 4'000 rpm for 4 min. Fixation was carried out with 3 % PFA for 90 min and cells were then subjected to immunofluorescence staining (see 2.4.7). For imaging, suspension cells were adhered on fibronectin-coated coverslips and then embedded in Mowiol.

2.4.4 Electron microscopic analysis of cell samples

293T cells were transfected using FuGENE HD (Roche Diagnostics GmbH, Mannheim, Germany) with pNLC4-3 or pNLC.SNAP, respectively. At 24 h post transfection the cells were fixed and processed for resin-embedding as described [240]. Briefly, cells were fixed with 4 % paraformaldehyde, 0.1 % glutaraldehyde in 0.1 M PHEM for at 90 min at RT then washed with 50 mM glycine in 0.1 M PHEM followed by 100 mM sodium-cacodylate, pH 7.4. Cells were scraped in 1 % BSA in 100 mM cacodylate, pelleted, washed with 100 mM cacodylate and post-fixed with 2.5 % GA for 1 h. Pellets were washed in 100 mM cacodylate, post-fixed with reduced Osmium (1 % OsO4, 1.5 % potassiumhexacyanoferrat in 100 mM cacodylate) and stained for 16 h with 1 % aequous uranyl acetate.

Cells were gradually embedded in epoxy-resin after dehydration with a series of increasing concentrations of acetone. Ultra-thin sections were post-stained with lead-citrate. All

sections were examined with a Zeiss EM10 TEM and images taken using a Gatan MultiScan™ camera and Digital Micrograph™ software and further processed using Adobe Photoshop CS2.

2.4.5 Flow cytometry of cells (FACS)

Adherent cells were detached with 5 mM EDTA in PBS for 5 min and washed with 10 % FCS/PBS. For pelletation of cells between different staining or washing steps, centrifugation was either performed in 1.5 ml reaction tubes at 4000 rpm for 5 min at 4°C or in 96-well plates at 1200 rpm for 5 min. If indicated, cells were fixed with 3 % PFA/PBS for 30 min and stained with antibodies against surface proteins in PBS at the given dilutions for 30 min at room temperature or on ice if unfixed samples were used. If primary antibodies were not available as directly coupled variants, species specific secondary antibodies coupled to the indicated fluorophore were used for staining for 30 min in PBS. Samples were briefly washed in PBS, resuspended thoroughly in PBS and then subjected to flow cytometry on a FACSCalibur, FACSAria, FACSCanto II or BD LSR II machine (BD Biosciences, Heidelberg, Germany). For some applications, dead cells were stained with propidium iodide or 7-aminoactinomycin D (7-AAD) which was added to the sample directly before measurement at a dilution of 1:1000.

2.4.6 Quantitative FACS measurements with QuantiBRITE

Affinofile cells were seeded at $3x10^5$ in 24-well plates and induced 18 h prior to the experiment. Cells were detached with 5 mM EDTA, transferred to test tubes, washed with PBS and surface staining of CD4, CCR5 and CXCR4 was performed as described above with monoclonal mouse antibodies directly coupled to PE. Flow cytometric analysis was performed with a FACSCalibur and a vial of QuantiBRITE PE (BD Biosciences, Heidelberg, Germany) was measured with the same instrument settings, only adjusting forward (FSC) and sideward scatter (SSC). This sample was gated on bead singlets and geometric mean values of PE fluorescence intensity were measured for the four bead-populations as described in the manufacturer's protocol. A standard curve was calculated from the Log_{10} of geometric mean values and lot-specific number of PE molecules per bead as given by the manual. Log_{10} of geometric mean values of individual cell measurements of FSC-SSC-gated Affinofile cell populations were then transformed to antibody molecules bound per cell (ABC) based on slope and intercept of the standard curve.

2.4.7 Immunofluorescence staining of cells

For intracellular p24 staining, C8166 cells infected with HIV-1 derivatives and control mock infected cells were fixed with 3 % PFA for 90 min and washed with PBS. $1x10^6$ cells were adhered to fibronectin coated cover slips and permeabilized by incubation with 0.1% TritonX-100/PBS for 3 min at room temperature and blocked with 3 % bovine serum albumin (BSA) in

PBS for 10 min. Intracellular p24 was detected by incubation with a rabbit antibody raised against HIV-1 CA for 30 min at room temperature. After washing with PBS, 30 min incubation at room temperature with a secondary goat anti-rabbit antibody coupled to Alexa 488 (Invitrogen, Karlsruhe, Germany) was utilized for visualization. Counterstaining of nuclei was performed using 1:500 Hoechst 33258 in the secondary antibody solution. Cells were washed again with PBS, rinsed with H_2O and embedded in Mowiol.

For surface detection of cellular proteins, cells were fixed and blocked directly without preceding permeabilization. Antibody staining was performed in PBS for 30 min each at room temperature. If coupled antibodies were applied, cells were subsequently kept in the dark. Affinofile cells were stained against CCR5 in a first step, using a mouse-antibody raised against CCR5, secondary goat anti-mouse antibodies coupled to Alexa 568 and cells were subsequently stained with an Alexa 647-coupled mouse-anti CD4 antibody. During the last two steps, Hoechst 33258 was present for nuclei counterstaining. Staining in 96-well plates was performed in 30 µl/well to minimize the amount of reagents needed. To ensure proper distribution of staining solution over the complete well, plates were gently agitated during the incubation periods. To prevent cell detachment, supernatants were decanted rather than aspirated.

For imaging on coverslips, adherent cells were grown on coverslips briefly rinsed in EtOH and flamed for sterilization. After fixation and blocking, cells were stained in 60 µl solution applied as a drop on top of the coverslip. Subsequently, cover slips were rinsed in H_2O and embedded in Mowiol.

2.4.8 Automated fluorescence microscopy

Affinofile cells transduced with equivalent amounts of isogenic viral vectors as described in 2.5.8, fixed and stained for cell surface molecules and nuclei as described in 2.4.7 were imaged in a fully automated inverted epifluorescence screening microscope equipped with the Scan^R acquisition software (Olympus Scan^R IX81 'inverted' microscope setup, Olympus Soft Imaging Solutions GmbH, Münster, Germany). 16 images per well were recorded in 4 channels using a 10x objective. The appropriate excitation and emission filters were used to acquire images in the channels DAPI for the detection of Hoechst staining of nuclei, GFP for reporter gene expression, TexasRed for CCR5 stained with Alexa 568 and Cy5 for CD4 staining with Alexa 647. Exposure times were adjusted for each experiment empirically but kept constant over the course of one experiment including all proper controls. The times were in the range of 2-5 ms for DAPI, 50-100 ms for GFP and 500-1000 ms for the two remaining channels.

2.5 Virological Methods

2.5.1 Particle preparation

293T cells were seeded at $3x10^6$ in 10 cm-dishes 24 h prior to transfection with the PEI-method. 15 µg pcHIV or a 1:1 mixture of pcHIV and a fluorescently labelled variant thereof were transfected per dish. Supernatants were harvested app. 40-48 h post transfection and cleared by brief centrifugation at 1500 rpm for 5 min at 4°C and subsequently filtered through 0.45 µm filters. App. 28 ml of supernatant were layered upon a 8 ml sucrose cushion (20 % sucrose (w/v) in PBS) and pelleted in the ultracentrifuge at 24'000 rpm for 2 h at 4°C. The pellet was the resuspended in 75 µl of PBS 20 mM Hepes and 10 % FCS. Aliquots of the virus preparation were shock-frozen in liquid nitrogen and then stored at -80°C. For smaller preparations, 293T cells were seeded in 6-well plates at $3x10^5$ or $8x10^4$ in 12-well plates and pelletation performed in a table-top ultracentrifuge at 44'000 rpm for 45 min-1 h.

HCV pseudoparticles were produced by transfection of 293T cells with the PEI method using 15 µg of proviral pcHIV.Env(-) or a mixture with the fluorescently labelled variant and 2.5 µg of pcDNA3ΔCE1E2. Harvesting and purification of particles was performed as described above.

Isogenic *gfp* reporter gene carrying vectors only varying in the Env protein incorporated were produced by transfection of 293T cells with the PEI method. To this end, $3x10^6$ 293T cells were seeded in 10 cm dishes and 24 h later transfected with a mixture of 11.29 µg pSEW, 6.72 µg pCMVΔR8.9 and 2.5 µg of the respective Env expression plasmid. Harvesting and purification of particles was performed as described above.

2.5.2 Virus Binding Assay

Adherent cells were seeded 24 h prior to the experiment at $1x10^4$ cells/well in 8-well chambered cover glasses (LabTek, Nunc, Wiesbaden, Germany) precoated with Collagen A for Lunet cells or $1x10^5$ HeLaP4 cells in 12-well plates with coverslips rinsed in EtOH and briefly heated over a flame. Suspension cells were directly used at a density of $1x10^6$ cells/100 µl. Cells were transferred to CO_2-independent medium, chilled on ice for 10 min and the indicated p24 equivalent of fluorescently labelled virus was added. Virus binding was allowed for 1 h on ice, excess virus was washed off with cold PBS and cells were then fixed with 3 % PFA on ice for 30 min. Suspension cells were then adhered to Fibronectin coated coverslips and embedded in Mowiol, whereas cells in LabTeks were overlayed with PBS and imaged directly.

Microscopy was performed using an inverted epifluorescence microscope (Zeiss Axiovert 200M, Carl Zeiss Imaging Solutions GmbH, München, Germany) equipped with the appropriate filter sets. To cover the complete cell volume, z-stacks were recorded. In case of the virus binding

assay to determine dependence on CD317 expression levels, single images at one z-position were acquired in the GFP and Alexa 647 channel in addition.

2.5.3 Virus Uptake Assay

Lunet cells were seeded 24 h prior to the experiment at $1x10^4$ cells/well in 8-well chambered cover glasses (LabTek, Nunc, Wiesbaden, Germany) precoated with Collagen A or at $3x10^5$ in 6-well plates with coverslips rinsed in EtOH and briefly heated over a flame. Cells were transferred to CO_2-independent medium, chilled on ice for 10 min and the indicated p24 equivalent of fluorescently labelled virus was added. Virus binding was allowed for 1 h on ice, medium was changed to warm DMEM thereby washing excess virus off and cells were incubated for the indicated time period at 37°C. Subsequently, cells were washed and fixed with 3 % PFA. To monitor cellular endocytosis, samples were incubated with virus in the presence of 50 µg/ml fluorescently coupled transferrin (Invitrogen, Karlsruhe, Germany).

Microscopy was performed using a confocal laser scanning microscope (Nikon C1Si, Nikon Imaging Center at University Heidelberg, Heidelberg, Germany; Nikon, Düsseldorf, Germany) equipped with the appropriate filter sets.

2.5.4 β-Lactamase Virion Fusion Assay

The β-Lactamase virion fusion assay was based on the method developed by Cavrois and colleagues [35]. Briefly, viral particles containing a fusion protein of Vpr and the bacterial protein β-Lactamase were produced from 293T cells as described in 2.5.1 by co-transfection of 1 µg of the plasmid pMM310 per 10 cm dish. Virus concentration was determined by p24-ELISA or quantitative Western Blot as described in 2.3.4 and 2.3.1, respectively.

Cells were seeded in 96-well plates at a density of $1\text{-}2x10^4$ for adherent cells app. 24 h before virus addition or $1x10^6$ suspension cells directly before virus addition, respectively. Virus dilutions of a given amount of p24 were added to the cells and incubated for 6 h at 37°C if not stated differently. Cells were then briefly washed with CO_2-independent media and 60 µl CCF2-AM, a fluorescent substrate for β-Lactamase (GeneBLAZER, Invitrogen Ltd., Paisley, UK), added according to the manufacturer's protocol. After o/n incubation at RT in the dark, cells were washed with PBS, fixed with 3 % PFA/PBS for at least 30 min and then subjected to further antibody staining if indicated.

Read-out was performed either microscopical, in a plate fluorimeter (Tecan Safire, Tecan Deutschland GmbH, Crailsheim, Germany) or with flow-cytometry in a FACSAria™ or FACSCanto™ II (BD Biosciences, Heidelberg, Germany) with the appropriate filters (Ex 409 nm, Em 447 nm and 520 nm). The entry efficiency was calculated in relation to a control where no virus was added.

2.5.5 Infectivity assay

TZM-bl cells were seeded in 96-well plates at $8x10^3$ cells/well in 100 µl. After 24 h cells were infected with 100 µl supernatant form transfected 293T cells (HIV, HIV^{SNAP} and HIV^{iSNAP} were produced by transfection with the plasmids pNLC, pNLC.SNAP and pNLCiSNAP, respectively) and serial 1:2 dilutions were performed in DMEM. Cells were incubated for 48 h at 37°C and supernatant was discarded. Cells were lysed with 50µl of Steady-Glo® reagent in 100µl DMEM (Steady-Glo® Luciferase Assay System, Promega, Mannheim, Germany) for 5 min at room temperature. 80 µl of cell lysate was transferred to a white 96-well plate and luminescence was measured in a plate luminometer.

2.5.6 Replication kinetics of HIV-1 derivatives

HIV, HIV^{SNAP} and HIV^{iSNAP} were produced by transfection of 293T cells with the plasmids pNLC, pNLC.SNAP and pNLCiSNAP, respectively. The amount of p24 in the supernatant was determined using qWB as described in 2.3.2 and 0.5 ng of p24 of each virus derivative were used to infect 1 x 10^5 MT4 cells in 200 µl per 96-well (V-bottom). 95 µl of supernatant were collected every 2 to 3 days and inactivated with 5 µl of 5 % Triton X-100, leading to a final concentration of 0.25 % of Triton X-100.

2.5.7 SNAP-labelling of HIV^{SNAP}

Non-infectious HIV^{SNAP} and HIV as a control were produced by transfection of 293T cells as described above. Viruses were purified by ultracentrifugation through a 20 % sucrose cushion and resuspended in PBS with 20 mM Hepes and 10 % FCS. 300 ng p24 equivalent were incubated with 1 µM TMR-Star and 5 mM DTT in PBS at 4°C over night. Virus was re-purified by ultracentrifugation in a tabletop centrifuge through 200 µl 20 % sucrose cushion, resuspended in PBS with 20 mM Hepes and 10 % FCS and imaged in a wide-field epifluorescence microscope.

2.5.8 Transduction of cells

Isogenic *gfp* reporter gene carrying vectors only varying in the Env protein incorporated were produced as described in 2.5.1. For a typical Affinofile transduction experiment, cells were seeded in 96-well plates at $8x10^3$ and induced for 18 h with the indicated concentration of inducing agents. Then, 5 ng p24 equivalent as determined by qWB (2.3.2) were added to the cells and incubated for 48 h at 37°C. Subsequently, cells were fixed with 3 % PFA for 30 min and immunofluorescence staining was performed if needed.

2.6 Computational Methods

2.6.1 Semi-automated Particle Counting and Colocalisation Analysis

A plug-in for the image analysis program ImageJ was complied which performed several subsequent analysis steps automatically. A batch read-in of pictures with the same base-name and incremented file numbering could be achieved. Then, depending on the file format, changes in bit depth and channel composition were performed to obtain 8-bit single channel images. The images were then filtered with a bandpass FFT (fast Fourier transformation) and a threshold was defined based on the mean background fluorescence signal or a fixed value which was determined empirically. A particle recognition program was applied on signals above this threshold and the intensity of the fluorescence signals in the different channels measured at the respective spots. To determine colocalization of spots in different channels, the thresholded images of both channels were divided by 255 and 127.5, respectively. The resulting images were added to each other, obtaining a new image with intensity values of 0, 1, 2 or 3, depending on the signal in the two original images with no signal in both channels resulting in 0, a signal in the first picture resulting in 1, in the other picture resulting in 2 and an overlapping signal in both original pictures resulting in 3. This resulting image was then analysed at the beforehand recognized spots.

2.6.2 Automated cell-segmentation and single cell read-out of microscopic data

Cell segmentation was performed in a two-step process, starting with the identification of each cell according to the nucleus signal in the DAPI channel. To this end, DAPI images were binarized, filtered and local maxima assigned to individual cell nuclei. The algorithm was performed as described in [22]. As the second step, cell bodies were segmented on a maximum projection of the two cellular surface molecule images in the Cy5 and TexasRed channel. A maximum projection was chosen to provide the strongest possible signal if one of the channels showed only weak signals. Perfect matching of both channels was beforehand controlled manually and a relocalization could be implemented if necessary. The seeded watershed segmentation method was used, where segmentation was started from the centre of the nuclei assigned before. In this method, the grey value intensities of the image are viewed as in a landscape, with low intensities building valleys and high intensities building hills. The algorithm simulates a rising level of water, starting from the assigned nuclei valleys. As soon as two neighbouring “basins” are about to merge, a barrier is built which reflects the line at which two cell bodies hit. In 2D, the line can be imagined growing from the centre (nucleus) until it hits a sharp intensity border or the border of a growing neighbouring cell. To prevent too big cells, a maximum area threshold was applied.

3 Results

This chapter is divided into two main parts. In the first part, the use of fluorescently labelled viruses as a tool to study the interactions of cells and viruses is described. While an emphasis is made on viral entry in this thesis, the establishment of a new internal labelling strategy also allows investigating virus egress. The second part (see page 69) describes a detailed analysis of virus entry into their host cells depending on different critical viral and cellular parameters. In order to find a better understanding of this process, the influence of the presence of different amounts of interfering drugs has also been investigated.

3.1 Fluorescently labelled viruses to study virus cell interactions

To study the kinetics and dynamics of the viral replication cycle, fluorescently labelled HIV-1 derivatives have widely been used in the past [117, 127, 147, 162]. In those studies, fluorescent proteins have been fused to various proteins of HIV-1, such as MA, Vpr or IN (compare chapter 1.3.1 for further details). For HCV, no such systems to directly label viral particles have been established, yet.

The first part of this chapter will describe the combination of the well-established virus tagging, fusion of the viral MA protein, with a new labelling technique, the SNAP-tag, which allows the usage of organic dyes as fluorochromes. The second part focuses on the establishment of a system to study and dissect the early steps of HCV entry, mainly with the help of fluorescently labelled particles but also with other methods. Finally, in the last part of this chapter the newly established methods to quantify virus binding to cells are applied to study also HIV-1 binding to cells.

3.1.1 SNAP-tag as a tool to study virus release

Major drawbacks of virus labelling by fluorescent proteins are the slow maturation kinetics, low quantum yield and fast photobleaching of those FPs. The recently described SNAP-tag [114] on the other hand provides a much more versatile tool to label viral structures since much more stable chemical fluorescent probes can be linked to it. These dyes are superior to fluorescent proteins as to stability, quantum yield, bleaching properties and the range of observation wavelengths. SNAP-tag allows covalent labelling if fused to a protein of interest by transfer of the fluorescently labelled moiety of O^6-Benzylguanine derivatives to its active site in a self-labelling reaction.

To make use of this labelling tool, I constructed a fusion of SNAP-tag to the main structural protein Gag in the proviral context to study virus formation and egress. The virus derivatives were characterized with respect to their protein composition, labelling properties and functional capacities. Preliminary data on the kinetics of Gag-trafficking were obtained using this tool.

3.1.1.1 Construction and characterization of an HIV-1 derivative carrying the SNAP-tag

In analogy to the previously described fluorescently labelled HIV-1 derivatives which can be used to study virus entry, the SNAP-tag was C-terminally fused to the viral protein MA. To achieve this, the *snap-tag* gene was amplified from the plasmid pSS26m by PCR and inserted in frame into the gag ORF shortly prior to the cleavage site of the HIV-1 protease between MA and CA (Fig. 3.1 A). A short fragment of the C-terminal end of MA was kept as a linker sequence and the protease cleavage site was fully retained. This results in a fully mature Gag protein that will be processed into its natural cleavage products CA, NC and p6. In addition, the virus will possess the fusion protein MA.SNAP which can be labelled by the addition of a fluorescently labelled SNAP-substrate (Fig. 3.1 B). To promote proper folding of the fusion protein, a short glycine rich linker sequence was introduced between the two protein coding sequences (Fig. 3.1 A).

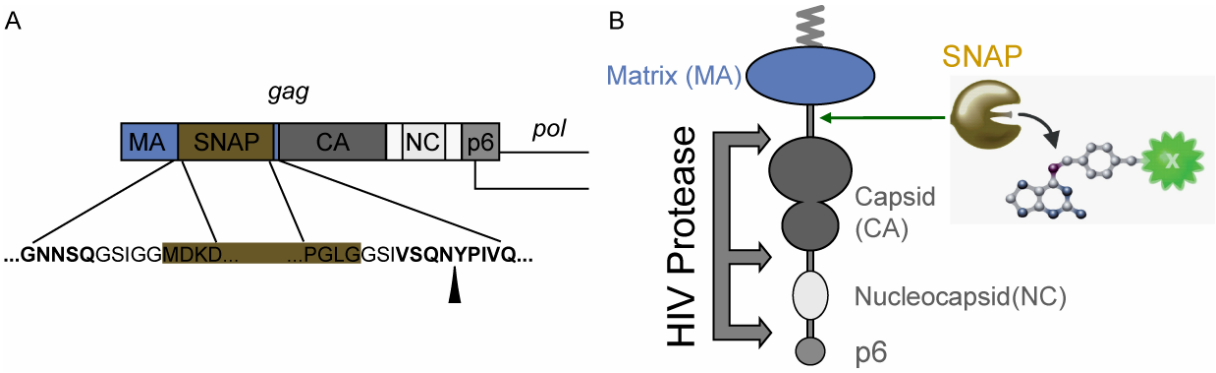

Fig. 3.1: Location of the SNAP-tag. (A) Schematic drawing of the HIV-1 gag ORF showing the snap-tag gene (brown) inserted between MA (blue) and CA (dark grey) coding regions. The expanded regions show the derived amino acid sequence at the domain borders, with HIV sequences displayed in boldface type and SNAP-tag sequences shown in black type on a brown background. An arrowhead indicates the PR cleavage site between MA and CA. (B) Schematic drawing the HIV-1 Gag protein with the approximate site of SNAP-tag insertion indicated by the green arrow. HIV-1 protease cleavage sites are indicated by grey arrows. Colour coding of protein domains according to the respective genes in (A).

To characterize the constructed plasmid pcHIV.SNAP, 293T cells were transfected with the plasmid and compared to pcHIV as well as a 1:1 mixture of pcHIV and pcHIV.SNAP. The particles produced from this transfection were purified by sucrose pelletation (2.5.1) and analyzed by western blotting (2.3.1) in regard to incorporation of viral proteins and processing of Gag protein. The modified Gag-protein was incorporated into particles and processed by the viral protease to comparable levels as wild-type Gag (Fig. 3.2 A). As expected, mixed particles harbouring both tagged and untagged Gag-proteins were released into the supernatant after co-

transfection of pcHIV and pcHIV.SNAP. To test if other viral proteins outside the *gag* ORF were affected by the insertion of the *snap-tag* gene, the particles were representatively analyzed for RT-incorporation. To this end, equal amounts of p24 as determined by ELISA were loaded for each sample. No difference in the intensity of both RT bands could be observed between wild-type and SNAP-tagged viruses (Fig. 3.2 B) which suggests a normal composition of HIV^{SNAP}.

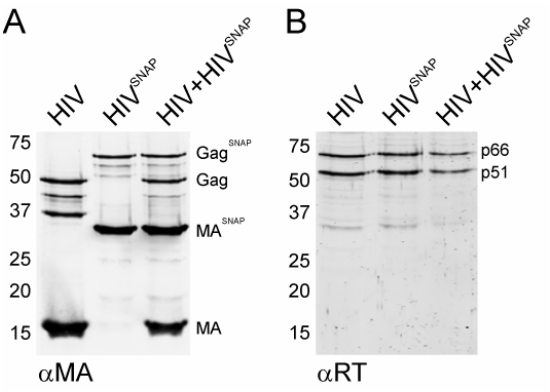

Fig. 3.2: Western Blot analysis of HIV-1 derived particles. HIV-1 derivatives were generated by transfection of 293T cells with pcHIV, pcHIV.SNAP or a mixture of both, particles were purified from the supernatant as described in 2.5.1 and subjected to Western Blot analysis. Membranes were probed against the viral proteins MA (A) or RT (B). Position of molecular mass standards is shown with numbers in kDa at the left and protein bands are labelled on the right.

To analyze the new construct to a greater depth, the ultrastructure of HIV^{SNAP} particles was investigated by electron microscopy (EM). 293T cells were transfected with pNLC4-3 or the SNAP-tagged variant thereof (pNLC.SNAP) and prepared for EM analysis as described in 2.4.4. Briefly, cells were fixed 24 h post transfection with PFA and GA, then transferred to a cacodylate buffer and scraped off the tissue culture dish. Pelleted cells were post-fixed with GA and Osmium and then stained with uranyl acetate. Cells were then embedded in an epoxy-resin, dehydrated and ultra-thin sections were post-stained with lead citrate. The samples were then examined with a Zeiss EM10 transmission electron microscope (TEM).

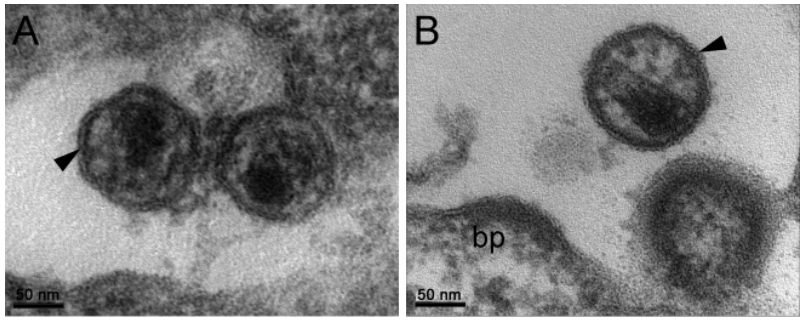

Fig. 3.3: Electron microscopic images of HIV and HIV^{SNAP}. 293T cells were transfected with pNLC4-3 (A) or pNLC.SNAP (B), respectively. After 24 h, cells were fixed and embedded in epoxy-resin for EM analysis as described in 2.4.4. Samples were analyzed in a TEM and pictures of viral structures taken at different magnifications. Images of free virus particles are displayed for HIV and HIV^{SNAP}. The bars represent 50 nm; bp = budding profile, arrowheads point at virus membranes. Sample embedding, processing and EM analysis performed by Anja Habermann.

Fig. 3.3 shows representative electron micrographs of HIV (A) and HIV^{SNAP} (B) produced from 293T cells. The cone-shaped core with dark dense material inside is characteristic for mature viral particles. The lipid bilayer surrounding the viral particles can be appreciated in both pictures (arrowheads). No obvious ultrastructural differences could be observed by comparison of

wt and HIV^{SNAP} particles. While a comparable number of budding profiles (bp), immature and mature viral particles were found in both samples, the electron dense material underlaying the viral membrane appeared to be marginally thicker in HIV^{SNAP} samples. To appreciate this, compare the thickness of the viral membrane at the arrowheads in Fig. 3.3 A and B, respectively. The difference seemed to be minor, though.

Next, the new constructs were tested for their release efficiency and entry competence of the released viral particles. 293T cells were transfected with FuGene6 to prevent unspecific release of vesicles containing p24 which can occur after the transfection of cells with PEI, Lipofectamine or other comparable transfection reagents (B. Müller, personal communication). The amount of p24 released into the supernatant was quantified by quantitative Western Blot or Dot Blot using rabbit antisera raised against HIV-1 CA protein.

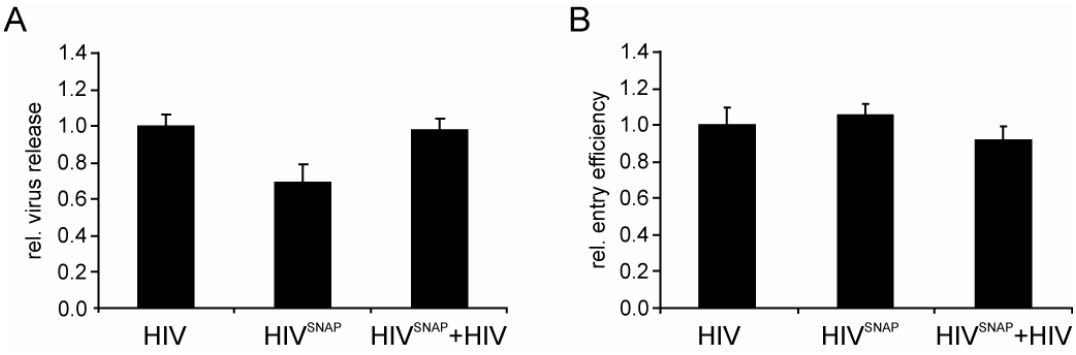

Fig. 3.4: Release and entry efficiency of HIV^{SNAP}. 293T cells were transfected with pcHIV, pcHIV.SNAP or a 1:1 mixture of both with FuGene6- (A) or PEI-method (B). (A) Amount of p24 released into the supernatant was quantified by quantitative Western Blot or Dot Blot and normalized to the release efficiency of HIV particles released from cells transfected with pcHIV. Error bars represent standard deviation of three independent experiments, each done in triplicate. (B) Entry efficiency of particles produced from 293T cells was tested on HeLaP4 cells as described in 2.5.4. Mean values of triplicates relative to entry efficiency of wild-type (HIV) are displayed. Error bars represent standard deviation.

Release of viral particles from transfected 293T cells was only moderately reduced for HIV^{SNAP} and could completely be restored by co-transfection of wt pcHIV in a ratio of 1:1 (Fig. 3.4 A). In addition, the relative entry efficiency on HeLaP4 cells compared to wild-type was not reduced for the SNAP-tagged virus or for the mixed particles (Fig. 3.4 B). Those data further emphasized the assumption that the particles containing the SNAP-tag within Gag are comparable in their features to wild-type HIV-1.

To further test this hypothesis, the SNAP-tagged HIV-derivative was subcloned into the infectious context of pNLC4-3 to test the infectivity and replication capacity of the constructed variants.

3.1.1.2 Infectivity and replication capacity of HIV^{SNAP}

First, the infectious derivative HIV^{SNAP} was tested for its infectivity on the reporter cell line TZMbl by titration of viruses produced from transfection of 293T and measurement of

luciferase activity of the reporter cells 48 h post infection.

Fig. 3.5 displays the relative infectivity of HIV^{SNAP}, which was reduced 4-fold in comparison to HIV wild-type. Mixed particles, produced from equimolar cotransfection of 293T cells with pNLC4-3 and pNLC.SNAP (HIV^{SNAP}+HIV) regained full infectivity.

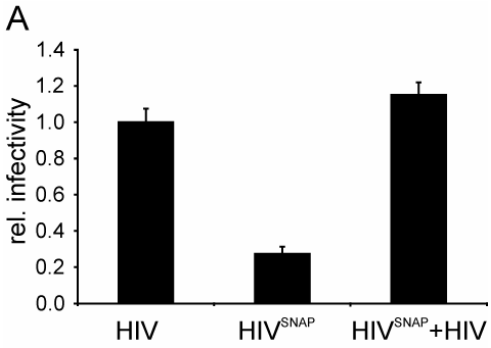

Fig. 3.5 Infectivity of HIVSNAP on TZMbl cells. Infectious HIV-1 particles were generated by transfection of 293T cells with pNLC4-3, pNLC.SNAP or an equimolar mixture of both.

During the course of this work, Hübner and colleagues published a GFP labelled HIV-derivative with only moderately reduced replication capacity compared to wt [98]. In this study, they inserted the GFP label into the *gag* ORF at exactly the same position as the SNAP-tag in the above described pNLC.SNAP, but a second PR cleavage site was inserted N-terminally of the tag to allow for full Gag processing including free MA.

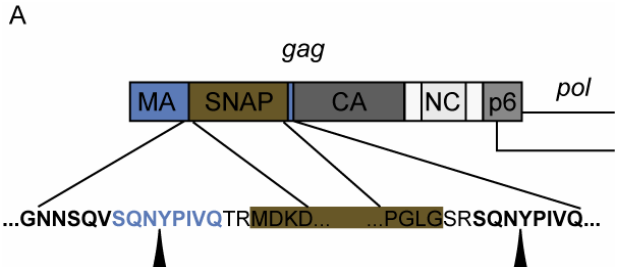

Fig. 3.6: Location of the SNAP-tag in pNLCiSNAP. (A) Schematic drawing of the HIV-1 *gag* ORF showing the *snap-tag* gene (brown) inserted between MA (blue) and CA (dark grey) coding regions. The expanded regions show the derived amino acid sequence at the domain borders, with HIV sequences displayed in boldface type and SNAP-tag sequences shown in black type on a brown background. Arrowheads indicate the PR cleavage site. The additional inserted PR cleavage site before the SNAP-tag sequence is highlighted in light blue.

To test if the full processing of Gag has an impact on the replication capacity of the SNAP-tagged HIV-1 derivatives, a comparable subviral plasmid was constructed. To this end, the *snap-tag* sequence was amplified by PCR from pSS26m with primers introducing the coding sequence for a second PR cleavage site. The fragment was then inserted into pNLCiGFP to obtain pNLCiSNAP. Analogously to the HIViGFP clone described by Hübner and colleagues, no special flanking sequence of the inserted label was chosen (Fig. 3.6).

To test the spread of HIV^{SNAP} and HIV^{iSNAP} in cell culture, a replication kinetic was performed on MT4 cells. For this, viral particles produced from 293T cells were added to MT4 cells at a defined concentration (0.5 ng p24 per well) and supernatants were monitored for p24 release every other day for a period of 17 days.

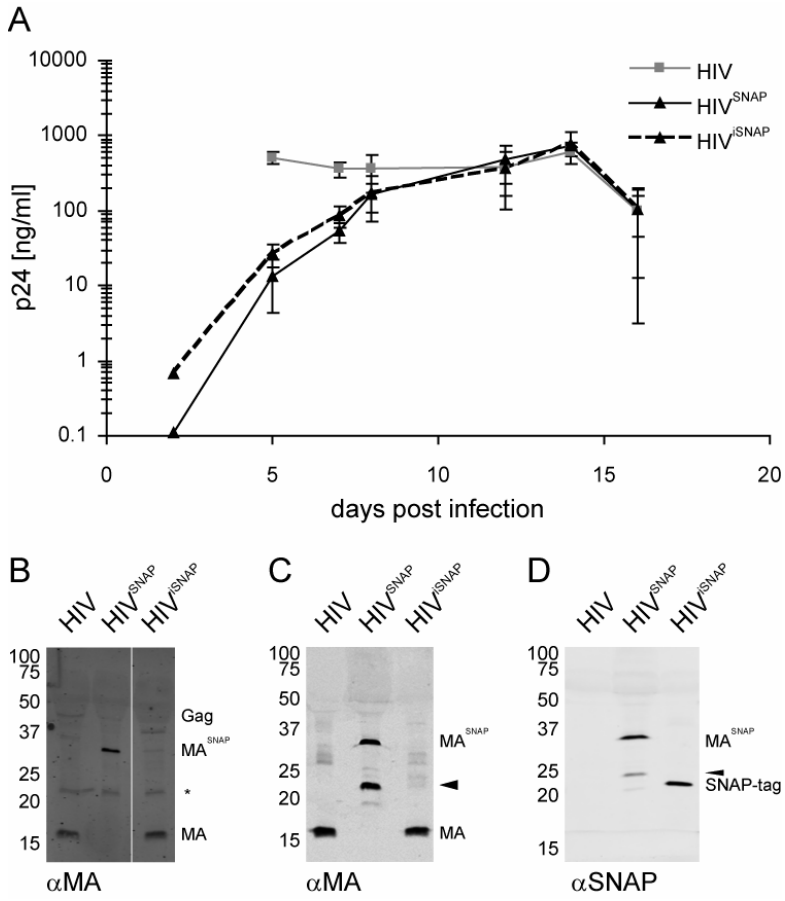

Fig. 3.7: Replication kinetics of HIV^{SNAP} and stability of SNAP-tag insertion over time. HIV, HIV^{SNAP} and HIV^{iSNAP} were produced from transfection of 293T cells with the plasmids pNLC, pNLC.SNAP and pNLCiSNAP, respectively. The amount of p24 in the supernatant was determined using qWB as described in 2.3.2 and 0.5 ng of p24 of each virus derivative were used to infect MT4 cells. A replication kinetic was performed as described in 2.5.6. Briefly, supernatants were collected every two to three days and the amount of p24 was determined utilizing the Dot Blot procedure (**2.3.3**) in comparison to CA standard. (A) The graph displays p24 amounts in ng/ml released into the supernatant over time for HIV (grey line), HIV^{SNAP} (black line) and HIV^{iSNAP} (dotted black line). Average of triplicate values and standard deviation of those are plotted. (B – D) show Western Blot analyses of input virus (B) and viral supernatants at day 14 of the replication kinetic (C + D). 293T (B) or MT4 (C + D) cell supernatants were analysed using antisera raised against the viral MA protein (B + C) or SNAP-tag protein (D). Approximate size of bands is shown with numbers in kDa at the left edge and protein bands are labelled on the right. Asterisk in (B) indicates background signal from αCA antibody staining which was performed in parallel. Arrowhead in (C) and (D) indicates cleavage product of MA^{SNAP}.

In Fig. 3.7 A, the amount of virus released into the supernatant is plotted over time for wt (HIV – grey line), HIV^{SNAP} (black line) and HIV^{iSNAP} (dotted line). Wt HIV reached a plateau of around 1µg/ml p24 after 5 days which only declined one log after 18 days. Both SNAP-tagged viruses showed a decreased spreading speed reaching the plateau of 1µg/ml p24 only after 14 days. Before this time, there was only a minor difference in replication capacity detectable between the two SNAP-tag variants with HIV^{SNAP} being slightly delayed compared to HIV^{iSNAP}. Comparable results could be obtained on C8166 cells (data not shown).

To test for stability of the inserted SNAP-tag over time, Western Blot analyses of the input virus in comparison to supernatant from late time points of the replication kinetic were

performed. Fig. 3.7 B shows the Western Blot analysis of the input viruses HIV, HIV^{SNAP} and HIV^{iSNAP} probed against the viral MA protein. While HIV^{SNAP} showed a band slightly below 37 kDa, corresponding to the fusion protein of MA and SNAP-tag (MA^{SNAP}), HIV^{iSNAP} harboured the fully processed MA band at 17 kDa at the same height as wild type HIV. The weak band that is marked with an asterisk in between the 20 and 25 kDa marker band represents a signal from an antibody contamination of αCA, proven by the simultaneous staining against CA (data not shown) and can therefore be neglected in further interpretations. After several rounds of replication in MT4 cells, the pattern of bands in the Western Blot remained the same for the three viruses tested (Fig. 3.7 C). Here, the supernatants of MT4 cells were analyzed 14 days post infection. The presence of a clear MA^{SNAP} band in the HIV^{SNAP} lane confirms the stability of the *snap-tag* gene within the HIV-1 genome and the persistence of the fusion protein within viral particles. As expected, HIV^{iSNAP} shows one single band at the expected height for MA only. To confirm that this virus still harboured the cleavable SNAP-tag protein, an additional Western Blot analysis was performed where the membrane was probed against SNAP-tag itself (Fig. 3.7 D). This Western Blot confirmed the presence of free SNAP-tag protein at the expected height of 20 kDa. It also confirmed that the MA^{SNAP} band in HIV^{SNAP} corresponded to a fusion protein of MA and SNAP-tag. In addition, the band labelled with the arrowhead in Fig. 3.7 C was also stained with antibody against SNAP-tag, hinting at the existence of a cleavage product of MA^{SNAP} which still harboured the recognition epitopes of both MA and SNAP-tag antibodies.

Taken together, these data suggested that the SNAP-tag introduced into HIV-1 had only minor effects on infectivity and replication in comparison to wt and was stable over prolonged replication within a standard T-cell line. Therefore, the constructed variants could be used to study intracellular Gag localization and trafficking.

3.1.1.3 Intracellular detection and localization of SNAP-tagged Gag protein

As the characterization of the SNAP-tag insertion into HIV-1 showed that those clones retained the characteristics of wild type HIV-1, they could now be used for the visualization of Gag proteins within cells. For this purpose, HeLa cells were transfected with pCHIV.SNAP in an equimolar mixture with the comparable eGFP-labelled variant pCHIV.eGFP. This strategy easily allowed identifying transfected cells and comparing the localization of the newly inserted tag with an already established viral label. At 24 h post transfection, cells were labelled with a SNAP-tag substrate coupled to TMR-*Star* (O^6-Benzylguanine-TMR-*Star*, referred to below as TMR-*Star*), cell nuclei were counterstained with Hoechst 33258 and cells were analyzed by confocal microscopy.

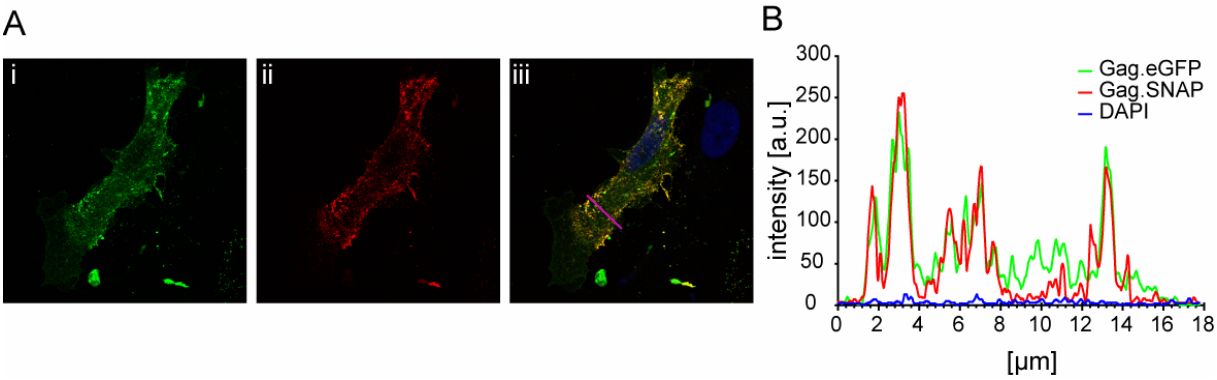

Fig. 3.8: Intracellular detection and localization of SNAP-tagged Gag protein. HeLa cells were transfected with an equimolar mixture of pCHIV.eGFP and pCHIV.SNAP. At 24 h post transfection, cells were labelled with TMR-Star for 15 min according to the manufactor's protocol and cell nuclei were stained with Hoechst 33258. Intracellular fluorescence was analyzed by confocal microscopy in a Leica SP2 setup with 60x oil immersion objective. (A) Microscopic images of a median section through a representative cell in the green GFP channel (i), red TMR-Star channel (ii) and a merged picture additionally showing the DAPI channel in blue (iii). (B) The histogram shows the intensities of GFP (green), TMR-Star (red) and DAPI (blue) fluorescence along the purple line in (A-iii). a.u. = arbitrary units.

Fig. 3.8 A shows a representative cell which was co-transfected with both non-infectious HIV derivatives, a GFP-labelled and a SNAP-tagged variant, respectively. Fig. 3.8 A-i displays the GFP channel in green with a characteristic punctuated pattern of Gag.eGFP all over the cell. A weak staining of the cytosol is also visible in this picture. Visualization of the SNAP-tag by labelling with TMR-*Star* reveals a comparable localization of Gag.SNAP with a similar dotted appearance (Fig. 3.8 A-ii). The diffuse staining in the cytosol is less visible here, though. The overlay of both channels (Fig. 3.8 A-iii) shows a high degree of overlap of the two Gag labels. This colocalization is confirmed by the line scan shown as a histogram in Fig. 3.8 B. Here, the fluorescence intensity of all three channels is plotted along a line of 20 µm drawn through the cell body as indicated in Fig. 3.8 A-iii (purple line). Fluorescence intensities of Gag.eGFP (green line) and Gag.SNAP (red line) peak at the same location, indicating a colocalization of both markers. The blue line indicates the fluorescence intensity in the DAPI channel which is at background levels at the chosen intersection through the cell body far away from the nucleus. Controls for background staining were always analyzed in parallel. The non-transfected cell in the upper right corner of Fig. 3.8 A (single blue nucleus in Fig. 3.8 A-iii) showed no signal in the red channel. Unspecific binding of TMR-*Star* to cellular or viral proteins could therefore be ruled out as confirmed in TMR-star treated control cells only transfected with pCHIV.eGFP which did not show a signal in the red channel (data not shown).

3.1.1.4 Labelling of cells infected with HIV^{SNAP}

To test if the SNAP-tag could also be stained after infection rather than transfection, C8166 cells were infected with the replication competent variant HIV^{SNAP} produced from transfection of 293T cells with pNLC.SNAP and passaged over several weeks. 23 days post

infection, cells were stained with TMR-*Star* as described in 2.4.3, fixed with 3 % PFA for 90 min, adhered to coverslips and counterstained with antisera raised against p24 (see 2.4.7) and a secondary antibody coupled to Alexa 488 analyzed by confocal microscopy.

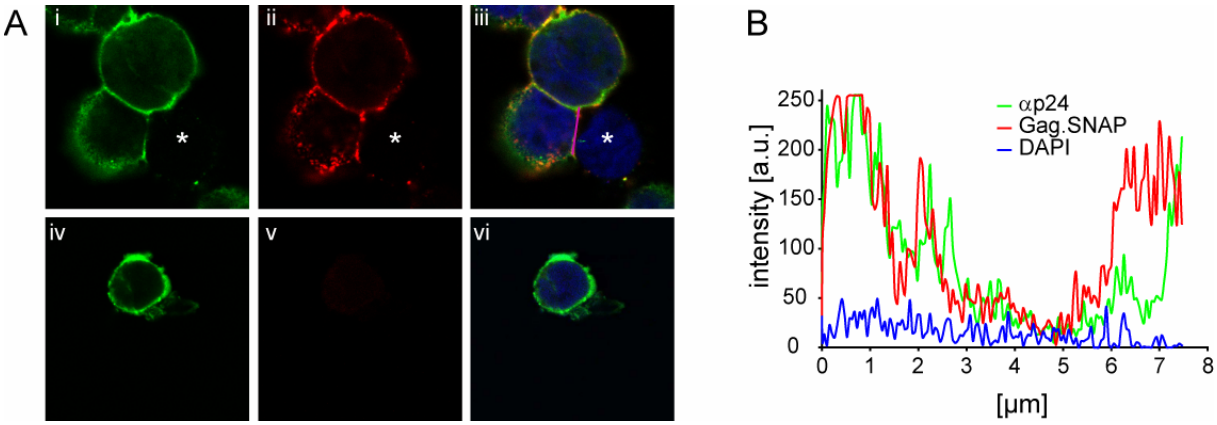

Fig. 3.9: Intracellular detection and localization of SNAP-tagged Gag protein in infected C8166 cells. HIV or HIV^{SNAP} were produced by transfection of 293T cells with pNLC4-3 and pNLC.SNAP, respectively. C8166 cells were infected with 100 ng of the respective virus and passaged for several weeks. 23 days post infection, cells were stained with TMR-*Star* and immunofluorescence against HIV-1 p24 was performed as described in 2.5.7 and 2.4.7, respectively. Cells were counterstained with Hoechst 33258 and imaged by confocal microscopy in a Leica SP2 setup. (A) Pictures of middle sections of representative cells are shown for p24 immunofluorescence in the green channel (i, iv), TMR-star signal in the red channel (ii, v) and overlay of Alexa 488, TMR-star and DAPI signals (blue) in iii and vi. The upper row shows cells infected with HIV^{SNAP} whereas the lower row shows a cell infected with HIV. The white asterisk indicates a non-infected cell. (B) The histogram shows the intensities of αp24 staining (Alexa 488, green), TMR-*Star* (red) and DAPI (blue) fluorescence along the purple line in (A iii). a.u. = arbitrary units.

A clear correlation between p24 staining and SNAP-labelling with TMR-*Star* could be observed in this experiment. Only cells infected with HIV^{SNAP} (Fig. 3.9 A i-iii) showed a signal in the TMR-*Star* channel, whereas cells infected with wt HIV (Fig. 3.9 A iv-vi) only stained positive for p24. An internal control for background staining was again present in the sample of HIV^{SNAP} infected C8166 cells: cells that had not been infected (e.g. the cell marked with a white asterisk in Fig. 3.9 A) did not show any signal in the TMR-*Star* channel (Fig. 3.9 A-ii) whereas a very slight background signal could be detected with Alexa 488 (Fig. 3.9 A-i). The overall distribution of the SNAP-tag signal varied slightly from the more diffuse immunofluorescence staining of p24. Whereas the antibody staining led to a diffuse signal which was also present all over the cell, TMR-star stained the SNAP-tag predominantly at the plasma membrane and in close vicinity to it. The SNAP-tag staining was also much more punctuated than the p24 staining. This differing pattern can be appreciated in Fig. 3.9 B where a histogram of fluorescence intensities along the purple line drawn in Fig. 3.9 A iii is depicted. The TMR-*Star* signal of the SNAP-tag showed more single peaks at positions where the green signal from the immunofluorescence of p24 was more diffuse, although the overall trend of the distribution of peaks was comparable in both stainings.

Taken together, those results showed that the inserted SNAP-tag within full length infectious HIV-1 can specifically be stained by adequate fluorescently labelled substrates. This provides a versatile tool to study Gag trafficking within transfected and infected cells.

3.1.1.5 Pulse chase experiments with Gag.SNAP

A major advantage of SNAP-tag over conventional protein labelling techniques is the variety of substrate colours in combination with the possibility to perform the labelling reaction in living cells. This provides the opportunity to perform pulse chase experiments in which the existing protein fraction can be labelled in one colour and the newly synthesized protein can be labelled in another colour after a certain chase period. This allows the direct comparison of the localization of the same protein produced at different time points within one cell.

To test this method and establish a suitable labelling protocol, HeLa cells were transfected with an equimolar mixture of pCHIV.eGFP and the SNAP-tagged variant pCHIV.SNAP. The GFP-tagged derivative was used in this setup to provide the reference point of Gag distribution within the cell over the whole course of the experiment. For those initial experiments, only one staining colour of SNAP-tag was chosen, TMR-*Star* as before. To only stain the portion of Gag.SNAP which was newly produced during the chase period, an approach was chosen where a non-labelled substrate (bromothenylpteridine, BTP, Covalys) was used in the beginning of the experiment to block all available SNAP-tag binding sites. BTP is a derivative of the SNAP-tag substrate O^6-Benzylguanine that contains a non-fluorescent moiety which will covalently be transferred to the active centre of SNAP-tag to block further self-labelling reactions. With this strategy, different time points (chase periods) can be chosen after which the newly synthesized SNAP-tag fusion proteins can be labelled with TMR-*Star*.

A representative proof of principle pulse chase experiment is depicted in Fig. 3.10. The figure shows single slice confocal microscopic images of HeLa cells expressing HIV^{eGFP} and HIV^{SNAP} which were stained with TMR-*Star* at the indicated time points after blocking with BTP. The first row (0 min) demonstrates that BTP blocked the SNAP-tag very efficiently as there was no detectable signal over background detectable in the red Gag.SNAP channel whereas the green eGFP signal was clearly visible and indicated that this particular cell had been transfected. In contrast to this, staining of cells after the shortest chase period tested in this experiment (30 min) yielded a detectable signal in the TMR-*Star* channel, which differed in intensity between individual cells. The overall signal intensity in the TMR-*Star* channel increased further at 60 min post blocking and reached an even higher level at the 2 h time point (120 min). Comparable results could be confirmed in several independent experiments (data not shown).

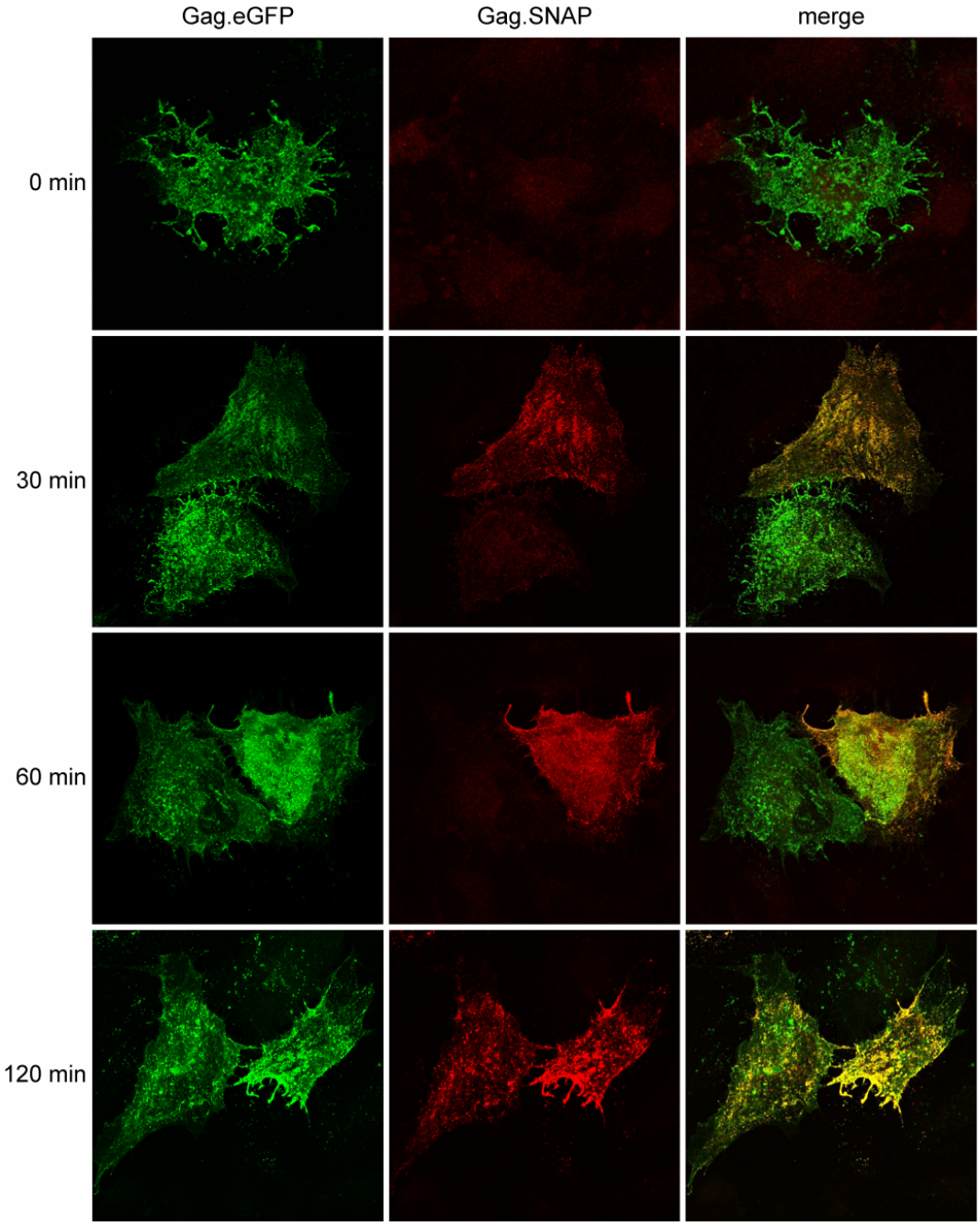

Fig. 3.10: Pulse chase labelling of Gag.SNAP. Pulse chase labelling of Gag.SNAP. HeLa cells were transfected with an equimolar mixture of pCHIV.eGFP and pCHIV.SNAP. At 24 h post transfection, cells were treated with BTP for 5 min at 37°C, washed 3 times with DMEM and incubated in DMEM at 37°C for the indicated chase periods of 0, 30, 60 or 120 min, respectively. Then, cells were stained with TMR-*Star* and fixed directly after the staining procedure. Embedded coverslips were imaged in a confocal Leica SP2 setting. Single confocal slices of representative cells are shown in the green (Gag.eGFP) and red (TMR-*Star*) channel and a merged picture of both.

No obvious difference in the distribution of both Gag-labels within the cell could be observed at any of the time points tested. Therefore, newly produced Gag protein did not seem to be transported to a single specific site but appeared to be quickly distributed relatively equal over the whole cell body. To narrow down the time that is needed to produce new SNAP-tagged Gag protein that can be labelled after the chase period, shorter time points were tested. Even the 5 min

chase yielded detectable TMR-Star signals (data not shown) which hints to a fast folding kinetic of the Gag.SNAP fusion protein.

3.1.1.6 Labelling of HIV^{SNAP} particles

Another application of the SNAP-tag introduced within the Gag protein consists of the use of the labelled particles in live cell experiments comparable to published studies where virus entry was investigated in real time using XFP labelled derivatives (e.g. [117, 127]). To this end, the possibilities to label HIV^{SNAP} particles *in vitro* was tested. Non-infectious HIV^{SNAP} particles were produced from transfected 293T co-transfected with pCHIV or an equimolar mixture of pCHIV and pCHIV.SNAP in combination with a construct coding for a fusion protein of Vpr and GFP, namely pVpr.eGFP [147]. The green fluorescent viral label Vpr.eGPF was introduced as a reference. Vpr.eGFP has been shown to be incorporated into HIV-1 particles in a quantitative manner [147] and shows very low background in non-viral particles. It therefore represents a good control to measure the labelling efficiency of SNAP-tagged particles by the membrane permeable SNAP-tag substrate TMR-*Star*. After purification through a sucrose cushion as described in 2.5.1, the particles were stained as described in 2.5.7. Briefly, 300 ng of particles were incubated with 2µM TMR-*Star* in the presence of 5 mM DTT at 4°C o/n and re-purified over a sucrose cushion. As a control, Vpr.eGFP labelled HIV particles not harbouring the SNAP-tag were treated in parallel to control for unspecific TMR-*Star* binding. In addition, HIV^{SNAP} particles were incubated with a solvent control to rule out possible bleed through from the GFP channel.

The labelled and purified particles were attached to fibronectin-coated coverslips and imaged in a wide-field fluorescence microscope. Particles were detected in the GFP channel and 10 z-stacks of 21 pictures each were taken at random positions of the coverslip in the green (GFP) and red (TMR-*Star*) channel. The results of this experiment are depicted in Fig. 3.11. Qualitative inspection of the images reveals that after labelling with TMR-*Star*, HIV^{SNAP} particle preparations showed strong punctuated particle signals in the red channel which colocalized to a great extent with the viral marker Vpr.eGFP in green (Fig. 3.11 A). In contrast to that, no signals in the TMR-*Star* channel were detected in control preparations (no SNAP-tag (HIV) or solvent control, respectively). For quantitative analysis, fluorescence micrographs were analyzed with the help of a semi automated ImageJ plug-in as described in 2.6.1. Briefly, maximum projections of both channels were filtered and individual signal spots were identified and counted. A new image depicting all picked spots was created for each channel which could then be used for colocalization analysis. For this, an overlay of both results images was created harbouring different numerical values for a spot found in either of the original channel images or in both which allowed to count the number of double labelled spots as well.

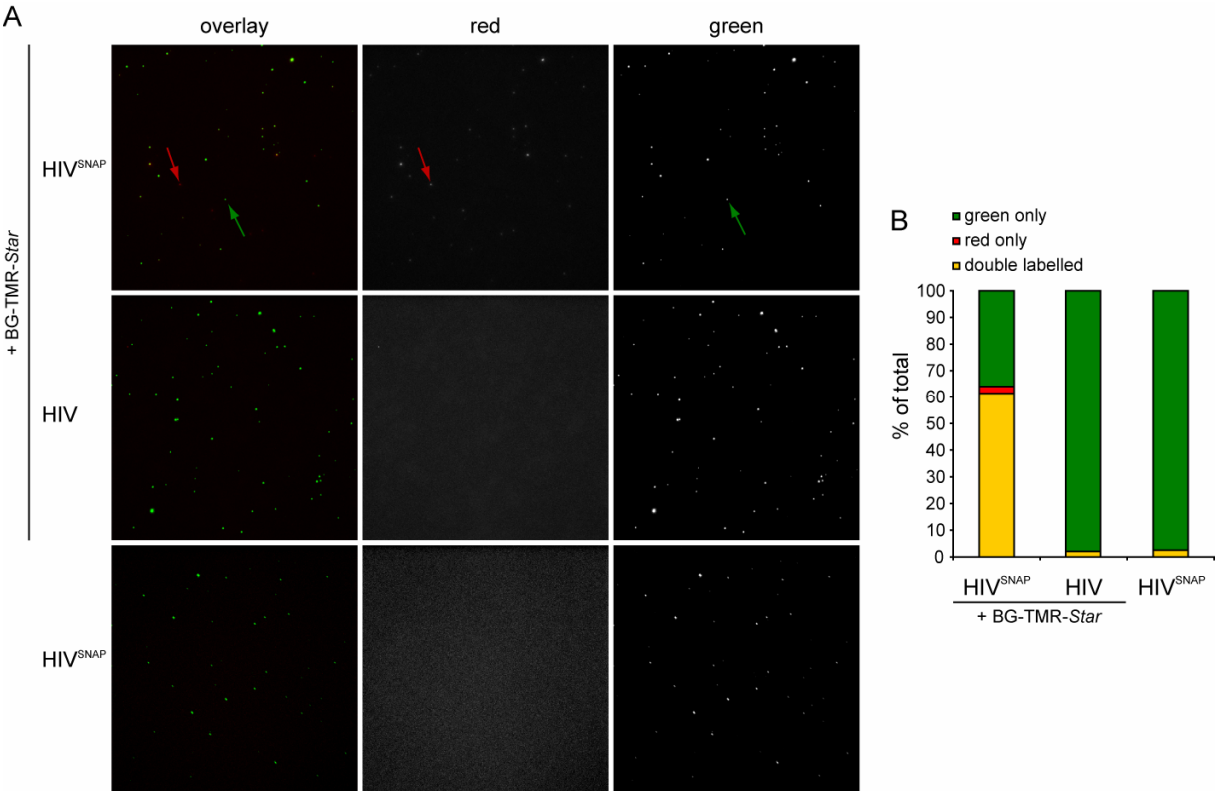

Fig. 3.11: Labelling of HIV^{SNAP} particles. Labelling of HIV^{SNAP} particles. HIV and HIV^{SNAP} particles incorporating Vpr.eGFP were produced from transfected 293T cells with pVpr.eGFP and pCHIV or an equimolar mixture of pCHIV and pCHIV.SNAP, respectively, and purified over a sucrose cushion. Particles were then labelled with TMR-*Star* (+ BG-TMR-*Star*) or treated with a solvent control and re-purified as described in 2.5.7. Particles were seeded on coverslips and imaged in a wide-field fluorescence microscope with a 100x oil-immersion objective. Z-stacks of 21 pictures each were taken at 10 random positions for each condition. (A) Maximum projections of representative fluorescence microscopic images are shown in the red and green channel as well as an overlay of both. Green and red arrows point to single labelled particles in the respective channel. (B) Double labelling efficiency was assessed with the help of a semi-automated ImageJ plug-in as described in 2.6.1. The graph shows the percentages of particles which were double labelled (yellow) or showed a signal in one of the channels exclusively (red and green, respectively). Average of 10 view fields for HIV^{SNAP} and HIV incubated in presence of substrate (+ BG-TMR-*Star*) or a solvent control are shown.

The percentage of double labelled particles (double) as well as particles only showing a signal in one of the two channels (red only and green only, respectively) are depicted in Fig. 3.11 B for all three samples. For HIV^{SNAP}, over 60 % of all spots were classified as double labelled. Only a minor fraction of signals (2.6 %) were found to be red only, indicating unspecific staining of non-viral structures within the sample. The remaining proportion of signals (36 %) was only detected in the green channel, indicating Vpr.eGFP labelled viral particles which were not successfully stained with TMR-*Star*. Only very low background staining was observed in the TMR-*Star* channel for particles not carrying the SNAP-tag (HIV, 2 %). A similar low number of double labelled particles (2.6 %) was observed in the solvent control sample of HIV^{SNAP}. Those particles most likely represent background fluorescence which can be assumed to be present in all other samples. The very low background in both controls indicated a very specific staining, which is in agreement with results from the previously described experiments in cells. Therefore, the

proposed strategy to use SNAP-tagged HIV derivatives in live cell imaging experiments could be accomplished with the above characterized newly established HIV^{SNAP} particles.

In conclusion, the insertion of the SNAP-tag into the ORF of HIV-1 Gag was well-tolerated by the virus. Particle release, morphology and entry into cells are not affected by the inserted tag. Infectivity was reduced, but could be restored in particles consisting of a 1:1 mixture of wt and tagged Gag proteins. Replication capacity was reduced but still detectable and the inserted tag proved to be stable over several replication cycles. The labelling of MA.SNAP was easily applicable for cells transfected with the constructs as well as viruses incorporating the tagged protein. Thus, the new labelling strategy for the HIV-1 MA protein presented here proves to be a versatile tool to study different aspects of the viral live cycle by microscopic techniques.

3.1.2 Fluorescently labelled HCV pseudoparticles to dissect the steps of virus entry

Although good progress towards an understanding of the early steps of the HCV replication cycle has been made since the establishment of tissue culture systems to study this virus, they are not yet understood completely. The use of fluorescently labelled HCV pseudoparticles (HCVpp) could help to dissect those early steps. Pseudoparticles are viral particles of a certain origin, in this case HIV-derived, which incorporate the envelope protein of a different virus, in this case HCV E1 and E2. This changes the tropism and mode of entry of the HCVpp accordingly [12]. HCVpp have previously been used by others to study the early steps of the HCV replication cycle [61, 148, 187] and results obtained with this system have been confirmed with the help of the infectious HCV cell culture system (HCVcc) [234].

In this study, fluorescent labelling of virus particles was achieved based on the previously established labelling of the MA protein of HIV [162]. I used unmodified HCV envelope glycoproteins incorporated into envelope protein deficient HIV derivatives carrying a MA.XFP fusion protein. This approach provides the unique opportunity to visualize the dynamic events of individual viral particles interacting with host cells and allows resolving distinct steps of the entry process. In particular, I dissected the first steps of entry, particle binding (chapter 3.1.2.2), endocytosis (chapter 0) and fusion (chapter 3.1.2.4), depending on CD81 expression and the presence of different stimulating or inhibiting factors.

3.1.2.1 Establishment of the system

In order to produce HCVpp which mimic HCV entry into host cells, the particles had to be devoid of HIV-1 Env proteins. For this purpose, subviral plasmids with a insertional frame-shift mutation in the beginning of the *env* gene were used. Cells transfected with pcHIV.Env(-) express all viral proteins except Nef and Env, since the plasmid harbours a deletion in the 3' end

of *nef* and a translational frame-shift mutation in the 5' of *env*. The plasmid does not contain LTR sequences and hence particles produced by transfection with this plasmid are non-infectious. The fluorescently labelled counterpart was constructed as described for the mCherry-tagged version in 2.2.4.1.

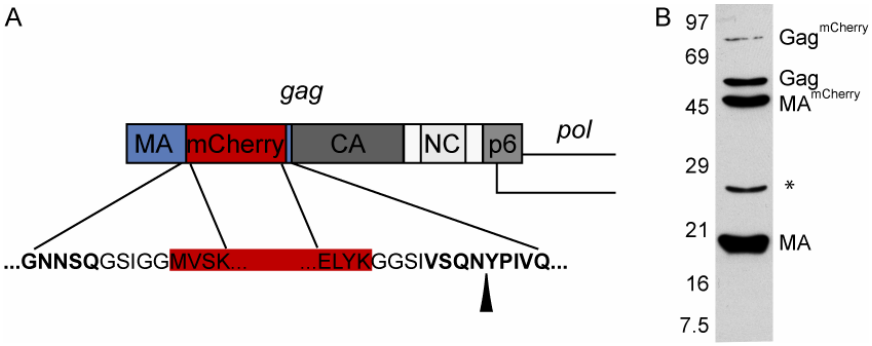

Fig. 3.12: Construction and characterization of a mCherry-tagged fluorescent HIV-1 derivative. (A) Schematic drawing of the HIV-1 gag ORF showing the *mcherry* gene (red) inserted between MA (blue) and CA (dark grey) coding regions. The expanded regions show the derived amino acid sequence at the domain borders, with HIV sequences displayed in boldface type and mCherry sequences shown in black type on a red background. An arrowhead indicates the PR cleavage site between MA and CA. (B) Western Blot analysis of HIV-1 derived particles. HIV-1 derivatives were generated by transfection of 293T cells with an equimolar mixture of pcHIV and pcHIV.mCherry, particles were purified from the supernatant and subjected to Western Blot analysis. The membrane was probed against the viral protein MA. Position of molecular mass standards is shown with numbers in kDa at the left and protein bands are labelled on the right. Asterisk indicates an unknown cleavage product of $MA^{mCherry}$.

The position of the mCherry label was chosen in exact analogy to the published pcHIV.eGFP derivative (Fig. 3.12 A; compare [162]). The modified Gag precursor was incorporated into particles produced from cotransfected 293T cells and showed protease processing comparable to wt Gag as shown by WB analysis. As represented in Fig. 3.12 B, an additional unidentified cleavage product of MA.mCherry could be detected (asterisk). Nevertheless, $HIV^{mCherry}$ particles were shown to be fusion competent and have successfully been used in a live-cell imaging study [117].

To incorporate the HCV genotype 1b (Con1) envelope proteins E1 and E2 into the viral lipid membrane, virus producing 293T cells were cotransfected with an additional expression plasmid, pcDNA3ΔCE1E2. WB analysis of particles purified from the supernatant by ultracentrifugation showed incorporation of the foreign Env protein, whereas no Env signal was detected in the control lacking an additional Env expression plasmid (Fig. 3.13 A). When incubated with target cells, for example the Huh-7 derived hepatocytic Lunet/CD81 cell line, the fluorescently labelled HCVpp (red dots) could readily be detected with a standard epifluorescence microscope (Fig. 3.13 B).

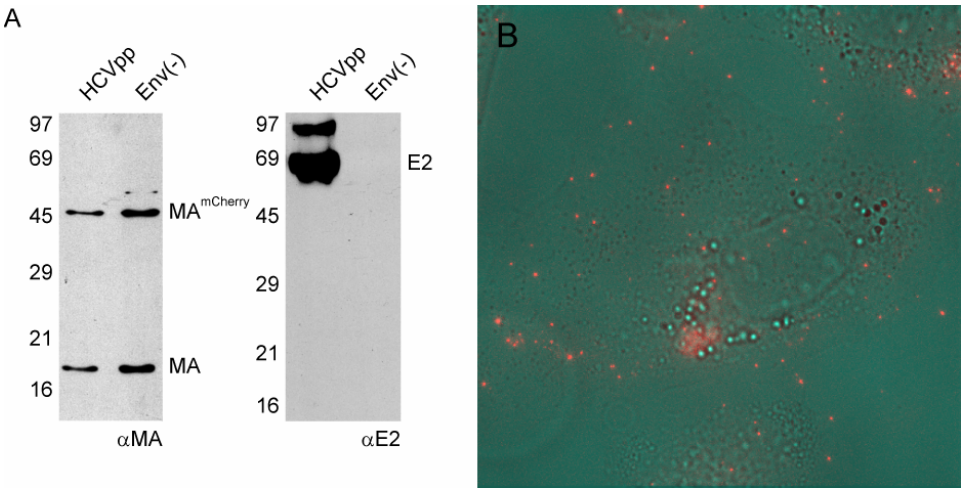

Fig. 3.13: Characterization of fluorescently labelled HCVpp. (A) Western blot analysis of virus particles purified by ultracentrifugation from 293T cells transfected with plasmids encoding for HIV.Env(-) and for the E1E2 of HCV (HCVpp) or the pCHIV.Env(-) alone (Env(-)). Membranes were probed against MA (left panel) and HCV E2 protein (right panel). Positions of molecular mass standards are shown with numbers in kDa at the left and protein bands are labelled on the right. (B) Overlay of bright field image and fluoerscence image of fluorescently labelled HCVpp (red) bound to Lunet/CD81 cells.

3.1.2.2 HCVpp binding to cells

Equipped with this useful tool, HCVpp binding to cells could be visualized and studied by microscopy. A virus binding assay based on fluorescently labelled HCVpp was established as illustrated in Fig. 3.14 and described in 2.5.2. Briefly, cells were seeded in 8-well chambered cover slides. After 24 h, cells were briefly pre-chilled on ice and fluorescently labelled virus was added and allowed to bind for 1 h on ice. This incubation in the cold was used to prevent particle endocytosis and other unspecific uptake into the cells. Subsequently, unbound virus was washed off with PBS and cells were fixed with cold PFA. Cell-bound virus particles were then imaged by wide-field fluorescence microscopy. In order to capture all virions bound, image stacks in z-direction were recorded covering the entire cell body.

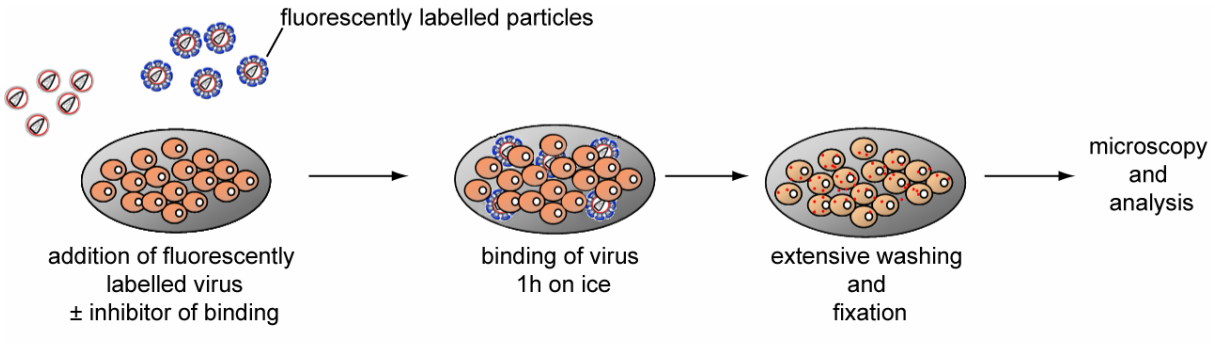

Fig. 3.14: Schematic illustration of the workflow of the virus binding assay. Details see text.

Image analysis was performed in a semi-automated system with the help of an ImageJ plug-in (based on a plug-in written by John Briggs). The workflow of this plug-in is depicted in Fig. 3.15. Maximum projections of fluorescence micrographs (Fig. 3.15 A) were transformed

with a bandpass filter to level out the background signal and to allow for single fluorescence spots of particles to be recognized more easily (Fig. 3.15 B). Then, an empirically set threshold was established to cut off the majority of background signals and to keep the signal intensity of individual viral particles (Fig. 3.15 C). Subsequently, an already implemented algorithm of ImageJ ("Analyze Particles…") was used to identify spots of a certain size and circularity. The location of each spot in x and y was recorded and output in a table. These coordinates were used to create a new combined image depicting the picked spots as crosses on top of the maximum projection image of the particle imaging channel, and either a brightfield image of the cell bodies or an image of a channel that depicted the autofluorescence signal of the cells in blue (Fig. 3.15 D). Either way, this overlaid picture was used to control for correct particle recognition and to manually count the approximate number of cells per image.

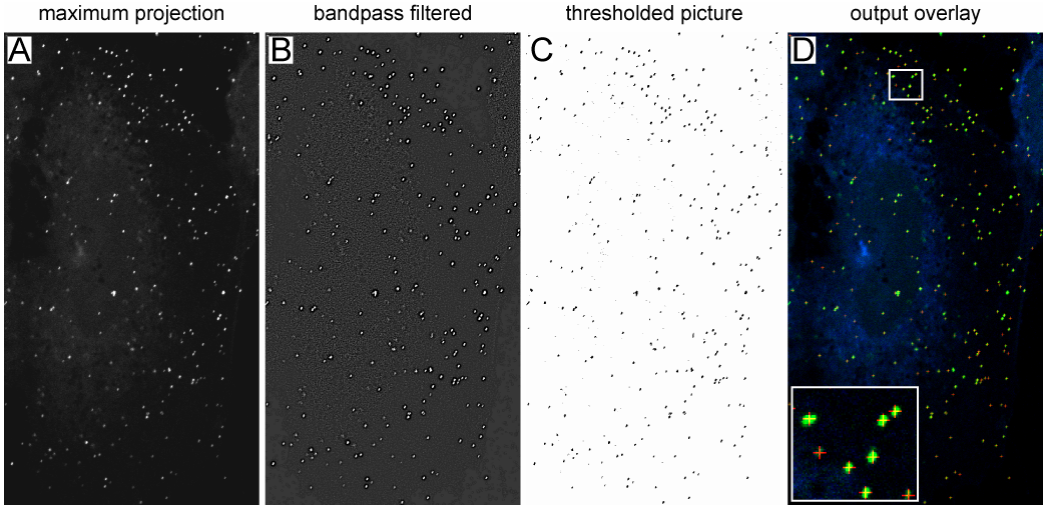

Fig. 3.15: Workflow of the "particle picker" ImageJ plug-in. Image output of the different steps within the "particle picker" plug-in are shown of an exemplary cell. (A) Maximum projection of a z-stack of fluorescence signals detected in the respective channel detecting individual fluorescently labelled viral particles. (B) Image after the bandpass filter to level out the background noise including autofluorescence. (C) Image after execution of an intensity threshold. Signals above threshold are depicted in black, whereas areas with signals below the threshold remain white. (D) To control for accuracy of the plug-in, an output file is created overlaying an image of the autofluorescence (blue) with the original maximum projection from (A) (green). The picked spots are displayed as red crosses. The inset in the lower left corner magnifies the boxed area from the top of the image to allow easier observation of the colocalization of green signals and red crosses.

As a proof of principle to test this new assay, I made use of the known fact that the addition of heparin decreases HCV binding to cells [122]. To this end, Lunet/CD81 cells were subjected to the virus binding assay in the presence of different concentrations of heparin. In addition, Heparinase I was used to enzymatically remove all heparin moieties from the cellular HSPGs, which should also abolish HCV binding to cells. For this purpose, Lunet/CD81 cells were incubated with 10 U of Heparinase I from *Flavobacterium heparinum* at 37°C for 30 min, washed with PBS and then subjected to the virus binding assay. Fig. 3.16 shows the representative results of two independent experiments. As expected, increasing amounts of heparin led to a decreased number of HCVpp bound to cells. The pre-treatment of cells with

Heparinase I also reduced particle binding to cells. Notably, Env(-) particles without any Env protein incorporated into their limiting membrane bound to the cells at comparable levels to HCVpp. This unspecific attachment of Env(-) viral particles could also be blocked by the addition of high amounts of heparin.

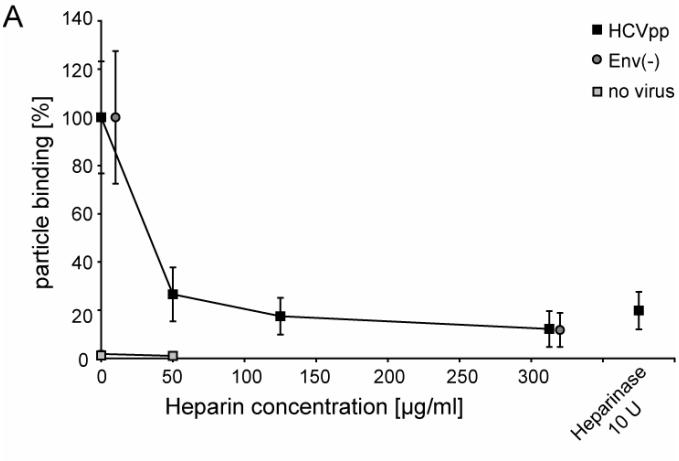

Fig. 3.16: Interference of heparin and Heparinase-treatment of cells with HCVpp binding to cells. Lunet/CD81 cells were incubated with HCVpp (black squares) or Env(-) particles (grey circles) in the presence of the indicated amount of heparin. Cells were subjected to the virus binding assay and particle binding per cell in the absence of heparin was normalized to 100 %. Mean values of 30 view fields and standard deviations are depicted as representative results from two independent experiments. In addition, one set of cells was pre-incubated with 10 U Heparinase I for 30 min at 37°C and HCVpp added only after this treatment (Heparinase 10 U). Images of mock treated cells served as a control (no virus).

After the successful proof of principle of this assay, the dependence of HCVpp binding to cells on the presence of HDL was tested, since a positive effect of those lipoprotein particles on HCVpp entry had been shown previously [56]. To this end, cells were subjected to the virus binding assay in the presence (HDL) or absence (no HDL) of 6 µg/ml HDL. Env(-) particles were always used as a control to monitor the contribution of unspecific attachment. As shown in Fig. 3.17, no clear correlation of particle binding to the presence of HDL, or the presence of the HCV Env proteins E1E2 could be observed on Lunet cells. The variability of particle binding on the single cell level was very high and is reflected by large and overlapping error bars.

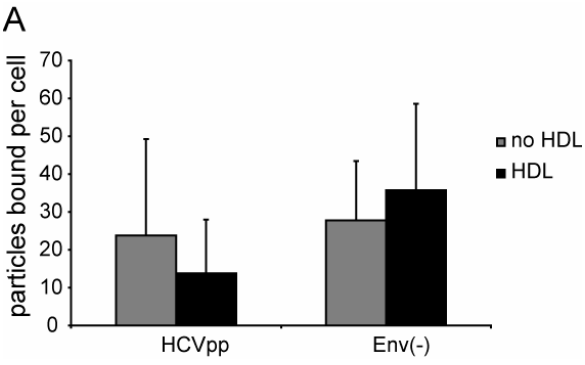

Fig. 3.17: Dependence of HCVpp binding on the presence of HDL. Lunet/CD81 cells were subjected to the virus binding assay with 100 ng fluorescently labelled HCVpp or Env(-) control particles in the presence (black) or absence (grey) of 6 µg/ml HDL. Mean number of particles bound per cell from 30 viewfields (corresponding to about 60 cells and a minimum of 500 particles per condition) and standard deviation is shown.

In conclusion, the high number of unspecifically bound Env(-) particles was found to be a problem for this single cell based method and hampered a detailed study of specific HCVpp binding to target cells. The newly established microscopic virus binding assay could nevertheless be shown to reflect known binding properties of HCV particles in dependence on HSPGs. Hence, this assay represents as a valuable tool to study binding of viruses to cells in a different setting (compare 3.1.3).

3.1.2.3 HCVpp uptake

The next step in HCV entry after the attachment to cells and receptor binding is the endocytic uptake of particles. In order to study this step in the viral replication cycle, an analogue assay to the virus binding assay described previously was established. After prebinding of virus particles and washing off excessive virus the cells were warmed up to 37°C and cellular uptake of particles was allowed for 1 h. In order to be able to monitor the efficiency of cellular endocytic uptake, cells were simultaneously incubated with transferrin coupled to Alexa 488 and mCherry labelled HCVpp. Transferrin has been shown to be taken up into cells by clathrin-mediated endocytosis, representing a reliable marker for endocytic uptake. As shown in Fig. 3.18, particles and transferrin only bound to the cell surface when cells were imaged after incubation with virus at 4°C, a temperature that precludes bulk endocytic uptake. When cells were warmed to 37°C, massive particle uptake could be observed. Also, endocytosed tranferrin could be observed in the green channel, whereas no obvious overall co-localization was detectable.

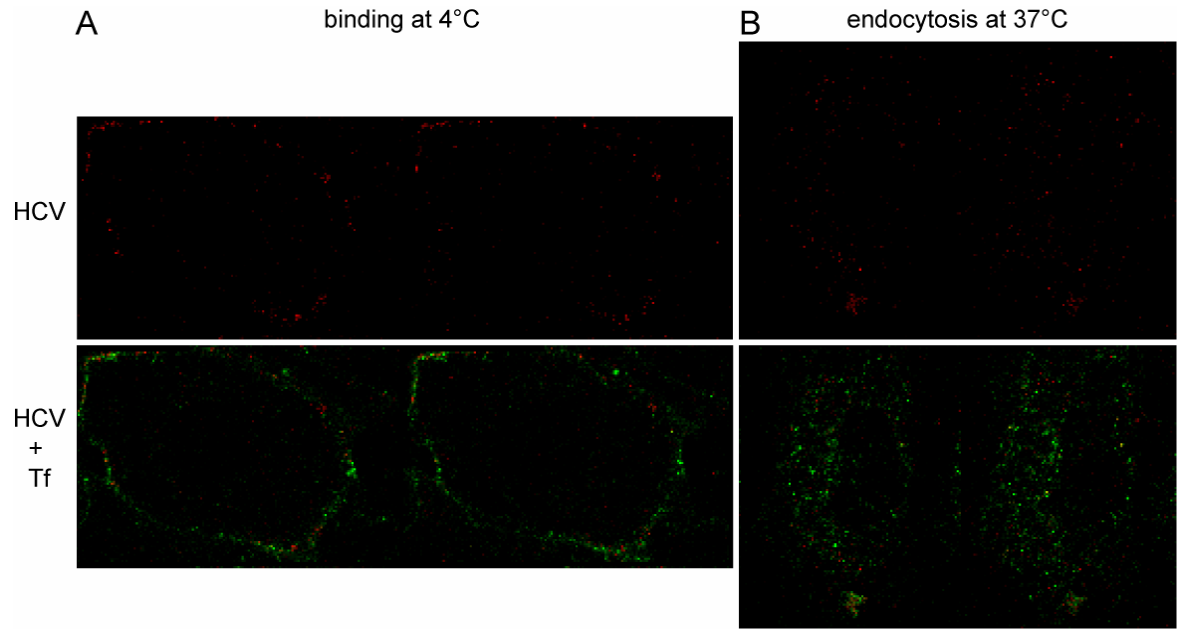

Fig. 3.18: HCVpp binding to the cell surface and endocytosis. Lunet/CD81 cells were incubated with mCherry labelled HCV^{mCherry}pp in the presence of transferrin-Alexa 488. Incubation was either conducted at 4°C for 30 min to monitor binding (A) or a subsequent warming of cells and incubation at 37°C was included to allow endocytosis (B). Cells were then fixed and z-stacks recorded with a confocal microscope. Representative fluorescence images of the red channel (HCV^{mCherry}pp – HCV, upper panel) and an overlay with the Transferrin (Tf) signals in the green channel (HCV + Tf, lower panel) are shown.

In line with the virus binding assay, no dependence of particle uptake on the presence of HCV Env could be observed on Lunet cells. Furthermore, the presence or absence of CD81 on the cell surface or blocking CD81 interaction with a neutralizing antibody did not influence the efficiency of HCVpp uptake (data not shown).

3.1.2.4 HCVpp fusion

Although many systems have been used to study the early steps of HCV entry, no system has yet been established to exclusively investigate the step of virus-cell fusion. To this end, I made use of a virion fusion assay that is well-established for HIV, the β-Lactamase assay (BlaM assay) [35]. The activity of the enzyme β-Lactamase which is incorporated into virus particles and released upon fusion into the cytoplasm of the target cell can be measured by a shift in emission wavelength of a florescent substrate. In order to use this assay for HCVpp, I adapted and optimized several steps, as the simple inclusion of Vpr.BlaM into HCVpp and the use of standard assay conditions did not yield reliable results (Barbara Müller, personal communication).

In a first step the amount of incorporated BlaM fusion protein was varied in HIV-derived particles pseudotyped with the glycoprotein of Vesicular Stomatitis Virus (VSV), below referred to as VSVpp. These pseudoparticles were chosen due to their very high entry efficiency so that virus input amounts could be kept minimal. Titration of these viral particles on HeLaP4 cells showed increasing BlaM activities with increasing amounts of cotransfected Vpr.BlaM expressing plasmid (pMM310), as seen in Fig. 3.19 A. In parallel, the particles were monitored for Gag processing in WB analysis with antibodies raised against the HIV-1 MA protein. Here, a strong increase in unprocessed Gag precursor protein could be detected with increasing amount of pMM310, which reached a plateau at 12.5 µg of cotransfected pMM310 (Fig. 3.19 B). Due to this, 10 µg pMM310 input per 10 cm dish of 293T cells during virus production was chosen as a compromise between increased entry efficiency (Fig. 3.19 A) and decreased Gag processing (Fig. 3.19 B). The signal of HCVpp entry could further be enhanced by prolonged incubation times (Fig. 3.19 C) as well as by the addition of 6 µg/ml HDL during virus incubation (Fig. 3.19 D). Increasing amounts of HCV Env-expressing plasmid on the other hand did not improve the entry efficiency (Fig. 3.19 E). In contrast, a threefold increase of E1E2-expressing plasmid even led to a decrease in entry efficiency.

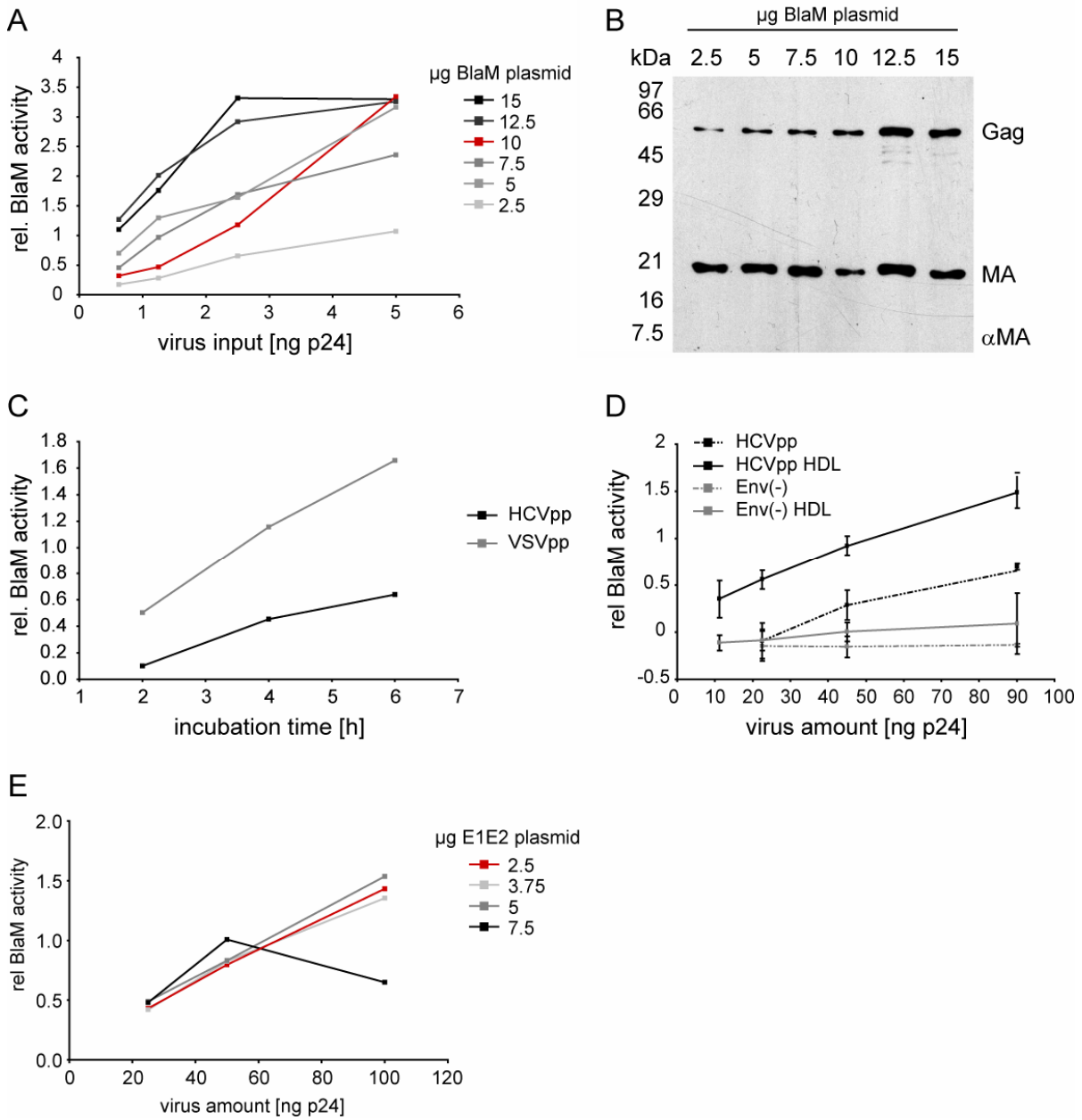

Fig. 3.19: Optimization of the β-Lactamase virion fusion assay for HCVpp. (A and B) Effect of amount of BlaM on entry efficiency. (A) VSVpp incorporating different amounts of Vpr.BlaM fusion protein were produced by cotransfection of the indicated amounts of pMM310 (BlaM plasmid). Purified viruses were titrated on Lunet/CD81 cells, the BlaM assay was performed as described and relative BlaM activity measured in a plate fluorimeter. (B) Viral particles from (A) were subjected to WB analysis with an antibody against HIV-1 MA protein to control for processing of Gag protein. Position of molecular mass standards is shown with numbers in kDa at the left and protein bands are labelled on the right. (C) Effect of incubation time on entry efficiency. Vpr.BlaM-containing HCVpp and VSVpp were produced as described and incubated with Lunet/CD81 cells for different time periods before addition of BlaM substrate and proceeding with the BlaM assay. Virus input: 100 ng p24 HCVpp, 1 ng p24 VSVpp. (D) Effect of HDL on particle entry. BlaM-containing HCVpp (black) and Env(-) control particles (grey) were titrated on Lunet/CD81 cells in the presence (solid lines) or absence (dotted lines) of 6 µg/ml HDL and BlaM assay was performed. Mean values of triplicate measurements and standard deviations are depicted. (E) Effect of E1E2 amount on entry efficiency. HCVpp incorporating different amounts of E1E2 were produced by cotransfection of the indicated amounts of pcDNA3ΔCE1E2 (E1E2 plasmid), titrated on Lunet/CD81 cells and BlaM assay was performed.

To test the specificity of the modified BlaM assay, the entry efficiency of HCVpp on cells expressing high (Lunet/CD81) or very low (Lunet/V) amounts of CD81 [121] was compared. The importance of CD81 for HCV entry has been proven in different systems and therefore offers a good possibility to test the validity of the HCVpp-adapted BlaM assay. VSVpp, which can enter both cell lines equally well, served as a control.

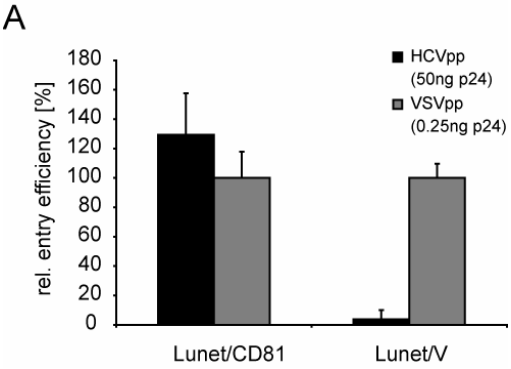

Fig. 3.20: Dependence of HCVpp entry on the presence of CD81. Entry efficiency of HCVpp (black) and VSVpp (grey) was tested with the BlaM assay on two different cell lines, Lunet/CD81 and Lunet/V, respectively. To obtain similar raw values of BlaM activity, different virus inputs had to be used (50 ng p24 equivalent for HCVpp and 0.25 ng p24 equivalent for VSVpp). Normalized entry efficiency in comparison to VSVpp of triplicate measurements with standard deviation is depicted.

Fig. 3.20 shows the entry efficiency of HCVpp in comparison to VSVpp. Note that due to much lower entry efficiencies of HCVpp, different concentrations of virus input were used to yield comparable BlaM acitivity (50 ng p24 HCVpp vs. 0.25 ng p24 VSVpp). Whereas HCVpp entered readily into CD81-expressing Lunet/CD81 cells, no BlaM activity could be detected after incubation with Lunet/V cells. In contrast to that, VSVpp entry was similar in both cell types. With this, the specificity of the BlaM assay adapted to HCVpp had been proven and several factors which had been shown to influence the early steps of replication of HCV could be tested regarding their influence on HCVpp fusion. To this end, the BlaM assay was performed in the presence of different agents that could potentially play a role in HCVpp fusion: HDL, oxidized high density lipoprotein (oxLDL), produced as described in 2.3.5, two different inhibitors of early endosome acidification, Concanamycin A (ConA) and Bafilomycin A (BafA), antibodies raised against CD81 (αCD81) and CD4 (αCD4) and two concentrations of Heparin.

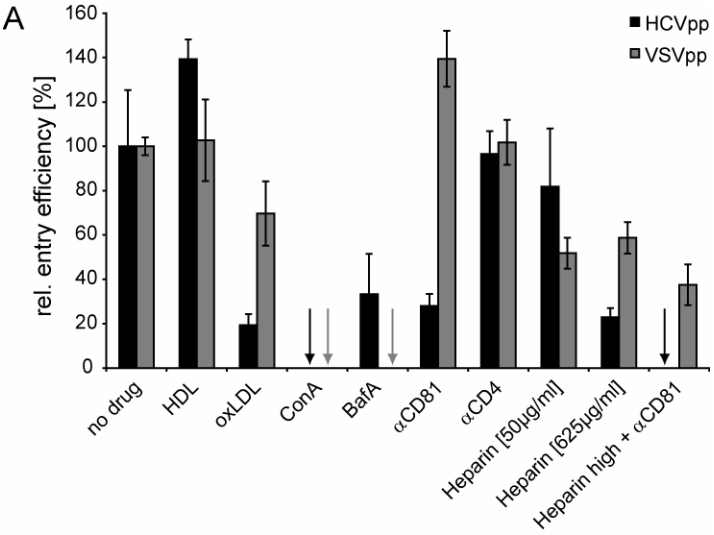

Fig. 3.21: Dependence of HCVpp and VSVpp fusion on different agents. Entry efficiency of HCVpp (black) and VSVpp (grey) was tested on Lunet/CD81 cells with the BlaM assay. Viruses were added in the presence of 6 µg/ml HDL, 100 µg/ml oxLDL, 5 nM Concanamycin A (ConA), 25 nM Bafilomycin A (BafA), 1.5 µg/ml antibody raised against CD81 (αCD81) or CD4 (αCD4), 50 or 625 µg/ml Heparin or a combination of 625 µg/ml Heparin and CD81 antibody (Heparin high + αCD81). Entry efficiencies were normalized to the values in the absence of drug. Mean values of triplicate measurements and standard deviations are shown.

As a control, VSVpp were subjected to the same treatment. In the case of the endosome acidification inhibitors, cells were preincubated for 45 min at 37°C and the drugs were also present during the overnight incubation with BlaM substrate, while the other compounds were only present during the incubation with virus at 37°C.

The relative entry efficiencies of both pseudoparticle types is shown in Fig. 3.21. Whereas HDL increased the entry efficiency of HCVpp, it did not have any effect on VSVpp. OxLDL had a negative effect on both types of pseudoparticles, although HCVpp were affected to a higher degree. Both inhibitors of endosome acidification strongly inhibited or completely blocked VSVpp and HCVpp entry. While both antibodies used did not reduce VSVpp entry, HCVpp entry efficiency was reduced more than threefold in the presence of αCD81, and HCVpp entry levels stayed stable in the presence of αCD4 antibodies. Treatment of cells with heparin blocked entry of HCVpp in a concentration dependent manner, while VSVpp was only reduced to about 50 % at both concentrations tested. The combination of the high heparin concentration with αCD81 antibody could block HCVpp entry completely, whereas VSVpp entry levels were comparable to the heparin-only treated samples.

In summary, the BlaM virion fusion assay was successfully adapted to HCVpp via several optimization steps. It provides a useful tool to study the early steps of HCV entry with fusion as an endpoint. The influence of several factors on those steps could be shown, confirming previous findings with systems looking at later time points in the replication cycle. In addition to the establishment of the virion fusion assay for HCV, microscopy-based assays were developed to investigate the steps preceding virus fusion with the target cell, namely virus uptake and cell binding as a first step. The validity of the binding assay was confirmed by showing the possibility to compete with cell binding of HCVpp by the addition of Heparin. Particle binding and endocytosis was nevertheless shown to be independent of the HCV Env proteins as well as the presence of CD81 on the cell surface. Both factors were in turn confirmed to be crucial for HCVpp cytosolic entry.

3.1.3 Fluorescently labelled HIV-1 derivatives

The microscopy-based virus binding assay established for HCVpp was also used to study cell binding of HIV-1. Binding efficiency to different cell lines as well as the dependence of virus binding on the newly identified virus restriction factor CD317/Tetherin was investigated.

3.1.3.1 Binding to different cell lines

Unspecific attachment of viral particles to heparan sulfate proteoglycans (HSPGs) on the cell surface can occur independent of the Env protein, as shown for HCVpp in comparison to Env(-) particles (see Fig. 3.16). In order to study the specific binding of HIV-1 particles to target

cells and eliminate background noise due to unspecific attachment, I sought to find the optimal conditions for HIV-1 cell binding. For this purpose, two different T-cell lines were compared in respect to efficiency of virus binding. SupT1 cells have been shown to possess a very low surface level of HSPGs (M. Lampe, personal communication).

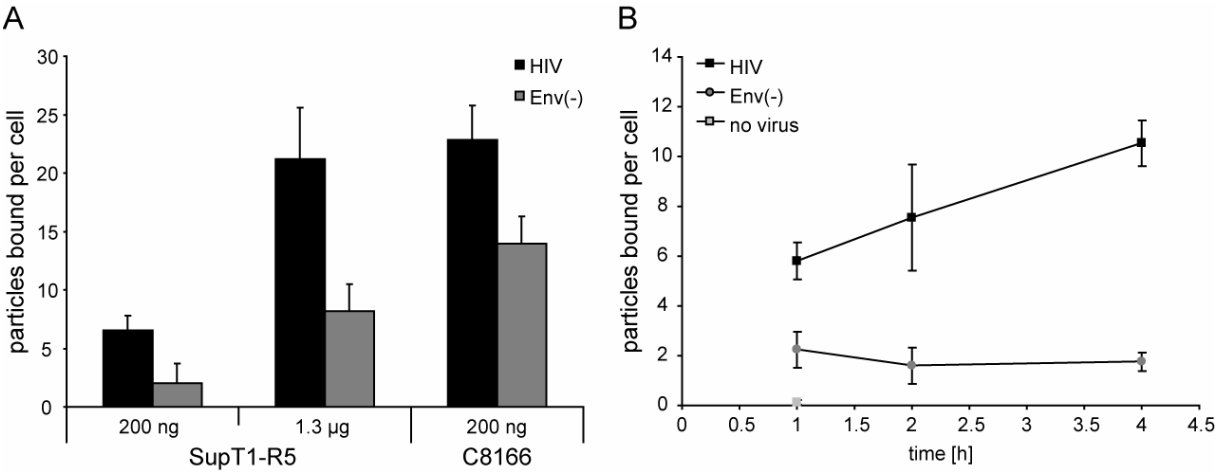

Fig. 3.22: HIV-1 binding to cells. HIV^{mCherry} (black) and Env(-)^{mCherry} (grey) were subjected to the virus binding assay and mean numbers of particles bound per cell determined. Standard deviations from app. 300 cells per condition are depicted. (A) Particle binding to SupT1-R5 cells with two depicted virus input concentrations of p24 equivalent, in comparison to C8166 cells. (B) Time course of particle binding to SupT1-R5 cells (200 ng p24 input). A control of mock treated cells (no virus, light grey) is included.

200 ng of fluorescently labelled HIV or Env(-) particles were incubated with 1x10^6 cells for 30 min on ice and subjected to the virus binding assay. As depicted in Fig. 3.22 A, HIV-1 binding was shown to be dependent on the presence of Env on both cell lines. Those differences were statistically significant as determined by student's T test ($p<0.0001$). The amount of bound particles was furthermore found to be dependent on the cell line, since on average 3.5 times more particles bound to C8166 than SupT1-R5 cells. This difference could be overcome by increasing the particle input (Fig. 3.22 A, 1.3µg p24), hinting at a concentration dependent mechanism. The time-dependence of Env-mediated cell binding could furthermore be shown in a time course experiment. While HIV binding to SupT1-R5 cells increased over time, unspecific Env(-) binding stayed at baseline over the course of 4 h (Fig. 3.22 B).

3.1.3.2 Binding to cells in dependence on CD317/Tetherin

The virus binding assay was furthermore applied in the context of a study on the distribution of the newly identified virion restriction factor CD317/Tetherin (also known as Bst-2 or HM1.24). CD317 is an interferon-inducible cellular protein that is able to inhibit the release of a variety of enveloped viruses by the proposed mechanism of physically tethering already budded particles to the plasma membrane [19, 165]. The accessory HIV-1 protein Vpu has been shown to counteract this restriction mechanism by downmodulating overall cell surface expression of CD317. The ultrastructural distribution of CD317 on the cell surface of infected and uninfected

cells had so far not been investigated. Incorporation of endogenous CD317 into budding viruses had been proposed but not been finally verified to this point [151, 181].

In a study utilizing mainly electron microscopy of cells endogenously expressing CD317, it was found to be downregulated from the plasma membrane in the presence of HIV-1 including Vpu (infection or transfection of cells). At the same time it was found to be enriched in budding structures of HIV-1 as well as in cell-bound and cell-free virions independent of the presence of Vpu [82]. In summary, these results indicated that CD317 function critically depends on the amount of CD317 at the plasma membrane as opposed to the virus membrane. This conclusion led to the hypothesis of differential binding of free CD317-containing HIV-1 particles depending on the surface expression levels of CD317 in a proposed CD317-dimer interaction model [181]. To test for this hypothesis, I produced fluorescently labelled $HIV^{mCherry}$ particles by transfection of HeLa P4 cells and used those in the virus binding assay. HeLa P4 cells were chosen for particle production in this experiment to mimic the situation of particles budding from producing cells and reattaching to the same cell in presence of CD4, to include the potential influence of CD4-dependent virus binding. To mimic HIV-1 infection of the cells on which binding was investigated, HeLa P4 cells were transfected with plasmids coding for Vpu.GFP or GFP prior to their employment in the binding assay.

Surface expression of CD317 was controlled for in microscopy- (Fig. 3.23 A) and flow cytometry-based experiments (Fig. 3.23 B). In a representative set of images, the downmodulation of CD317 (rαBst-2, blue in overlay) can clearly be seen in the two highly Vpu.GFP-positive cells (marked with asterisks) in Fig. 3.23 A. The two cells that show an intermediate Vpu.GFP signal (GFP, green in overlay) show an intermediate phenotype in CD317 surface expression. $HIV^{mCherry}$ signals ($HIV^{mCherry}$, red in overlay) can be detected distributed over the cell body independent of the other two channels. The second line of verification in regard to CD317 downregulation can be seen in Fig. 3.23 B. Cells harvested in parallel to the performance of the virus binding assay were stained against CD317 surface expression and monitored in a flow cytometer. CD317 expression (y-axis) is plotted against GFP expression (x-axis) for both transfection conditions. A clear decrease in CD317-Alexa 660 signal could be observed with medium to high expression of Vpu.GFP, whereas the expression of GFP alone did not correlate with the amount of CD317 surface expression. For clarity, mean fluorescence intensities (MFI) for the different expression levels of GFP are shown in the upper part of the plots. Quantification of the virus binding assay is depicted in Fig. 3.23 C with single dots and squares representing individual cells and the mean of virus bound per cell represented by horizontal lines. The difference between the number of particles bound to non-transfected versus Vpu.GFP expressing cells with a clear phenotype in CD317 downmodulation was shown to be very minor. On average 46 particles were found to be bound to non-transfected cells and only 39 to Vpu.GFP expressing

cells, resulting in a difference of 7 ± 4 particles. Statistical analysis using the unpaired two-tailed student's t-test showed a non-significant p-value of 0.1071.

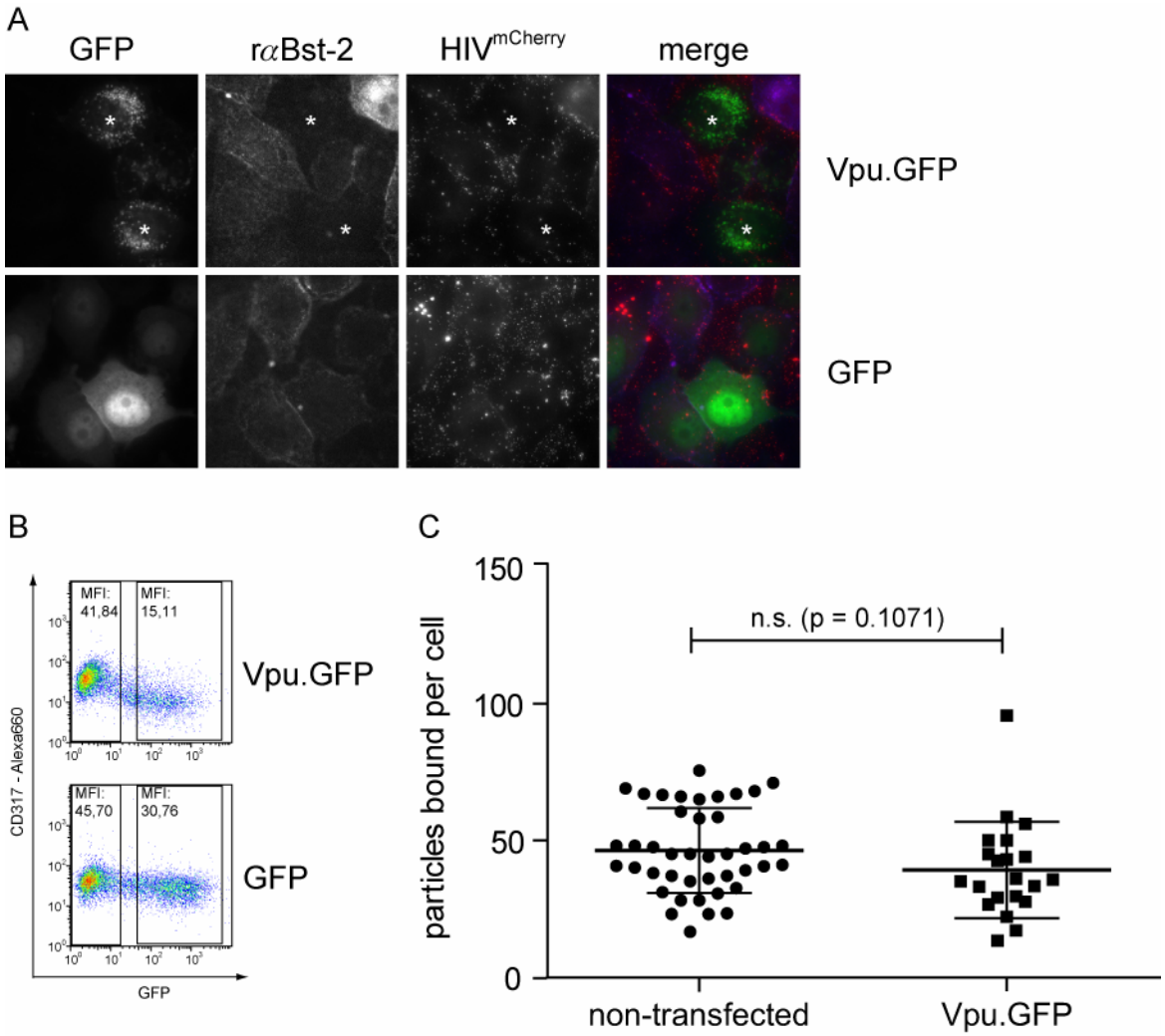

Fig. 3.23: HIV-1 binding to cells in dependence of CD317/Tetherin surface expression. (A) HeLa P4 cells were transfected with pVpuGFP or peGFP-N1, treated at 48 h with 20 U/ml Heparinase I for 45 min at 37°C washed, and purified HIV^{mCherry} produced from transfected HeLa P4 cells (200 ng p24) allowed to bind for 1 h at 16°C. Cells were labelled for CD317 surface expression with anti-Bst-2 and Atto647N-conjugated antibodies and cell nuclei were counterstained with Hoechst33258. Fluorescence images of the three individual channels and an overlay (GFP, green; HIVmCherry, red; αBst-2, blue) is shown. Asterisks indicate cells that have been taken into account for quantification. (B) FACS analysis of CD317 surface expression of HeLa P4 cells transfected for 48 h with pVpuGFP or peGFP-N1 using a mouse anti-CD317 and anti-mouse-Alexa660. Numbers represent the mean fluorescence intensity (MFI) for cell surface-exposed CD317 on cells with medium to high GFP expression and of GFP-negative cells, respectively. (C) Quantitation of virions bound per cell by virus binding assay. Only cells with clear CD317-phenotype (medium to high surface staining for non-tranfected cells (n=42) or no surface staining for Vpu.GFP expressing cells (n=21), respectively) from triplicate transfections were taken into account. Single values (dots and squares), mean values (horizontal bars) and standard deviations are shown in a scatter plot. n.s. = not significant.

In summary, no correlation of virus binding to cells on the surface expression level of CD317 could be shown. However, the utility of the newly established virus binding assay could be proven by this application.

3.2 Patient- and drug-specific models of HIV-1 entry

HIV-1 entry is a multistep process, involving interactions between the viral Env protein and the cellular receptor CD4 and a CXCR4 or CCR5 co-receptor molecule. The viral co-receptor tropism is at least in part determined by the third variable loop (V3) of Env. With the approval and use of co-receptor antagonists as a new class of antiviral drugs, a detailed understanding of co-receptor tropism and accurate prediction of co-receptor usage of virus from patient samples has become essential.

The goal of this study was to develop a better understanding of the dependence of viral entry efficiency and sensitivity towards entry inhibitors on critical cellular and viral determinants. The interplay of viral Env sequence with receptor and co-receptor density on the cell surface, and prototype entry inhibitors from different classes (receptor blocker, co-receptor antagonist, fusion inhibitor) has been investigated. Computational models based on this comprehensive set of quantitative data should lead to a better understanding of the mechanisms and development of resistance against HIV entry inhibitors.

3.2.1 Experimental systems to create multidimensional data

This study was designed as a multidimensional analysis of HIV-1 entry. Therefore, several parameters had to be varied within a fixed system measuring HIV-1 entry efficiency. The variable parameters were chosen to be

- surface concentration of CD4 receptor molecules on the target cell,
- surface concentration of CCR5 co-receptor molecules on the target cell,
- V3-loop sequence of HIV-1 Env protein and
- presence of different concentrations of prototype entry inhibitors.

In this chapter, the different experimental systems used to create this multidimensional setup will be described.

3.2.1.1 Receptor and Co-Receptor expression on different cell lines

To make use of different surface expression levels of the HIV-1 receptor CD4 and on of the co-receptors, CCR5, we took two different approaches. On the one hand, I made use of the 293 derived Affinofile cell line, established by the Lee lab [105] which can be induced to express a wide variety of CD4 and CCR5 levels independent of each other. Those cells offered the possibility to examine the dependence of virus entry efficiency on the presence of different

concentrations of those two receptors. On the other hand, T-cell lines which may mimic the natural target cells of HIV-1 infection more closely were utilized: the T-cell line pairs C8166 [204] and C8166/CCR5 [69] (below referred to as C8166-R5) as well as SupT1/CCR5 (below referred to as SupT1-R5). Both parental T-cell lines (C8166 and SupT1 [136]) express CD4 and CXCR4, but no CCR5, which was in both cases added by stable transfection, resulting in the cell lines C8166-R5 and SupT1-R5, respectively.

To analyze the surface concentration of the three receptors on all cell lines used, quantitative flow cytometry was performed. With the help of the BD QuantiBRITE kit, the amuont of antibody molecules bound per cell (ABC) can easily be estimated. To this end, monoclonal antibodies directly coupled to Phycoerythrin (PE) recognizing the receptors of interest (CD4, CCR5 and CXCR4) were utilized to stain the respective cells. Beads with 4 distinct surface labelling densities of PE molecules were used to calibrate correlate the number of ABC with identical settings of the FACS machine. The resulting standard curve was then used to correlate the fluorescence intensity measured from an unknown sample to PE-molecules bound per cell, corresponding to the estimated amount of antibody molecules bound per cell.

To analyze the surface expression of CD4 and CCR5 on the dually inducible Affinofile cell line, cells were seeded in 24-well plates in presence of different concentrations of the two inducing agents, Tetracycline (Tet) to induce CD4 expression and Ponasterone A (PonA) to induce CCR5 expression, respectively. 18 to 24 h after induction, cells were detached from the culture plate, stained with the different PE-coupled antibodies and subjected to quantitative FACS measurement as described in 2.4.6.

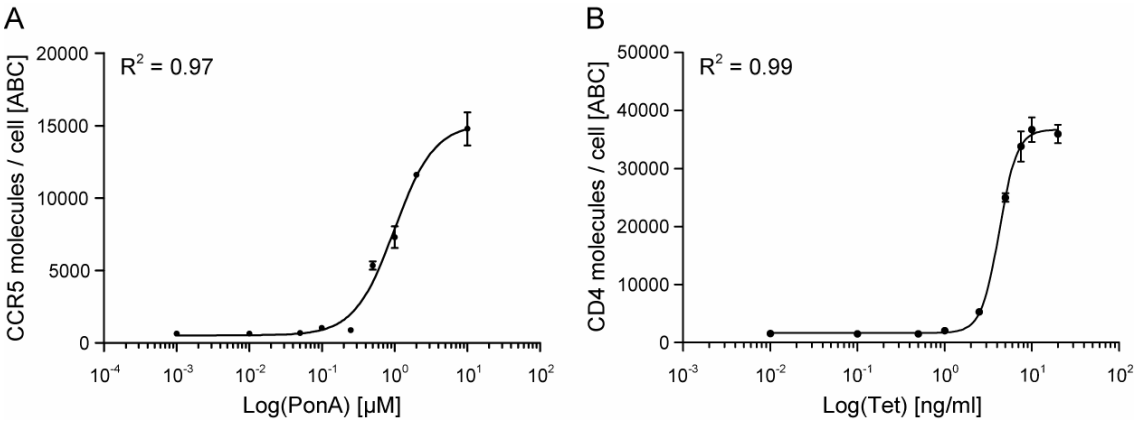

Fig. 3.24: HIV-1 Co-receptor and receptor density on Affinofile cells upon differential induction of expression. Affinofile cells were seeded in multiwell plates and induced with increasing concentrations of Ponasterone A (A) or Tetracycline (B). 18 h post induction, cells were detached with 5 mM EDTA and stained with PE-coupled antibodies raised against CCR5 (A) or CD4 (B) for 45 min on ice. Samples were then subjected to flow cytometry analysis in comparison to QuantiBRITE-PE beads. Antibody molecules bound per cell were estimated from the standard curve. The graphs display mean values with standard deviations of triplicate measurements of CCR5-antibody molecules bound per cell (A) or CD4-antibody molecules bound per cell (B) and a four parameter dose-response curve fitted to the data. PonA = Ponasterone A, Tet = Tetracycline, ABC = antibody molecules bound per cell. R^2 describes the correlation of data and fit.

Induction of CCR5 surface expression with PonA was concentration dependent (Fig. 3.24 A). Increasing concentrations of 0.1 µM up to 2 µM PonA led to a steep increase in CCR5-expression, followed by saturation at higher concentrations, with an calculated effective concentration inducing 50 % of response (EC_{50}) of ~1 µM. In the presence of 1 µM PonA and concentrations above, the cells started to grow in islands and appeared less vital with increasing numbers of cells rounding up and detaching from the culture plate (data not shown). Thus, 1 µM was chosen as the upper limit of PonA concentration. In contrast to this, the expression of CD4 could be induced up to saturating amounts on the cell surface without obvious damage to the cells. CD4 saturation was reached at a Tet concentration of 7.5 ng/ml to 10 ng/ml with app. 35'000 CD4 ABC (Fig. 3.24 B). EC50 of 4.2 ng/ml was calculated and a working range between 0.5 and 7.5 ng/ml Tet was chosen for further experiments. Of note, expression of residual amounts of CD4 (~1'200 ABC) could also be detected in the absence of inducing agent. This "leakage" of the inducible promoter could not be detected for CCR5 expression, where the background level of CCR5 molecules/cell was in the same range as background of cells without any antibody staining (no stain, ~500 ABC).

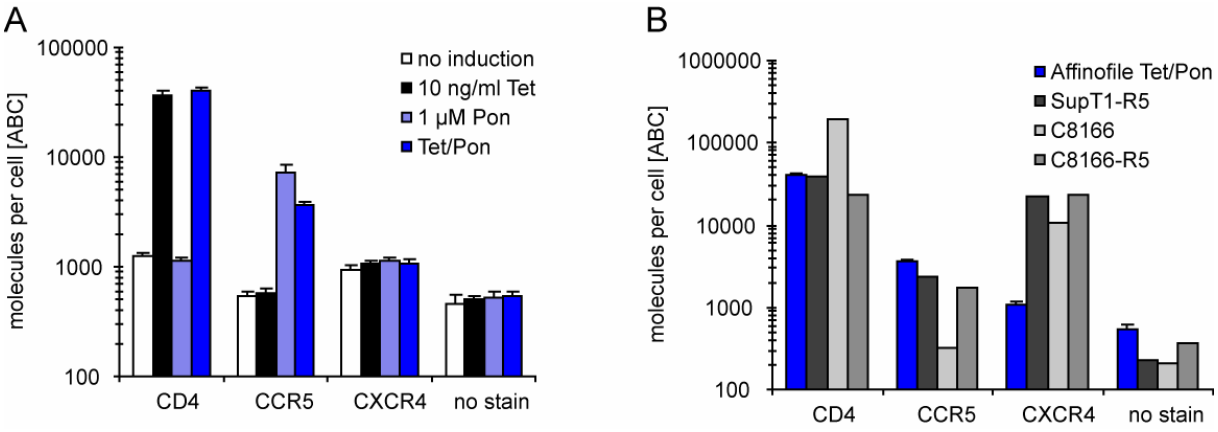

Fig. 3.25: Amount of receptor molecules on the surface of different cell lines determined by QuantiBRITE flow cytometry analysis. (A) Affinofile cells were induced as depicted in the graph. 18-24 h later, cells were detached with EDTA, stained against the receptor molecules CD4, CXCR4 or CCR5, respectively. Mean values of triplicate measurements and standard deviations are shown (B) $1x10^6$ SupT1-R5 (dark grey), C8166 (grey) or C8166-R5 (light grey) cells were stained using antibodies raised against the receptor molecules CD4, CXCR4 or CCR5, respectively. The graphs show the estimated number of antibody molecules bound per cell (ABC). Background of unstained samples is shown as a reference (no stain). For comparison, the data set of dually induced Affinofile cells (Affinofile Tet/PonA, dark blue) is also depicted in (B).

Fig. 3.25 shows a comparison of receptor expression on the surface of different cell lines. In panel (A), the amount of receptor and co-receptor molecules, CD4, CCR5 and CXCR4, respectively, is shown for different induction conditions of Affinofile cells. The maximum concentrations of both inducting agents, 10 ng/ml Tet and 1 µM PonA, were chosen for this analysis. As described above, the level of CCR5 remained at background without induction (white bars), whereas a low basal expression of CD4 could be detected. CD4 expression levels could be increased by more than one order of magnitude by the addition of 10 ng/ml Tet (black

bars), without affecting CCR5 levels. The addition of 1 µM PonA (blue bars) led to an increase of CCR5 expression by at least one order of magnitude with CD4 levels remaining at the same low basal expression level as without induction. Upon dual induction (dark blue bars), CD4 levels increased to comparable amounts as with single Tet induction, whereas the level of CCR5 induction was app. twofold lower than with PonA induction alone. With respect to CXCR4, which should not be affected by Tet or PonA, the different induction conditions had a small but detectable impact. Affinofile cells that were induced with Tet, PonA or a combination of both showed an app. twofold increase in CXCR4 surface expression. To compare the range of receptor surface levels of Affinofile cells with more physiological target cells, the analysis was expanded to human T-cell lines. As shown in Fig. 3.25 B CXCR4 levels on Affinofile cells were more than one order of magnitude lower than on the T-cells (~1'500 ABC as compared to ~10'000-20'000 ABC). CD4 was detected to comparable amounts of about 40'000 molecules per cell on dually induced Affinofile cells, SupT1-R5 and C8166-R5 cells, whereas C8166 cells showed increased CD4 surface levels of over 100'000 ABC. As expected, C8166 cells showed no expression of CCR5 on the cell surface. The CCR5-expressing T-cell lines on the other hand displayed about 2'000 CCR5 ABC, which in a similar range than the level on dually induced Affinofile cells. Overall, the surface expression levels of CD4 as well as CCR5 detected on the Affinofile cell line was found to be comparable to physiologically more relevant T-cell lines.

In summary, the cell lines tested here represented a panel of model cells suitable for differential expression patterns of HIV-1 receptor and co-receptors. Thus, they represent a valuable tool to investigate different surface levels of CD4 and CCR5 without the necessity to utilize different cell lines.

3.2.1.2 Selection of patient-derived V3-loop sequences

In order to keep provide a system with reduced complexity for initial modelling approaches we decided to compare isogenic virus derivatives varying only in the V3-loop of Env. To this end, a pseudotyping system was used for the production of viral particles, with a subviral plasmid (pCHIV.Env(-)) harbouring a translational frame-shift in the beginning of the *env* ORF to provide all viral proteins except for Env, and expression plasmids encoding the NL4-3 Env carrying modified V3-loop sequences inserted as described in 2.2.4.3. Briefly, V3-loop sequences were amplified by PCR from patient's samples and inserted into a pCAGGS-based expression vector encoding the complete NL4-3 Env protein.

In order to obtain a comprehensive set of variants for initial experiments, 8 divergent patient derived V3-loop sequences were selected. To this end, we made use of a pool of patient samples from the Bonn haemophiliac cohort, collected in the 1980s [111]. Those samples, kindly provided by Rolf Kaiser (Department of Virology, University Hospital of Cologne, Cologne, Germany) provide a very valuable tool as by the time of sample collection, no anti-retroviral

drugs had been introduced into the market, yet, so that all patients were completely therapy-naïve. In addition, naturally evolved broadly variable viral quasispecies pools without the selective pressure of drugs are present in those samples, which is in contrast to modern patient's samples.

Viruses from 94 patient samples had been propagated in PBMCs over a period up to 3 months and characterized according to their CPE (cytopathic effect) phenotype. The samples were grouped according to SI (syncytium inducing) or NSI (non-syncytium inducing). Bulk sequencing of the virus populations was performed for a subset of the samples[1]. 60 different V3-loop sequences of viruses isolated from 36 patient samples yielded evaluable sequences, which were then further characterized by our collaborators with the help of computational biology[2]. For this purpose, the sequences were subjected to several different analyses, including Splitstree analysis [99], analysis of their localization in sequence space, genotypic prediction outcome of three different methods (geno2pheno [216], WebPSSM [104], 11/25 rule [67]) and the overall clustering trend.

patient #	clone #	phenotype	V3-loop sequence	bioinformatical analysis
220	X4_C3	SI	CTRPNNNTIK**G**ISI--GPGRAVIATR**K**IIGDIRQAHC	**clearly X4**
286	X4_7b	SI	CTRPHNNI-K**R**HRIHIGPGRSFHTTK**G**ITGNIRQAHC	**clearly X4**
409	X4_C15	SI	CTRPGNNTRK**S**ITR--TPGRVIYATG**A**IIGDIRQAHC	**ambiguous - X4**
651	X4_25a	SI	CTRPNNNTRK**S**VRI--GPGDIFITT-**D**IIGNIRQAHC	**ambiguous - X4**
685	X4_C26	SI	CTRPNNNIMR**R**IHI--GPGRAFYATR**K**IIGNIRQAHC	**clearly X4**
822	R5_C29	NSI	CTRPNNNTRR**S**IHI--APGRAFYTTG**Q**IIGDIRQAHC	**clearly R5**
838	R5_C30	NSI	CTRPNNNTRK**S**IHI--GPGKAFYTTG**E**IIGDIRQAHC	**clearly R5**
924	X4_36b	NSI	CFRPNNNTRK**G**IHI--GPGRAFYTTG**E**IIGDIRRAYC	**ambiguous - X4**
	NL4-3	SI	CTRPNNNTRK**S**IRIQRGPGRAFVTIG**K**I-GNMRQAHC	**clearly X4**
	NL4-3 R5		CTRPNNNTRK***G***I***H***I**--**GPGRAFYTTG***E***I***I***G***DI***RQAHC	**clearly R5**

Tab. 3.1: Comparison of selected V3-loop sequences with those of two standard clones NL4-3 and its R5-tropic variant, NL4-3 R5. The table shows CPE determined for original patient's isolate, amino acid sequence of the V3-loop of the respective clone and overall outcome of bioinformatical analysis. Point mutations within the NL4-3 R5 V3-loop that led to the R5-tropism are highlighted in bold italic. Positions 11 and 25 with respect to the consensus subtype B V3-loop sequence are highlighted in bold type. V3-loop sequences yielding a clear prediction for X4-tropism (clearly X4) are labelled in red, those yielding a clear prediction for R5-tropism (clearly R5) are labelled in blue and those receiving an ambiguous result (ambiguous) are labelled in black and have the geno2pheno tropism prediction assigned (X4 or R5). SI = syncytium inducing, NSI = non-syncytium inducing.

Tab. 3.1 summarizes the characteristics of the V3-loop sequences selected for this study.

[1]Virus propagation, RNA isolation and sequencing performed by Saleta Sierra-Arragon and Rolf Kaiser, Department of Virology, University Hospital of Cologne, Cologne, Germany.

[2]Computational biology analysis was always performed by Kasia Bozek, AG Lengauer, Department of Computational Biology and Applied Algorithmics, Max-Planck-Institute for Computer Sciences, Saarbrücken, Germany.

NL4-3 represents the V3-loop sequence of the standard X4-tropic laboratory HIV-1 strain NL4-3 [1]. To obtain a comparable R5-tropic standard clone, NL4-3 R5 was used, a clone harbouring several point mutations in the V3-loop conferring R5-tropism (changes highlighted in bold italic in Tab. 3.1). The patient # indicates the AIDS number of the patient carrying the virus species with the respective sequence, whereas the clone # is derived from the geno2pheno prediction outcome (X4 = X4-tropic, R5 = R5-tropic) in combination with internal numbering system of the sequences obtained. The character "C" within the clone # indicates that sequencing of the isolate yielded a single clonal sequence, whereas samples lacking the "C" had ambiguous nucleotide sequences that could be arranged in several variants of which only one sequence was cloned for our analyses. The vast majority (63 of 94) of all viruses expanded in culture were shown to have a SI-type CPE. This is in part reflected in the selection, as over 50 % of the clones (5 of 8) also showed this phenotype. All V3-loop sequences selected had a length of 33 to 36 aa, with different degrees of sequence overlap. For better visualisation of differences, amino acid sequences are aligned and gaps are filled with a dash (–) in Tab. 3.1. Prediction of the 11/25 rule (positively charged aa at position 11 and/or 25 indicates a SI phenotype [67]) corresponded to the actually determined CPE phenotype for all clones, except for X4_C15 and X4_25a. After computational analysis of all sequences, the clones were either labeled "clearly X4" (marked with red color in all following schemes), "clearly R5" (marked with blue color in all following schemes) or "ambiguous" (marked with black or purple color in all following schemes) if the bioinformatic analyses yielded conflicting outcomes.

The location in sequence space of all selected variants is depicted exemplarily in a Splitstree analysis in Fig. 3.26. Splitstree analyses provide the basis to depict phylogenetic networks taking into account also conflicting relations. Here, every individual dot represents the location of one V3-loop sequence from a randomly selected sample of the Los Alamos Database (www.hiv.lanl.gov). Line distances between individual sequences in the graph represent the relative degree of relatedness between the respective V3-loop sequences, whereas the branches depict different possible connections between the sequences. R5 sequences (blue dots) tended to form more compact clusters with higher sequence similarity, whereas X4 sequences (red dots) varied to a higher degree (compare also [24]). The clones considered ambiguous (black labels) did not follow this overall trend or fell in between the clear boundaries of X4 and R5 clusters.

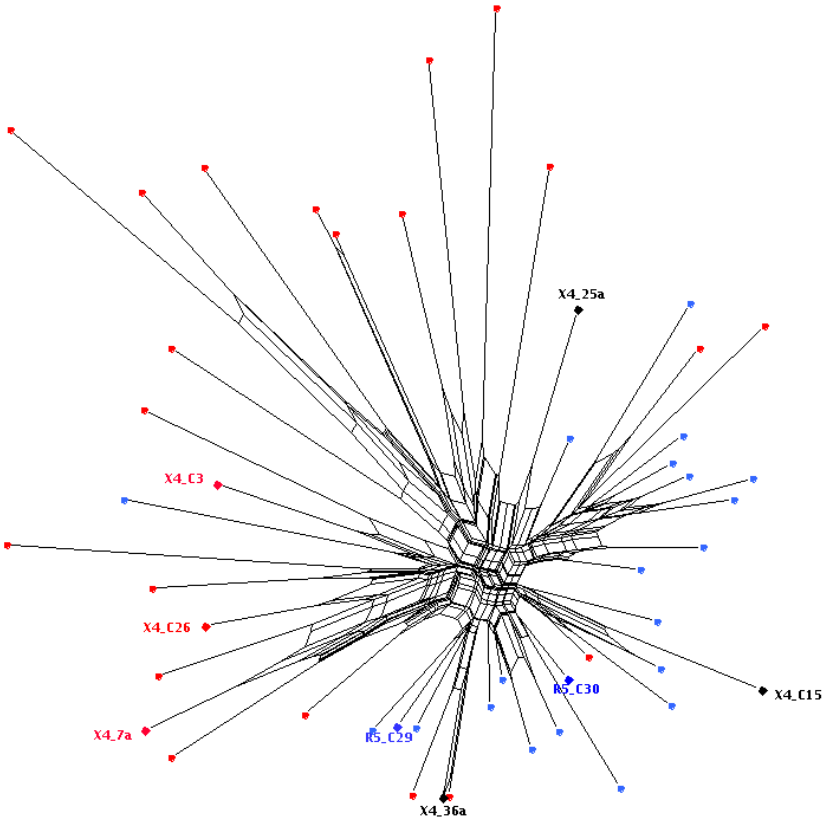

Fig. 3.26: Splitstree analysis of patient derived V3-loop sequences. V3-loop sequences selected for the study were subjected to Splitstree analysis together with random sequences from the Los Alamos Database (www.hiv.lanl.gov). Sequences that obtained a R5-tropic prediction outcome according to geno2pheno analysis (or phenotypic data from LA DB) are labelled in blue, whereas sequences predicted to be X4-tropic are labelled in red. The sequences selected for the current study are labelled with the respective names. Black labels correspond to sequences that were judged to be "ambiguous" (see below for details).

In combination with the usage of prototype drugs from of the class of entry inhibitors, these systems allowed the variation of the desired parameters, surface concentration of receptor and/or co-receptor molecules on the target cell, and V3-loop sequence of the Env protein on the virus independently of each other. Hence, a reliable system to monitor entry efficiency had to be chosen to study the dependencies of HIV-1 entry efficiency on all those factors.

3.2.2 Two systems to measure entry efficiency of HIV-1

The method of choice to investigate HIV-1 entry independent of any further steps of the viral replication cycle is the so-called β-Lactamase virion fusion assay (referred to below as BlaM Assay) as described by Cavrois and colleagues [35]. Briefly, viral particles are produced that, by a fusion to Vpr, incorporate the bacterial enzyme β-Lactamase which is delivered to the cytosol of the target cell upon fusion of viral and cellular membrane. The presence or absence of β-Lactamase in the target cell can then be visualized by loading of cells with a cleavable fluorescent substrate (CCF2) that shows different emission wavelengths in its cleaved (blue) or un-cleaved (green) state. This method was used for the analysis of T-cell lines but could, due to high background signals, not be used in combination with the Affinofile cell line. Hence, I used an additional entry assay, namely GFP transduction of cells. To this end, viral particles incorporating a self inactivating (SIN) vector encoding for GFP [257], were produced and viral entry could be detected by the green fluorescence of target cells 48 h after transduction.

3.2.2.1 FACS-based read-out for BlaM assay

The BlaM assay can be evaluated by flow cytometry using a 405 nm laser to excite the BlaM substrate CCF2. This method allowed the parallel determination of expression of the three relevant surface proteins CD4, CCR5 and CXCR4, respectively, could be monitored with the help of simultaneous immunostaining. Cells that had been incubated for 6 h with BlaM carrying virus at 37°C were subsequently loaded with BlaM substrate over night at room temperature, then fixed and stained against the three receptors with directly labelled primary antibodies. To control for the possibility of virus-induced receptor downregulation, the time point of staining was carefully evaluated. Staining of cells before incubation with the virus (green), before the overnight incubation (pink) or before fixation (light blue) yielded comparable results (Fig. 3.27), whereas overnight incubation (orange) with the antibody increased the overall staining due to increased incubation time and temperature (room temperature vs. 4°C for all other samples). As unspecific antibody-uptake during this prolonged incubation time at elevated temperature could not be excluded, this method was however considered inferior to the other three and staining after fixation was finally considered as the method of choice.

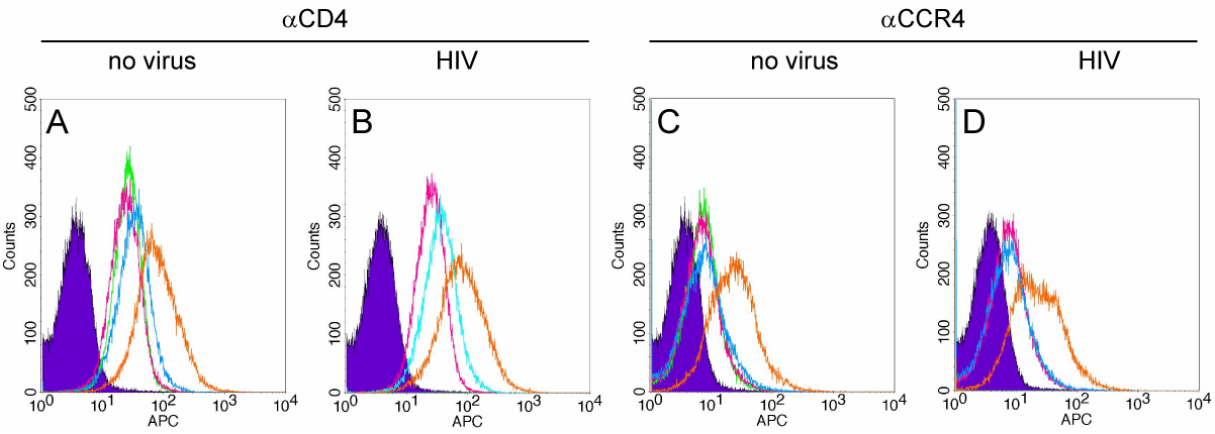

Fig. 3.27: Comparison of different antibody staining time points. C8166 cells were subjected to BlaM assay in presence of no virus (A, C) or 10 ng BlaM-containing virus (HIV; B, D) and stained for receptor (A, B) and co-receptor (C, D) at different time points with APC-coupled antibodies. APC-fluorescence spectra (arbitrary units) of cell population are depicted as histograms. The different coloured lines represent the population at the individual staining time points: before infection (green), after infection (pink), overnight (orange) and after overnight incubation (light blue). The purple-shaded population represents the distribution of an unstained control.

Overlapping fluorescence spectra of CCF2 and the chromophors used to detect the receptors (compare Fig. 3.28) demanded compensation controls during data recording. In the standard experiment, the following antibody labels were used: CD4-APC-H7, CCR5-PE and CXCR4-APC, with the need of proper compensation between PE and the green emission of CCF2 resulting from excitation of its FITC moiety (CCF2 – green) by the 488 nm laser and standard compensation between APC and APC-H7.

A

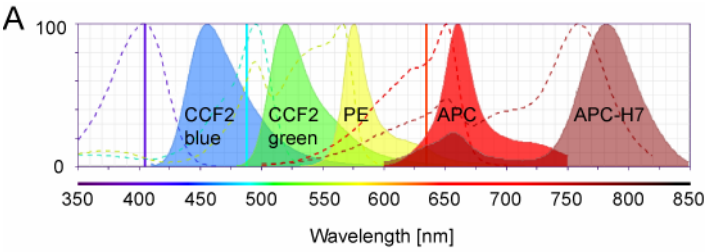

B

Fluorochrome	Ex_{max} [nm]	laser [nm]	Em_{max} [nm]
CCF2 - blue	409	405	447
CCF2 - green	409 (488)	405	520
PE	(493) 566	488	575
APC	650	635	660
APC-H7	(650) 757	635	780

Fig. 3.28: Characteristics of fluorochromes used for FACS analysis. (A) Fluorescence excitation (dotted lines) and emission (filled curves) spectra for all fluorochromes used, including both spectra of cleaved (blue) and uncleaved (green) CCF2, PE (yellow), APC (red) and APC-H7 (dark purple). The three utilized laser lines (purple = 405 nm, turquoise = 488 nm, orange = 635 nm) are depicted as vertical lines. (B) Table of excitation (Ex) and emission (Em) maxima (max) with additional local maxima indicated in brackets. The wavelength of the respective laser used for excitation is indicated in the column "laser".

To allow for analysis of single cell data, the data recorded by flow cytometry had to be extracted and converted to formats that could be used with the computational methods developed by our cooperation partners. In a first step, the standard binary fcs-files were converted to an ASCII text format using the program FCSExtract Utility [73] to access the data. To preserve the compensation corrected fluorescence intensity values throughout this extraction, original FACS-data had to be stored in the FCS2.0 file format, as FCS3.0 files keep raw values for the data and only apply a compensation matrix within the flow cytometric analysis program. Data extracted like this could then be analysed using methods established for the computer software R [190] and other specialized software.

This workflow allowed the simultaneous observation of entry efficiency and receptor expression of CD4, CCR5 and CXCR4 on the single cell level.

3.2.2.2 Microscopy-based read-out for Affinofile cells

For all T-cell lines utilized in this study, the above described FACS-based read-out represented the most convenient technique. For the adherent Affinofile cell line, on the other hand, this read-out was found to be very time-consuming and could only be operated in a very low-throughput scale. Therefore, a semi-automated medium-throughput microscopy based system was established instead[3]. To this end, cells were seeded in 96-well plates. As Affinofile cells are HEK293-derived and hence very lightly adherent, several different plates were tested in regard to cell adherence and performance in fluorescence microscopy: Corning #3603 black with clear bottom, Corning #3340 with CellBIND surface black with clear bottom, BD PureCoat™

[3]In cooperation with Christoph Sommer, AG Hamprecht, Heidelberg Collaboratory for Image Processing (HCI), Interdisciplinary Center for Scientific Computing (IWR), University of Heidelberg, Heidelberg, Germany

black with clear bottom and BD Biocoat^{R} clear plates. The latter were excluded due to fluoerescence spill from well to well. The specially treated CellBIND plate from Corning proved to be most suitable with regard to the amount of cells that could be kept on the plates after the multistep staining protocol. Cells were seeded in the presence of the desired concentration of Tet and PonA and transduced with 5 ng p24 equivalent of isogenic viruses harbouring the different Env proteins. After 48 h cells were fixed with 3 % PFA and briefly incubated with 2 % BSA in PBS to block unspecific antibody binding sites. Afterwards, a sequential immunostaining protocol against CCR5 and CD4 was applied. Monoclonal mouse antibodies raised against CCR5 (clone 2D7) were used in combination with a secondary antibody coupled to Alexa 568 and a directly labelled monoclonal CD4-Alexa 647 mouse antibody (clone RPA-T4) was used to monitor CD4 surface expression. Nuclei were counterstained with Hoechst 33258 and cells were then subjected to automated fluorescence microscopy. For high-throughput image acquisition a fully automated epifluorescence Scan^{R} screening microscope equipped with the Scan^{R} acquisition software (Olympus Biosystems GmbH, Münster, Germany) was used. Images were acquired with a 10x objective at 16 positions per well in four channels with the respective filter sets: DAPI to detect Hoechst stained nuclei, GFP to detect transduced cells, TexasRed to detect CCR5 stained with Alexa 568 and Cy5 to detect CD4 stained with Alexa 647. Segmentation of cell nuclei was performed as described in [22]. Then, a maximum projection of the TexasRed and Cy5 channel was created which was then used to segment the single cell bodies. For this purpose, the images of the two channels had to be corrected for a minor location shift to obtain completely overlapping frames. The segmentation of cell bodies was computed using the seeded watershed algorithm as described in 2.6.2. Briefly, the segmentation line was started at the previously identified nuclei boundaries and allowed to grow until they hit a sharp intensity cut in the segmentation channel or another growing border from an adjacent cell. In addition, the growing of segmentation borders was restricted to an empirically fixed size cutoff to avoid oversized cell bodies when no clear intensity cut was hit.

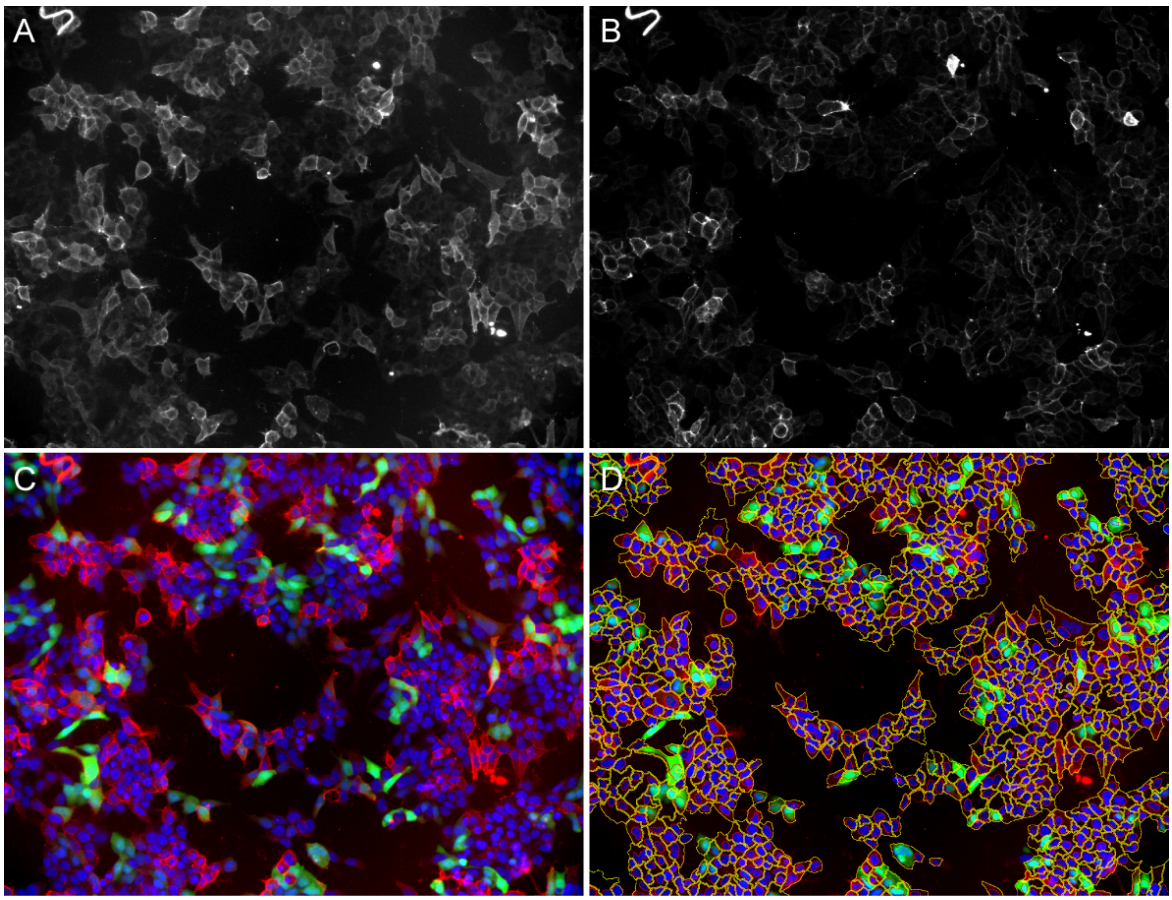

Fig. 3.29: Steps of a microscopy based single cell read-out. Affinofile cells were induced with 2.5 ng/ml Tet and 0.25 µM PonA and after 18 h transduced with 5 ng p24 equivalent of a GFP-coding HIV-1 derivative. Cells were fixed with 3 % PFA 48 h p.t. and stained against CD4 and CCR5 expression. Cell nuclei were counterstained with Hoechst 33258 and cells imaged in an automated fluorescence microscope at a magnification of 10x. 16 images per well were taken in 4 channels (DAPI for nuclei, CCR5-Alexa 568, CD4-Alexa 647 and GFP), maximum projection of CCR5 and CD4 pictures calculated and cells were segmented based on DAPI and this maximum projection. Fluorescence intensities in CCR5, CD4 and GFP-channel were then read-out based on the single segmented cells. Fluorescence microscopic images of a representative experiment are shown for CCR5 staining (A) and CD4 staining (B). Overlay of DAPI (blue), maximum projection of CCR5 and CD4-channels (red) and GFP channel (green) is shown in (C). (D) graphically depicts the segmentation out-put with the picture from (C) overlaid with the segmentation of nuclei (blue lines) and cell bodies (yellow lines).

In Fig. 3.29, the consecutive steps of the image analysis are shown. Fig. 3.29 A and Fig. 3.29 B show microscopic images of CCR5 and CD4 surface expression immunofluorescence staining in the TexasRed and Cy5 channel, respectively. Here, the staining of the cellular plasma membrane could be observed, while also the whole cell body appeared to show some background signal. This background signal was higher in the CCR5 staining (Fig. 3.29 A), which exhibited overall higher fluorescence intensities than the CD4 staining. In both images, the presence of different fluorescence intensities of single cells was clearly visible. Comparison of both images showed stronger signal in either one of the channels for some single cells, representing the independent induction of CD4 and CCR5 in each single cell. With the chosen induction conditions, nevertheless most of the cells showed an intermediate fluorescence intensity. A segmentation of cell bodies based on one of the channels showed promising results, but could be

improved by combining both channels in a maximum projection (data not shown). With this method, cells that only expressed one of the receptors induced for could more easily and reliably be subjected to segmentation as a signal in one of the channels was sufficient to guide the segmentation algorithm. Fig. 3.29 C shows an overlay of DAPI (blue) and GFP (green) channels with the maximum projection of TexasRed and Cy5 channels (red) is shown. To visualize the segmentation outcome of this set of images, Fig. 3.29 D displays an overlay of Fig. 3.29 C with segmented nuclei (red lines) and segmented cell bodies (yellow lines). For the majority of cells within one image, this segmentation yielded an exact representation of the cell body's contour. Reliability of this segmentation was dependent on cell density. Also, a negligible fraction of cell bodies were depicted as merged or mal-shaped in the segmentation. Nonetheless, the developed algorithm reliably allowed segmentation of cells which could then be used to quantify the fluorescence intensities of every single cell in the three channels GFP, TexasRed and Cy5 to determine if the single cell had been transduced (GFP positive) and expressed CCR5 (TexasRed) and/or CD4 (Cy5) on the surface.

The results of individual images were extracted as a table (csv format), which could be merged for further analysis. An average of 800 nuclei were counted per image, resulting in over 10'000 cells included in the analysis per single well, compared to 10'000 to 300'000 cells per single condition in the FACS-based measurements.

3.2.3 Establishment of single-cell analyses of entry efficiency[4]

The data output from both the microscopic as well as the FACS-based read-outs were transferred to bioinformatics analysis in large tables via a SVN server. Data was merged if necessary and processed as follows: first, a binary classification of entry positive cells was established. For that purpose, the fluorescence intensities were scored in comparison to a mock-infected control of cells.

For GFP, a gamma distribution was fitted to the distribution of GFP fluorescence in the no virus control (Fig. 3.30 A, black line). With this method, the overestimation of single outlier cells within the uninfected control displaying high fluorescence intensity in the GFP channel due to autofluorescence or dust particles above the cell body could be avoided. Based on this gamma fitting, a threshold was established, which was set to a positive score of only 0.01 % of cells in the negative control (Fig. 3.30 A, red verical line). Cells displaying GFP fluorescence intensities

[4]In cooperation with Kasia Bozek, PhD student in the group of Thomas Lengauer, Department of Computational Biology and Applied Algorithmics, Max-Planck-Institute for Computer Sciences, Saarbrücken, Germany.

above the threshold were scored as GFP- and therefore entry-positive, whereas cells displaying lower GFP-fluorescence were scored as negative (Fig. 3.30 B).

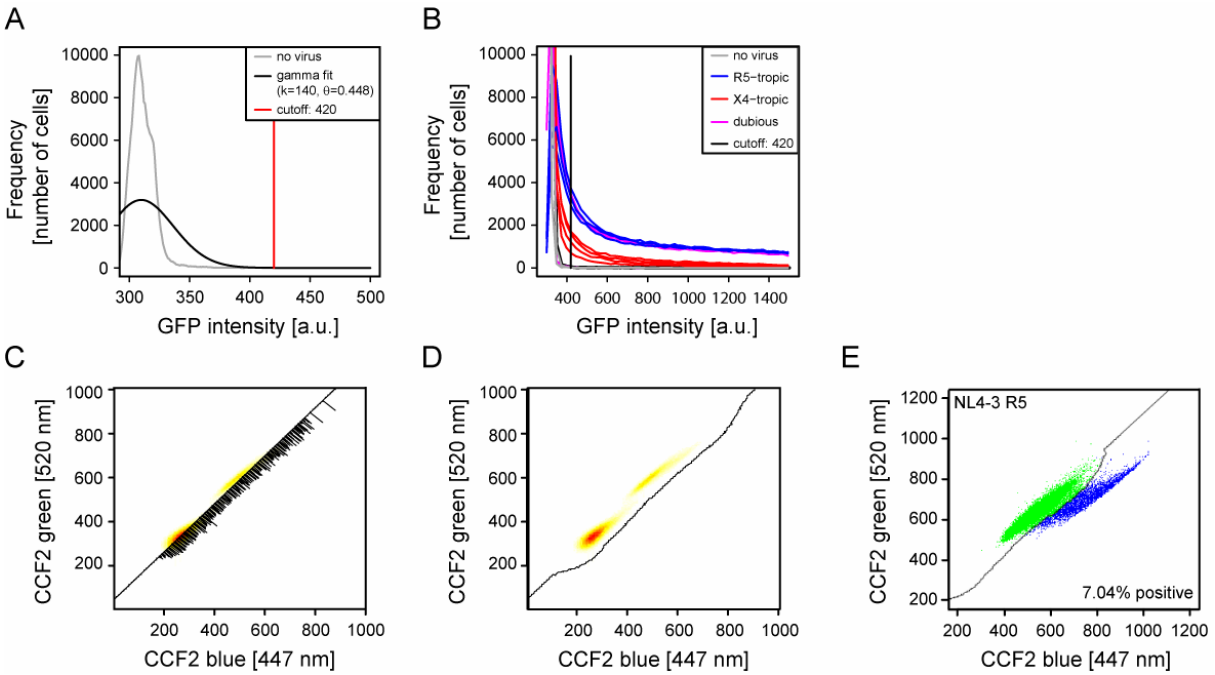

Fig. 3.30: Establishment of a threshold for binary classification. (A-B) GFP classifictation. (A) GFP-distribution of mock infected cells (no virus, grey line), gamma fit to this curve (black line) and thereby established threshold (red vertical line) are shown for a representative data set. (B) GFP-distribution of cells infected with R5-tropic (blue), X4-tropic (red) or ambiguous (pink) virus variants are shown in comparison to the mock-infected control (no virus, grey). The cutoff established in (A) is shown as black vertical line. (C-E) BlaM classification. Distribution of the two emission wavelengths of CCF2, blue (x-axis) and green (y-axis) is shown in dot plots. (C) and (D) show densitiy heat maps ranging from yellow (few cells) to red (many cells). (C) A line is fitted through the mock infected controls and distances from the line established over the whole population (black bars perpendicular to diagonal). (D) A gate surrounding the negative control is established along the averaged distances from (C). (E) Example of data from a NL4-3 R5 infected cell population with cells within the negative gate depicted in green and cells within the positive gate in blue. Percentage of BlaM-positive cells is shown in the lower right corner. a.u. = arbitrary units.

In the BlaM assay, entry-positive cells were defined with a scoring technique closely mimicking FACS-gating (Fig. 3.30 C-E). In standard FACS-gating, the user has to set gates according to control values, a method which can be biased at times. To provide an objective method and deal with the great amounts of data in reasonable time, we developed this gating method based exclusively on computational methods. To this end, fluorescence intensities of both uncleaved (green) and cleaved (blue) CCF2 β-Lactamase substrate were plotted in dotplots against each other for every individual cell in the control samples (mock treated cells merged with the unstained control). A linear function was fitted to the plotted points and the distance of the points from the fitted line was measured (Fig. 3.30 C, black diagonal and black lines perpendicular to this diagonal). The averaged distances of the most distant points from the fitted line were used to define the negative gate (Fig. 3.30 D). Data points lying below the fitted line and further away from it than the distances established using the control were scored to be BlaM- and therefore entry-positive (e.g. Fig. 3.30 E). After this binary classification of each individual

cell, the expression patterns of CD4, CCR5, and in FACS-measured samples also CXCR4, could be taken into account in the next step.

To illustrate the interdependencies of receptor/co-receptor usage and entry efficiency, the data were represented as 3D plots. For this purpose, the extreme 0.5 % of data were rejected on both horizontal axes to avoid misleading effects of outliers, and the remaining 99 % of data were binned in a 30x30 grid. The ratio of entry positive cells per bin was quantified and depicted in dependence of two other parameters. To smoothen the appearance of the plots for better interpretability, values in neighboring bins were averaged as shown exemplarily in Fig. 3.31. Empty bins are colored in black, whereas those yielding unreliable results due to a low number of individual cells (less than 0.11 % of total cells) were labelled in grey.

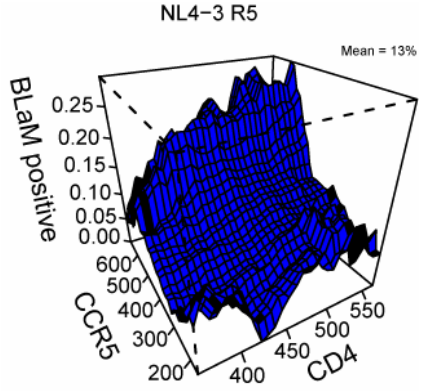

Fig. 3.31: 3D plot of single-cell data analysis. SupT1-R5 cells were incubated with BlaM carrying virus and subjected to BlaM entry assay and stained for surface expression of CD4, CCR5 and CXCR4. Single cell analysis was performed as described. Plot shows entry efficiency represented by the percentage of BlaM positive cells in dependence of CD4 and CCR5 for the virus harbouring Env proteins with NL4-3 R5 V3-loop.

This method of data display allowed a comprehensive visualization of the multiparameter analysis. The 3D plots were used for an initial estimate of data quality and indicated potential technical or systematical problems which could impede with future mathematical models if the respective data set would be taken into account. Furthermore, analysis of the data plotted in this way allowed for an initial interpretation guiding subsequent steps in experimental design to generate further data sets for a good and valid mathematical model.

3.2.4 Effect of the amount of virus-incorporated Env protein on entry efficiency

Since the viruses used to investigate entry efficiency had to be produced as isogenic pseudoparticles (see 3.2.1.2), the amount of incorporated Env protein could in principle vary from particle preparation to particle preparation. To monitor for those possible changes, quantitative Western Blot (qWB) analyses were performed using antibodies against CA protein and gp41 – the transmembrane part of Env. The intensities of CA and gp41 bands were quantified for every sample and normalized to a wt control, consisting of a particle preparation of pCHIV transfected 293T cells, applied to each single qWB as a standard.

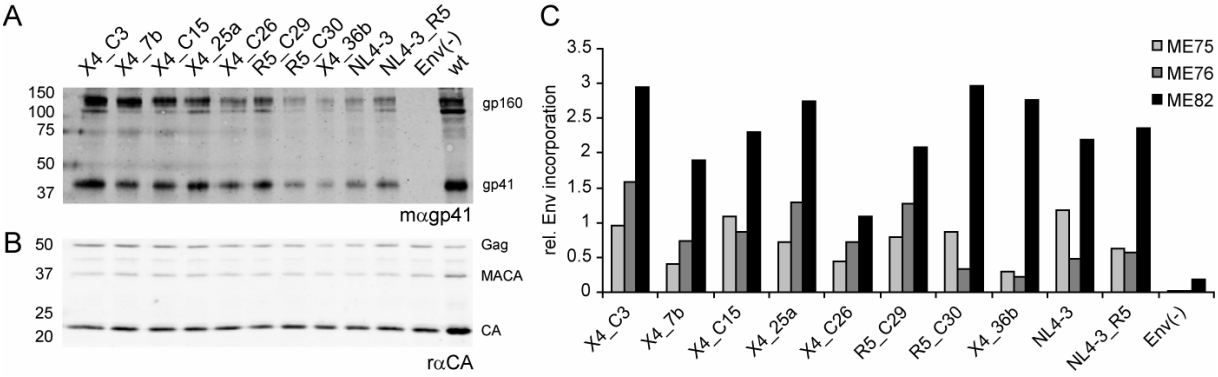

Fig. 3.32: Quantitation of Env incorporation into HIV-1 pseudoparticles. Isogenic viruses only differing in the Env protein incorporated were produced from 293T cells. Samples were diluted in SDS-sample buffer and subjected to quantitative Western Blot analysis probing against gp41 (A) and CA (B) at the same time. Lanes are labelled with the clone number of the Env protein used for pseudotyping. Env(-) = no envelope protein, wt = proviral plasmid encoding for the Env protein within the viral sequence (pCHIV). Position of molecular mass standards is shown with numbers in kDa at the left edge and protein bands are labelled on the right. (C) Single band intensities were quantitated using the LiCor Odyssey 2.1 software. The ratio of gp41 to CA was determined for every sample and normalized to wt. The graph shows the relative Env incorporation (ratio of gp41 per CA protein) for the different isogenic viruses of different particle preparations (ME75, ME76, ME82, respectively).

Fig. 3.32 A and B show qWB images of a representative particle preparation. The Chessie-8 antibody (A) stained gp41-containing proteins, namely the precursor protein gp160, which was present in all pseudotyped samples (lanes 1-10), as well as gp41 itself. This band occurred somewhat blurry, which was due to differently glycosylated species of the protein. As expected, no gp41 bands could be detected in the Env(-) sample (lane 11). In contrast to that, the wt sample (lane 12) showed a stronger gp41 signal compared to the other viruses. The CA antibody (B) showed as expected free CA protein (24 kDa) as well as a weak pattern of Gag processing products, including Gag precursor and MACA cleavage intermediate at the expected heights of 55 and 43 kDa, respectively. In order to have a more comprehensive picture of the incorporation of Env protein into viral particles, the ratio of gp41 signal to CA signal was calculated for each sample. Those ratios were then normalized to wt and are displayed for different particle preparations in Fig. 3.32 C. Here, the varying incorporation between different Env protein variants as well as over different particle preparations (ME75, ME76 and ME82, respectively) can easily be appreciated.

This result led to the question, if different amounts of Env protein incorporated per CA protein – and assuming a more or less constant amount of CA protein per virion also Env/virion – had an effect on entry efficiency of the respective viral particles. To investigate this, BlaM carrying pseudoparticles incorporating different amounts of Env protein were produced by co-transfection of differing amounts of pCAGGS-NL4-3*Xba*I over a wide range corresponding to plasmid amounts of 0 to 5 µg per 10 cm dish (with 2.5 µg Env-plasmid as the standard procedure). Those viruses were characterized in respect to their gp41/CA ratio in comparison to

the wt control as described above and then subjected to BlaM assay measurements on C8166 cells. The entry efficiency was quantified in a FACS read-out and percentage of BlaM positive cells plotted against the Env incorporation ratio (gp41/CA) in Fig. 3.33.

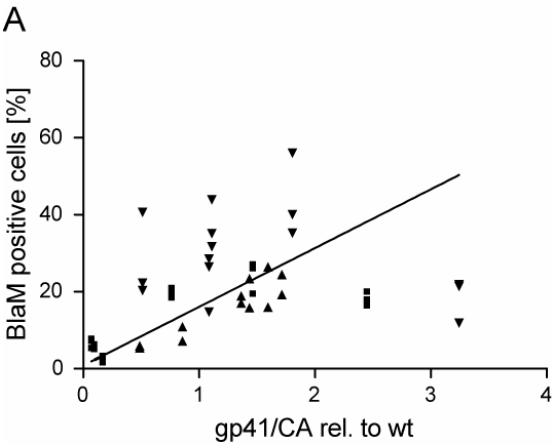

Fig. 3.33: Dependency of entry efficiency on Env incorporation. Different amounts of NL4-3 Env expression plasmid were co-transfected with a proviral plasmid lacking the *env* gene (pCHIV.Env(-)) into 293T cells to obtain a panel of isogenic viruses differing in their Env incorporation levels. Env incorporation ratio of gp41/CA was determined as described in Fig. 3.34. Relative entry efficiencies were determined by BlaM assay on C8166 cells and plotted against the relative gp41/CA ratio compared to a wt preparation. Values of three independent triplicate experiments are plotted. Line represents Deming regression with the assumption of errors with standard deviation of 0.7 for x-values and standard deviation of 8 for y-values (as estimated from multiple measurements).

An increase of entry efficiency could be observed in relation to the incorporation ratio of gp41 per virus. This dependency occurred to be roughly linear, as indicated by the fitting of the curve with a Deming regression (line in Fig. 3.33) which was significantly different from zero. While the standard linear regression method assumes that only the y measurements are associated with random errors, the Deming method takes errors for both measurements into account. Higher ratios of Env incorporation were also tested, but seemed to lead to a "saturation" of the function. The two triplicate values above the gp41/CA ratio of 2 seem to fall in this high Env classification already, but are taken into account in the regression. All particle preparations used in this study however showed gp41/CA ratios below the point where saturation was reached.

In conclusion, the amount of Env protein incorporated into a viral particle plays a role in entry efficiency, at least in the lower range of gp41/CA which was relevant for the further experiments. Hence, all particle preparations were subjected to gp41/CA-quantification by quantitative western blot analysis and the linear correlation can be incorporated in future models.

3.2.5 Dependency of entry efficiency on different receptor concentrations

For an initial characterization of the selected virus variants, the quantitative dependence of entry efficiency on receptor concentrations was tested. Hence, the different model cell lines were challenged with the isogenic reporter vectors carrying various V3-loop sequences. Entry efficiency was monitored by flow cytometry of GFP expression 48 h post transduction. Fig. 3.35 shows the distinct entry patterns of the selected vector variants into C8166 (orange), C8166-R5 (light blue) and differently induced Affinofile cells. The surface expression levels of CD4, CCR5 and CXCR4 were monitored by bulk quantitative FACS measurement at the time point of

transduction, as well as at the time point of GFP read-out and were shown to be similar for both time points and in the expected range for all cell lines (compare Fig. 3.25).

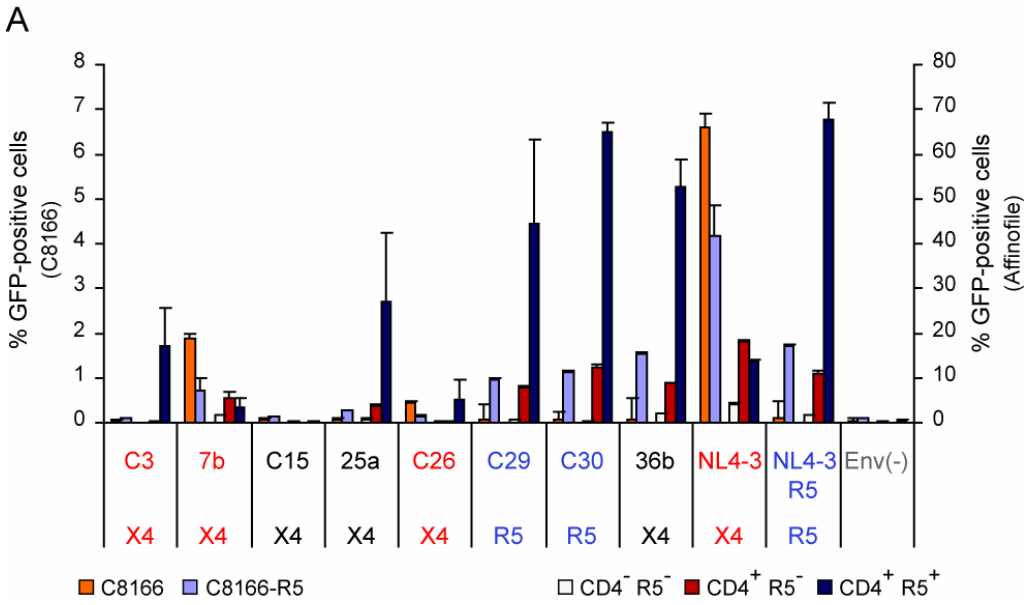

Fig. 3.35: Bulk entry efficiencies of the selected variants into different cell types. C8166 and C8166-R5 cells (left axis; orange and light blue bars, respectively) and Affinofile cells (right axis) not induced (white bars) or induced with 10 ng/ml Tet to express CD4 alone (red bars) or with a combination of 10 ng/ml Tet and 1 µM PonA to express CD4 and CCR5 (blue bars) were incubated with 25 ng (T-cell) and 5 ng p24 equivalent (Affinofile) of isogenic GFP-coding viruses carrying different Env proteins harboring the selected V3-loop sequences, respectively. Cells were tested for GFP fluorescence 48 h after transduction by flow cytometry. Mean percentage of GFP-positive cells of triplicate measurements and standard deviation are depicted for the different clones. Note the different scaling due to higher overall entry efficiencies on Affinofile cells.

Regarding entry efficiency, both T-cell lines showed GFP-expression of the reporter gene to a significantly lower level than Affinofile cells (note different scales of left (T-cells) and right (Affinofile) y-axes). As a control, viruses lacking any Env protein on their surface (Env(-)), were also tested and did not enter into any of the tested cell lines. Only clearly X4-predicted clones (marked in red on the x-axis) showed detectable entry into C8166 cells, with only clone X4_C3 failing in this regard. On the other hand, entry efficiency of these X4-tropic variants was decreased in the related cell line, C8166-R5, which expresses a lower concentration of CD4 than the parental clone (compare Fig. 3.25 B). In contrast to that, all clearly R5-predicted clones showed detectable entry only on the CCR5-expressing T-cell line, C8166-R5. In this regard, the standard clone NL4-3 R5 showed the highest entry levels, followed by one ambiguous variant, X4_36b, and the two clearly R5-predicted clones, R5_C29 and R5_C30. In addition, also another ambiguous variant, X4_25a showed very low but detectable entry efficiency on C8166-R5 cells. Affinofile cells not induced for CD4 or CCR5 (white) showed low levels of entry efficiency for some variants, most prominent in case of the standard X4-tropic variant NL4-3 and to a lesser degree for X4_7b, X4_36b and NL4-3 R5. Those low levels of entry efficiency could be increased in Affinofile cells expressing high CD4 levels for clones X4_7b, X4_25a, R5_C29 and X4_36b

and reached over 10 % GFP-positive cells for clones R5_C30, NL4-3 and NL4-3 R5. After additional induction of high levels of CCR5 (red), all clones except for the ambiguously predicted clone X4_C15, that showed no entry in either cell line, were shown to exhibit GFP-positive cells of up to nearly 70 % (R5_C30 and NL4-3 R5). All clearly R5-predicted clones displayed markedly increased entry efficiencies in comparison to Affinofile cells only induced for CD4, whereas the clearly X4-predicted clones X4_7b and NL4-3, showed no further increase of entry efficiency. In contrast to that, the also clearly X4-predicted clone X4_C3 was only able to enter Affinofile cells with high CD4 and CCR5 levels, hinting at a CCR5-dependence of this clone which was unexpected with the clear prediction outcome. The ambiguously predicted clones X4_25a and X4_36b showed matching increase in entry efficiency in presence of CCR5 surface expression on C8166-R5 and dually induced Affinofile cells, with the latter yielding overall higher entry efficiencies than the former. Of note, the standard X4-tropic clone NL4-3 showed, in comparison to all other clones, relatively much higher entry efficiencies on both T-cell lines than on the adherent Affinofile cells, which can be explained by its need for high CXCR4 expression levels, only present on the T-cell lines tested (compare Fig. 3.25 B).

In conclusion, the overall entry pattern of both standard clones and most of the clones tested proved to be in line with their predicted tropism, with some unexpected patterns in co-receptor usage for one clearly predicted clone (e.g. X4_C3) and as expected for the ambiguously predicted clones X4_25a, X4_36b. One ambiguous clone, X4_C15, did not gain entry in any of the cell lines tested at the chosen experimental settings.

Next, a deeper differential analysis was performed with 16 different induction levels of CD4 and CCR5 on Affinofile cells. To achieve this, the cells were induced with all possible combinations of the two induction agents at the concentrations of 0, 2.5, 3.75 and 10 ng/ml Tet and 0, 0.25, 0.5 and 1 μM PonA, respectively. Cells were again transduced with GFP-coding viruses harboring the individual Env sequences selected and entry efficiency was quantified with the help of the microscopic single-cell read-out. First, a bulk analysis of these data was performed to describe the overall CD4/CCR5-dependencies of entry efficiency of the different clones in a comprehensive way. Hence, the mean percentages of GFP-positive cells for each condition were analyzed and patterns were mathematically transformed into 3D surface plots with the web-based tool V.E.R.S.A. (Viral Entry Receptor Sensitivity Analysis; [105]; http://versa.biomath.ucla.edu). For CD4 and CCR5 expression levels, the mean fluorescence intensities of the respective immunostain were taken into account.

Fig. 3.36 shows the 3D surface plots drawn from the polynomial functions of the web-tool output. NL4-3 (Fig. 3.36 A) displayed a clear dependence on CD4 levels, whereas variation of CCR5 levels did not affect entry. In contrast to this, NL4-3 R5 (Fig. 3.36 B) was dependant on the presence of high expression levels of both CD4 and CCR5. In uninfected cells (no virus; Fig. 3.36 C), GFP-positive cells were found only at background levels and no dependence on either of the receptors could be detected. All patient derived variants tested showed distinct patterns of CD4 and CCR5 dependency, with R5_C29, R5_C30 and X4_36b (Fig. 3.36 I-K) most closely mimicking NL4-3 R5, whereas no variant showed an exclusive CD4 dependence comparable to NL4-3. In contrast, all clearly X4-predicted clones showed a mixed dependency on both receptors tested, with highest entry efficiencies in the presence of high surface expression levels of both CD4 and CCR5. This entry efficiency pattern was also displayed by the ambiguous clone X4_25a. Clones X4_C3 and X4_C26 both showed a very clear dependence from CCR5, although they both were clearly predicted to be X4-tropic. The ambiguous clone X4_C15 again showed entry levels not significantly above background (not exceeding 0.8 % GFP-positive cells under any condition, resulting in a smoothed 3D plot function not exceeding 0.5 % entry efficiency). The saddle-shaped surface pattern was considered to be an artifact of low entry efficiencies and therefore neglected in further analyses.

Note that X4-classified variants (red) again showed overall lower entry efficiencies than R5-tropic variants (blue). In this regard, the ambiguous clones (black), except the above mentioned clone X4_C15, behaved more like R5-tropic variants, displaying medium to high entry efficiencies.

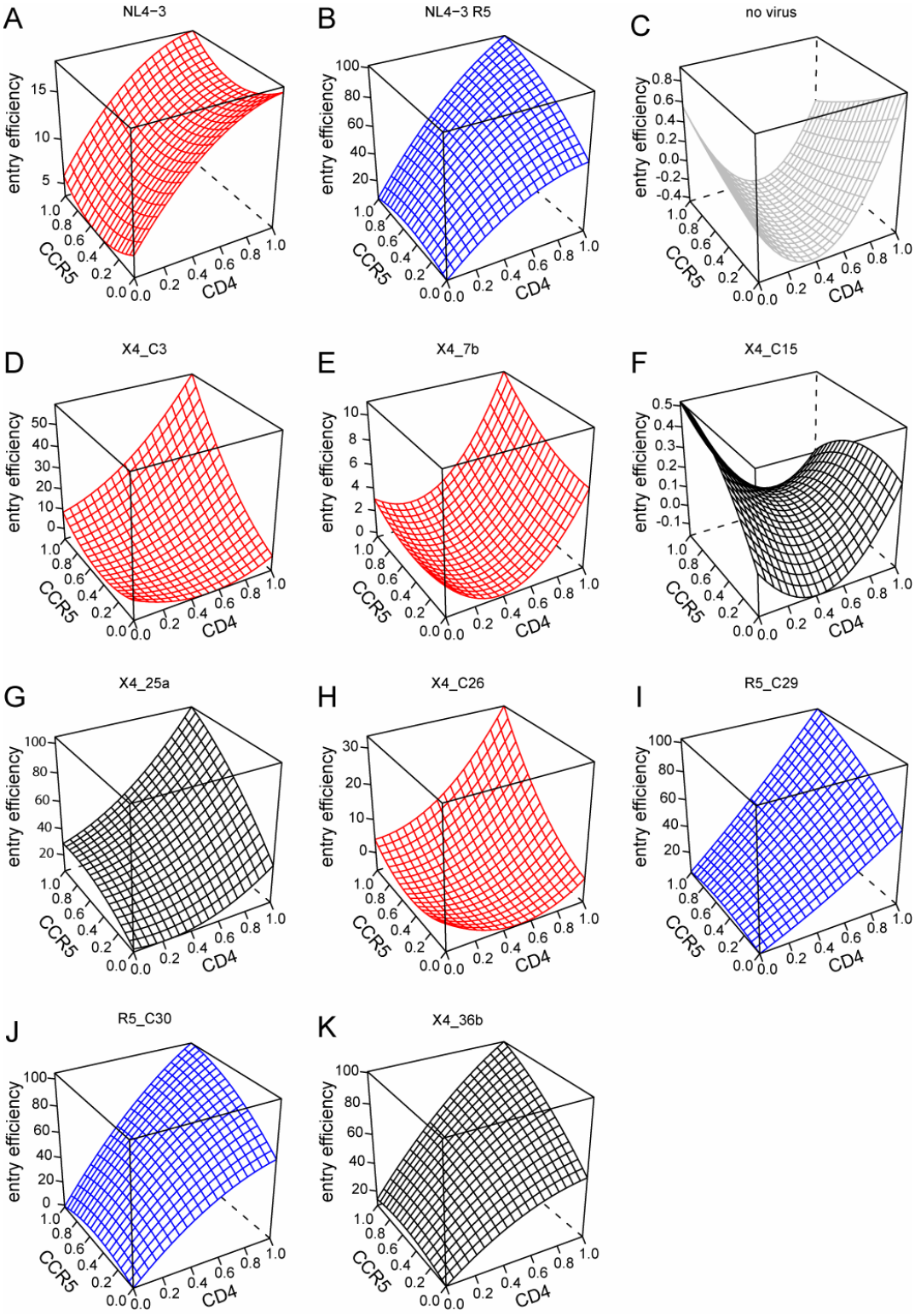

Fig. 3.36: Viral Entry Receptor Sensitivity Analysis (V.E.R.S.A.) of all clones selected. See page 89.

Another way to interpret the data obtained from the VERSA analysis web-tool is depicted in Fig. 3.37. Here, the sensitivity vector angle θ, a measure to describe the gross feature of the 3D surface plots (for details see [105]), is plotted for the different clones. The closer this angle is to 90°, the more CCR5-dependent is the respective virus clone, whereas angles close to 0° represent almost exclusive sensitivity to CD4 levels. To correlate this sensitivity vector with the overall

entry efficiency, the length of the arrows was drawn with respect to the vector magnitude, which is a direct measure for entry efficiency. The longer an arrow, the higher the overall entry efficiency, with R5_C30 showing the highest vector magnitude (86.3) and X4_C15 showing the lowest vector magnitude (0.2) in the same range as the mock-infected control (0.29). X4_C15 will therefore be ignored for further interpretation and is thus neglected in the plot. The length differences of the arrows again stresses the overall difference in entry efficiency of the clearly X4-predicted clones (labelled in red), which all showed low vector magnitudes, and the clearly R5-predicted as well as two of the ambiguously predicted clones (labelled in blue and black, respectively), which showed much higher vector magnitudes.

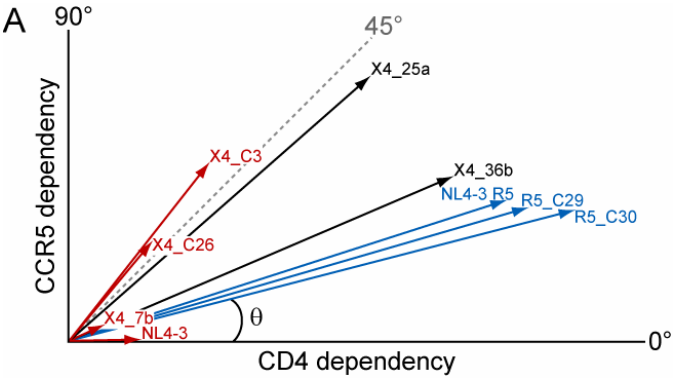

Fig. 3.37: Sensitivity Vector Angles for the different clones. Additional analysis output from VERSA of the data from Fig. 3.36. Length of arrow reflects sensitivity vector magnitude. A sensitivity vector angle θ close to 0° represents high CD4-dependency of a clone whereas an angle of close to 90° high CCR5-dependency. Grey dotted line indicates an angle of 45°.

In regard to the actual sensitivity vector angle, only the standard X4-tropic clone NL4-3 showed an exclusive CD4-dependence, whereas all other clones exhibited mixed dependencies. Surprisingly, two clearly X4-predicted clones, X4_C3 and X4_C26, displayed sensitivity vector angles above 45°, hinting of a strong CCR5-dependency. An angle close to 45° could otherwise only be reached by the ambiguous clone X4_25a (41.28°), whereas all clearly R5-tropic variants as well as the third ambiguous clone X4_36b showed angles below 25°.

Fig. 3.36 (page 88): Viral Entry Receptor Sensitivity Analysis (V.E.R.S.A.) of all clones selected. Affinofile cells were induced with 16 different combinations of Tet and PonA concentrations for 18 h, and then infected with isogenic viruses carrying the 10 selected Env-proteins. 48 h later, cells were fixed, stained for CCR5 and CD4 surface expression, nuclei were counterstained with Hoechst, fluorescence microscopy performed, images were segmented and percentage of GFP-positive cells determined. Entry efficiency expressed in % GFP-positive cells for the different viral strains and CD4 and CCR5 levels expressed as mean fluorescence values were uploaded to the VERSA analysis web-tool ([105], http://versa.biomath.ucla.edu) and fitting polynomials were plotted with R ([190], http://www.R-project.org). The graphs, showing the respective clone number on top, show entry efficiency in % GFP-positive cells (z-axis) plotted against normalized surface expression levels of CD4 (x-axis) and CCR5 (y-axis). Functions of viruses predicted to be X4-tropic are plotted in red, those of viruses predicted to be R5-tropic in blue, those of ambiguous clones in black and a control without virus (C, no virus) is depicted in grey as a background control.

3.2.6 Quantifying the effect of entry inhibitors

In addition to the direct correlation of entry efficiency and the presence of receptor and/or co-receptor on the surface of target cells, sensitivity to entry inhibitors also provides valuable information about the behaviour of the different isogenic viruses. To include this component into our multivariable study, the complete virus panel was tested for entry efficiency at the fully inhibitory concentrations of three prototype entry inhibitors. C46 [93], a derivative of T-20/Enfuvirtide ([66, 116]; trade name Fuzeon (Roche Pharmaceuticals, Basel, Switzerland)), is a peptidic fusion inhibitor of HIV-1 that blocks six-helix bundle formation of gp41 during the fusion process of viral and cellular membrane. It should therefore inhibit entry of all HIV-1 variants selected in this study, independent of their respective co-receptor tropism [68]. In addition to this broadly acting fusion inhibitor I also utilized two prototype co-receptor antagonists. AMD-3100 (AMD) is a bicyclam that has been shown to potently inhibit HIV-1 entry by antagonizing the CXCR4 co-receptor molecule [47, 210]. It is nevertheless not used in HIV-1 therapy due to massive adverse effects observed in humans [91]. On the other hand, the CCR5 co-receptor can easily be blocked by the small compound Maraviroc (MVC) [9], which was approved for antiretroviral treatment in Europe in 2007 ([63]; trade name Celsentri (ViiV Healthcare, Brentford, UK)).

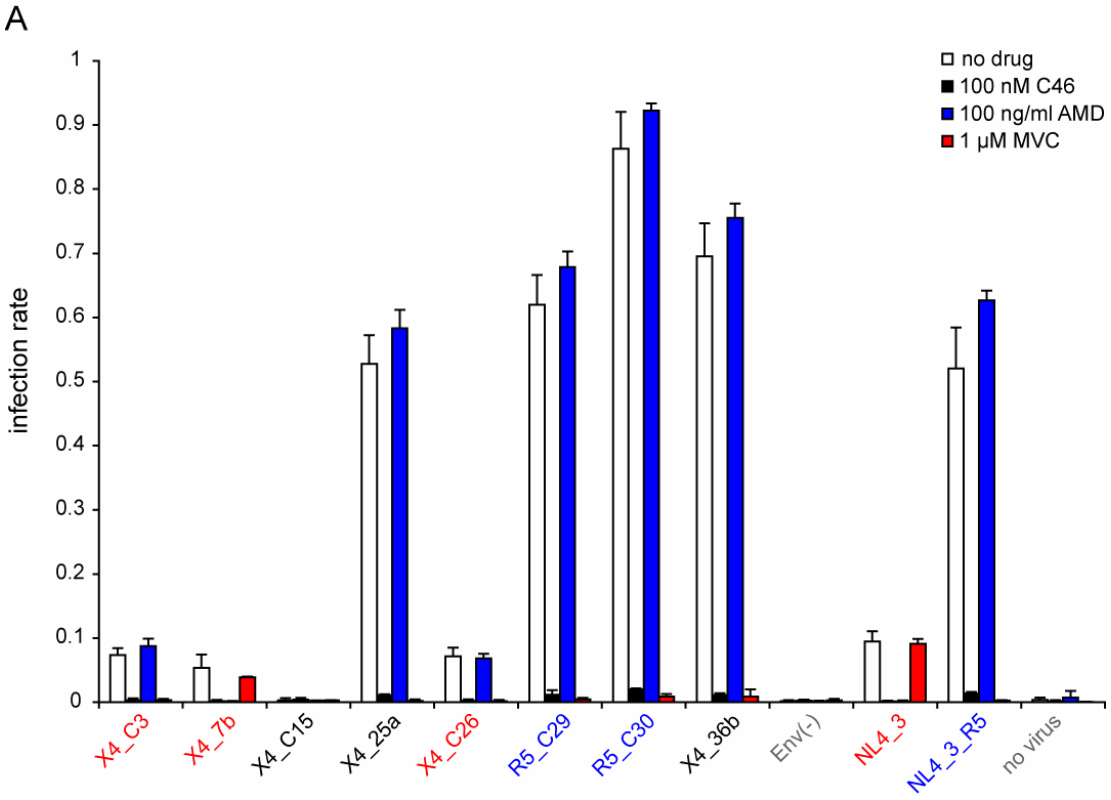

Fig. 3.38: Sensitivity towards prototype entry inhibitors. GFP-coding viruses with the different Env proteins (x-axis) where used to transduce Affinofile cells induced for low expression levels of CD4 and CCR5 in the presence of the indicated concentrations of three prototype entry inhibitors. After 48 h, infection rate (ratio of GFP-positive cells) was determined by microscopic read-out. Mean values of triplicate measurements (6 measurements for no drug) and standard deviations are shown.

To investigate the sensitivity of all selected V3-loop variants, Affinofile cells induced for a low bulk expression level of CD4 and CCR5 (2.5 ng/ml Tet and 0.25 μM PonA) were transduced with GFP-coding isogenic vectors in the absence (no drug – white bars) or presence of fully inhibitory concentrations of C46 (black bars), AMD-3100 (blue bars) and MVC (red bars). Fig. 3.38 summarizes the bulk results of the microscopic read-out of this experiment after 48 h. As expected, all vectors were sensitive to the addition of 100 nM C46. Clones showing a higher initial infection rate (R5-tropic variants labelled in blue on the x-axis and two of the ambiguous clones, labelled in black on the x-axis) retained a higher background infection rate in the presence of C46, demonstrating a virus specific effect of the decrease in the number of GFP-positive cells. In contrast to those very clear results, both co-receptor antagonists showed less definite inhibition patterns. A clear match of expectations and tested sensitivity could be observed with the control viruses NL4-3, which was inhibited by AMD, but not MVC, and NL4-3 R5, which in turn was inhibited only by MVC and not by AMD. This clear phenotype was only mimicked by both clones clearly predicted to be R5-tropic as well as one of the clearly X4-predicted clones (labelled in red on the x-axis), namely X4_7b. The two remaining clearly X4-predicted clones showed an "inverted" phenotype: they were both inhibited by MVC but not AMD. The ambiguous clones all (except for X4_C15 which again showed insignificant overall entry levels) displayed a clear sensitivity towards MVC, but their entry efficiency was not affected by the presence of AMD.

In order to obtain a more detailed picture of the sensitivity of the different virus variants to the presence of entry inhibitors, titration experiments were performed. For this purpose, SupT1-R5 (Fig. 3.39) or Affinofile cells (Fig. 3.40) were incubated with the isogenic virus variants in the presence of different concentrations of MVC.

On SupT1-R5 cells, the BlaM assay was used as a read-out. Fig. 3.39 displays dose-response curves for the different variants labelled on top of each plot. The fits were calculated with the software GraphPad Prism and IC50 values for curves reaching the non-inhibited plateau and a correlation of the fit over R2 = 0.8 are shown. Variants X4_7b (Fig. 3.39 B), X4_C15 (Fig. 3.39 C), X4_C26 (Fig. 3.39 E) as well as the standard X4-tropic clone NL4-3 (Fig. 3.39 I) did not show any response to increasing amounts of the CCR5-antagonist MVC. The remaining variants displayed strong inhibition with IC50 values in the low- to mid-nanomolar range. The control variant for R5-tropic viruses, NL4-3 R5 (Fig. 3.39 J) displayed the highest IC50 of 62.3 nM, followed by one ambiguous variant (X4_36b, IC50 = 40.1 nM, Fig. 3.39 H), the two clearly R5-predicted variants (R5_C30 and R5_C29, IC50 = 30.4 nM and 16.5 nM, respectively, Fig. 3.39 G and F) and the second ambiguous variant, X4_25, with the lowest calculated IC50 value of 3.9 nM (Fig. 3.39 D). The clearly X4-predicted variant X4_C3 (Fig. 3.39 A) showed a very steep MVC-response curve not allowing to calculate a reliable IC50 value as the plateau was not reached with the administered concentrations of drug. To properly illustrate the strong inhibition, an additional display of this data set was chosen on a linear scale (Fig. 3.39 K).

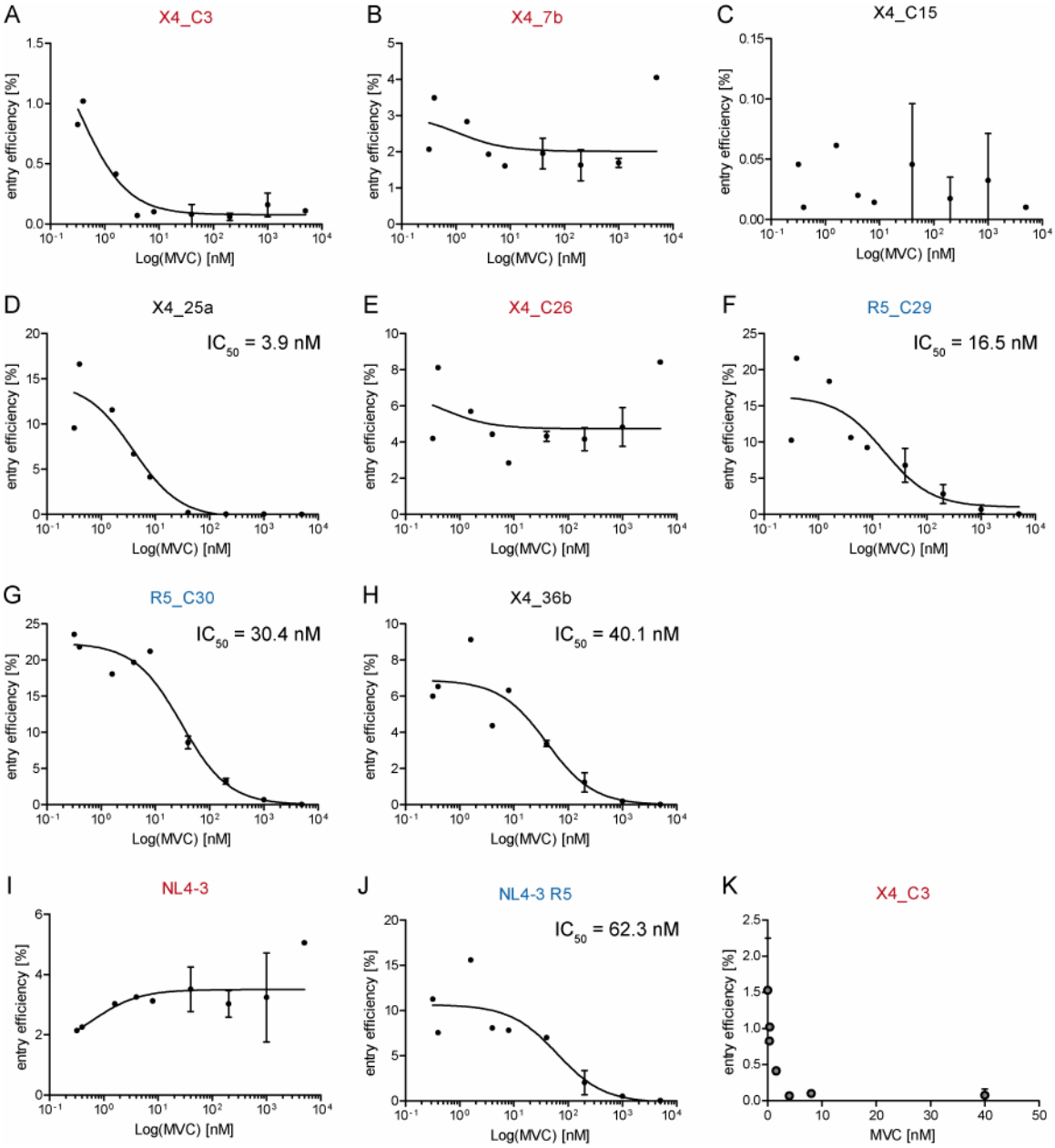

Fig. 3.39: Sensitivity of different virus variants towards MVC on SupT1-R5 cells. Entry efficiency of isogenic viruses into SupT1-R5 cells was investigated using the BlaM assay in the presence of different concentrations of MVC. Data of two independent experiments are shown (mean value of overlapping data points with standard deviation). Dose response curves were fitted with the GraphPad Prism software. The Env variant is indicated above the respective plot. IC_{50} values in nM are depicted for reliable curves. Note the non-logarithmic x-axis in (K) to display the data point without MVC.

A similar analysis was conducted on the Affinofile cell line to compare the two model systems. Affinofile cells were induced with 2.5 ng/ml Tet and 0.25 µM PonA for this purpose and transduced with 10 ng GFP-coding isogenic vector variants carrying the different Env proteins. Entry efficiency was analyzed using the microscopic read-out 48 h post transduction. The results of this experiment are depicted in Fig. 3.40.

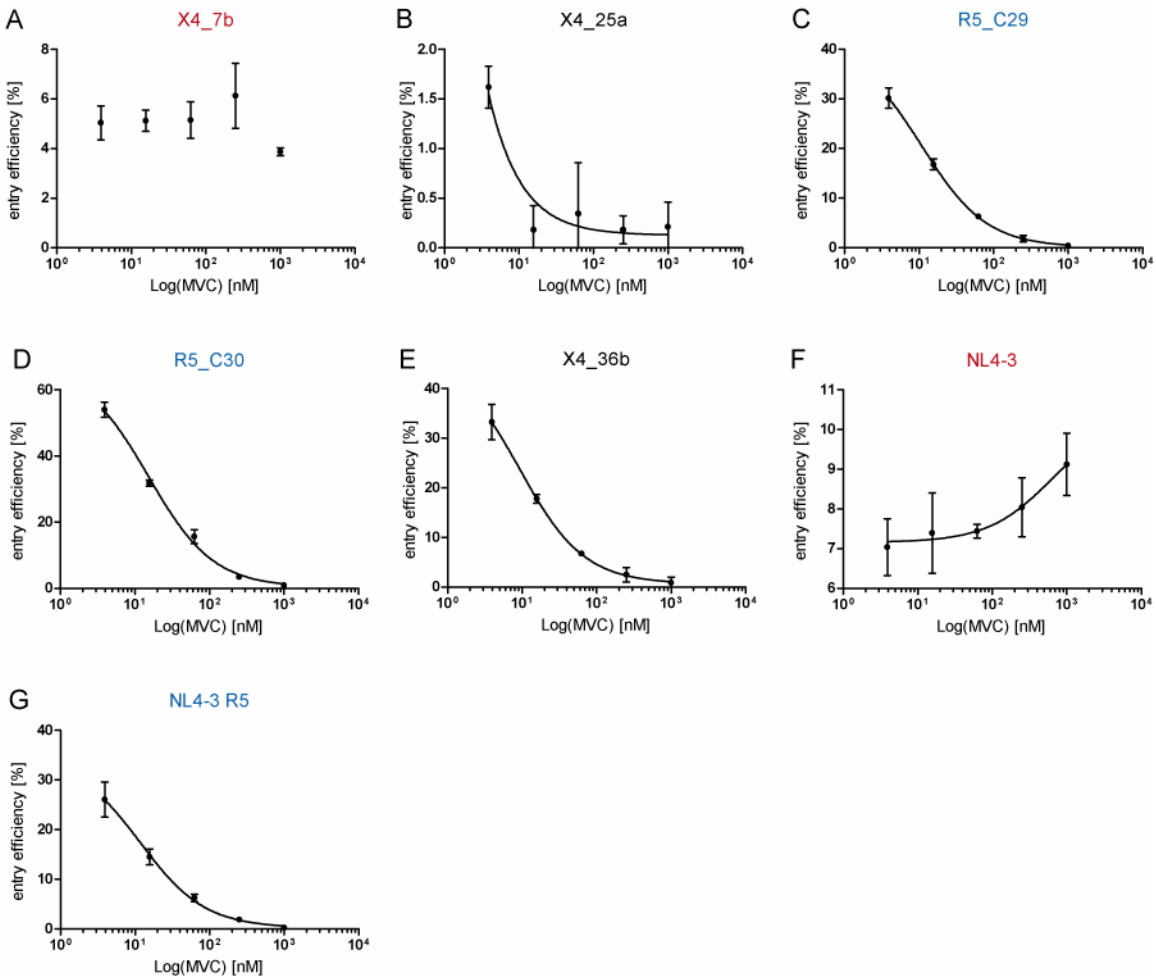

Fig. 3.40: Sensitivity of different virus variants towards MVC on Affinofile cells. Entry efficiency of isogenic viruses into Affinofile cells induced for a low expression of CD4 and CCR5 was investigated with the microscopic GFP-transduction assay in the presence of different concentrations of MVC. Data of two triplicate measurements and standard deviations are shown. The Env variant is indicated above the respective plot. Logarithmic curves fitted with dose response functions using the GraphPad Prism software are shown.

Only two X4-tropic variants were insensitive to MVC inhibition (Fig. 3.40 A and Fig. 3.40 F). All other clones were inhibited in a dose-dependent manner. Dose-response curves were fitted to the data sets showing clear phenotypes, although the lowest MVC concentration did not allow the detection of the upper plateau for any of the variants. Thus, the IC_{50} values calculated are not considered reliable and have not been displayed, here. The standard R5-tropic clone, NL4-3 R5 (Fig. 3.40 G), as well as the two clearly R5-predicted variants (Fig. 3.40 C-D) and one ambiguously predicted clone, X4_36b (Fig. 3.40 E), showed a clear MVC sensitivity in the same range as observed on SupT1-R5 cells (compare Fig. 3.39).

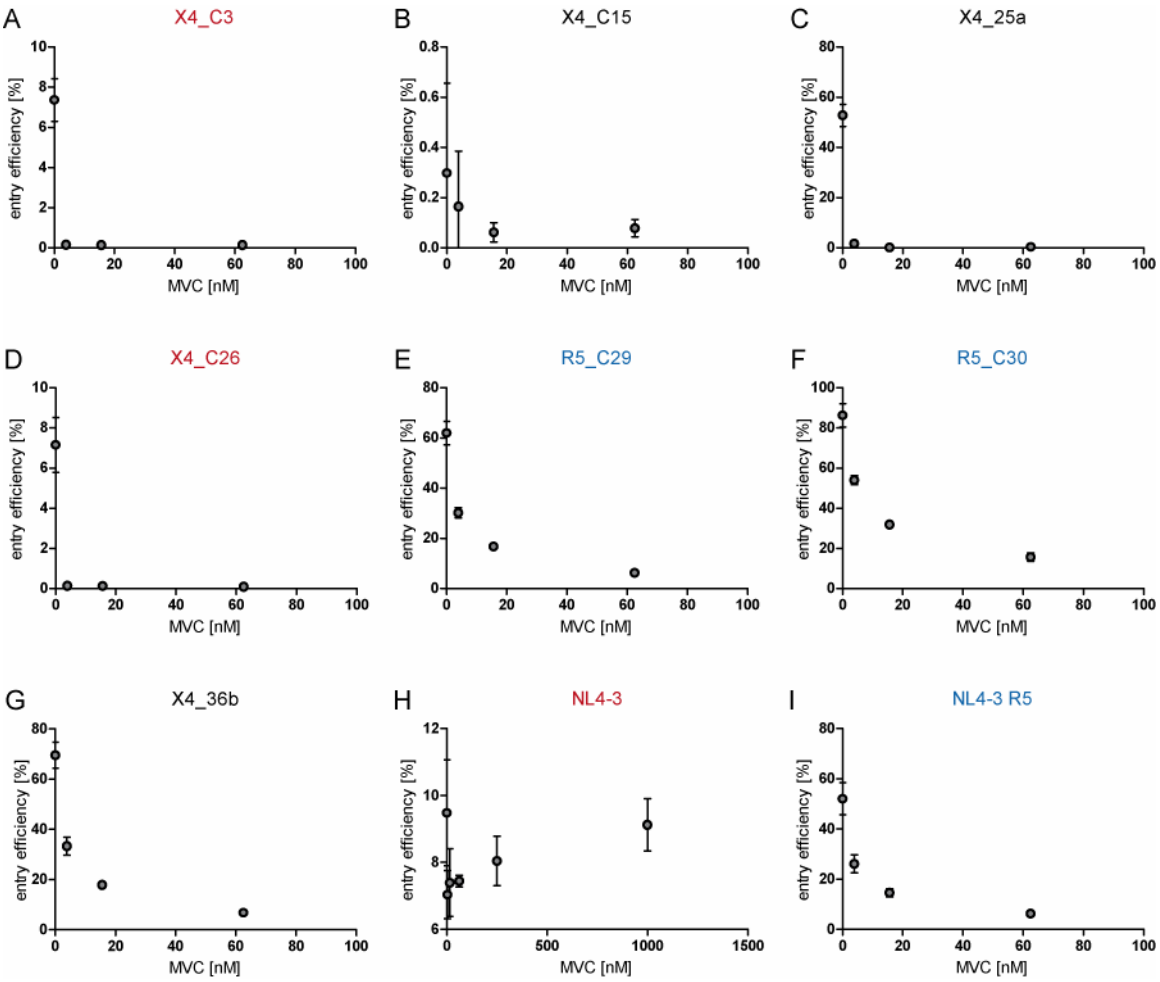

Fig. 3.41: Sensitivity of different virus variants towards MVC on Affinofile cells. Linear display of a subset of Env variants depicted above the respective plots. Details see Fig. 3.40.

For clarity, the response curves of some variants are depicted in a linear display in Fig. 3.41 to highlight the strong drop in entry efficiency from the first data point (0 nM MVC) to the second (0.015625 nM MVC). Those graphs are restricted to 100 nM MVC input to easily visualize the low drug concentrations. However, note the extended scale in Fig. 3.41 H to illustrate the resistance of the standard X4-tropic clone NL4-3 to CCR5-antagonist inhibition even in presence of high drug concentrations. A very steep decrease in entry efficiencies can nevertheless be seen in the subnanomolar range for the variants X4_C3 (Fig. 3.41 B), X4_25a (Fig. 3.41 C) and X4_C26 (Fig. 3.41 D). Two of those, X4_C3 and X4_C26, display entry efficiencies of below 10 % already at the baseline (no MVC) and the steepness of the curve could therefore result from the overall low entry efficiency with this virus input. In contrast to this, X4_25a is inhibited from an initial entry efficiency of over 50 %, laying further stress on the strong R5-dependence of this variant. The ambiguous variant X4_C15 (Fig. 3.41 B) seemed to show a slight sensitivity towards MVC despite very low overall entry efficiencies.

For easier comparison, Tab. 3.2 summarizes the sensitivities of entry efficiency into the two different cell lines for the individual clones.

		Inhibition by MVC		
patient #	clone #	SupT1-R5	IC_{50} [nM]	Affinofile
220	X4_C3	+	n.d.	+
286	X4_7b	-	n.d.	-
409	X4_C15	-	n.d.	(+)
651	X4_25a	+	3.9	++
685	X4_C26	-	n.d.	+
822	R5_C29	+	16.5	+
838	R5_C30	+	30.4	+
924	X4_36b	+	40.1	+
	NL4-3	-	n.d.	-
	NL4-3 R5	+	62.3	+

Tab. 3.2: Summary of MVC sensitivity on different cell lines. The sensitivity of individual clones is expressed as ++ for very strong inhibition, + for inhibition, (+) for minor reduction and - for lacking inhibition. IC_{50} values in nM on SupT1-R5 cells are indicated if determined. n.d. = not determined.

In order to test whether variants that were inhibited by the CCR5-antagonist MVC could further be influenced by the presence of a CXCR4-antagonist by blocking the second available major co-receptor, an experiment was conducted where the two drugs MVC and AMD were titrated against each other. For this purpose, Affinofile cells were again induced for medium levels of CD4 and CCR5 (2.5 ng/ml Tet and 0.25 µM PonA) and transduced with the panel of isogenic GFP-vectors for 48 h. Concentrations which did not lead to full inhibition of the standard clones NL4-3 and NL4-3 R5, respectively, were used, leading to a 4x4 inhibition grid with AMD concentrations of 0, 0.4, 2 and 10 ng/ml AMD and 0, 8, 40 and 200 nM MVC, in each combination.

Fig. 3.42 depicts the 16 data points of the individual data sets for each virus variant in a 3D plot with bulk entry efficiencies from two merged independent experiments displayed on the z-axis in dependence of increasing AMD (x-axis) and MVC (y-axis) concentrations towards the right front of the plot. The overall sensitivities to the drugs could be confirmed as tested before by these results: The X4-tropic standard NL4-3 (Fig. 3.42 A) and the clearly X4-predicted variant X4_7b (Fig. 3.42 D) were shown to display a clear sensitivity to increasing AMD concentrations, but they were not inhibited by the addition of MVC. In contrast to this, the two remaining clearly X4-predicted variants, X4_C3 (Fig. 3.42 C) and X4_C26 (Fig. 3.42 F), respectively, as well as two of the ambiguously predicted clones, X4_25a (Fig. 3.42 E) and X4_36b (Fig. 3.42 I), and the clearly R5-predicted variants and standard, R5_C29 (Fig. 3.42 G), R5_C30 (Fig. 3.42 H) and NL4-3 R5 (Fig. 3.42 B), respectively, were shown to be sensitive to MVC but not AMD. However, no additive effect of the two drugs could be observed in this experiment.

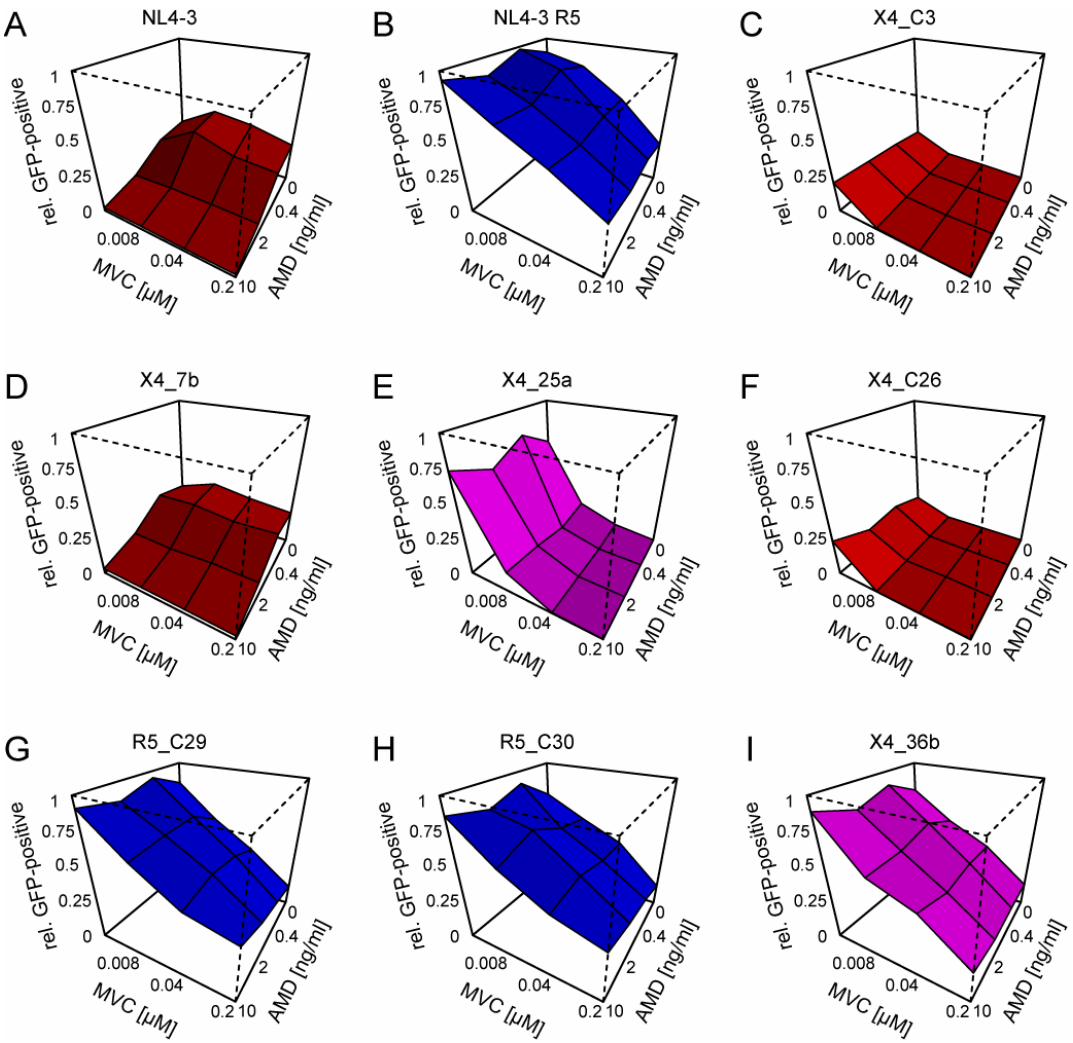

Fig. 3.42: Dependence of entry efficiency on the combination of two co-receptor antagonists. Affinofile cells were induced for low level expression of both CD4 and CCR5 for 18 h, incubated for 48 h with GFP-expressing virus with different Env proteins as indicated above the plots and subjected to microscopic read-out. Ratio of GFP-positive cells per total cells is depicted in dependence of increasing amounts of AMD and MVC towards the frontal corner.

The single-cell analysis method developed in this study was able to reveal a much more detailed picture of those experimental results. The dependency of entry efficiency on CD4- and CCR5 levels in the presence of increasing drug amounts is depicted exemplary for three virus variants in Fig. 3.43 and Fig. 3.44. Reflecting the overall results of the bulk analysis, AMD-sensitivity could only be detected for NL4-3 (Fig. 3.43 B), whereas X4_C3 (Fig. 3.43 A) and NL4-3 R5 (Fig. 3.43 C) showed no sensitivity towards this drug. Accordingly, a clear dependence on CCR5-levels can be observed for X4_C3 with a steep gradient of high entry efficiency towards high surface concentrations of this co-receptor, which is not changed dramatically in the presence of increasing amounts of AMD. In contrast to this, for NL4-3 the flat plateau of entry positive cells distributed more equally over the range of CCR5-expression levels is vanishing evenly with increasing AMD concentrations. The very high entry efficiencies of NL4-3 R5 impede the correct interpretation of receptor- and co-receptor-dependence in this case as the high entry efficiency-

pattern is not changed dramatically in the presence of AMD.

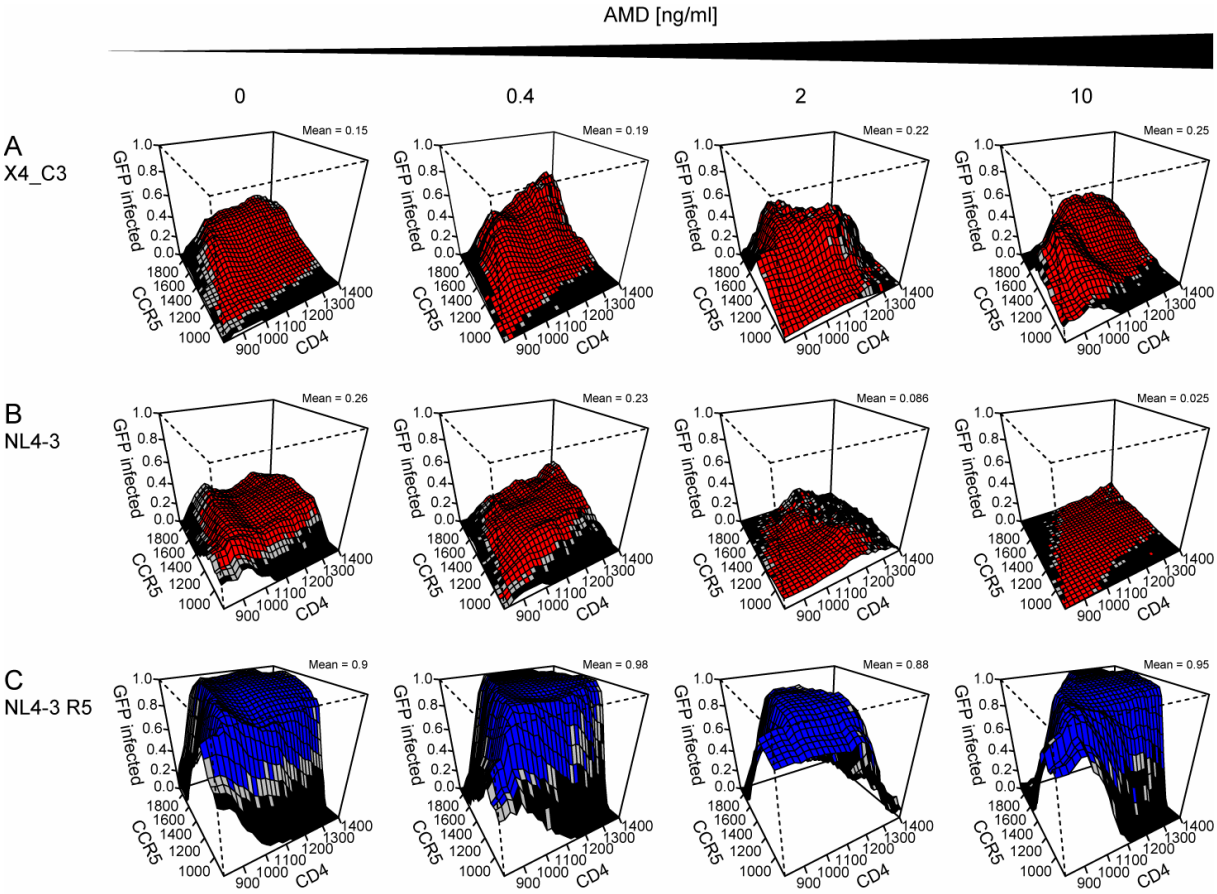

Fig. 3.43: Single cell analysis of entry dependency on CD4 and CCR5 expression levels with increasing amounts of AMD. Affinofile cells were induced with 2.5 ng/ml Tet and 0.25 µM PonA and entry efficiency of isogenic vector variants in presence of increasing amounts of AMD assessed with the microscopic assay. 3D-plots of relative entry efficiency (z-axis) in dependence on CD4- (x-axis) and CCR5- (y-axis) surface expression levels are shown as determined by the single cell analysis method developed in 3.2.3 for clone X4_C3 (A) as well as the two standard clones NL4-3 (B) and NL4-3 R5 (C). AMD concentrations from left to right: 0, 0.4, 2 and 10 ng/ml.

In contrast to this, the sensitivity towards MVC on the single cell level is shown in Fig. 3.44. Both variants that did not react to AMD, X4_C3 (Fig. 3.44 A) and NL4-3 R5 (Fig. 3.44 C) showed a clear sensitivity towards MVC. With respect to receptor dependence of this reduction in entry efficiency, a peculiar phenotype could be observed: in presence of MVC, viruses seemed to enter cells that expressed low CD4-levels to a higher degree than in the absence of drug. This could be observed for both variants, although more obvious for NL4-3 R5 due to higher overall entry efficiencies, where it could best be seen at 0.04 and 0.2 µM MVC. The same phenotype was observed for all virus variants that were sensitive to MVC. Surprisingly, NL4-3 (Fig. 3.44 B) also showed a similar phenotype, although only in the presence of the highest MVC concentration and not as pronounced as for the R5-tropic variants.

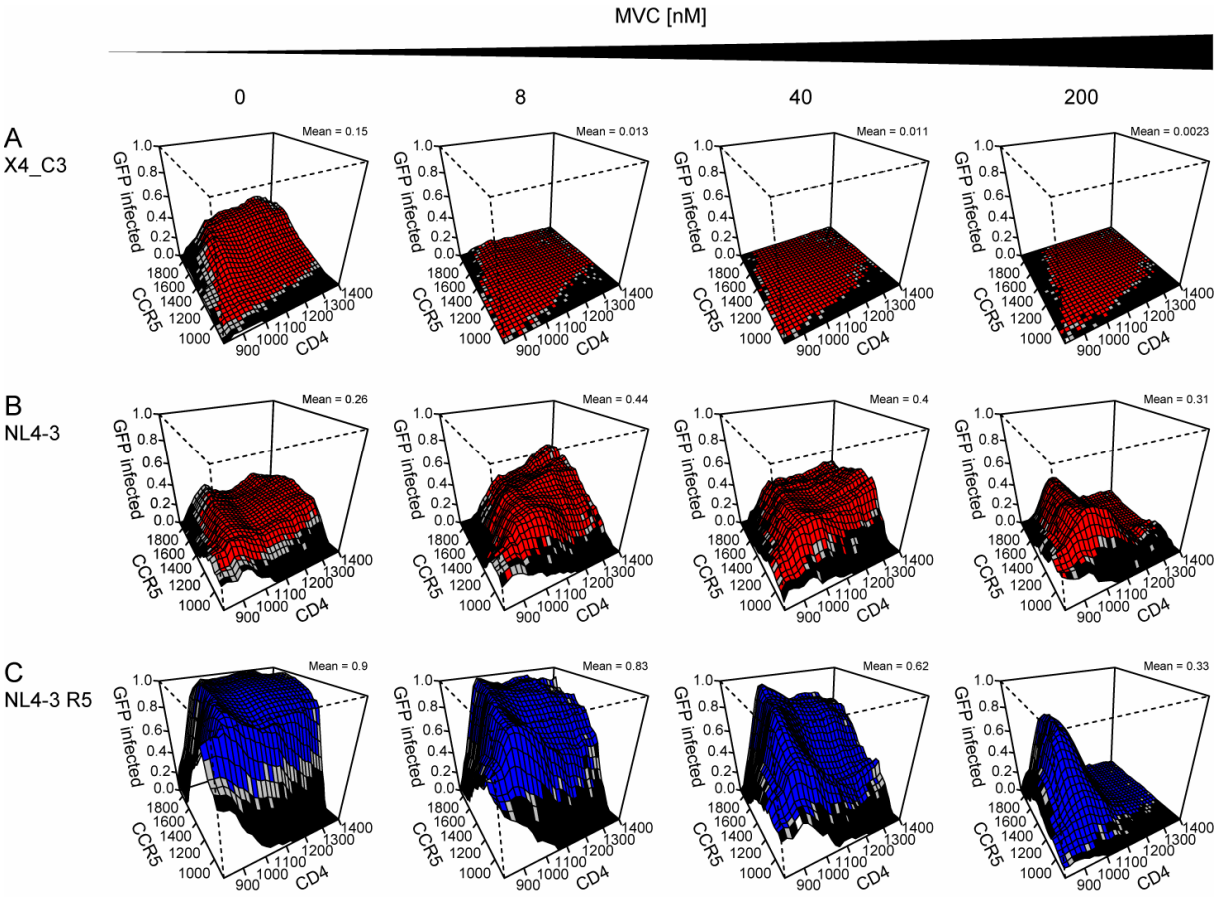

Fig. 3.44: Single cell analysis of entry dependency on CD4 and CCR5 expression levels with increasing amounts of MVC. Affinofile cells were induced with 2.5 ng/ml Tet and 0.25 µM PonA and entry efficiency of isogenic vector variants in presence of increasing amounts of MVC assessed with the microscopic assay. 3D-plots of relative entry efficiency (z-axis) in dependence on CD4- (x-axis) and CCR5- (y-axis) surface expression levels are shown as determined by the single cell analysis method developed in 3.2.3 for clone X4_C3 (A) as well as the two standard clones NL4-3 (B) and NL4-3 R5 (C). MVC concentrations from left to right: 0, 8, 40 and 200 nM.

3.2.7 Comparison of different analysis methods

The subtle differences described above were invisible in the bulk analysis of the same data, proving an advantage of the single-cell analysis of entry efficiencies developed here. To compare the different analysis methods side by side, all data obtained with the differential induction experiment (compare 3.2.5) was analyzed in three different ways. To compare the results of those analyses, three representative graphs are shown for each method in Fig. 3.45.

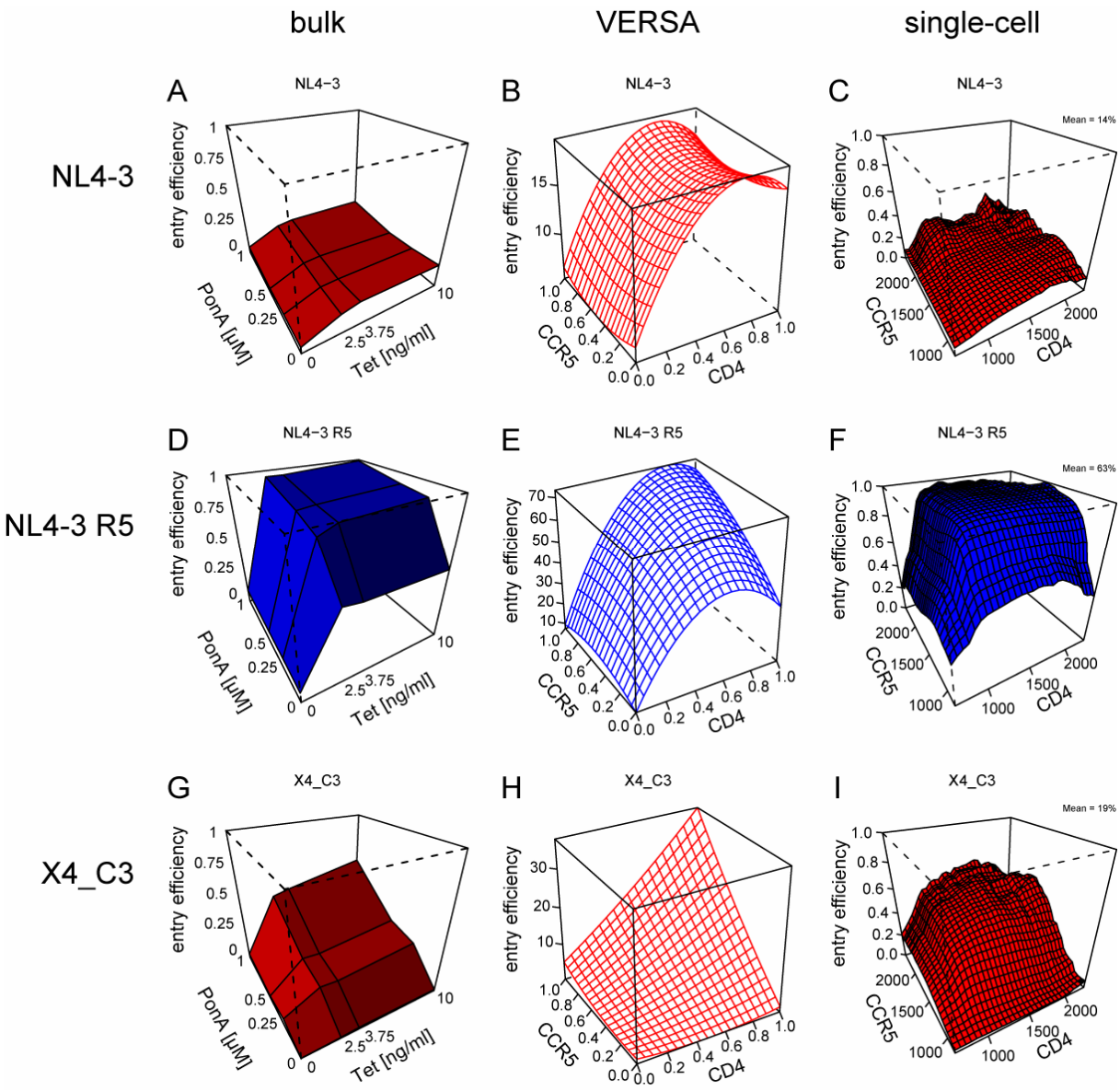

Fig. 3.45: Comparison of different analyses of the same data set. Affinofile cells were induced with 16 different combinations of Tet and PonA concentrations for 18 h, and then infected with viruses coding for GFP. 48 h later, cells were fixed, stained for CCR5 and CD4 surface expression, nuclei were counterstained with Hoechst, fluorescence microscopy performed, images were segmented and percentage of GFP-positive cells determined as described above. Entry efficiency expressed in % GFP-positive cells (z-axis) were either plotted as a function of the concentration of both induction agents Tetracycline (Tet) and PonasteroneA (PonA) in A, D and G or as a function of CD4 (x-axis) and CCR5 (y-axis) levels expressed as mean fluorescence values. Values were either uploaded to the VERSA analysis web-tool ([105], http://versa.biomath.ucla.edu) and fitting polynomials were plotted with R ([190], www.R-project.org) (B, E and H) or single-cell analysis performed as described above (C, F and I). Analyses for viruses carrying three different Env-proteins are shown: NL4-3 (A-C), NL4-3 R5 (D-F) and X4_C3 (G-I).

The roughest analysis is represented by plotting the mean entry efficiency for each single of the 16 induction conditions (first column; Fig. 3.45 A, D, G). No information on the actual expression level of both receptors CD4 and CCR5 after induction with different concentrations of the two inducing agents, Tet and PonA, respectively, was included here. The graphs give a coarse impression of the dependence of entry efficiency on the presence of different concentrations of both inducing agents. The second column (Fig. 3.45 B, E, H) represents the graphic output of the

VERSA analysis. Those graphs have been discussed in detail above (compare page 86). Finally, the third column (Fig. 3.45 C, F, I) depicts single-cell analysis of the same data sets. In contrast to the other two methods, those graphs reveal subtle differences in entry efficiencies with minor changes in receptor concentrations. While all three methods of analysis revealed the same trend in entry dependency on induction intensity of the Affinofile cell line, an increase in analysis depth could clearly be seen from left to right in every row of Fig. 3.45.

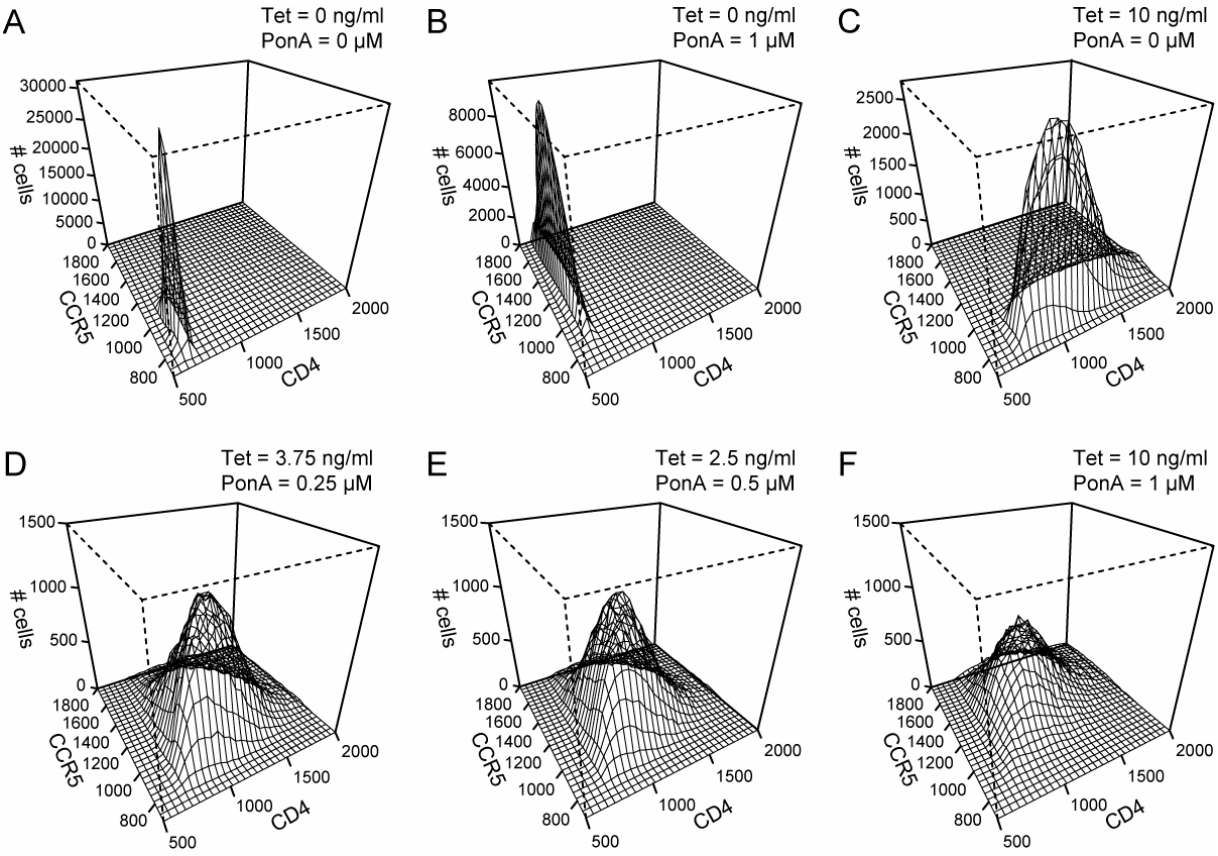

Fig. 3.46: Distinct CD4/CCR5 surface expression levels at different induction conditions. Affinofile cells were induced with different combinations of Tet and PonA. Surface expression of CD4 and CCR5 was measured by immunofluorescence after 66 h. 3D plots show number (#) of cells in the respective CD4/CCR5 bin for different induction conditions indicated in Tet and PonA concentration in the upper right corner of each plot.

The much more detailed pattern of the dependence of entry efficiency on the levels of CD4 and CCR5 in the single cell analysis can be explained by the broad distribution of different expression levels of both receptors at the individual induction conditions. This is visualized in Fig. 3.46, where the frequency of distinct CD4/CCR5 expression levels (i.e. number of cells in a given bin) is shown for several induction conditions. Although the overall expression level is clearly dependent on the concentration of the respective inducing agent (compare also Fig. 3.24), the picture is different on the level of single cells. Even in the presence of only low amounts of an inducing agent resulting in low bulk levels of receptor expression, some individual cells expressed high amounts of the induced receptor molecule. This is neglected in the VERSA analysis, where mean values of expression levels were taken into account for the individual induction condition.

In contrast to this, the single cell analysis established here assigns the entry efficiency to the actual expression level of every single cell and thus integrates outliers within one induction condition in the right way.

In conclusion, single cell analysis established in this study represents a superior method for the generation of detailed quantitative data as a basis for mathematical modeling of the entry process.

3.2.8 Summary of phenotypes determined for the individual clones

For easier discussion of the differences between the selected V3-loop variants, a summary of characteristics of every individual clone is helpful and is hence described in the following paragraphs.

3.2.8.1 The standard clones, NL4-3 and NL4-3 R5

The two clones chosen as standard variants proved to behave as expected in most of the tests performed. A very clear CXCR4-dependence of NL4-3 could be shown by comparison of entry efficiencies on T-cell lines expressing high amounts of this co-receptor in contrast to the Affinofile cell line that displays only very low surface levels of CXCR4. In addition, NL4-3 showed a very clear and exclusive CD4-dependence on Affinofile cells, establishing the independence of this clone from any surface concentration of CCR5. Furthermore, a strong sensitivity towards the CXCR4-antagonist AMD-3100 could be established. NL4-3 showed no sensitivity towards MVC, although a minor decrease in entry efficiency could be observed in some experiments.

This is in contrast to the second control virus, NL4-3 R5. This variant showed a very strong sensitivity to CCR5-expression on the T-cell line pair C8166 and C8166-R5. Low background entry efficiency was observed on Affinofile cells not induced for CCR5-expression, which could be increased markedly upon induction of this co-receptor. On both cell lines tested, NL4-3 R5 could easily be inhibited by the addition of MVC, with an estimated IC_{50} in the nanomolar range on SupT1-R5 cells.

3.2.8.2 The clearly X4-predicted clone X4_C3

All selection parameters used clearly predicted that this clone was an X4-tropic variant. All genotyping algorithms used, including the 11/25 charge rule were in agreement, as well as the phenotypic analysis which stated a SI-phenotype. Surprisingly, the viruses produced to incorporate the Env protein with this particular V3-loop did not behave X4-tropic at all. Entry into both C8166 cell lines was at background levels. However, entry into SupT1-R5 cells demonstrated the viability of this variant. A clear CCR5-dependence could furthermore be shown

on Affinofile cells, where induction of both CD4 and CCR5 was needed for entry. Overall low entry efficiencies of this variant hampered the calculation of IC_{50} values in response to MVC treatment. However, a clear sensitivity towards the CCR5-antagonist could be established, while the virus did not respond to the CXCR4-antagonist.

3.2.8.3 The clearly X4-predicted clone X4_7b

The likewise very clearly X4-predicted clone X4_7b reacted as expected in all tests and in line with its predicted X4-tropism. It entered into all cell lines tested, independent of the expression level of CCR5. A slight decrease in entry efficiency was observed in the cell line C8166-R5 in comparison to its parental cell line, C8166. On Affinofile cells, a dependence on CD4-levels was visible, although not as exclusive as for the standard X4-tropic variant NL4-3. In regard to drug sensitivity, X4_7b behaved as expected as well: inhibition was achieved only by AMD, whereas even high concentrations of MVC did not inhibit entry of this variant.

3.2.8.4 The ambiguous-predicted clone X4_C15

X4_C15 did not show significant entry into any of the systems tested. Even very high virus input levels did not rescue entry efficiency.

3.2.8.5 The ambiguous-predicted clone X4_25a

This clone lacking any clear tropism prediction behaved clearly as a R5-tropic virus in all cellular assays. It only entered cells when CCR5 was present and was inhibited by MVC but not AMD. The R5-tropism had been predicted by webPSSM and the lack of a charged amino acid at position 11 or 25 equally hinted at this phenotype. However, the SI-classification of the original patient's sample was in favour for the wrong X4-prediction.

3.2.8.6 The clearly X4-predicted clone X4_C26

This variant showed an ambiguous behaviour opposed to the very clear tropism prediction by all different methods tested. On T-cell lines, the virus was readily able to enter into cells lacking the CCR5-co-receptor. However, it was not shown to be sensitive to AMD and slightly sensitive to MVC. This hint towards a dual-tropic behaviour was strengthened on Affinofile cells. In these cells, X4_C26 only entered when they had been induced for CCR5-expression. In addition, a strong sensitivity towards MVC was observed on this cell line.

3.2.8.7 The clearly R5-predicted clone R5_C29 and R5_C30

Both clearly R5-predicted clones that we chose to take into the initial selection were found to behave as expected. No entry was observable on cell lines without CCR5-expression and a clear inhibition was detected in the presence of increasing amounts of MVC but not AMD.

3.2.8.8 The ambiguous-predicted clone X4_36b

The last ambiguous clone in this panel was found to be clearly R5-tropic in all assays including drug sensitivity.

In conclusion, the whole spectrum of outcomes was observed, ranging from confirmation of the predicted phenotype (two standard clones as well as one X4-variant and both R5-variants), over the clear characterization of ambiguously predicted variants, to the revelation of opposing phenotype (one clearly X4-predicted variant proved to be R5-tropic) and the discovery of one dual-tropic variant. The overall bias in the selection towards X4-prediction (6/8) was therefore turned upside down with the majority of clones proving clearly R5-tropic after careful examination (5/8).

4 Discussion

4.1 Fluorescently labelled viruses to study virus cell interactions

In the first part of the thesis, an alternative labelling approach was developed which offers new possibilities to study virus entry and egress. Furthermore, the system of fluorescently labelled HIV-1 derivatives has, for the first time, successfully been implemented for HCVpp. In addition, new single-particle techniques making use of theses fluorescently labelled viruses could be established and were utilized also to study the binding of HIV-1 derivatives to individual cells in dependence of different factors.

4.1.1 SNAP-tag as a tool to study virus release

The insertion of the SNAP-tag into the ORF of HIV-1 *gag* proved to be a promising expansion of the already existing palette of fluorescence labelling tools for viruses. The effects of this modification on particle release, entry efficiency and infectivity were minor and completely restorable by the equimolar addition of wt Gag. The most promising part of this full characterization of HIV^{SNAP} is the non-detrimental effect on replication capacity without the need for mixing with wt HIV. In contrast to similar constructs with a fusion of MA to eGFP (B. Müller, personal communication), the spreading in culture was observed to similar final levels as wt, although with a lower initial speed, and the inserted tag proved to be expressed stably over several replication rounds. This offers the possibility to use the constructed HIV^{SNAP} variants in infected T-cells and to easily label particles produced from those.

The introduction of an additional HIV-1 protease cleavage site before the MA-SNAP-tag junction did not improve the impaired replication speed any further. This is in contrast to the eGFP label, which could be shown to replicate to significantly higher degrees if the second cleavage site was present (data not shown and [98]). In the case of HIV^{SNAP} the second cleavage site may even represent a drawback rather than an improvement: The original MA.SNAP fusion should allow studying of tagged and labelled MA even after entry into newly infected cells, whereas this possibility would be lost with the full cleavage of SNAP-tag from the viral components.

Labelling of HIV^{SNAP} particles and of the tagged Gag precursor within transfected cells was easily applicable and initial pulse-chase experiments have been conducted. The quite rapid labelling of newly synthesized Gag^{SNAP} after 5 min of chase period seemed surprising. However, under closer examination this result may in part be influenced by the design of the experiment.

First, the synthesis of new protein had not been inhibited, e.g. with cycloheximide [172]. Thus, already translated proteins which had not been folded properly at the time of blocking with non-labelled SNAP-substrate, could finish folding within this short time period and then be ready for labelling. Second, the staining protocol itself harbours the possibility of underestimation of the time needed to produce new fusion protein: The fluorescently labelled substrate was offered for staining according to manufacturer's suggestions for 15 min at 37°C, thereby prolonging the chase period to 20 min instead of the assumed 5 min. Besides reduction of staining time, which might come at the expense of lower signals, another strategy could be possible to circumvent this issue. It has been shown that the SNAP-tag retains its self-labelling activity even after fixation (manufacturer's information and personal communication with J. Chojnacki). This could be used by fixing cells directly after the chase period and only subject them to labelling afterwards in order to minimize the overlap of chase period and staining time.

This method would also render HIV^{SNAP} amenable to labelling with e.g. Atto or Dyomics dyes. These organic dyes display a higher quantum yield, enhanced photostability and an improved spectrum of available excitation and emission wavelengths. With this method, new imaging techniques, such as simulated emission depletion (STED) microscopy [90] or stochastic optical reconstruction microscopy (STORM) [202] could also be applied to study trafficking of HIV-1 Gag. These methods allow the detailed investigation of protein interactions with a resolution below the diffraction limit [96]. For example, interactions of HIV-1 Gag with the cellular components of the ESCRT complex at individual budding sites would be of major interest and those studies are pursued in our department as well as in collaboration with others (W. Muranyi, S. Ivanchenko, personal communication). However, available Atto or Dyomics dyes have the disadvantage of often being cell impermeable. Therefore, one challenge to make use of the SNAP-tag also in live cell experiments is the development of a wider variety of cell-permeable organic dyes. Several methods aiming at this have been developed and are currently under investigation [142].

4.1.2 Fluorescently labelled HCV pseudoparticles to dissect the steps of virus entry

The combination of fluorescently labelled HIV-1 derivatives and HCVpp was successfully established in this study, creating fluorescently labelled HCVpp which were used to investigate binding and endocytosis. Until very recently, binding of HCV particles has been studied by indirect measurements exclusively. For example, a soluble version of E2 (sE2) was used to mimic cell binding of HCV [11]. In addition, HCV binding to cells was studied with insect cell-derived HCV-like particles [14] and by quantification of the amount of bound viral RNA [159]. In contrast, the virus binding assay established in this thesis provides information on the single particle level by direct visualization of particles bound to host cells. Inhibition of HCVpp binding to cells by competition with heparin proved the functionality of this assay, as this phenotype had

been shown already by other techniques [11, 122]. The observed independence of HCVpp binding to Lunet cells from HDL is also in line with previous findings on a different cell line [55].

Single-cell analysis comes at the expense of high cell to cell variations. The differences of e.g. surface expression of proteins during the replication cycle of each individual cell are levelled out in bulk analyses. Each individual cell will add to the overall population, resulting in a Gaussian shaped distribution of cellular marker proteins as well as other parameters that might be dependent on the stage of the cell cycle. The width of variation is not shrinking with increasing sample sizes, although differences may statistically become more significant. In bulk assays, the width of these single-cell variations is the same, but basically never surfaces, as it is included in the mean values that are measured. In single-cell analyses, these variations often handicap easy interpretation of data and only very strong phenotypes can easily be observed. On the other hand, this technique provides a much more detailed picture of the individual steps during virus entry.

The advantage in resolution that is obtained with single particle analysis is unfortunately accompanied by another drawback. The very low specific infectivity of HCVcc (on average, app. only every 1000^{th} - 10000^{th} particle is infectious [137]) leads to a very high number of "background" events which is counter-productive for single-particle methods. The low number of infectious particles per total amount of particles is most likely even further decreased in the HCVpp system. Although this model system has very successfully been used in the past to study various aspects of the early steps of the HCV replication cycle, many limitations have been discussed repeatedly. First, the incorporation of HCV E1E2 into retroviral particles occurs randomly. Due to an ER retention signal, E1E2 are normally forced to stay at the predicted site of HCV particle assembly [57]. However, this localization is undesired for incorporation into retroviral particles, as budding of HIV-1 occurs predominantly at the plasma membrane [167, 241]. In addition, the amount of Env protein incorporated per virion is most likely different for HCV and HIV-1. HIV-1 has been shown to incorporate a very low number of Env proteins into its lipid envelope, probably as few as 10 to 20 Env trimers [254]. In contrast to this, the closest relatives of HCV that has been studied in this regard, i.e. Dengue virus, showed a dense packing of Env proteins (~180 per virion) covering the entire viral particle surface [125]. The amount of E1E2 incorporated into wild type HCV particles is not known yet, but similar high levels could be assumed. The unspecific binding to as well as uptake into cells observed with fluorescently labelled HCVpp in this study could result from this hurdle. Minor differences in binding and endocytosis which are dependent on the presence of E1E2 would be missed if they are obscured by the presence of particles carrying too few glycoproteins on their surface.

In addition, another issue of HCVpp has to be taken into account. HCV produced in cell culture or isolated from patients has been found to possess a variety of buoyant densities, which results from the close association of virus particles with different lipoproteins, i.e. LDL and

VLDL [7, 71]. Infectivity of different particle fractions has closely been linked with this association: Particles of low density show much higher infectivity than the majority of the preparation. This fact, as well as the involvement of cellular molecules which interact with lipoproteins in their original function, i.e. the attachment factor LDLr and one of the receptor molecules of HCV, SR-BI, imply an important contribution of lipoproteins to the entry process of HCV. Due to their production from non-hepatic cells as well as the changed budding location and mechanism driven by their retroviral core, HCVpp do not associate with lipoproteins *per se*, therefore lacking this important facet of the entry process. The presence of HDL during infection with HCVpp can mimic the association with lipoproteins and enhance entry efficiency [56], although the clear mechanism of this association has not yet been elucidated.

Nevertheless, the fact that HCVpp can be produced easily and handled under lower safety conditions than fully infectious HCVcc makes them a valuable tool for many fields of study. The dissection of HCV entry into several clearly defined parts has been the goal of this part of my thesis. Binding and cellular uptake of particles were studied with the above described fluorescently labelled HCVpp, whereas the next step in early replication, fusion of viral and cellular membranes, was approached with another technique.

The β-Lactamase virion fusion assay has long been established for quantification of HIV-1 cytosolic entry. It measures the steps up to cytosolic entry uncoupled from any subsequent steps in the replication cycle by incorporation of the enzyme β-Lactamase into virions which can upon cytosolic delivery cleave a substrate loaded to cells. Several optimization steps accomplished in this thesis led to the successful implementation of this assay for HCVpp entry into susceptible cells. With this, the dependence of HCVpp cytosolic entry on several factors could be proven: enhancement of cytosolic entry by HDL, opposed to its inhibition by oxLDL, αCD81 antibody, inhibition of endosomal acidification and the presence of heparin.

While this assay is completely uncoupled from later steps in the replication cycle, it is still tightly associated with the steps preceding fusion. Therefore, no clear conclusion can be drawn whether these factors influence only fusion itself or the attachment and specific binding before. For heparin, a clear implication in binding has been shown by the virus binding assay, as described above. In contrast to this, HDL was dispensable for binding and uptake but clearly enhanced cytocolic entry of HCVpp. In the same line, CD81 expression on the target cell surface and the presence of E1E2 on the particle surface could not been shown to be involved in particle binding and uptake, but were clearly shown to be necessary for cytosolic entry in Lunet cells. This implies an involvement in a step between endocytic uptake and cytosolic delivery of the virus core. The clear temporal confinement of CD81 action is in agreement with a current model of HCV entry, in which HCV glycoprotein binding to CD81 is thought to trigger the transport of bound virus towards tight junctions in an actin-dependent way [27]. The model proposes that

only there, it can then engage the two subsequent receptors CLDN and OCLN, which both are tight junction proteins. A similar mode of entry has been shown for coxsackievirus group B, where primary binding to a receptor triggers actin-dependent transport to the tight junction localized receptor that promotes particle internalization [43].

The shortcomings of HCVpp as discussed above also apply for the BlaM assay established here. Incorporation of β-Lactamase into HCVcc could therefore be a desired goal. HCV reporter viruses used so far contain a reporter gene coding for luciferase or a FP inserted into the viral genome (e.g. [122, 228]). This requires the expression of the reporter inside the infected cell and thus is a less direct measure for virus entry than provided by the BlaM assay. Incorporation of viral fusion proteins provided in *trans* comparable to the method applied with HIV-1 and Vpr fusion proteins, has not been adopted, yet. Recently, a reporter system based on the cleavage of a cellular expressed FP fusion protein by the viral protease has been established with two different readouts: secretion of the FP [100] and change of subcellular localization of a FP fusion protein [108]. Other than that, fluorescence labelling techniques of HCV mostly comprise the fusion of single viral proteins to FPs to study their subcellular localization and interaction with several cellular proteins (e.g. [212]). The use of fluorescently labelled HCV in real-time single particle imaging would have been an implication of the fluorescently labelled HCVpp described in this thesis. The above mentioned hurdles however hampered this plan, so far. Although the authors using the change of subcellular localization as a marker of infection claim real-time imaging of HCV entry with this technique [108], another recent report fulfils this task using live cell microscopy [41]. There, Coller and colleagues describe the labelling of HCVcc with the lipophilic dyes DiD and DiI, analogue to studies with other viruses, including Dengue virus [230, 231]. The use of HCVcc offers the advantage of production of particles in relevant hepatic cells, which leads to the association with lipoproteins and the possibility of isolation of highly infectious fractions of virus associated with a certain buoyant density thus circumventing the problems arising from the use of HCVpp.

4.1.3 Fluorescently labelled HIV-1 derivatives

In contrast to the findings with HCV pseudoparticles, HIV-1 attachment to T-cell lines was found to be dependent on the presence of Env in viral particles. This finding is in line with a report showing the CD4-dependency of HIV-1 cell binding by inhibition with soluble CD4 and blocking antibodies [17]. The amount of particles bound per single cell was cell-type specific, with more particles binding to C8166 than SupT1-R5 cells. The unspecific binding of Env(-) particles was also increased on C8166 cells, hinting at an at least partial contribution of non-CD4-specific interactions. T-cell lines have been shown to harbour differing levels of HSPGs whereas primary

T-cells display only low levels on their surface [173]. C8166 cells display high surface levels of HSPGs (M. Lampe, personal communication), which probably contribute to this enhanced binding. In addition, several other attachment factors could play a role. The most prominent attachment factor known for HIV-1 is DC-SIGN, which is expressed on dentritic cells and helps them to capture virus to facilitate spread to T-cells [131]. In addition, the incorporation of the cellular protein ICAM-1 (intercellular adhesion molecule-1) into viral particles has been shown to facilitate virus binding to host cells expressing the ligand LFA1 (leucocyte function associated antigen 1) [94]. In conclusion, the high level of unspecific binding of HIV-1 to C8166 cells has implications on studies of the early events of HIV-1 replication: To enhance the chance of observing meaningful interactions of the virus with its host cell, cells with a low amount of unspecific binding should be chosen. The SupT1-R5 cell line therefore represents a good tool to study HIV-1 attachment and binding in greater detail and on the single-cell level.

The observed time-dependent increase in Env-dependent binding to cells over 4 h is most likely explained by a "scanning" mechanism of viral particles along the cell surface for CD4-molecules. Time-course studies of HIV-1 infectivity showed that the majority of entry occurs during the first two hours after virus addition at 37°C (B. Glass, personal communication). The virus binding assay has been carried out at room temperature, thus possibly prolonging this increase in specific binding over a period of four hours.

HIV-1 binding to cells was shown to be independent from the surface concentration of the cellular restriction factor CD317. It has recently been shown that CD317 acts as the physical tether between newly budded viruses to the membrane of infected cells [85]. The observed phenotype seems to be counter-intuitive for this proposed mechanism. Since incorporation of CD317 into virus particles is not changed in the presence or absence of the viral countermeasure Vpu [82], the tethering activity in dependence of Vpu should be explained by the cellular part in some way. This could then also lead to a positive effect in cell-free virus infection of neighbouring cells by enhanced attachment. However, an artificial system had to be used to study this aspect: fluorescently labelled particles were produced by transfection of cells and then purified and concentrated by ultra centrifugation. After this step, the particles were resuspended in FCS-containing buffer to prevent aggregation in the following freezing step. One possible explanation is that this freeze-thaw circle harmed the tethering activity of Tetherin in some way. Another possibility would be the shielding of interaction sites by the high protein amounts in the added FCS. In addition, the unspecific attachment of virus particles to cells could also play a role. To prevent this, HSPGs were removed from cells by heparinase I treatment before the addition of virus. The effect of significantly lowered virus binding to cells in comparison to untreated control cells could be shown, although the decrease of cellular heparan sulphate could not be proven by

flow cytometry. This argues that residual amounts of HSPGs could still mask specific differences in particle binding. Assessment of virus binding on more relevant cells such as primary T-cells could shed more light in this question.

Another explanation is the time point of establishment of the intermolecular interaction. The tethering phenotype has been observed in cells producing virus progeny. The interactions between adjacent CD317 molecules will therefore most likely be established during this budding process. An interference with the interaction at this stage could block the tethering phenotype, not only by depletion of the molecule from the cell surface. The incorporation of one of its membrane anchors in either of the tethered membranes, viral and cellular, could be a possibility for this. This model of tethering is in line with results from Perez-Caballero and colleagues who favour the integration of parallel homodimers of CD317 in a fashion that either the C- or the N-terminus of both molecules are anchored in one and the other terminus is anchored in the opposing membrane [181]. Another very recent report implied the existence of long connections between tethered particles or cells, hinting at the involvement of several dimers of CD317 [85]. This establishment of multimers of CD317 would also point in the direction that tethering of particles can only occur during budding and not be established retrospectively after this process is finished.

4.2 Patient- and drug-specific models of HIV-1 entry

In this part of the thesis, new techniques to study the entry efficiency of HIV-1 in dependence on multiple parameters have been established. All of these have been designed to provide a very detailed insight on the interdependencies of viral and host cellular factors during entry and were hence developed on single cell basis. These multidimensional data are currently being used to develop and compute mathematical models of HIV-1 entry and should lead to a better understanding of this process and the impact of entry inhibitors.

4.2.1 Experimental systems to create multidimensional data

In order to create a system in which reliable and quantitative data on the entry efficiency of HIV-1 derivatives could be gathered, several decisions had to be made. On the one hand, the system had to be variable enough to provide a wide span of data. On the other hand, these variables had to be controlled tightly so that quantitative data could be obtained. In addition, all variables should be well defined to provide a solid basis for mathematical modelling.

To do so, we chose the following parameters to be varied: Surface concentration of CD4 receptor molecules on the target cell, surface concentration of CCR5 co-receptor molecules on the

target cell, V3-loop sequence of HIV-1 Env protein and presence of different concentrations of prototype entry inhibitors.

4.2.1.1 Cell systems with variable receptor and co-receptor levels

For the purpose of variation of receptor and co-receptor molecules on the cell surface, several options were considered. The HeLa-derived cell line collection described by the Kabat laboratory [110] is composed of a panel of cell lines that express differential amounts of CD4 and got later on extended by cells with different CCR5-expression levels [186]. These cells nevertheless possess the drawback of the possibility of subtle differences between the different cell clones as also discussed below. A B-cell line inducible for CD4 expression [124] had also been discussed, but was dismissed due to the availability of a more versatile option. The recently established dual inducible cell line Affinofile [105] proved as a useful tool. Levels of both surface markers were found to be readily inducible in a wide range, although to a moderately lower bulk level as described in the literature. These differences can easily be explained by differing culturing conditions, e.g. the permanent selective pressure with all four antibiotics in contrast to the minimized setup of only one in the Lee lab. The expression range reached in this study however provided a wide variability of CD4 and CCR5 levels which can be resolved by single-cell analysis. Single-cell analysis of surface expression revealed a broad distribution of different expression levels of both receptors at the individual induction conditions (compare Fig. 3.46). Although the overall expression level was clearly dependent on the concentration of the respective inducing agent (compare also Fig. 3.25), the picture was different on the level of single cells. This becomes obvious if the Gaussian shape of receptor level distribution is taken into account, whereas only the mean value of the whole distribution is used in bulk analysis, which was also the case in the VERSA analysis. In contrast to this, the single cell analysis established in this thesis assigns the entry efficiency to the actual expression level of every single cell and thus appropriately integrates outliers within one induction condition. The much more detailed pattern of the dependence of entry efficiency on the levels of CD4 and CCR5 in single cell analysis can easily be explained by this.

The fact that CCR5-levels on Affinofile cells were found to be at the background of unstained cells does not exclude residual “leaky” CCR5-expression even in the non-induced control. Under some experimental conditions, CCR5-detection was hard to achieve in flow cytometry measurements. Interestingly, the entry of clearly R5-tropic viruses turned out to be much more sensitive than the CCR5-staining. A titration of a clearly R5-tropic strain down to very low CCR5-induction levels in direct comparison to co-receptor detection in flow cytometry could add to the answer of sensitivity.

Application of the Affinofile cell line is limited by the low expression level of the second major co-receptor, CXCR4. This resulted in low overall entry efficiencies of X4-dependent virus

variants, decreasing the effective range of observation. Therefore, the dependencies of those clones need to be evaluated further with higher virus inputs. In addition, the low expression level of CXCR4 also abolished the evaluation of its expression on the single cell level. Both read-out methods used, flow cytometry as well as the microscopic assay, rely on antibody recognition of the respective cellular surface molecules. Specific CXCR4-antibody binding to cells was below the detection limit in the microscopic assay and hence no direct evaluation of CXCR4 levels can be extracted from these single-cell data. To compensate for this, the Affinofile cells will be assigned a mean CXCR4-expression level based on the quantitative bulk FACS-measurements. Another possibility would be to establish a high-throughput FACS-based assay for the adherent Affinofile cell line, preferentially using a 96-well device.

Another way to circumvent the low CXCR4-expression on Affinofile cells is the use of another cell line. In this regard, the T-cell lines used in this study represent a valuable addition to the spectrum of data generated. The major cause why we initially decided to use the inducible Affinofile cell line system was the lack of a comparable variable system in T-cell lines. To be able to distinguish viruses with different tropisms, we used T-cell line pairs originally negative for CCR5 and only rendered $CCR5^+$ upon stable transfection. Although this strategy allowed comparing virus entry in presence and absence of CCR5, an identical cellular background is not given in this system. Upon transfection of the CCR5-expression plasmid, the parental cell line had to be put under selective pressure to select for clones stably expressing the desired co-receptor. This procedure, as well as individual adaptations of the individual cell lines could lead to small but significant effects on the evaluation of entry efficiency. This becomes evident when comparing the different CD4 expression level of C8166-R5 cells in comparison to the parental cell line, C8166 (compare Fig. 3.25). The advantage of the Affinofile cell line becomes obvious in this regard: the same pool of cells is seeded and will only be induced to express different levels of the desired receptor and co-receptor. However, the presence of inducing agents could also influence the cell's behaviour, as can be seen by the slightly altered CXCR4 levels under different induction conditions. Effects of these agents on the expression of the marker protein, GFP, have not been studied, but could also pose a possible interference. In addition, the presence of the inducing agent could in theory also interfere with the entry efficiency of viruses *per se*. This could be investigated by monitoring entry efficiency of a CD4- and CCR5-independent virus, such as VSVpp. This could rule out possible general effects of the inducing agents, although a final conclusion concerning HIV-1 entry cannot be drawn from this.

In this regard, the T-cell lines used again have an advantage over the Affinofile system. These cells, although being cell lines as well, are closer to the physiological target cells of HIV-1, primary T-cells. The cell culture system mimicking a physiological infection even better are freshly isolated human primary blood mononuclear cells (PBMC). These cells have already been used in initial experiments. However, the degrees of freedom increase with such a variable

system. Thus, the inclusion of PBMCs, which always pose a mixture of subpopulations of cells, will only be considered at a later stage of this project. To circumvent donor variations in $CD4^+$ percentages, $CD4^+$ enriched cell populations could also be used.

4.2.1.2 Systems to monitor entry efficiency

I made use of two different systems to monitor entry efficiencies of the diverse viral variants in this study. The BlaM assay proved to be a very useful tool in this, since it exclusively measures cytosolic entry of viruses [35]. If analysed by flow cytometry, it allows for single-cell data and the parallel surface staining of several cellular molecules. This strategy therefore allows extracting several parameters at once from every single cell: cell entry, CD4-, CCR5-, and CXCR4-levels. Furthermore, by combination of the raw fluorescence read-out and quantitative measurements of bulk receptor levels, the calculation of approximate numbers of receptor molecules on the single cell level is possible.

Due to very high background levels, the BlaM assay was not applicable for the Affinofile cell line. This high cellular background signal most likely stems from the stable transfection of four plasmids into those cells. β-Lactamase is a bacterial protein that confers resistance to antibiotics by cleaving the β-lactam ring of e.g. ampicillin. It is thus encoded in every plasmid harbouring the *amp*^{r} gene for bacterial selection. Although the gene is usually inserted in antisense orientation in relation to the gene of interest on eukaryotic expression vectors and is driven from a prokaryotic promoter, there could be leaky expression as described in early studies of bacteriophage expression in mammalian cells [149]. Also, random integration of the plasmid DNA could lead to the positioning of the bacterial gene downstream of a mammalian promoter and hence lead to gene expression of the β-Lactamase gene. I tried to deactivate the intrinsic β-Lactamase in Affinofile cells by incubation at elevated temperatures. This markedly decreased the intrinsic BlaM signal in these cells and allowed the detection of a virus-delivered heat-stable β-Lactamase [88]. However, the heat-treatment interfered with the controlled detection of fusion-dependent signals, as also Env(-) particles were able to deliver the heat-stable β-Lactamase. Therefore, this system cannot be used.

Due to this, another technique was sought to easily monitor entry efficiencies. The GFP-transduction system proved as a very useful tool in this regard. Although this assay does not exclusively measure cytosolic entry of the virus but relies on the expression of a marker protein, it has widely been used to study the entry of different viruses into their host cells. Results obtained with this method showed higher entry efficiencies in Affinofile cells than on the two tested T-cell lines. This might reflect the entry efficiency, but could also be an artefact of higher expression from the *gfp* reporter gene in Affinofile cells. Comparing the entry efficiency of similar virus input on the T-cell line in the BlaM assay versus GFP-transduction would strengthen this point, but a

clear correlation is hard to be made due to different virus preps used. A combination of both systems by incorporation of Vpr.BlaM into the GFP-transducing vector particles would allow a direct correlation of this issue, though.

The microscopic assay established in this study allows the quantitative investigation of the relationship between entry efficiency and the expression of receptor and co-receptor molecules on the single cell level. The key step in this assay possibly is the segmentation of single cell bodies. This step has been shown to be possible for example on actin staining of cells (K. Börner & Ch. Sommer, personal communication). This additional staining step however would slow down the complete procedure of this method by requiring more processing time of the sample, accompanied by the possible loss of cells due to additional washing steps, and the recording of additional images which also implies the usage of additional filter sets not interfering with the original microscopy. To circumvent this, the segmentation process was adapted to the already existent cell surface stainings for receptor and co-receptor. In a setup with different induction conditions, the lack of expression of either of those receptors poses a hurdle for proper segmentation in this channel. Thus, a maximum projection of both channels was used as the segmentation input. With this, the lack of a strong signal in one of the two channels could be compensated.

In this study, only entry efficiency of cell-free virus was taken into account. Viruses of several families, including HIV-1, have been shown to use direct transmission routes from cell to cell [206]. For HIV-1, the most prominent way to do so is via the formation of a so-called virological synapse (VS). This area of cell-cell contact between an infected cell and an uninfected target cell is enriched in receptor and co-receptor molecules on the target cell side as well as Env protein at the surface of the infected cell. Cells are held in close contact by interactions of cellular surface molecules as well as Env-receptor interactions [106, 107]. This method of spread is much more efficient than cell-free virus infection; reports range from 1 to 4 orders of magnitude [38, 217] and is thought to play a crucial role in *in vivo* infection. The possibility to inhibit this cell-to-cell spread by entry inhibitors has been discussed controversially. However, a recent report showed the accessibility of even preformed VS to a broad range of entry inhibitors, including T20 and two co-receptor antagonists [146]. A minor preference of cell-free virus entry inhibition was found with the CCR5-antagonist TAK 779 resulting in a slightly shifted dose-response curve, while no significant difference in IC_{50} values was observed. The fact that in this study, free virions were found within the gap between both cells engaged in the VS argues in favour of similar overall entry mechanisms for both transmission routes, cell-free versus cell-to-cell spread.

Another issue that has been discussed in regard to sensitivity towards entry inhibitors is the involvement of endocytic entry for HIV-1, which has recently been proposed to be the

predominant route of entry [152]. Regardless of the route of entry, many years of research have clearly validated the necessity of the HIV-1 Env protein in the entry process. It has been speculated that entry via the endocytic route may prevent the accessibility of entry inhibitors to the site of entry. *In vivo*, the drug will however be present before encounter of virus and uninfected cell – no matter if the transmission will occur via cell-free virus or cell-to-cell spread. To mimic this scenario, we preincubated cells with the respective drug before the addition of virus. With this, the simultaneous uptake of drug and virus into endosomes which may lead to productive infection is enabled. The influence of endocytosis on virus entry should nevertheless be considered. Unspecific uptake of virus may end in an unproductive dead-end. The amount of unspecific binding and uptake is a cell-type dependent feature (compare 3.1.3.1), thus introducing possible differences between the systems used here and the *in vivo* situation. In SupT1-R5 cells, the CD4- and Env-dependence of viral endocytosis suggests a specific entry mechanism via this route (N. Herold, personal communication), whereas other cell lines have been shown to display massive unspecific particle uptake. The thereby created difference of virus available for specific interactions could lead to a difference in entry efficiency and should be included if data of different cell types are compared.

4.2.2 Evaluation of the selected V3-loop variants

The V3-loop is, as its name implies, a highly variable sequence within the HIV-1 Env protein. During the course of an infection, the virus evolves very quickly to escape immune recognition and potential antiviral treatment. Variations in nucleotide sequences are mostly acquired by random errors of the viral reverse transcriptase lacking a proof-reading function [196]. However, exogenous sequences originating from the host cell genome can be incorporated into the viral genome, as described by a recent study where a 15 bp insertion from the gene of a transcription factor into the V3-loop sequence resulted in a co-receptor switch of the respective virus variant [245]. Even smaller changes in the V3-loop can change the tropism of the virus carrying it, which makes this short sequence an optimal target for variation when studying virus tropism.

In this work, the selection process of the V3-loop variants was conducted based on the comparison of the outcome of several prediction tools in combination with the reported SI/NSI-phenotype of the original patient's sample the sequences were obtained from. The selection from this pool of samples could be viewed as biased *per se*. All samples were sequenced from frozen stocks of virus supernatant of the co-culturing of primary isolates from patients with uninfected PBMCs. It has been reported that X4-tropic viruses can be expanded *in vitro* more easily than R5-variants, leading to a bias towards more X4-tropic clones. Samples from patients with exclusively R5-tropic variants may not have spread in the cell culture in the first place. An additional factor would be the outgrowth of minority X4-tropic populations under those uncontrolled conditions.

No means to prevent this have been available at the time of collection (1986 until 1989). If samples would be collected today, the viral sequences could be obtained directly from patient's plasma without any intermediate *in vitro* expansion step. This bias in X4-selectivity was also clearly reflected in the fact that the majority of primary samples showed an SI phenotype (63/94).

The set of V3-loops used for this analysis nevertheless lead to an interesting panel of results. Tab. 4.1 summarizes the initial prediction as well as the experimental outcome for all individual clones. Taken together, these results led to the conclusion regarding the true tropism shown at the end of the table.

		Prediction					Entry efficiency			Affinofile		Inhibition by MVC			Conclusion
patient #	clone #	g2p	FPR	PSSM	11/25	SI/NSI	C8166	C8166-R5	SupT1-R5	$CD4^+$	$CD4^+CCR5^+$	SupT1-R5	IC_{50} [nM]	Affinofile	
220	X4_C3	X4	1.7%	X4	+	SI	-	-	+	-	+	+	n.d.	+	R5
286	X4_7b	X4	0.2%	X4	+	SI	+	+	+	(+)	(+)	-	n.d.	-	X4
409	X4_C15	X4	2.9%	X4	-	SI	-	-	-	-	-	-	n.d.	(+)	n.d.
651	X4_25a	X4	8.6%	R5	-	SI	-	(+)	++	(+)	++	+	3.9	++	R5
685	X4_C26	X4	0.2%	X4	+	SI	(+)	-	++	-	(+)	-	n.d.	+	dual
822	R5_C29	R5	55.7%	R5	-	NSI	-	+	++	+	++	+	16.5	+	R5
838	R5_C30	R5	24.7%	R5	-	NSI	-	+	++	+	+++	+	30.4	+	R5
924	X4_36b	X4	3.9%	X4	-	NSI	-	+	+	+	+++	+	40.1	+	R5
	NL4-3	X4	0.7%	n.d.	+	SI	+	++	+	++	+	-	n.d.	-	X4
	NL4-3 R5	R5	20.7%	n.d.	-	n.d.	-	+	++	+	+++	+	62.3	+	R5

Tab. 4.1: Summary of selected variants. Prediction outcome, entry efficiency, sensitivity to MVC and conclusion of tropism drawn from all data are depicted for the individual clones. g2p = geno2pheno$_{[coreceptor]}$, FPR = false positive rate at which prediction would switch to X4 in g2p, PSSM = webPSSM, 11/25 = charge rule, SI/NSI = phenotype. Entry efficiencies are indicated by symbols with different margins for the different cell lines. C8166 and C8166-R5: -<0.2 %, (+)<0.5 %, +>0.5 %, ++>5 %; SupT1-R5: -<2 %, +<10 %, ++>10 %; Affinofile: -<1 %, (+)<5 %, +<20 %, ++<50 %, +++>50 %. n.d. = not determined.

In summary, all clearly R5-predicted clones were shown to behave as predicted, whereas the X4-prediction was much less accurate. Only the standard clone NL4-3 as well as one selected variant, X4_7b displayed a clear X4-phenotype after careful investigation.

One of the clearly X4-predicted clones (X4_C3) was shown to be wrongly predicted and displayed a clear R5-tropism instead. Evaluation of the factors that led to the wrong classification of this clone with all available prediction programs despite the very clear *in vitro* phenotype will be very interesting. The counter-intuitive SI-phenotype could easily be explained by the existence of X4-tropic variants within the patient's quasispecies [200]. Deep-sequencing of this patient's sample and retesting several clonal V3-loop sequences in our assay system could therefore be interesting.

The case of variant X4_C26 is particularly interesting, as the viruses harbouring this V3-loop showed an ambiguous behaviour in all experimental setups opposed to the very clear X4-tropism prediction by all different methods tested. The most possible explanation for the displayed phenotype in concordance with the seemingly wrong X4-prediction by the various algorithms is the following scenario: The V3-loop present in this variant is capable of utilizing

CXCR4 as a co-receptor for entry, hence the prediction algorithms were right with their prediction. All of the web-tools available have been trained to distinguish if a sequence would hint at the possibility of CXCR4-usage or not. If this possibility exists, the output will be X4-tropic, while only purely R5-tropic variants will be assigned as such (see also below). Syncitium-formation with T-cell lines is therefore also an expected phenotype, as the utilized reporter cells express this receptor and therefore infected cells will be able to form syncitia with neighbouring uninfected cells. If CXCR4 is not present or blocked, this particular V3-loop sequence allows the utilization of CCR5 as a co-receptor, as well. Obviously, Affinofile cells express too low CXCR4-levels on the cell surface to be able to act as a co-recetor for X4_C26. Hence, on these cells the entry efficiency is CCR5-dependent. This also explains the lack of sensitivity to AMD-treatment on these cells as well as on SupT1-R5 cells (data not shown). MVC on the other hand can efficiently block the only remaining alternative for X4_C26 to enter into Affinofile cells, whereas the virus will still utilize CXCR4 on MVC-treated T-cell lines. For this clone, it would be of particular interest to establish the dependence towards combinations of both drugs on T-cell lines expressing both co-receptors.

Whereas two variants that had been ambiguously predicted turned out to be clearly R5-tropic (X4_25a and X4_36b), X4_C15 did not show significant entry in any of the systems tested. Therefore, a problem of this variant seems to be very likely. In the light of the way that all sequences were obtained, this is nevertheless not easily understood. The V3-loop sequence of this variant, as well as all other sequences used in this study, was amplified from a coculture of patient's sample with PBMCs. Hence, this particular V3-loop sequence must have existed in the patient's sample and most likely also to a high extend, given the clonal sequence obtained from this amplification. Sequencing of the whole *env* gene of this variant could maybe give a clue whether just the combination of this particular V3-loop with the gp120 backbone of NL4-3 is defective.

4.2.2.1 Overrepresentation of R5-tropism

The fact that the majority of sequences were found to display an R5-tropic phenotype after careful examination is in the range of expectations. R5-tropic variants have been shown to be transmitted between infected individuals in the majority of cases [16]. This is in line with current tropism-testing, where 85 % of all viral sequences in patients that are treatment-naïve were R5-tropic [39]. Even in treatment-experienced individuals, this number only went down to 56 %. However, if cultured *in vitro*, X4-tropic variants have an advantage over R5-tropic strains. This fact most likely explains the overrepresentation of SI-phenotypes in the pool of sequences in the first place. However, some of these variants with SI-phenotype were shown to harbour an R5-tropism.

4.2.2.2 Overrepresentation of X4-prediction

A discrepancy between more sequences in our selection being predicted to be X4-tropic and more of those variants displaying a clear R5-tropic phenotype in the experimental systems was observed in this study. All available co-receptor prediction algorithms have been developed in respect to the introduction of CCR5-co-receptor antagonists into the market. Due to the concurrence of disease progression and the emergence of X4-tropic variants [143], one goal during therapy with this new drug has been to avoid a shift of R5- to X4-tropism of the patient's virus population. Resistance development has been shown to mainly occur through the outgrowth of pre-existing minor populations of X4-tropic variants [134], and hence an emphasis has been made on avoiding the administration of the R5-antagonist in the presence of X4-tropic viruses within the patient. A positive treatment outcome has also been linked to the exclusive existence of R5-tropic viruses in the patient's quasispecies at baseline [86, 89]. Thus, prediction programs have been designed to detect X4-tropic variants with a high accuracy, therefore taking the risk of misinterpretation of possible R5-tropic variants. This tendency is reflected in the quite stringent recommendations to use the co-receptor tropism prediction program geno2pheno$_{[coreceptor]}$. The German recommendations that are currently in effect [235] suggest a false positive rate (FPR) of 20 % for patient's with other treatment options. This translates into 20 % of R5-tropic sequences to be falsely predicted as X4-tropic. For patients with strongly limited treatment options they recommend a FPR of 12.5 % and an additional phenotypic assay is advised. However, the web-tool also displays the FPR at which a switch from X4- to R5-tropic prediction would occur as a measure of accuracy of the prediction. This actual FPR was given as 1.7 % for the wrongly predicted clone X4_C3, which would be interpreted as a very good prediction of X4-tropism. Nevertheless, the FPR for the two clones that proved to be X4-tropic in all experimental systems, X4_7b and the standard NL4-3, had FPRs below 1 % (0.2 and 0.7 %, respectively). No clone that had been predicted to be R5-tropic proved to be X4-tropic in the end. This displays the high emphasis on safety of theses algorithms, while it clearly shows that there might be more room for specificity. The overrepresentation of X4-prediction in this study is in contrast to another report, where the overrepresentation of R5-prediction of clinical isolates was described [141]. Low and colleagues reported the tropism misinterpretation of primary clinical isolates by genotypic methods in contrast to phenotypic assays. The major difference to this study is the used of bulk sequencing data, whereas we applied the prediction algorithms on single clonal data.

In regard to the SI/NSI phenotype of the variants selected, some inconsistencies have been unravelled as well. The two clones X4_C3 and X4_25a have been reported to show an SI phenotype. Nevertheless, they clearly proved to be dependent on CCR5 as a co-receptor, hence a NSI phenotype would rather be expected. The weakness of this early phenotyping scheme clearly is the biased read-out. The judgement is based solely on visual inspection of T-cell lines

cocultured with cells infected with the patient's virus sample. The inherent possibility of misjudgement is obvious, as the phenotype itself is not restricted to virus infected cells alone. The spontaneous formation of syncytia has also been reported. In addition, if cocultured with PBMCs, cells from this latter population could be able to form syncytia when infected with R5-tropic strains, as those primary cells harbour both major co-receptors – at least parts of the population. Nevertheless, the expectation would have been to over-interpret the actual number of NSI-samples, as the formation of syncytia can sometimes hard to be seen. The read-out is therefore highly dependent on the person interpreting it, which introduces a wide error margin. These data were recorded at the time of sample collection, so a re-evaluation under today's standards would maybe shed more light on this aspect.

Due to the fact that disease progression has been linked to the emergence of X4-tropic variants during the course of HIV-1 infection [143], the prediction of their development is a major goal. Mild and colleagues have described the several factors in gp120 that could hint towards the development of an X4-shift, including V2-loop length, glycosylation density of gp120 and V3-loop net charge [150]. By observing longitudinal data, they found that those values can be predictive of a R5 population of patient's isolate to shift to X4 or not. The reduction of net charge of the amino acids of the V3-loop was significantly higher in virus of patients that did not display an X4-shift over the course of the study (up to 12 years). In our study, the variants shown to be able to utilize CXCR4, including the dual tropic variant, all showed net charges of 7 or higher, whereas the clearly R5-dependent variants had a mean net charge of 3.3 (scores: arginine and lysine = +1, aspartic acid and glutamic acid = -1), which is in line with previous findings [87]. In this analysis, clone X4_C3, which acted R5-tropic in our assays shows a relatively high value of 5, which could hint at a development towards X4-usage and probably explains the wrong initial prediction by all genotyping tools.

One of the ambiguously predicted clones that was proven to be R5-tropic in this study (X4_36b) could offer some deeper insight into the prediction process. While both web-based tools failed to predict the clear R5-tropism, the 11/25 rule as well as the NSI phenotype hinted in this direction. Nevertheless, it has been found to be quite far from other R5-sequences in sequence space (compare also location in Splitstree analysis, Fig. 3.26), which does not fit to the clear R5-tropism. A closely related sequence to clone X4_36b was included in the primary sequence pool, differing in only one single amino acid. This sequence was predicted R5-tropic by all methods used, so a direct comparison of both sequences could be of interest to elucidate why the two web-based prediction tools failed to correctly classify this sequence. In regard to the distance in sequence space, Bozek and colleagues have demonstrated that 98 % of all R5-sequences cluster

together [24]. This leads to a very low probability (2 %) that a clone with a V3-loop sequence as far in sequence space as X4_36b is truly R5-tropic. Exceptions of this are however observed, which can also be appreciated in the Splitstree analysis (Fig. 3.26), where a single blue dot (representing a random R5-tropic sequence from the Los Alamos Database) is found spread between the far separated red dots (X4-tropic sequences). The authors of the above mentioned study also report that sequences which were misclassified by all different genotypic methods were found to behave discordant in the sequence space and hence only a very slight improvement of prediction outcome could be observed when this analysis was integrated into existing classification methods.

4.2.3 Outlook and perspective

The data presented in this study represent a comprehensive quantitative analysis of the dependence of entry efficiency on several factors. The detailed characterization of several prototype sequences has been carried out successfully, although some further tests will be needed. These comprise mainly the evaluation of drug sensitivity of the individual clones to a greater extent. As mentioned above, the evaluation whether the two co-receptor antagonists show additive or even cooperative effects on the entry efficiency of the dual-tropic variant X4_C26 will be of great interest. Furthermore, the results describing the variants with low overall entry efficiencies will be repeated with higher virus input to increase the dynamic range of the experiments. On the other hand, transduction of Affinofile cells with R5-tropic variants resulted in very high numbers of positive cells. To exclude a masking effect of multiple integration events of the reporter virus which could lead to an underestimation of entry efficiency, these experiments should be repeated with lower virus input.

In addition, the correlation of results obtained with the newly established single-cell methods with already existing analyses will be crucial. The easiest way to do so will be the correlation with the VERSA analysis provided by the Lee lab and already applied to data from this study [105]. Comparable sensitivity vectors calculated on the single-cell data could serve as a control in reference to the VERSA analysis using bulk data.

4.2.3.1 Modelling

The huge amount of data obtained during this study will now be used to calculate mathematical models describing the complex relations between the different varied parameters and virus entry efficiency. To this end, preliminary models have already been calculated by our collaboration partners (K. Bozek, MPI for Computer Sciences, Saarbrücken, Germany). Multivariate regression models were used to describe and compare the entry efficiency

dependencies of the analyzed clones on the measured parameters. Regression analysis allows describing the entry efficiency as a function of the input parameters. Models have been trained on two variants with a clear R5- or X4-tropism outcome in all experimental systems. For this purpose, R5_C29 and R5_C30 were chosen as clearly R5-tropic, while the standard X4-variant NL4-3 and clone X4_7b were chosen as clearly X4-tropic. Vectors of parameter coefficients that depict each parameter effect on the cell entry efficiency of the respective model were extracted from the trained models. The normalized vectors of these multidimensional models were then compared to the normalized coefficient vectors of models trained on the data of all individual variants. A clone characteristic is quantified as the correlation between a vector of the given clone and vectors of the R5/X4-models. In these initial experimental models, data obtained on SupT1-R5 cells with the BlaM assay were used and experiments with two MVC-titrations and one AMD-titration were taken into account. The dependence of entry efficiency on all three monitored cellular molecules, CD4, CXCR4 and CCR5 as well as the drug response was included.

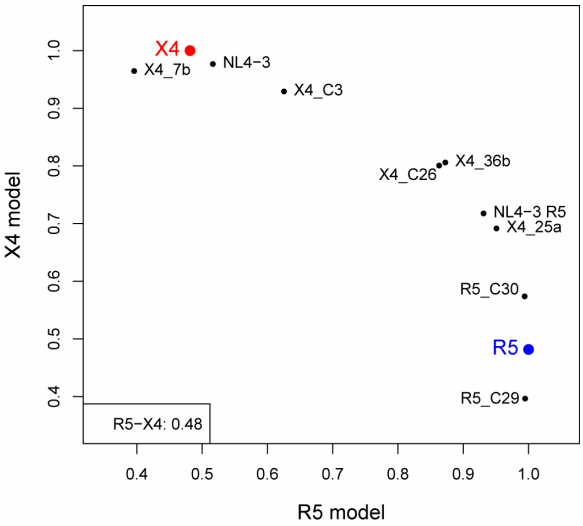

Fig. 4.1: Correlation of vectors describing mathematical models for the individual variants. X4 (red) model is trained on variants NL4-3 and X4_7b, whereas R5 (blue) is trained on variants R5_C29 and R5_C30. Correlation with both standard models is shown for distinct models trained on the individual variants. The overall correlation of both standard models is depicted in the lower left corner.

Fig. 4.1 depicts the correlation of these normalized vectors to the vectors of the R5- and X4- models. The blue and red dots symbolize the R5- and X4-tropic test-models, respectively, while all variants are labelled accordingly. A high correlation of a clone vector to a vector of either R5- or X4-model indicates similar entry efficiency dependencies. The overall correlation of the standard X4- and R5-models was 0.48 in this experiment, which reflects the interdependencies of the tropism of clearly defined variants. For example, all of the variants tested showed a clear CD4-dependency, which will increase the overall correlation of both phenotypes. The inclusion of CD4-independent viral variants could be of interest in this regard. Entry efficiency of the simian immunodeficiency virus clone 316 for example has been described to be strongly dependent on CCR5 but independent from CD4 [58]. This comparison of models for the different variants can help to distinguish between the impact of different factors if they are included in the process or not. An observed correlation of CXCR4- and CCR5-staining on cells

will have to be evaluated further and the impact of including only one of the co-receptors on the modelling outcome will have to be closely examined.

4.2.3.2 Inclusion of larger parts of Env

When modelling biological processes by mathematical methods, a lot of presumptions have to be made. For exact modelling outcome, all variables of the system have to be defined as exactly as possible. This is mostly hampered by the complexity of biological systems, where most of the interdependencies are not known, yet, and are therefore hard to take into account. Due to this, mathematical models of biological processes are always restricted to the conditions the model has been trained on.

Based on this thought, we decided to keep the variables of our system as small as possible, thereby aiming at the most precise mathematical model. On the viral side, we therefore started with the variation of a very small proportion of the Env protein, the V3-loop. Although this part of Env has been shown to play an essential role in co-receptor tropism [40], other regions of gp120 have also been implicated in this regard [176, 195]. Inclusion of the V2-loop for example has been reported not to increase the predictive value of co-receptor-tropism, however [24]. The probable importance of other Env regions is stressed by a study describing an *env* sequence with a partial V3-loop deletion that retains entry competence by adaptive mutations in both gp120 and gp41 [3]. Concerns that the Env backbone used in this study, namely the one of the X4-tropic standard clone NL4-3, could lead to a misinterpretation of the effect of the respective V3-loops inserted on entry efficiency could be raised. It has been reported that the insertion of an R5 V3-loop led to an incomplete shift in tropism [97] and the authors reported a role of sequences in gp41 to contribute to this phenotype. However, in the present study this does not seem to be very likely since most of the variants tested showed an R5-phenotype. If anything, an increase in X4-tropism would have been assumed. The complete *env* sequence could nevertheless shed more light on the involvement of other regions within the Env protein.

In this regard, another point from this study could also be important. It was shown here, that the amount of Env protein incorporated into viral particles correlated with the entry efficiency of the respective virus preparation, although the correlation was found to be associated with a high error rate. The importance of Env incorporation is stressed by another report, where differential incorporation of Env proteins from different virus isolates into pseudoparticles was observed and a correlation with entry efficiency was reported [189]. In conclusion, even if the amount of Env/virus is monitored closely and integrated into the calculations, an error will still result from pseudotyping. The inclusion of the varying V3-loop sequences into an *env*-containing proviral plasmid would pose a marked increase in reliability of Env-incorporation levels and rule out this source of error completely.

4.2.3.3 Longitudinal data from patients under MVC treatment and deep-sequencing of patient's samples

Although the course of HIV-1 infection can efficiently slowed down by the administration of HAART, escape of virus populations by resistance mutations is a major issue for successful treatment. Those mechanisms cannot easily be predicted, as for example a very unexpected resistance pathway has been described for protease inhibitors, where the virus escapes by mutation of the protease target sequence (Gag) rather than classical mutations within the active site of the enzyme [170]. The analysis of resistance development against the newly introduced co-receptor antagonist will be of major interest. The cooperation with the Department of Virology in Cologne offers the possibility to include longitudinal data from patients under MVC treatment, which will provide a useful data set for the quantitative analysis of these processes. Concerning this strategy, the possibility of ultra-deep sequencing of patient's samples will be of major interest. With this, the tracking of virus evolution under selective pressure is possible and could add to the understanding of resistance development. In particular, sequence variants that display an interesting genotype would be selected and tested quantitatively in the systems established here. Initial models developed from the data obtained so far will be helpful to decide on features of the sequences that could lead to the most insightful results.

The newly emerged field of systems biology is built on the premise that complex biological systems consist of several interdependent factors that interact in a non-linear, non-additive way [128]. This implies the need to look at the whole picture of biological events, rather than the separated small parts of them. Complex diseases like cancer are widely being studied by systems biology approaches [123]. Viruses are relatively simple organism which makes them amenable for the development of mathematical models. Although this study focused on one aspect of virus replication and thereby impeded with the non-reductive strategy, we still served the idea of systems biology by recording data including simultaneous information on several factors on the single cell level.

5 References

1. **Adachi, A., H. E. Gendelman, S. Koenig, T. Folks, R. Willey, A. Rabson, and M. A. Martin.** 1986. Production of acquired immunodeficiency syndrome-associated retrovirus in human and nonhuman cells transfected with an infectious molecular clone. J Virol **59**(2):284-91.
2. **Agnello, V., G. Abel, M. Elfahal, G. B. Knight, and Q. X. Zhang.** 1999. Hepatitis C virus and other flaviviridae viruses enter cells via low density lipoprotein receptor. Proc Natl Acad Sci U S A **96**(22):12766-71.
3. **Agrawal-Gamse, C., F. H. Lee, B. Haggarty, A. P. Jordan, Y. Yi, B. Lee, R. G. Collman, J. A. Hoxie, R. W. Doms, and M. M. Laakso.** 2009. Adaptive mutations in a human immunodeficiency virus type 1 envelope protein with a truncated V3 loop restore function by improving interactions with CD4. J Virol **83**(21):11005-15.
4. **Albanese, A., D. Arosio, M. Terreni, and A. Cereseto.** 2008. HIV-1 pre-integration complexes selectively target decondensed chromatin in the nuclear periphery. PLoS One **3**(6):e2413.
5. **Alkhatib, G., C. Combadiere, C. C. Broder, Y. Feng, P. E. Kennedy, P. M. Murphy, and E. A. Berger.** 1996. CC CKR5: a RANTES, MIP-1alpha, MIP-1beta receptor as a fusion cofactor for macrophage-tropic HIV-1. Science **272**(5270):1955-8.
6. **Alter, M. J.** 2007. Epidemiology of hepatitis C virus infection. World J Gastroenterol **13**(17):2436-41.
7. **Andre, P., F. Komurian-Pradel, S. Deforges, M. Perret, J. L. Berland, M. Sodoyer, S. Pol, C. Brechot, G. Paranhos-Baccala, and V. Lotteau.** 2002. Characterization of low- and very-low-density hepatitis C virus RNA-containing particles. J Virol **76**(14):6919-28.
8. **Arhel, N., A. Genovesio, K. A. Kim, S. Miko, E. Perret, J. C. Olivo-Marin, S. Shorte, and P. Charneau.** 2006. Quantitative four-dimensional tracking of cytoplasmic and nuclear HIV-1 complexes. Nat Methods **3**(10):817-24.
9. **Baba, M., O. Nishimura, N. Kanzaki, M. Okamoto, H. Sawada, Y. Iizawa, M. Shiraishi, Y. Aramaki, K. Okonogi, Y. Ogawa, K. Meguro, and M. Fujino.** 1999. A small-molecule, nonpeptide CCR5 antagonist with highly potent and selective anti-HIV-1 activity. Proc Natl Acad Sci U S A **96**(10):5698-703.
10. **Barre-Sinoussi, F., J. C. Chermann, F. Rey, M. T. Nugeyre, S. Chamaret, J. Gruest, C. Dauguet, C. Axler-Blin, F. Vezinet-Brun, C. Rouzioux, W. Rozenbaum, and L. Montagnier.** 1983. Isolation of a T-lymphotropic retrovirus from a patient at risk for acquired immune deficiency syndrome (AIDS). Science **220**(4599):868-71.
11. **Barth, H., C. Schafer, M. I. Adah, F. Zhang, R. J. Linhardt, H. Toyoda, A. Kinoshita-Toyoda, T. Toida, T. H. Van Kuppevelt, E. Depla, F. Von Weizsacker, H. E. Blum, and T. F. Baumert.** 2003. Cellular binding of hepatitis C virus envelope glycoprotein E2 requires cell surface heparan sulfate. J Biol Chem **278**(42):41003-12.
12. **Bartosch, B., J. Dubuisson, and F. L. Cosset.** 2003. Infectious hepatitis C virus pseudo-particles containing functional E1-E2 envelope protein complexes. J Exp Med **197**(5):633-42.
13. **Basu, A., T. Kanda, A. Beyene, K. Saito, K. Meyer, and R. Ray.** 2007. Sulfated homologues of heparin inhibit hepatitis C virus entry into mammalian cells. J Virol **81**(8):3933-41.
14. **Baumert, T. F., S. Ito, D. T. Wong, and T. J. Liang.** 1998. Hepatitis C virus structural proteins assemble into viruslike particles in insect cells. J Virol **72**(5):3827-36.
15. **Berger, E. A., R. W. Doms, E. M. Fenyo, B. T. Korber, D. R. Littman, J. P. Moore, Q. J. Sattentau, H. Schuitemaker, J. Sodroski, and R. A. Weiss.** 1998. A new classification for HIV-1. Nature **391**(6664):240.
16. **Berger, E. A., P. M. Murphy, and J. M. Farber.** 1999. Chemokine receptors as HIV-1 coreceptors: roles in viral entry, tropism, and disease. Annu Rev Immunol **17**657-700.

17. **Berlinger, L., P. Rusert, and A. Trkola.** 2009. P04-40. Dissecting pre- and post-attachment activity of HIV-1 entry inhibitors and neutralizing antibodies. Retrovirology **6**(Suppl 3):P68.
18. **Biebricher, C. K., and M. Eigen.** 2005. The error threshold. Virus Res **107**(2):117-27.
19. **Bieniasz, P. D.** 2009. The cell biology of HIV-1 virion genesis. Cell Host Microbe **5**(6):550-8.
20. **Biswas, P., G. Tambussi, and A. Lazzarin.** 2007. Access denied? The status of co-receptor inhibition to counter HIV entry. Expert Opin Pharmacother **8**(7):923-33.
21. **Blanchard, E., S. Belouzard, L. Goueslain, T. Wakita, J. Dubuisson, C. Wychowski, and Y. Rouille.** 2006. Hepatitis C virus entry depends on clathrin-mediated endocytosis. J Virol **80**(14):6964-72.
22. **Borner, K., J. Hermle, C. Sommer, N. P. Brown, B. Knapp, B. Glass, J. Kunkel, G. Torralba, J. Reymann, N. Beil, J. Beneke, R. Pepperkok, R. Schneider, T. Ludwig, M. Hausmann, F. Hamprecht, H. Erfle, L. Kaderali, H. G. Krausslich, and M. J. Lehmann.** 2009. From experimental setup to bioinformatics: An RNAi screening platform to identify host factors involved in HIV-1 replication. Biotechnol J.
23. **Bour, S., R. Geleziunas, and M. A. Wainberg.** 1995. The human immunodeficiency virus type 1 (HIV-1) CD4 receptor and its central role in promotion of HIV-1 infection. Microbiol Rev **59**(1):63-93.
24. **Bozek, K., A. Thielen, S. Sierra, R. Kaiser, and T. Lengauer.** 2009. V3 loop sequence space analysis suggests different evolutionary patterns of CCR5- and CXCR4-tropic HIV. PLoS One **4**(10):e7387.
25. **Brandenburg, B., L. Y. Lee, M. Lakadamyali, M. J. Rust, X. Zhuang, and J. M. Hogle.** 2007. Imaging poliovirus entry in live cells. PLoS Biol **5**(7):e183.
26. **Brandenburg, B., and X. Zhuang.** 2007. Virus trafficking - learning from single-virus tracking. Nat Rev Microbiol **5**(3):197-208.
27. **Brazzoli, M., A. Bianchi, S. Filippini, A. Weiner, Q. Zhu, M. Pizza, and S. Crotta.** 2008. CD81 is a central regulator of cellular events required for hepatitis C virus infection of human hepatocytes. J Virol **82**(17):8316-29.
28. **Briggs, J. A., T. Wilk, R. Welker, H. G. Krausslich, and S. D. Fuller.** 2003. Structural organization of authentic, mature HIV-1 virions and cores. EMBO J **22**(7):1707-15.
29. **Brumme, Z. L., J. Goodrich, H. B. Mayer, C. J. Brumme, B. M. Henrick, B. Wynhoven, J. J. Asselin, P. K. Cheung, R. S. Hogg, J. S. Montaner, and P. R. Harrigan.** 2005. Molecular and clinical epidemiology of CXCR4-using HIV-1 in a large population of antiretroviral-naive individuals. J Infect Dis **192**(3):466-74.
30. **Bukrinsky, M.** 2004. A hard way to the nucleus. Mol Med **10**(1-6):1-5.
31. **Bullough, P. A., F. M. Hughson, J. J. Skehel, and D. C. Wiley.** 1994. Structure of influenza haemagglutinin at the pH of membrane fusion. Nature **371**(6492):37-43.
32. **Burniston, M. T., A. Cimarelli, J. Colgan, S. P. Curtis, and J. Luban.** 1999. Human immunodeficiency virus type 1 Gag polyprotein multimerization requires the nucleocapsid domain and RNA and is promoted by the capsid-dimer interface and the basic region of matrix protein. J Virol **73**(10):8527-40.
33. **Caffrey, M., M. Cai, J. Kaufman, S. J. Stahl, P. T. Wingfield, D. G. Covell, A. M. Gronenborn, and G. M. Clore.** 1998. Three-dimensional solution structure of the 44 kDa ectodomain of SIV gp41. EMBO J **17**(16):4572-84.
34. **Campbell, E. M., O. Perez, M. Melar, and T. J. Hope.** 2007. Labeling HIV-1 virions with two fluorescent proteins allows identification of virions that have productively entered the target cell. Virology **360**(2):286-93.
35. **Cavrois, M., C. De Noronha, and W. C. Greene.** 2002. A sensitive and specific enzyme-based assay detecting HIV-1 virion fusion in primary T lymphocytes. Nat Biotechnol **20**(11):1151-4.
36. **Chan, D. C., and P. S. Kim.** 1998. HIV entry and its inhibition. Cell **93**(5):681-4.

37. **Charneau, P., M. Alizon, and F. Clavel.** 1992. A second origin of DNA plus-strand synthesis is required for optimal human immunodeficiency virus replication. J Virol **66**(5):2814-20.
38. **Chen, P., W. Hubner, M. A. Spinelli, and B. K. Chen.** 2007. Predominant mode of human immunodeficiency virus transfer between T cells is mediated by sustained Env-dependent neutralization-resistant virological synapses. J Virol **81**(22):12582-95.
39. **Coakley, E., J. Benhamida, C. Chappey, J. Whitcomb, and colleagues.** 2006. An evaluation of tropism profiles and other characteristics among 3988 individuals screened from A4001026, A4001027 (MOTIVATE 1) and A4001028 (MOTIVATE 2) studies for maraviroc. Second International Workshop on Targeting HIV Entry. Boston, MA, USA. Oct 20–21 2006. Abstract 8.
40. **Cocchi, F., A. L. DeVico, A. Garzino-Demo, A. Cara, R. C. Gallo, and P. Lusso.** 1996. The V3 domain of the HIV-1 gp120 envelope glycoprotein is critical for chemokine-mediated blockade of infection. Nat Med **2**(11):1244-7.
41. **Coller, K. E., K. L. Berger, N. S. Heaton, J. D. Cooper, R. Yoon, and G. Randall.** 2009. RNA interference and single particle tracking analysis of hepatitis C virus endocytosis. PLoS Pathog **5**(12):e1000702.
42. **Collman, R., N. F. Hassan, R. Walker, B. Godfrey, J. Cutilli, J. C. Hastings, H. Friedman, S. D. Douglas, and N. Nathanson.** 1989. Infection of monocyte-derived macrophages with human immunodeficiency virus type 1 (HIV-1). Monocyte-tropic and lymphocyte-tropic strains of HIV-1 show distinctive patterns of replication in a panel of cell types. J Exp Med **170**(4):1149-63.
43. **Coyne, C. B., and J. M. Bergelson.** 2006. Virus-induced Abl and Fyn kinase signals permit coxsackievirus entry through epithelial tight junctions. Cell **124**(1):119-31.
44. **Crabb, C.** 2006. GlaxoSmithKline ends aplaviroc trials. AIDS **20**(5):641.
45. **Daecke, J., O. T. Fackler, M. T. Dittmar, and H. G. Krausslich.** 2005. Involvement of clathrin-mediated endocytosis in human immunodeficiency virus type 1 entry. J Virol **79**(3):1581-94.
46. **Day, R. N., and M. W. Davidson.** 2009. The fluorescent protein palette: tools for cellular imaging. Chem Soc Rev **38**(10):2887-921.
47. **De Clercq, E., N. Yamamoto, R. Pauwels, M. Baba, D. Schols, H. Nakashima, J. Balzarini, Z. Debyser, B. A. Murrer, D. Schwartz, and et al.** 1992. Potent and selective inhibition of human immunodeficiency virus (HIV)-1 and HIV-2 replication by a class of bicyclams interacting with a viral uncoating event. Proc Natl Acad Sci U S A **89**(12):5286-90.
48. **Deng, H., R. Liu, W. Ellmeier, S. Choe, D. Unutmaz, M. Burkhart, P. Di Marzio, S. Marmon, R. E. Sutton, C. M. Hill, C. B. Davis, S. C. Peiper, T. J. Schall, D. R. Littman, and N. R. Landau.** 1996. Identification of a major co-receptor for primary isolates of HIV-1. Nature **381**(6584):661-6.
49. **Di Primio, C., D. Arosio, D. Gallo, D. Dylla, G. Cianci, T. J. Hope, and A. Cereseto.** 2009. Nuclear Trafficking of HIV-1 pre-Integration Complexes in Living Cells. 34th annual meeting on Retroviruses. Cold Spring Harbor, NY, USA. May 18 - 23 2009.
50. **Dimitrov, A.** 2007. Ibalizumab, a CD4-specific mAb to inhibit HIV-1 infection. Curr Opin Investig Drugs **8**(8):653-61.
51. **Doms, R. W., and J. P. Moore.** 1997. HIV-1 Coreceptor Use: A Molecular Window into Viral Tropism, p. IV-25-36. *In* B. Korber, C. Brander, B. Haynes, R. Koup, J. Moore, and B. Walker (ed.), HIV Molecular Immunology Database 1997. Theoretical Biology and Biophysics Group, Los Alamos, NM.
52. **Dong, X., H. Li, A. Derdowski, L. Ding, A. Burnett, X. Chen, T. R. Peters, T. S. Dermody, E. Woodruff, J. J. Wang, and P. Spearman.** 2005. AP-3 directs the intracellular trafficking of HIV-1 Gag and plays a key role in particle assembly. Cell **120**(5):663-74.

53. **Dorr, P., M. Westby, S. Dobbs, P. Griffin, B. Irvine, M. Macartney, J. Mori, G. Rickett, C. Smith-Burchnell, C. Napier, R. Webster, D. Armour, D. Price, B. Stammen, A. Wood, and M. Perros.** 2005. Maraviroc (UK-427,857), a potent, orally bioavailable, and selective small-molecule inhibitor of chemokine receptor CCR5 with broad-spectrum anti-human immunodeficiency virus type 1 activity. Antimicrob Agents Chemother **49**(11):4721-32.
54. **Douek, D. C., L. J. Picker, and R. A. Koup.** 2003. T cell dynamics in HIV-1 infection. Annu Rev Immunol **21**265-304.
55. **Dreux, M., B. Boson, S. Ricard-Blum, J. Molle, D. Lavillette, B. Bartosch, E. I. Pecheur, and F. L. Cosset.** 2007. The exchangeable apolipoprotein ApoC-I promotes membrane fusion of hepatitis C virus. J Biol Chem **282**(44):32357-69.
56. **Dreux, M., T. Pietschmann, C. Granier, C. Voisset, S. Ricard-Blum, P. E. Mangeot, Z. Keck, S. Foung, N. Vu-Dac, J. Dubuisson, R. Bartenschlager, D. Lavillette, and F. L. Cosset.** 2006. High density lipoprotein inhibits hepatitis C virus-neutralizing antibodies by stimulating cell entry via activation of the scavenger receptor BI. J Biol Chem **281**(27):18285-95.
57. **Duvet, S., L. Cocquerel, A. Pillez, R. Cacan, A. Verbert, D. Moradpour, C. Wychowski, and J. Dubuisson.** 1998. Hepatitis C virus glycoprotein complex localization in the endoplasmic reticulum involves a determinant for retention and not retrieval. J Biol Chem **273**(48):32088-95.
58. **Edinger, A. L., J. L. Mankowski, B. J. Doranz, B. J. Margulies, B. Lee, J. Rucker, M. Sharron, T. L. Hoffman, J. F. Berson, M. C. Zink, V. M. Hirsch, J. E. Clements, and R. W. Doms.** 1997. CD4-independent, CCR5-dependent infection of brain capillary endothelial cells by a neurovirulent simian immunodeficiency virus strain. Proc Natl Acad Sci U S A **94**(26):14742-7.
59. **Eigen, M., and P. Schuster.** 1977. The hypercycle. A principle of natural self-organization. Part A: Emergence of the hypercycle. Naturwissenschaften **64**(11):541-65.
60. **Este, J. A., and A. Telenti.** 2007. HIV entry inhibitors. Lancet **370**(9581):81-8.
61. **Evans, M. J., T. von Hahn, D. M. Tscherne, A. J. Syder, M. Panis, B. Wolk, T. Hatziioannou, J. A. McKeating, P. D. Bieniasz, and C. M. Rice.** 2007. Claudin-1 is a hepatitis C virus co-receptor required for a late step in entry. Nature **446**(7137):801-5.
62. **Fatkenheuer, G., M. Nelson, A. Lazzarin, I. Konourina, A. I. Hoepelman, H. Lampiris, B. Hirschel, P. Tebas, F. Raffi, B. Trottier, N. Bellos, M. Saag, D. A. Cooper, M. Westby, M. Tawadrous, J. F. Sullivan, C. Ridgway, M. W. Dunne, S. Felstead, H. Mayer, and E. van der Ryst.** 2008. Subgroup analyses of maraviroc in previously treated R5 HIV-1 infection. N Engl J Med **359**(14):1442-55.
63. **Fatkenheuer, G., A. L. Pozniak, M. A. Johnson, A. Plettenberg, S. Staszewski, A. I. Hoepelman, M. S. Saag, F. D. Goebel, J. K. Rockstroh, B. J. Dezube, T. M. Jenkins, C. Medhurst, J. F. Sullivan, C. Ridgway, S. Abel, I. T. James, M. Youle, and E. van der Ryst.** 2005. Efficacy of short-term monotherapy with maraviroc, a new CCR5 antagonist, in patients infected with HIV-1. Nat Med **11**(11):1170-2.
64. **Feng, Y., C. C. Broder, P. E. Kennedy, and E. A. Berger.** 1996. HIV-1 entry cofactor: functional cDNA cloning of a seven-transmembrane, G protein-coupled receptor. Science **272**(5263):872-7.
65. **Fenyo, E. M., L. Morfeldt-Manson, F. Chiodi, B. Lind, A. von Gegerfelt, J. Albert, E. Olausson, and B. Asjo.** 1988. Distinct replicative and cytopathic characteristics of human immunodeficiency virus isolates. J Virol **62**(11):4414-9.
66. **Fletcher, C. V.** 2003. Enfuvirtide, a new drug for HIV infection. Lancet **361**(9369):1577-8.
67. **Fouchier, R. A., M. Brouwer, S. M. Broersen, and H. Schuitemaker.** 1995. Simple determination of human immunodeficiency virus type 1 syncytium-inducing V3 genotype by PCR. J Clin Microbiol **33**(4):906-11.
68. **Furuta, R. A., C. T. Wild, Y. Weng, and C. D. Weiss.** 1998. Capture of an early fusion-active conformation of HIV-1 gp41. Nat Struct Biol **5**(4):276-9.

69. **Gaddis, N. C., E. Chertova, A. M. Sheehy, L. E. Henderson, and M. H. Malim.** 2003. Comprehensive investigation of the molecular defect in vif-deficient human immunodeficiency virus type 1 virions. J Virol **77**(10):5810-20.
70. **Gallo, R. C., S. Z. Salahuddin, M. Popovic, G. M. Shearer, M. Kaplan, B. F. Haynes, T. J. Palker, R. Redfield, J. Oleske, B. Safai, and et al.** 1984. Frequent detection and isolation of cytopathic retroviruses (HTLV-III) from patients with AIDS and at risk for AIDS. Science **224**(4648):500-3.
71. **Gastaminza, P., S. B. Kapadia, and F. V. Chisari.** 2006. Differential biophysical properties of infectious intracellular and secreted hepatitis C virus particles. J Virol **80**(22):11074-81.
72. **Gheysen, D., E. Jacobs, F. de Foresta, C. Thiriart, M. Francotte, D. Thines, and M. De Wilde.** 1989. Assembly and release of HIV-1 precursor Pr55gag virus-like particles from recombinant baculovirus-infected insect cells. Cell **59**(1):103-12.
73. **Glynn, E. F.** 2006. FCSExtract Utility. Stowers Institute for Medical Research. http://research.stowers-institute.org/efg/ScientificSoftware/Utility/FCSExtract/index.htm
74. **Goff, S. P.** 2007. Host factors exploited by retroviruses. Nat Rev Microbiol **5**(4):253-63.
75. **Goffard, A., N. Callens, B. Bartosch, C. Wychowski, F. L. Cosset, C. Montpellier, and J. Dubuisson.** 2005. Role of N-linked glycans in the functions of hepatitis C virus envelope glycoproteins. J Virol **79**(13):8400-9.
76. **Gosert, R., D. Egger, V. Lohmann, R. Bartenschlager, H. E. Blum, K. Bienz, and D. Moradpour.** 2003. Identification of the hepatitis C virus RNA replication complex in Huh-7 cells harboring subgenomic replicons. J Virol **77**(9):5487-92.
77. **Gottwein, J. M., T. K. Scheel, T. B. Jensen, J. B. Lademann, J. C. Prentoe, M. L. Knudsen, A. M. Hoegh, and J. Bukh.** 2009. Development and characterization of hepatitis C virus genotype 1-7 cell culture systems: role of CD81 and scavenger receptor class B type I and effect of antiviral drugs. Hepatology **49**(2):364-77.
78. **Gould, S. J., A. M. Booth, and J. E. Hildreth.** 2003. The Trojan exosome hypothesis. Proc Natl Acad Sci U S A **100**(19):10592-7.
79. **Gousset, K., S. D. Ablan, L. V. Coren, A. Ono, F. Soheilian, K. Nagashima, D. E. Ott, and E. O. Freed.** 2008. Real-time visualization of HIV-1 GAG trafficking in infected macrophages. PLoS Pathog **4**(3):e1000015.
80. **Grewe, C., A. Beck, and H. R. Gelderblom.** 1990. HIV: early virus-cell interactions. J Acquir Immune Defic Syndr **3**(10):965-74.
81. **Gu, M., J. Rappaport, and S. H. Leppla.** 1995. Furin is important but not essential for the proteolytic maturation of gp160 of HIV-1. FEBS Lett **365**(1):95-7.
82. **Habermann, A., J. Krijnse Locker, H. Oberwinkler, M. Eckhardt, S. Homann, A. Andrew, K. Strebel, and H. G. Krausslich.** 2010. CD317/Tetherin is Enriched in the HIV-1 Envelope and Downregulated from the Plasma Membrane upon Virus Infection. J Virol[Epub ahead of print: 2010/02/12].
83. **Hallenberger, S., M. Moulard, M. Sordel, H. D. Klenk, and W. Garten.** 1997. The role of eukaryotic subtilisin-like endoproteases for the activation of human immunodeficiency virus glycoproteins in natural host cells. J Virol **71**(2):1036-45.
84. **Haller, C., S. Rauch, N. Michel, S. Hannemann, M. J. Lehmann, O. T. Keppler, and O. T. Fackler.** 2006. The HIV-1 pathogenicity factor Nef interferes with maturation of stimulatory T-lymphocyte contacts by modulation of N-Wasp activity. J Biol Chem **281**(28):19618-30.
85. **Hammonds, J., J. J. Wang, H. Yi, and P. Spearman.** 2010. Immunoelectron microscopic evidence for Tetherin/BST2 as the physical bridge between HIV-1 virions and the plasma membrane. PLoS Pathog **6**(2):e1000749.

86. **Hardy, D., J. Reynes, I. Konourina, D. wheeler, S. Moreno, E. van der Ryst, W. Towner, A. Horban, H. Mayer, and J. Goodrich.** 2008. Efficacy and Safety of Maraviroc plus Optimized Background Therapy in Treatment-experienced Patients Infected with CCR5-Tropic HIV-1: 48-Week Combined Analysis of the MOTIVATE Studies. 15th Conference on Retroviruses and Opportunistic Infections (CROI). Boston, MA, USA. February 3-6 2008. Abstract 792.
87. **Hartley, O., P. J. Klasse, Q. J. Sattentau, and J. P. Moore.** 2005. V3: HIV's switch-hitter. AIDS Res Hum Retroviruses **21**(2):171-89.
88. **Hecky, J., and K. M. Muller.** 2005. Structural perturbation and compensation by directed evolution at physiological temperature leads to thermostabilization of beta-lactamase. Biochemistry **44**(38):12640-54.
89. **Heera, J., M. Saag, P. Ive, J. Whitcomb, M. Lewis, L. McFadyen, J. Goodrich, H. Mayer, E. van der Ryst, and M. Westby.** 2008. Virological Correlates Associated with Treatment Failure at Week 48 in the Phase 3 Study of Maraviroc in Treatment-Naive Patients. 15th Conference on Retroviruses and Opportunistic Infections (CROI). Boston, MA, USA. February 3–6 2008. Abstract 40LB.
90. **Hell, S. W., and J. Wichmann.** 1994. Breaking the diffraction resolution limit by stimulated emission: stimulated-emission-depletion fluorescence microscopy. Opt Lett **19**(11):780-2.
91. **Hendrix, C. W., A. C. Collier, M. M. Lederman, D. Schols, R. B. Pollard, S. Brown, J. B. Jackson, R. W. Coombs, M. J. Glesby, C. W. Flexner, G. J. Bridger, K. Badel, R. T. MacFarland, G. W. Henson, and G. Calandra.** 2004. Safety, pharmacokinetics, and antiviral activity of AMD3100, a selective CXCR4 receptor inhibitor, in HIV-1 infection. J Acquir Immune Defic Syndr **37**(2):1253-62.
92. **Hermida-Matsumoto, L., and M. D. Resh.** 2000. Localization of human immunodeficiency virus type 1 Gag and Env at the plasma membrane by confocal imaging. J Virol **74**(18):8670-9.
93. **Hildinger, M., M. T. Dittmar, P. Schult-Dietrich, B. Fehse, B. S. Schnierle, S. Thaler, G. Stiegler, R. Welker, and D. von Laer.** 2001. Membrane-anchored peptide inhibits human immunodeficiency virus entry. J Virol **75**(6):3038-42.
94. **Hildreth, J. E., and R. J. Orentas.** 1989. Involvement of a leukocyte adhesion receptor (LFA-1) in HIV-induced syncytium formation. Science **244**(4908):1075-8.
95. **Hoxie, J. A., C. C. LaBranche, M. J. Endres, J. D. Turner, J. F. Berson, R. W. Doms, and T. J. Matthews.** 1998. CD4-independent utilization of the CXCR4 chemokine receptor by HIV-1 and HIV-2. J Reprod Immunol **41**(1-2):197-211.
96. **Huang, B., M. Bates, and X. Zhuang.** 2009. Super-resolution fluorescence microscopy. Annu Rev Biochem **78**993-1016.
97. **Huang, W., J. Toma, S. Fransen, E. Stawiski, J. D. Reeves, J. M. Whitcomb, N. Parkin, and C. J. Petropoulos.** 2008. Coreceptor tropism can be influenced by amino acid substitutions in the gp41 transmembrane subunit of human immunodeficiency virus type 1 envelope protein. J Virol **82**(11):5584-93.
98. **Hubner, W., P. Chen, A. Del Portillo, Y. Liu, R. E. Gordon, and B. K. Chen.** 2007. Sequence of human immunodeficiency virus type 1 (HIV-1) Gag localization and oligomerization monitored with live confocal imaging of a replication-competent, fluorescently tagged HIV-1. J Virol **81**(22):12596-607.
99. **Huson, D. H.** 1998. SplitsTree: analyzing and visualizing evolutionary data. Bioinformatics **14**(1):68-73.
100. **Iro, M., J. Witteveldt, A. G. Angus, I. Woerz, A. Kaul, R. Bartenschlager, and A. H. Patel.** 2009. A reporter cell line for rapid and sensitive evaluation of hepatitis C virus infectivity and replication. Antiviral Res **83**(2):148-55.
101. **Ivanchenko, S., W. J. Godinez, M. Lampe, H. G. Krausslich, R. Eils, K. Rohr, C. Brauchle, B. Muller, and D. C. Lamb.** 2009. Dynamics of HIV-1 assembly and release. PLoS Pathog **5**(11):e1000652.

102. **Jacobson, J. M., D. R. Kuritzkes, E. Godofsky, E. DeJesus, J. A. Larson, S. P. Weinheimer, and S. T. Lewis.** 2009. Safety, pharmacokinetics, and antiretroviral activity of multiple doses of ibalizumab (formerly TNX-355), an anti-CD4 monoclonal antibody, in human immunodeficiency virus type 1-infected adults. Antimicrob Agents Chemother **53**(2):450-7.
103. **Jäger, S.** 2008. HIV-1 Gag Ubiquitination and the Role of ESCRT Factors in Retroviral Release. PhD Thesis. University of Heidelberg, Heidelberg, Germany.
104. **Jensen, M. A., F. S. Li, A. B. van 't Wout, D. C. Nickle, D. Shriner, H. X. He, S. McLaughlin, R. Shankarappa, J. B. Margolick, and J. I. Mullins.** 2003. Improved coreceptor usage prediction and genotypic monitoring of R5-to-X4 transition by motif analysis of human immunodeficiency virus type 1 env V3 loop sequences. J Virol **77**(24):13376-88.
105. **Johnston, S. H., M. A. Lobritz, S. Nguyen, K. Lassen, S. Delair, F. Posta, Y. J. Bryson, E. J. Arts, T. Chou, and B. Lee.** 2009. A quantitative affinity-profiling system that reveals distinct CD4/CCR5 usage patterns among human immunodeficiency virus type 1 and simian immunodeficiency virus strains. J Virol **83**(21):11016-26.
106. **Jolly, C., K. Kashefi, M. Hollinshead, and Q. J. Sattentau.** 2004. HIV-1 cell to cell transfer across an Env-induced, actin-dependent synapse. J Exp Med **199**(2):283-93.
107. **Jolly, C., I. Mitar, and Q. J. Sattentau.** 2007. Adhesion molecule interactions facilitate human immunodeficiency virus type 1-induced virological synapse formation between T cells. J Virol **81**(24):13916-21.
108. **Jones, C. T., M. T. Catanese, L. M. Law, S. R. Khetani, A. J. Syder, A. Ploss, T. S. Oh, J. W. Schoggins, M. R. MacDonald, S. N. Bhatia, and C. M. Rice.** 2010. Real-time imaging of hepatitis C virus infection using a fluorescent cell-based reporter system. Nat Biotechnol **28**(2):167-71.
109. **Jouvenet, N., P. D. Bieniasz, and S. M. Simon.** 2008. Imaging the biogenesis of individual HIV-1 virions in live cells. Nature **454**(7201):236-40.
110. **Kabat, D., S. L. Kozak, K. Wehrly, and B. Chesebro.** 1994. Differences in CD4 dependence for infectivity of laboratory-adapted and primary patient isolates of human immunodeficiency virus type 1. J Virol **68**(4):2570-7.
111. **Kamradt, T., D. Niese, K. E. Schneweis, H. H. Brackmann, B. Kamps, B. van Loo, and U. Hammerstein.** 1989. Natural history of HIV-infection in hemophiliacs: clinical, immunological, and virological findings. Klin Wochenschr **67**(20):1033-41.
112. **Karlsson Hedestam, G. B., R. A. Fouchier, S. Phogat, D. R. Burton, J. Sodroski, and R. T. Wyatt.** 2008. The challenges of eliciting neutralizing antibodies to HIV-1 and to influenza virus. Nat Rev Microbiol **6**(2):143-55.
113. **Keppler, A., S. Gendreizig, T. Gronemeyer, H. Pick, H. Vogel, and K. Johnsson.** 2003. A general method for the covalent labeling of fusion proteins with small molecules in vivo. Nat Biotechnol **21**(1):86-9.
114. **Keppler, A., M. Kindermann, S. Gendreizig, H. Pick, H. Vogel, and K. Johnsson.** 2004. Labeling of fusion proteins of O6-alkylguanine-DNA alkyltransferase with small molecules in vivo and in vitro. Methods **32**(4):437-44.
115. **Keppler, A., H. Pick, C. Arrivoli, H. Vogel, and K. Johnsson.** 2004. Labeling of fusion proteins with synthetic fluorophores in live cells. Proc Natl Acad Sci U S A **101**(27):9955-9.
116. **Kilby, J. M., S. Hopkins, T. M. Venetta, B. DiMassimo, G. A. Cloud, J. Y. Lee, L. Alldredge, E. Hunter, D. Lambert, D. Bolognesi, T. Matthews, M. R. Johnson, M. A. Nowak, G. M. Shaw, and M. S. Saag.** 1998. Potent suppression of HIV-1 replication in humans by T-20, a peptide inhibitor of gp41-mediated virus entry. Nat Med **4**(11):1302-7.
117. **Koch, P., M. Lampe, W. J. Godinez, B. Muller, K. Rohr, H. G. Krausslich, and M. J. Lehmann.** 2009. Visualizing fusion of pseudotyped HIV-1 particles in real time by live cell microscopy. Retrovirology **6**84.

118. **Koch, P., M. J. Lehmann, and H. G. Krausslich.** 2010. Triple labelled pseudotyped HIV-1 particles to visualize fusion by live cell microscopy. Department of Infectious Diseases, Virology, Heidelberg, Germany. Unpublished work.
119. **Koot, M., I. P. Keet, A. H. Vos, R. E. de Goede, M. T. Roos, R. A. Coutinho, F. Miedema, P. T. Schellekens, and M. Tersmette.** 1993. Prognostic value of HIV-1 syncytium-inducing phenotype for rate of CD4+ cell depletion and progression to AIDS. Ann Intern Med **118**(9):681-8.
120. **Koot, M., A. H. Vos, R. P. Keet, R. E. de Goede, M. W. Dercksen, F. G. Terpstra, R. A. Coutinho, F. Miedema, and M. Tersmette.** 1992. HIV-1 biological phenotype in long-term infected individuals evaluated with an MT-2 cocultivation assay. AIDS **6**(1):49-54.
121. **Koutsoudakis, G., E. Herrmann, S. Kallis, R. Bartenschlager, and T. Pietschmann.** 2007. The level of CD81 cell surface expression is a key determinant for productive entry of hepatitis C virus into host cells. J Virol **81**(2):588-98.
122. **Koutsoudakis, G., A. Kaul, E. Steinmann, S. Kallis, V. Lohmann, T. Pietschmann, and R. Bartenschlager.** 2006. Characterization of the early steps of hepatitis C virus infection by using luciferase reporter viruses. J Virol **80**(11):5308-20.
123. **Kreeger, P. K., and D. A. Lauffenburger.** 2010. Cancer systems biology: a network modeling perspective. Carcinogenesis **31**(1):2-8.
124. **Kruger, U., T. Pfeiffer, and V. Bosch.** 1996. Generation of lymphocyte cell lines coexpressing CD4 and wild-type or mutant HIV type 1 glycoproteins: implications for HIV type 1 Env-induced cell lysis. AIDS Res Hum Retroviruses **12**(9):783-92.
125. **Kuhn, R. J., W. Zhang, M. G. Rossmann, S. V. Pletnev, J. Corver, E. Lenches, C. T. Jones, S. Mukhopadhyay, P. R. Chipman, E. G. Strauss, T. S. Baker, and J. H. Strauss.** 2002. Structure of dengue virus: implications for flavivirus organization, maturation, and fusion. Cell **108**(5):717-25.
126. **Kwong, P. D., R. Wyatt, J. Robinson, R. W. Sweet, J. Sodroski, and W. A. Hendrickson.** 1998. Structure of an HIV gp120 envelope glycoprotein in complex with the CD4 receptor and a neutralizing human antibody. Nature **393**(6686):648-59.
127. **Lampe, M., J. A. Briggs, T. Endress, B. Glass, S. Riegelsberger, H. G. Krausslich, D. C. Lamb, C. Brauchle, and B. Muller.** 2007. Double-labelled HIV-1 particles for study of virus-cell interaction. Virology **360**(1):92-104.
128. **Laubenbacher, R., V. Hower, A. Jarrah, S. V. Torti, V. Shulaev, P. Mendes, F. M. Torti, and S. Akman.** 2009. A systems biology view of cancer. Biochim Biophys Acta **1796**(2):129-39.
129. **Lehmann, M. J., N. M. Sherer, C. B. Marks, M. Pypaert, and W. Mothes.** 2005. Actin- and myosin-driven movement of viruses along filopodia precedes their entry into cells. J Cell Biol **170**(2):317-25.
130. **Leitner, T., B. Foley, B. Hahn, P. Marx, F. McCutchan, J. Mellors, S. Wolinsky, and B. Korber (ed.).** 2005. HIV Sequence Compendium 2005. Theoretical Biology and Biophysics Group, Los Alamos National Laboratory.
131. **Lekkerkerker, A. N., Y. van Kooyk, and T. B. Geijtenbeek.** 2006. Viral piracy: HIV-1 targets dendritic cells for transmission. Curr HIV Res **4**(2):169-76.
132. **Lengauer, T., O. Sander, S. Sierra, A. Thielen, and R. Kaiser.** 2007. Bioinformatics prediction of HIV coreceptor usage. Nat Biotechnol **25**(12):1407-10.
133. **Leonard, C. K., M. W. Spellman, L. Riddle, R. J. Harris, J. N. Thomas, and T. J. Gregory.** 1990. Assignment of intrachain disulfide bonds and characterization of potential glycosylation sites of the type 1 recombinant human immunodeficiency virus envelope glycoprotein (gp120) expressed in Chinese hamster ovary cells. J Biol Chem **265**(18):10373-82.

134. **Lewis, M., P. Simpson, S. Fransen, W. Huang, J. Whitcomb, M. Mosley, D. L. Robertson, R. Mansfield, G. Ciaramella, and M. Westby.** 2007. CXCR4-using virus detected in patients receiving maraviroc in the Phase III studies MOTIVATE 1 and 2 originates from a pre-existing minority of CXCR4-using virus. XVI International HIV Drug Resistance Workshop. Barbados, West Indies. 12-16 June 2007. Abstract 10.
135. **Liesnard, C., M. L. Delforge, M. Tchetcheroff, V. De Maertelaer, C. M. Farber, and J. P. Van Vooren.** 1997. Importance of method in the determination of syncytium-inducing phenotype of human immunodeficiency virus type 1 clinical isolates. J Virol Methods **64**(2):137-45.
136. **Lifson, J. D., G. R. Reyes, M. S. McGrath, B. S. Stein, and E. G. Engleman.** 1986. AIDS retrovirus induced cytopathology: giant cell formation and involvement of CD4 antigen. Science **232**(4754):1123-7.
137. **Lindenbach, B. D., M. J. Evans, A. J. Syder, B. Wolk, T. L. Tellinghuisen, C. C. Liu, T. Maruyama, R. O. Hynes, D. R. Burton, J. A. McKeating, and C. M. Rice.** 2005. Complete replication of hepatitis C virus in cell culture. Science **309**(5734):623-6.
138. **Lippincott-Schwartz, J., and G. H. Patterson.** 2003. Development and use of fluorescent protein markers in living cells. Science **300**(5616):87-91.
139. **Littman, D. R.** 1998. Chemokine receptors: keys to AIDS pathogenesis? Cell **93**(5):677-80.
140. **Liu, R., W. A. Paxton, S. Choe, D. Ceradini, S. R. Martin, R. Horuk, M. E. MacDonald, H. Stuhlmann, R. A. Koup, and N. R. Landau.** 1996. Homozygous defect in HIV-1 coreceptor accounts for resistance of some multiply-exposed individuals to HIV-1 infection. Cell **86**(3):367-77.
141. **Low, A. J., W. Dong, D. Chan, T. Sing, R. Swanstrom, M. Jensen, S. Pillai, B. Good, and P. R. Harrigan.** 2007. Current V3 genotyping algorithms are inadequate for predicting X4 co-receptor usage in clinical isolates. AIDS **21**(14):F17-24.
142. **Lymperopoulos, K., A. Kiel, A. Seefeld, K. Stohr, and D. P. Herten.** 2010. Fluorescent probes and delivery methods for single-molecule experiments. Chemphyschem **11**(1):43-53.
143. **Maas, J. J., S. J. Gange, H. Schuitemaker, R. A. Coutinho, R. van Leeuwen, and J. B. Margolick.** 2000. Strong association between failure of T cell homeostasis and the syncytium-inducing phenotype among HIV-1-infected men in the Amsterdam Cohort Study. AIDS **14**(9):1155-61.
144. **Maddon, P. J., A. G. Dalgleish, J. S. McDougal, P. R. Clapham, R. A. Weiss, and R. Axel.** 1986. The T4 gene encodes the AIDS virus receptor and is expressed in the immune system and the brain. Cell **47**(3):333-48.
145. **Marsh, M., and A. Helenius.** 2006. Virus entry: open sesame. Cell **124**(4):729-40.
146. **Martin, N., S. Welsch, C. Jolly, J. A. Briggs, D. Vaux, and Q. J. Sattentau.** 2010. Virological synapse-mediated spread of human immunodeficiency virus type 1 between T cells is sensitive to entry inhibition. J Virol **84**(7):3516-27.
147. **McDonald, D., M. A. Vodicka, G. Lucero, T. M. Svitkina, G. G. Borisy, M. Emerman, and T. J. Hope.** 2002. Visualization of the intracellular behavior of HIV in living cells. J Cell Biol **159**(3):441-52.
148. **Meertens, L., C. Bertaux, and T. Dragic.** 2006. Hepatitis C virus entry requires a critical postinternalization step and delivery to early endosomes via clathrin-coated vesicles. J Virol **80**(23):11571-8.
149. **Merril, C. R., M. R. Geier, and J. C. Petricciani.** 1971. Bacterial virus gene expression in human cells. Nature **233**(5319):398-400.
150. **Mild, M., A. Kvist, J. Esbjornsson, I. Karlsson, E. M. Fenyo, and P. Medstrand.** 2010. Differences in molecular evolution between switch (R5 to R5X4/X4-tropic) and non-switch (R5-tropic only) HIV-1 populations during infection. Infect Genet Evol **10**(3):356-364.

151. **Miyagi, E., A. J. Andrew, S. Kao, and K. Strebel.** 2009. Vpu enhances HIV-1 virus release in the absence of Bst-2 cell surface down-modulation and intracellular depletion. Proc Natl Acad Sci U S A **106**(8):2868-73.
152. **Miyauchi, K., Y. Kim, O. Latinovic, V. Morozov, and G. B. Melikyan.** 2009. HIV enters cells via endocytosis and dynamin-dependent fusion with endosomes. Cell **137**(3):433-44.
153. **Miyoshi, I., H. Taguchi, M. Fujishita, K. Niiya, T. Kitagawa, Y. Ohtsuki, and T. Akagi.** 1982. Asymptomatic type C virus carriers in the family of an adult T-cell leukemia patient. Gann **73**(2):339-40.
154. **Mondor, I., S. Ugolini, and Q. J. Sattentau.** 1998. Human immunodeficiency virus type 1 attachment to HeLa CD4 cells is CD4 independent and gp120 dependent and requires cell surface heparans. J Virol **72**(5):3623-34.
155. **Moore, J. P., J. A. McKeating, R. A. Weiss, and Q. J. Sattentau.** 1990. Dissociation of gp120 from HIV-1 virions induced by soluble CD4. Science **250**(4984):1139-42.
156. **Moradpour, D., F. Penin, and C. M. Rice.** 2007. Replication of hepatitis C virus. Nat Rev Microbiol **5**(6):453-63.
157. **Mori, J., M. Lewis, P. Simpson, and colleagues.** 2008. Characterization of maraviroc resistance in patients failing treatment with CCR5-tropic virus in MOTIVATE 1 and MOTIVATE2 (24 week analysis). European HIV Drug Resistance Workshop. Budapest, Hungary. March 26-28 2008. Abstract 51.
158. **Mori, J., M. Mosley, M. Lewis, P. Simpson, J. Toma, W. Huang, J. Whitcomb, G. Ciaramella, and M. Westby.** 2007. Characterization of maraviroc resistance in patients failing treatment with CCR5-tropic virus in MOTIVATE 1 and MOTIVATE2. XVI International HIV Drug Resistance Workshop: Basic Principles & Clinical Implications. Barbados, West Indies. June 12-16 2007. Abstract 10.
159. **Morikawa, K., Z. Zhao, T. Date, M. Miyamoto, A. Murayama, D. Akazawa, J. Tanabe, S. Sone, and T. Wakita.** 2007. The roles of CD81 and glycosaminoglycans in the adsorption and uptake of infectious HCV particles. J Med Virol **79**(6):714-23.
160. **Moyle, G. J., E. DeJesus, and M. Boffito.** 2007. Presented at the 14th Conference on Retroviruses and Opportunistic Infection, Los Angeles, CA, USA, Feb 25–28 2007.
161. **Moyle, G. J., A. Wildfire, S. Mandalia, H. Mayer, J. Goodrich, J. Whitcomb, and B. G. Gazzard.** 2005. Epidemiology and predictive factors for chemokine receptor use in HIV-1 infection. J Infect Dis **191**(6):866-72.
162. **Muller, B., J. Daecke, O. T. Fackler, M. T. Dittmar, H. Zentgraf, and H. G. Krausslich.** 2004. Construction and characterization of a fluorescently labeled infectious human immunodeficiency virus type 1 derivative. J Virol **78**(19):10803-13.
163. **Murakami, T., and E. O. Freed.** 2000. Genetic evidence for an interaction between human immunodeficiency virus type 1 matrix and alpha-helix 2 of the gp41 cytoplasmic tail. J Virol **74**(8):3548-54.
164. **Neil, S. J., S. W. Eastman, N. Jouvenet, and P. D. Bieniasz.** 2006. HIV-1 Vpu promotes release and prevents endocytosis of nascent retrovirus particles from the plasma membrane. PLoS Pathog **2**(5):e39.
165. **Neil, S. J., T. Zang, and P. D. Bieniasz.** 2008. Tetherin inhibits retrovirus release and is antagonized by HIV-1 Vpu. Nature **451**(7177):425-30.
166. **Nguyen, D. G., A. Booth, S. J. Gould, and J. E. Hildreth.** 2003. Evidence that HIV budding in primary macrophages occurs through the exosome release pathway. J Biol Chem **278**(52):52347-54.
167. **Nguyen, D. H., and J. E. Hildreth.** 2000. Evidence for budding of human immunodeficiency virus type 1 selectively from glycolipid-enriched membrane lipid rafts. J Virol **74**(7):3264-72.
168. **Nicholson, J. K., S. W. Browning, R. L. Hengel, E. Lew, L. E. Gallagher, D. Rimland, and J. S. McDougal.** 2001. CCR5 and CXCR4 expression on memory and naive T cells in HIV-1 infection and response to highly active antiretroviral therapy. J Acquir Immune Defic Syndr **27**(2):105-15.

169. **NIH** 2010. Dose-Response Study of Ibalizumab (Monoclonal Antibody) Plus Optimized Background Regimen in Patients With HIV-1 (TMB-202). http://clinicaltrials.gov/ct2/show/NCT00784147. [Online.]
170. **Nijhuis, M., N. M. van Maarseveen, S. Lastere, P. Schipper, E. Coakley, B. Glass, M. Rovenska, D. de Jong, C. Chappey, I. W. Goedegebuure, G. Heilek-Snyder, D. Dulude, N. Cammack, L. Brakier-Gingras, J. Konvalinka, N. Parkin, H. G. Krausslich, F. Brun-Vezinet, and C. A. Boucher.** 2007. A novel substrate-based HIV-1 protease inhibitor drug resistance mechanism. PLoS Med **4**(1):e36.
171. **Oberlin, E., A. Amara, F. Bachelerie, C. Bessia, J. L. Virelizier, F. Arenzana-Seisdedos, O. Schwartz, J. M. Heard, I. Clark-Lewis, D. F. Legler, M. Loetscher, M. Baggiolini, and B. Moser.** 1996. The CXC chemokine SDF-1 is the ligand for LESTR/fusin and prevents infection by T-cell-line-adapted HIV-1. Nature **382**(6594):833-5.
172. **Obrig, T. G., W. J. Culp, W. L. McKeehan, and B. Hardesty.** 1971. The mechanism by which cycloheximide and related glutarimide antibiotics inhibit peptide synthesis on reticulocyte ribosomes. J Biol Chem **246**(1):174-81.
173. **Ohshiro, Y., T. Murakami, K. Matsuda, K. Nishioka, K. Yoshida, and N. Yamamoto.** 1996. Role of cell surface glycosaminoglycans of human T cells in human immunodeficiency virus type-1 (HIV-1) infection. Microbiol Immunol **40**(11):827-35.
174. **Ono, A., S. D. Ablan, S. J. Lockett, K. Nagashima, and E. O. Freed.** 2004. Phosphatidylinositol (4,5) bisphosphate regulates HIV-1 Gag targeting to the plasma membrane. Proc Natl Acad Sci U S A **101**(41):14889-94.
175. **Op De Beeck, A., R. Montserret, S. Duvet, L. Cocquerel, R. Cacan, B. Barberot, M. Le Maire, F. Penin, and J. Dubuisson.** 2000. The transmembrane domains of hepatitis C virus envelope glycoproteins E1 and E2 play a major role in heterodimerization. J Biol Chem **275**(40):31428-37.
176. **Pastore, C., R. Nedellec, A. Ramos, S. Pontow, L. Ratner, and D. E. Mosier.** 2006. Human immunodeficiency virus type 1 coreceptor switching: V1/V2 gain-of-fitness mutations compensate for V3 loss-of-fitness mutations. J Virol **80**(2):750-8.
177. **Pegg, A. E.** 2000. Repair of O(6)-alkylguanine by alkyltransferases. Mutat Res **462**(2-3):83-100.
178. **Pelchen-Matthews, A., B. Kramer, and M. Marsh.** 2003. Infectious HIV-1 assembles in late endosomes in primary macrophages. J Cell Biol **162**(3):443-55.
179. **Pelkmans, L., J. Kartenbeck, and A. Helenius.** 2001. Caveolar endocytosis of simian virus 40 reveals a new two-step vesicular-transport pathway to the ER. Nat Cell Biol **3**(5):473-83.
180. **Perez-Caballero, D., T. Hatziioannou, J. Martin-Serrano, and P. D. Bieniasz.** 2004. Human immunodeficiency virus type 1 matrix inhibits and confers cooperativity on gag precursor-membrane interactions. J Virol **78**(17):9560-3.
181. **Perez-Caballero, D., T. Zang, A. Ebrahimi, M. W. McNatt, D. A. Gregory, M. C. Johnson, and P. D. Bieniasz.** 2009. Tetherin inhibits HIV-1 release by directly tethering virions to cells. Cell **139**(3):499-511.
182. **Perlman, M., and M. D. Resh.** 2006. Identification of an intracellular trafficking and assembly pathway for HIV-1 gag. Traffic **7**(6):731-45.
183. **Pierson, R.** 2010. Merck HIV drug from Schering merger fails trials, 21.01.2010 ed. www.reuters.com.
184. **Pileri, P., Y. Uematsu, S. Campagnoli, G. Galli, F. Falugi, R. Petracca, A. J. Weiner, M. Houghton, D. Rosa, G. Grandi, and S. Abrignani.** 1998. Binding of hepatitis C virus to CD81. Science **282**(5390):938-41.
185. **Pillai, S., B. Good, D. Richman, and J. Corbeil.** 2003. A new perspective on V3 phenotype prediction. AIDS Res Hum Retroviruses **19**(2):145-9.
186. **Platt, E. J., K. Wehrly, S. E. Kuhmann, B. Chesebro, and D. Kabat.** 1998. Effects of CCR5 and CD4 cell surface concentrations on infections by macrophagetropic isolates of human immunodeficiency virus type 1. J Virol **72**(4):2855-64.

187. **Ploss, A., M. J. Evans, V. A. Gaysinskaya, M. Panis, H. You, Y. P. de Jong, and C. M. Rice.** 2009. Human occludin is a hepatitis C virus entry factor required for infection of mouse cells. Nature **457**(7231):882-6.
188. **Prasher, D. C., V. K. Eckenrode, W. W. Ward, F. G. Prendergast, and M. J. Cormier.** 1992. Primary structure of the Aequorea victoria green-fluorescent protein. Gene **111**(2):229-33.
189. **Provine, N. M., W. B. Puryear, X. Wu, J. Overbaugh, and N. L. Haigwood.** 2009. The infectious molecular clone and pseudotyped virus models of human immunodeficiency virus type 1 exhibit significant differences in virion composition with only moderate differences in infectivity and inhibition sensitivity. J Virol **83**(17):9002-7.
190. **R_Development_Core_Team.** 2009. R: A Language and Environment for Statistical Computing. R Foundation for Statistical Computing. http://www.R-project.org
191. **Regoes, R. R., and S. Bonhoeffer.** 2005. The HIV coreceptor switch: a population dynamical perspective. Trends Microbiol **13**(6):269-77.
192. **Resh, M. D.** 2005. Intracellular trafficking of HIV-1 Gag: how Gag interacts with cell membranes and makes viral particles. AIDS Rev **7**(2):84-91.
193. **Resh, M. D.** 2004. A myristoyl switch regulates membrane binding of HIV-1 Gag. Proc Natl Acad Sci U S A **101**(2):417-8.
194. **Rimsky, L. T., D. C. Shugars, and T. J. Matthews.** 1998. Determinants of human immunodeficiency virus type 1 resistance to gp41-derived inhibitory peptides. J Virol **72**(2):986-93.
195. **Rizzuto, C. D., R. Wyatt, N. Hernandez-Ramos, Y. Sun, P. D. Kwong, W. A. Hendrickson, and J. Sodroski.** 1998. A conserved HIV gp120 glycoprotein structure involved in chemokine receptor binding. Science **280**(5371):1949-53.
196. **Roberts, J. D., K. Bebenek, and T. A. Kunkel.** 1988. The accuracy of reverse transcriptase from HIV-1. Science **242**(4882):1171-3.
197. **Ronaghi, M., M. Uhlen, and P. Nyren.** 1998. A sequencing method based on real-time pyrophosphate. Science **281**(5375):363, 365.
198. **Roos, M. T., J. M. Lange, R. E. de Goede, R. A. Coutinho, P. T. Schellekens, F. Miedema, and M. Tersmette.** 1992. Viral phenotype and immune response in primary human immunodeficiency virus type 1 infection. J Infect Dis **165**(3):427-32.
199. **Rowell, J. F., P. E. Stanhope, and R. F. Siliciano.** 1995. Endocytosis of endogenously synthesized HIV-1 envelope protein. Mechanism and role in processing for association with class II MHC. J Immunol **155**(1):473-88.
200. **Rozera, G., I. Abbate, A. Bruselles, C. Vlassi, G. D'Offizi, P. Narciso, G. Chillemi, M. Prosperi, G. Ippolito, and M. R. Capobianchi.** 2009. Massively parallel pyrosequencing highlights minority variants in the HIV-1 env quasispecies deriving from lymphomonocyte sub-populations. Retrovirology **6**15.
201. **Rudner, L., S. Nydegger, L. V. Coren, K. Nagashima, M. Thali, and D. E. Ott.** 2005. Dynamic fluorescent imaging of human immunodeficiency virus type 1 gag in live cells by biarsenical labeling. J Virol **79**(7):4055-65.
202. **Rust, M. J., M. Bates, and X. Zhuang.** 2006. Sub-diffraction-limit imaging by stochastic optical reconstruction microscopy (STORM). Nat Methods **3**(10):793-5.
203. **Rust, M. J., M. Lakadamyali, F. Zhang, and X. Zhuang.** 2004. Assembly of endocytic machinery around individual influenza viruses during viral entry. Nat Struct Mol Biol **11**(6):567-73.
204. **Salahuddin, S. Z., P. D. Markham, F. Wong-Staal, G. Franchini, V. S. Kalyanaraman, and R. C. Gallo.** 1983. Restricted expression of human T-cell leukemia--lymphoma virus (HTLV) in transformed human umbilical cord blood lymphocytes. Virology **129**(1):51-64.
205. **Samson, M., O. Labbe, C. Mollereau, G. Vassart, and M. Parmentier.** 1996. Molecular cloning and functional expression of a new human CC-chemokine receptor gene. Biochemistry **35**(11):3362-7.

206. **Sattentau, Q.** 2008. Avoiding the void: cell-to-cell spread of human viruses. Nat Rev Microbiol **6**(11):815-26.
207. **Scarselli, E., H. Ansuini, R. Cerino, R. M. Roccasecca, S. Acali, G. Filocamo, C. Traboni, A. Nicosia, R. Cortese, and A. Vitelli.** 2002. The human scavenger receptor class B type I is a novel candidate receptor for the hepatitis C virus. EMBO J **21**(19):5017-25.
208. **Schaller, T., N. Appel, G. Koutsoudakis, S. Kallis, V. Lohmann, T. Pietschmann, and R. Bartenschlager.** 2007. Analysis of hepatitis C virus superinfection exclusion by using novel fluorochrome gene-tagged viral genomes. J Virol **81**(9):4591-603.
209. **Scherer, W. F., J. T. Syverton, and G. O. Gey.** 1953. Studies on the propagation in vitro of poliomyelitis viruses. IV. Viral multiplication in a stable strain of human malignant epithelial cells (strain HeLa) derived from an epidermoid carcinoma of the cervix. J Exp Med **97**(5):695-710.
210. **Schols, D., S. Struyf, J. Van Damme, J. A. Este, G. Henson, and E. De Clercq.** 1997. Inhibition of T-tropic HIV strains by selective antagonization of the chemokine receptor CXCR4. J Exp Med **186**(8):1383-8.
211. **Sena-Esteves, M., Y. Saeki, S. M. Camp, E. A. Chiocca, and X. O. Breakefield.** 1999. Single-step conversion of cells to retrovirus vector producers with herpes simplex virus-Epstein-Barr virus hybrid amplicons. J Virol **73**(12):10426-39.
212. **Shavinskaya, A., S. Boulant, F. Penin, J. McLauchlan, and R. Bartenschlager.** 2007. The lipid droplet binding domain of hepatitis C virus core protein is a major determinant for efficient virus assembly. J Biol Chem **282**(51):37158-69.
213. **Shugars, D. C., C. T. Wild, T. K. Greenwell, and T. J. Matthews.** 1996. Biophysical characterization of recombinant proteins expressing the leucine zipper-like domain of the human immunodeficiency virus type 1 transmembrane protein gp41. J Virol **70**(5):2982-91.
214. **Sierra, S., R. Kaiser, A. Thielen, and T. Lengauer.** 2007. Genotypic coreceptor analysis. Eur J Med Res **12**(9):453-62.
215. **Simmonds, P.** 1995. Variability of hepatitis C virus. Hepatology **21**(2):570-83.
216. **Sing, T., A. J. Low, N. Beerenwinkel, O. Sander, P. K. Cheung, F. S. Domingues, J. Buch, M. Daumer, R. Kaiser, T. Lengauer, and P. R. Harrigan.** 2007. Predicting HIV coreceptor usage on the basis of genetic and clinical covariates. Antivir Ther **12**(7):1097-106.
217. **Sourisseau, M., N. Sol-Foulon, F. Porrot, F. Blanchet, and O. Schwartz.** 2007. Inefficient human immunodeficiency virus replication in mobile lymphocytes. J Virol **81**(2):1000-12.
218. **Spearman, P., R. Horton, L. Ratner, and I. Kuli-Zade.** 1997. Membrane binding of human immunodeficiency virus type 1 matrix protein in vivo supports a conformational myristyl switch mechanism. J Virol **71**(9):6582-92.
219. **Starcich, B. R., B. H. Hahn, G. M. Shaw, P. D. McNeely, S. Modrow, H. Wolf, E. S. Parks, W. P. Parks, S. F. Josephs, R. C. Gallo, and et al.** 1986. Identification and characterization of conserved and variable regions in the envelope gene of HTLV-III/LAV, the retrovirus of AIDS. Cell **45**(5):637-48.
220. **Tersmette, M., R. A. Gruters, F. de Wolf, R. E. de Goede, J. M. Lange, P. T. Schellekens, J. Goudsmit, H. G. Huisman, and F. Miedema.** 1989. Evidence for a role of virulent human immunodeficiency virus (HIV) variants in the pathogenesis of acquired immunodeficiency syndrome: studies on sequential HIV isolates. J Virol **63**(5):2118-25.
221. **Tessmer, U., and H. G. Krausslich.** 1998. Cleavage of human immunodeficiency virus type 1 proteinase from the N-terminally adjacent p6* protein is essential for efficient Gag polyprotein processing and viral infectivity. J Virol **72**(4):3459-63.
222. **Thomssen, R., S. Bonk, C. Propfe, K. H. Heermann, H. G. Kochel, and A. Uy.** 1992. Association of hepatitis C virus in human sera with beta-lipoprotein. Med Microbiol Immunol **181**(5):293-300.

223. **Tilton, J. C., and R. W. Doms.** 2010. Entry inhibitors in the treatment of HIV-1 infection. Antiviral Res **85**(1):91-100.
224. **Tremblay, M. J., J. F. Fortin, and R. Cantin.** 1998. The acquisition of host-encoded proteins by nascent HIV-1. Immunol Today **19**(8):346-51.
225. **Trinh, L., D. Han, W. Huang, T. Wrin, J. A. Larson, L. D. Kiss, E. Coakley, C. J. Petropoulos, N. T. Parkin, J. Whitcomb, and J. D. Reeves.** 2008. Technical Validation of an Enhanced Sensitivity Trofile HIV Co-receptor Tropism Assay for Selecting Patients for Therapy with Entry Inhibitors Targeting CCR5. XVII HIV Drug Resistance Workshop. Sitges, Spain. June 10-14 2008.
226. **Trkola, A., S. E. Kuhmann, J. M. Strizki, E. Maxwell, T. Ketas, T. Morgan, P. Pugach, S. Xu, L. Wojcik, J. Tagat, A. Palani, S. Shapiro, J. W. Clader, S. McCombie, G. R. Reyes, B. M. Baroudy, and J. P. Moore.** 2002. HIV-1 escape from a small molecule, CCR5-specific entry inhibitor does not involve CXCR4 use. Proc Natl Acad Sci U S A **99**(1):395-400.
227. **Trouplin, V., F. Salvatori, F. Cappello, V. Obry, A. Brelot, N. Heveker, M. Alizon, G. Scarlatti, F. Clavel, and F. Mammano.** 2001. Determination of coreceptor usage of human immunodeficiency virus type 1 from patient plasma samples by using a recombinant phenotypic assay. J Virol **75**(1):251-9.
228. **Tscherne, D. M., C. T. Jones, M. J. Evans, B. D. Lindenbach, J. A. McKeating, and C. M. Rice.** 2006. Time- and temperature-dependent activation of hepatitis C virus for low-pH-triggered entry. J Virol **80**(4):1734-41.
229. **UNAIDS.** 2009. 2009 AIDS Epidemic update. UNAIDS.
230. **van der Schaar, H. M., M. J. Rust, C. Chen, H. van der Ende-Metselaar, J. Wilschut, X. Zhuang, and J. M. Smit.** 2008. Dissecting the cell entry pathway of dengue virus by single-particle tracking in living cells. PLoS Pathog **4**(12):e1000244.
231. **van der Schaar, H. M., M. J. Rust, B. L. Waarts, H. van der Ende-Metselaar, R. J. Kuhn, J. Wilschut, X. Zhuang, and J. M. Smit.** 2007. Characterization of the early events in dengue virus cell entry by biochemical assays and single-virus tracking. J Virol **81**(21):12019-28.
232. **von Hahn, T., B. D. Lindenbach, A. Boullier, O. Quehenberger, M. Paulson, C. M. Rice, and J. A. McKeating.** 2006. Oxidized low-density lipoprotein inhibits hepatitis C virus cell entry in human hepatoma cells. Hepatology **43**(5):932-42.
233. **von Schwedler, U. K., M. Stuchell, B. Muller, D. M. Ward, H. Y. Chung, E. Morita, H. E. Wang, T. Davis, G. P. He, D. M. Cimbora, A. Scott, H. G. Krausslich, J. Kaplan, S. G. Morham, and W. I. Sundquist.** 2003. The protein network of HIV budding. Cell **114**(6):701-13.
234. **Wakita, T., T. Pietschmann, T. Kato, T. Date, M. Miyamoto, Z. Zhao, K. Murthy, A. Habermann, H. G. Krausslich, M. Mizokami, R. Bartenschlager, and T. J. Liang.** 2005. Production of infectious hepatitis C virus in tissue culture from a cloned viral genome. Nat Med **11**(7):791-6.
235. **Walter, H., J. Eberle, H. Müller, C. Noah, E. Wolf, M. Stürmer, P. Braun, K. Korn, M. Däumer, T. Berg, M. Obermeier, A. Thielen, and R. Kaiser.** 2009. Empfehlung zur Bestimmung des HIV-1-Korezeptor-Gebrauchs. National Reference Center for Retroviruses, University of Erlangen.
236. **Watson, C., S. Jenkinson, W. Kazmierski, and T. Kenakin.** 2005. The CCR5 receptor-based mechanism of action of 873140, a potent allosteric noncompetitive HIV entry inhibitor. Mol Pharmacol **67**(4):1268-82.
237. **Wei, X., J. M. Decker, H. Liu, Z. Zhang, R. B. Arani, J. M. Kilby, M. S. Saag, X. Wu, G. M. Shaw, and J. C. Kappes.** 2002. Emergence of resistant human immunodeficiency virus type 1 in patients receiving fusion inhibitor (T-20) monotherapy. Antimicrob Agents Chemother **46**(6):1896-905.
238. **Weissenborn, K., A. B. Tryc, M. Heeren, H. Worthmann, H. Pflugrad, G. Berding, M. Bokemeyer, H. L. Tillmann, and A. Goldbecker.** 2009. Hepatitis C virus infection and the brain. Metab Brain Dis **24**(1):197-210.

239. **Weissenhorn, W., A. Dessen, S. C. Harrison, J. J. Skehel, and D. C. Wiley.** 1997. Atomic structure of the ectodomain from HIV-1 gp41. Nature **387**(6631):426-30.
240. **Welsch, S., A. Habermann, S. Jager, B. Muller, J. Krijnse-Locker, and H. G. Krausslich.** 2006. Ultrastructural analysis of ESCRT proteins suggests a role for endosome-associated tubular-vesicular membranes in ESCRT function. Traffic **7**(11):1551-66.
241. **Welsch, S., O. T. Keppler, A. Habermann, I. Allespach, J. Krijnse-Locker, and H. G. Krausslich.** 2007. HIV-1 buds predominantly at the plasma membrane of primary human macrophages. PLoS Pathog **3**(3):e36.
242. **Westby, M., M. Lewis, J. Whitcomb, M. Youle, A. L. Pozniak, I. T. James, T. M. Jenkins, M. Perros, and E. van der Ryst.** 2006. Emergence of CXCR4-using human immunodeficiency virus type 1 (HIV-1) variants in a minority of HIV-1-infected patients following treatment with the CCR5 antagonist maraviroc is from a pretreatment CXCR4-using virus reservoir. J Virol **80**(10):4909-20.
243. **Westby, M., C. Smith-Burchnell, J. Mori, M. Lewis, M. Mosley, M. Stockdale, P. Dorr, G. Ciaramella, and M. Perros.** 2007. Reduced maximal inhibition in phenotypic susceptibility assays indicates that viral strains resistant to the CCR5 antagonist maraviroc utilize inhibitor-bound receptor for entry. J Virol **81**(5):2359-71.
244. **Whitcomb, J. M., W. Huang, S. Fransen, K. Limoli, J. Toma, T. Wrin, C. Chappey, L. D. Kiss, E. E. Paxinos, and C. J. Petropoulos.** 2007. Development and characterization of a novel single-cycle recombinant-virus assay to determine human immunodeficiency virus type 1 coreceptor tropism. Antimicrob Agents Chemother **51**(2):566-75.
245. **White, E. J., B. McColgan, S. Kassaye, L. Zijenah, and D. Katzenstein.** 2010. Unusual five amino acid insert within subtype C HIV-1 envelope contributes to dual-tropism (X4R5). AIDS.
246. **WHO.** 2009. Rapid Advice: Antiretroviral Therapy for HIV Infection in Adults and Adolescents.
247. **Wild, C. T., D. C. Shugars, T. K. Greenwell, C. B. McDanal, and T. J. Matthews.** 1994. Peptides corresponding to a predictive alpha-helical domain of human immunodeficiency virus type 1 gp41 are potent inhibitors of virus infection. Proc Natl Acad Sci U S A **91**(21):9770-4.
248. **Wilkin, T. J., Z. Su, D. R. Kuritzkes, M. Hughes, C. Flexner, R. Gross, E. Coakley, W. Greaves, C. Godfrey, P. R. Skolnik, J. Timpone, B. Rodriguez, and R. M. Gulick.** 2007. HIV type 1 chemokine coreceptor use among antiretroviral-experienced patients screened for a clinical trial of a CCR5 inhibitor: AIDS Clinical Trial Group A5211. Clin Infect Dis **44**(4):591-5.
249. **Wu, L., N. P. Gerard, R. Wyatt, H. Choe, C. Parolin, N. Ruffing, A. Borsetti, A. A. Cardoso, E. Desjardin, W. Newman, C. Gerard, and J. Sodroski.** 1996. CD4-induced interaction of primary HIV-1 gp120 glycoproteins with the chemokine receptor CCR-5. Nature **384**(6605):179-83.
250. **Wyatt, R., P. D. Kwong, E. Desjardins, R. W. Sweet, J. Robinson, W. A. Hendrickson, and J. G. Sodroski.** 1998. The antigenic structure of the HIV gp120 envelope glycoprotein. Nature **393**(6686):705-11.
251. **Wyatt, R., and J. Sodroski.** 1998. The HIV-1 envelope glycoproteins: fusogens, antigens, and immunogens. Science **280**(5371):1884-8.
252. **Zanetti, G., J. A. Briggs, K. Grunewald, Q. J. Sattentau, and S. D. Fuller.** 2006. Cryo-electron tomographic structure of an immunodeficiency virus envelope complex in situ. PLoS Pathog **2**(8):e83.
253. **Zheng, A., F. Yuan, Y. Li, F. Zhu, P. Hou, J. Li, X. Song, M. Ding, and H. Deng.** 2007. Claudin-6 and claudin-9 function as additional coreceptors for hepatitis C virus. J Virol **81**(22):12465-71.

254. **Zhu, P., E. Chertova, J. Bess, Jr., J. D. Lifson, L. O. Arthur, J. Liu, K. A. Taylor, and K. H. Roux.** 2003. Electron tomography analysis of envelope glycoprotein trimers on HIV and simian immunodeficiency virus virions. Proc Natl Acad Sci U S A **100**(26):15812-7.
255. **Zignego, A. L., C. Giannini, M. Monti, and L. Gragnani.** 2007. Hepatitis C virus lymphotropism: lessons from a decade of studies. Dig Liver Dis **39 Suppl 1**S38-45.
256. **Zimmerman, C., K. C. Klein, P. K. Kiser, A. R. Singh, B. L. Firestein, S. C. Riba, and J. R. Lingappa.** 2002. Identification of a host protein essential for assembly of immature HIV-1 capsids. Nature **415**(6867):88-92.
257. **Zufferey, R., T. Dull, R. J. Mandel, A. Bukovsky, D. Quiroz, L. Naldini, and D. Trono.** 1998. Self-inactivating lentivirus vector for safe and efficient in vivo gene delivery. J Virol **72**(12):9873-80.

6 Abbreviations

7AAD	7-Aminoactinomycin D
a.u.	arbitrary units
ABC	antibodies bound per cell
AMD	AMD3100 – CXCR4 antagonist
APC	allophycocyanin
APC-H7	APC-cyanine tandem conjugate
app.	approximately
ASCII	American Standard Code for Information Interchange (computer file format)
BlaM	β-Lactamase
BSA	bovine serum albumin
BTP	bromothenylpteridine
CA	HIV-1 capsid protein
CCR5	CC chemokine receptor 5 – HIV-1 coreceptor
conc.	concentration
CPE	cytopathic effect
csv	comma separated values (computer file format for tabular data)
CXCR4	CXC chemokine receptor 4 – HIV-1 coreceptor
DAPI	4',6-diamidino-2-phenylindole
DMEM	Dulbecco's modified Eagle medium
DMSO	dimethylsulfoxyd
DNA	desoxyribonucleic acid
dNTP	desoxy-nucleoside-triphosphate
DTT	dithiotreitol
EDTA	ethylenediaminetetraacetic acid
EM	electron micrsocopy
Env	envelope protein
ER	endoplasmic reticulum
FACS	fluorescence assisted cell sorting – also used for 'flow cytometry' in general
FASTA	text-based file format for nucleotide or amino acid sequences
FCS	fetal calf serum
fcs	flow cytometry standard (computer file format for FACS data)
FDA	Food and Drug Administration (US government)
FFT	fast Fourier transformation
FP	fluorescent protein
GA	glutaraldehyde
Gag	group specific antigen – HIV-1 structural precursor protein
gp41	glycoprotein (number indicates size in kDa, e.g. gp41 – 41kDa)
HIV	Human Immunodeficiency Virus – also used to abbreviate HIV-1
IN	HIV-1 integrase protein
kb	kilo bases (unit for DNA and RNA – 1000 nucleotides)
kDa	kilo Daltons (unit for protein mass)

LA DB	Los Alamos Database
LTR	long terminal repeat
MA	HIV-1 matrix protein
MFI	mean fluorescence intensity
MIP-1	macrophage inflammatory protein 1
MVC	maraviroc – CCR5 antagonist
NC	HIV-1 nucleocapsid protein
Nef	negative factor – accessory protein of HIV-1
NK cells	natural killer cells (lymphocyte subset)
o/n	over night
ORF	open reading frame
p6	protein (number indicates size in kDa, e.g. p6 – 6kDa)
PBMC	peripheral blood mononuclear cells
PE	phycoerythrin
PEI	polyethyleneimine
PFA	paraformaldehyde
PI	propidium iodide
Pol	polymerase – HIV-1 replication machinery precursor protein
PonA	Ponasterone A
PR	HIV-1 protease protein
qWB	quantitative Western Blot
RANTES	"regulated upon activation, normal T-cell expressed and secreted" – chemokine of the CXC group
RNA	ribonucleic acid
rpm	revolutions per minute
RT	HIV-1 reverse transcriptase protein or room temperature
SDF-1	stromal cell-derived factor 1
SDS	sodium dodecyl sulfate
SIN	self-inactivating
sp1	spacer peptide (number indicates size in kDa, e.g. sp1 – 1kDa)
Tat	transactivator – accessory protein of HIV-1
TEM	transmission electron microscope
Tet	Tetracycline
V.E.R.S.A. or VERSA	viral entry receptor sensitivity analysis
Vpr	HIV-1 viral protein R
Vpu	viral protein U – accessory protein of HIV-1
VSV	Vesicular Stomatitis Virus
w/o	without
WB	Western Blot
wt	wild-type

List of publications

Journal papers:

Manon Eckhardt, K. Bozek, Ch. Sommer, S. Sierra-Aragon, F. Hamprecht, R. Kaiser, Th. Lengauer, H.-G. Kräusslich and B. Müller. Quantitative Multidimensional Analysis of HIV-1 Entry Efficiency on Single Cell Level**.** ***In preparation***.

Irene C. Schneider, Manon Eckhardt, Julia Brynza, Mary Collins, Klaus Cichutek and Christian J. Buchholz. 2010. Escape from R-peptide deletion in a γ-retrovirus. ***Ready for submission***.

Anja Habermann, Jacomine Krijnse Locker, Heike Oberwinkler, Manon Eckhardt, Stefanie Homann, Amy Andrew, Klaus Strebel, and Hans-Georg Kräusslich. 2010. CD317/Tetherin is Enriched in the HIV-1 Envelope and Downregulated from the Plasma Membrane upon Virus Infection. J Virol:[Epub ahead of print: 2010/02/12].

Oral presentations:

Manon Eckhardt, K. Bozek, E. Heger, S. Sierra-Aragon, R. Kaiser, Th. Lengauer, H.-G. Kräusslich and B. Müller. Comparative analysis of HIV-1 attachment and fusion efficiency. AREVIR-GenaFor-Meeting 2009, April 2009, Bonn, Germany.

Manon Eckhardt, M. Lampe, Th. Pietschmann, H.-G. Kräusslich and B. Müller. Fluorescently labelled HIV-1 derivatives as a tool to study virus cell interactions. Symposium of the Cell Entry group of SPP1230, May 2008, Langen, Germany.

Manon Eckhardt, J. Bitzegeio, G. Koutsoudakis, M. Lampe, H.-G. Kräusslich, Th. Pietschmann and B. Müller. Studying HCV entry using fluorescently labelled pseudoparticles. Workshop "Cell Biology of Viral Infections", October 2007, Deidesheim, Germany.

Poster presentations:

Manon Eckhardt, K. Bozek, Ch. Sommer, E. Heger, S. Sierra-Aragon, S. Delair, B. Lee, R. Kaiser, F. Hamprecht, Th. Lengauer, H.-G. Kräusslich and B. Müller. Quantitative Multidimensional Analysis of HIV-1 Entry Efficiency on Single Cell Level. 4th European Congress of Virology, April 2010, Como, Italy.

Manon Eckhardt, K. Bozek, Ch. Sommer, E. Heger, S. Sierra-Aragon, S. Delair, B. Lee, R. Kaiser, F. Hamprecht, Th. Lengauer, H.-G. Kräusslich and Barbara Müller. Quantitative Multidimensional Analysis of HIV-1 Entry Efficiency on Single Cell Level. 17th Conference on Retroviruses and Opportunistic Infections (CROI), February 2010, San Francisco, CA, USA.

Manon Eckhardt, K. Bozek, E. Heger, S. Sierra-Aragon, S. Delair, B. Lee, R. Kaiser, Th. Lengauer, H.-G. Kräusslich & B. Müller. Multidimensional Quantitative Analysis of HIV-1 Entry Efficiency. Cold Spring Harbor Retrovirus Meeting, May 2009, Cold Spring Harbor, NJ, USA.

Manon Eckhardt, K. Bozek, E. Heger, S. Sierra-Aragon, S. Delair, B. Lee, R. Kaiser, Th. Lengauer, H.-G. Kräusslich & B. Müller. Multidimensional Quantitative Analysis of HIV-1 Entry Efficiency. MedSys Kick-off Meeting, May 2009, Heidelberg, Germany.

Manon Eckhardt, Peter Koch, M. Adal, M. Lampe, M. Anders, K. Stöhr, H.-G. Kräusslich, D. Herten and B. Müller. SNAP-tagged HIV-1 derivatives as tools for the study of viral entry and egress. Annual Meeting of the German Society of Virology (GfV), March 2008. Heidelberg, Germany.

Manon Eckhardt, J. Bitzegeio, G. Koutsoudakis, Th. Pietschmann, M. Lampe, J. Briggs, A. Meier, H.-G. Kräusslich and B. Müller. Studying HCV entry using fluorescently labelled pseudoparticles. Third European Congress of Virology, September 2007, Nürnberg, Germany.

Acknowledgments

I am truly thankful to everybody who contributed to my thesis in any way – but there won't be enough space to mention everyone.

First of all, I would like to thank Hans-Georg Kräusslich, my first referee and head of department, as well as Barbara Müller, my supervisor, for the opportunity to perform this work, and their advice at various stages.

I'd also like to thank Ralf Bartenschlager for agreeing to be the second referee and participating in my two thesis advisory committees with helpful suggestions.

Thomas Pietschmann, Freddy Frischknecht and Oliver Keppler participated in the fruitful discussions of my thesis advisory committee, which I would like to acknowledge.

I thank my collaborators, mainly Kasia Bozek for great communication and stimulating discussions about our data, Christoph Sommer for the fast and efficient implementation of the segmentation algorithm and patient help with computer programs, but also Thomas Lengauer, Rolf Kaiser and the 'Cologne girls' as well as Fred Hamprecht. In this regard I'd also like to acknowledge Benhur Lee, who contributed the Affinofile cell line and showed constant interest in my work. Robert Doms, Mike Malim, Klaus Strebel and Thomas Pietschmann also contributed reagents.

Parts of microscopy were performed at the Nikon Imaging Center at the University of Heidelberg and I thank Ulrike Engel and Christian Ackermann for their help. I was allowed to use the FACS machines in ZMBH under the technical assistance of Monika Langlotz.

I am grateful to all current and former members of the lab – this includes the whole department of virology – for support, helpful comments and the nice working atmosphere. Maria Anders and Anke-Mareil Heuser contributed excellent technical assistance and continuous guidance and support. I thank Marko Lampe for his introduction to microscopy and the department, Anja Habermann for electron microscopy she performed for me, Steffi Homann for help with the SNAP-tag and CD317. Julia Bitzegeio, Kathleen Börner, Jessica Janus, Marko Lampe and Vanda Lux contributed helpful comments to parts of the manuscript. I am very grateful to Christiane Jost, Steffi Jäger and Sonja Welsch for continuous support and encouragement as well as critical reading of this manuscript.

I deeply appreciate the constant encouragement, support and strength that my friends and great big family offered to me. Without their belief in me, I would not have been able to get through this tough time. I dedicate this work to my late grandparents.